2014

Micro (Wind) Generation: 'Urban Resource Potential & Impact on Distribution Network Power Quality'

Keith Sunderland
Technological University Dublin, keith.sunderland@tudublin.ie

Micro (Wind) Generation: *'Urban Resource Potential & Impact on Distribution Network Power Quality'*

Keith Sunderland

School of Electrical and Electronic Engineering
Dublin Institute of Technology

A thesis submitted in fulfilment of the requirements for the degree of Doctor of Philosophy

Under the Supervision of

Prof. Michael Conlon and Dr. Gerald Mills

Abstract

Of the forms of renewable energy available, wind energy is at the forefront of the European (and Irish) green initiative with wind farms supplying a significant proportion of electrical energy demand. This type of distributed generation (DG) represents a 'paradigm shift' towards increased decentralisation of energy supply. However, because of the distance of most DG from urban areas where demand is greatest, there is a loss of efficiency. The solution, placing wind energy systems in urban areas, faces significant challenges. The complexities associated with the urban terrain include planning, surface heterogeneity that reduces the available wind resource and technology obstacles to extracting and distributing wind energy. Yet, if a renewable solution to increasing energy demand is to be achieved, energy conversion systems where populations are concentrated, that is cities, must be considered.

This study is based on two independent strands of research into: low voltage (LV) power flow and modelling the urban wind resource.

The urban wind resource is considered by employing a physically-based empirical model to link wind observations at a conventional meteorological site to those acquired at urban sites. The approach is based on urban climate research that has examined the effects of varying surface roughness on the wind-field above buildings. The development of the model is based on observational data acquired at two locations across Dublin representing an urban and sub-urban site. At each, detailed wind information is recorded at a height about 1.5 times the average height of surrounding buildings. These observations are linked to data gathered at a conventional meteorological station located at Dublin Airport, which is outside the city. These observations are linked through boundary-layer meteorological theory that accounts for surface roughness. The resulting model has sufficient accuracy to assess the wind resource at these sites and allow us to assess the potential for micro–turbine energy generation.

One of the obstacles to assessing this potential wind resource is our lack of understanding of how turbulence within urban environments affects turbine productivity. This research uses two statistical approaches to examine the effect of

turbulence intensity on wind turbine performance. The first approach is an adaptation of a model originally derived to quantify the degradation of power performance of a wind turbine using the Gaussian probability distribution to simulate turbulence. The second approach involves a novel application of the Weibull Distribution, a widely accepted means to probabilistically describe wind speed and its variation.

On the technological side, incorporating wind power into an urban distribution network requires power flow analysis to investigate the power quality issues, which are principally associated with imbalance of voltage on distribution lines and voltage rise. Distribution networks that incorporate LV consumers must accommodate a highly unbalanced load structure and the need for grounding network between the consumer and grid operator (TN-C-S earthing). In this regard, an asymmetrical 3-phase (plus neutral) power flow must be solved to represent the range of issues for the consumer and the network as the number of wind-energy systems are integrated onto the distribution network. The focus in this research is integrating micro/small generation, which can be installed in parallel with LV consumer connections. After initial investigations of a representative Irish distribution network, a section of an actual distribution network is modelled and a number of power flow algorithms are considered. Subsequently, an algorithm based on the admittance matrix of a network is identified as the optimal approach. The modelling thereby refers to a 4-wire representation of a suburban distribution network within Dublin city, Ireland, which incorporates consumer connections at single-phase (230V-N). Investigations relating to a range of network issues are considered. More specifically, network issues considered include voltage unbalance/rise and the network neutral earth voltage (NEV) for increasing levels of micro/small wind generation technologies with respect to a modelled urban wind resource. The associated power flow analysis is further considered in terms of the turbulence modelling to ascertain how turbulence impinges on the network voltage/voltage-unbalance constraints.

Declaration

I hereby certify that this thesis which I now submit for examination for the award of Doctor of Philosophy, is entirely my own work and has not been taken from the work of others, save and to the extent that such work has been cited and acknowledged within the text of my work.

This thesis was prepared according to the regulations for postgraduate study by research of the Dublin Institute of Technology and has not been submitted in whole or in part for another award in any Institute.

The work reported on in this thesis conforms to the principles and requirements of the Institute's guidelines for ethics in research.

The Institute has permission to keep, lend or copy this thesis in whole or in part, on condition that any such use of the material of the thesis be duly acknowledged.

…….

2014

Author Keith Sunderland
keith.sunderland@dit.ie
School of Electrical & Electronic Engineering
Dublin Institute of Technology, Ireland

Supervisor Professor Michael Conlon
michael.conlon@dit.ie
School of Electrical & Electronic Engineering
Dublin Institute of Technology, Ireland

Supervisor Dr. Gerald Mills
gerald.mills@ucd.ie
School of Geography, Planning & Environmental Policy
University College Dublin, Ireland

Reviewer Professor Alison Tomlin
a.s.tomlin@leeds.ac.uk
School of Process, Environmental and Materials Engineering
University of Leeds,
Leeds, UK

Reviewer Associate Professor Alberto Borghetti
alberto.borghetti@unibo.it
Associate Professor of Electrical Engineering
University of Bologna
Bologna, Italy

Acknowledgements

I would like to acknowledge my colleagues, past and present, in the School of Electrical and Electronic Engineering, who supported me through this research.

To my supervisors, Dr. Michael Conlon and Dr. Gerald Mills, your support was matched only by your patience over the duration of this research. Your guidance was instrumental and I am both forever grateful and appreciative for all you have done.

To my parents, Martin and Ann, your encouragement and belief in me have been constant for as long as I can remember. Your strength and conviction are my inspiration and your faith in me is something I can only hope to realise with my own children. Words could never truly express how grateful I am.

To my sisters, Tara and Sharon, you, along with my brother in-law, Richie, have been behind me in so many ways, particularly as perpetual baby sitters over many...many weekends.

I would also like to acknowledge my other family, the Pruntys. You too have provided me so much support along the way and I will be forever grateful.

Finally, to my wife Janet and my children, Robyn, Jack and Daisy, you have borne the brunt of this process and my ambition. I dedicate this work to you. It would not have been possible without you and I want you to know that I will endeavour to repay - with interest - all the time that was 'borrowed' to get me to this point.

List of Abbreviations

AMC	Admittance Matrix Correction
BRE	Building Research Establishment
BUBBLE	Basel Urban Boundary Layer Experiment
CCM	Current Correction Matrix
CENELEC	Comité Européen de Normalisation Electrotechnique
CER	Commission for Energy Regulation
CFD	Computational Fluid Dynamics
CHP	Combined Heat and Power
COE	Cost of Energy
DCENR	Department of Communications, Energy and Natural Resources (Ireland)
DCMNR	Department of Marine, Communications and Natural Resources
DECC	Department of Energy and Climate Change (UK)
DG	Distributed Generation
DN	Distribution Network
DNO	Distribution Network Operator
DUBLex	Dublin Boundary Layer Experiment
EEA	European Environment Agency
EIA	Energy Information Agency (US)
ELR	Environment Lapse Rate
EN	European Normative
EREC	European Renewable Energy Council
ESB	Electricity Supply Board (Now Electric Ireland)
ESDU	Engineering Sciences Data Unit
EST	Energy Saving Trust
EU	European Union
EU	European Union
EWEA	European Wind Energy Association
FiT	Feed in Tariff

GHG	Green House Gas(es)
GWEC	Global Wind Energy Council
HAWT	Horizontal Axis Wind Turbine
HOMER^{TM}	Hybrid Optimisation Model for Electric Renewables (software platform)
HV	High Voltage
IEA	International Energy Agency
IEC	International Electrotechnical Commission
ISL	Inertial sub layer
IWEA	Irish Wind Energy Association
LCZ	Local Climate Zone
LOM	Loss of Mains
LV	Low Voltage
MAE	Mean absolute error
MATLAB^{TM}	Matrix Laboratory (software platform)
MCS	Microgeneration Certification Scheme
MEES	Middle East Economic Survey
MPPT	Maximum Power Point Tracking
MV	Medium Voltage
NAKBA	Aluminium conductor sub distribution cable
NOABL	Numerical Objective Analysis of Boundary Layer
NR	Newton Raphson
NRE	Non-conventional Renewable Energy
NREAP	National Renewable Energy Action Plan
NTM	Normal Turbulence Model
NV	Not Viable
OPEC	Organisation of the Petroleum Exporting Countries
PDF	Probability Density Function
PQ	Power Quality
PV	Photo Voltaic
RESE	Renewable Energy Supply (Electrical)
RMDS	Retail Market Design Service
RMSE	Root mean squared error

RSL	Roughness sub layer
SEAI	Sustainable Energy Authority of Ireland
SECO	State Energy Conservation Service
SIAM	System Integration of Additional Micro Generation
SL	Surface Layer
SSEG	Small Scale Embedded Generation
SSEZ	Small Scale Energy Zone
SSWT	Small Scale Wind Turbines
SUB1	Suburban location containing high resolution anemometry (Sonic, CSAT3)
SWT	Small Wind Turbine
UBL	Urban Boundary Layer
UCL	Urban Canopy Layer
UK	United Kingdom
URB1	Urban location containing high resolution anemometry (Sonic, CSAT3)
US	United States
VAT	Value Added Tax
VAWT	Vertical Axis Wind Turbine
WADE	World Alliance for Decentralised Energy
WMO	World Meteorological Organisation
WWEA	World Wind Energy Association
WWEA	World Wind Energy Council
XLPE	Cross-linked Polyethylene cable insulation

Nomenclature

A	Cross-sectional area (m^2)
A_{rotor}	Rotor cross-sectional area (m^2)
A_F	Frontal area of roughness element(s) (m^2)
A_P	Total plan area of the roughness element (m^2)
A_T	Total surface area of the roughness element (m^2)
c	Scaling factor (Weibull and Rayleigh distribution functions)
$C_{ann,tot}$	Total annualised cost of system (€/Year)
C_{cap}	Initial capital cost (€)
C_D	Drag coefficient
$\overline{C_{DH}}$	Mean drag coefficient (for surface mounted cubes)
C_H	Urban High-platform wind observations
COE	Cost of Energy
C_p	Wind turbine power coefficient
C_L	Urban Low-platform wind observations
$CRF(i,N)$	Capital recovery factor, with i the annual interest and N the number of years
d_{ab}	Horizontal distance between conductors a and b (per unit-length)
E_{def}	Deferrable load served (kWh/year)
$E_{grid,sales}$	Total grid sales (kWh/year)
E_{prim}	Primary load served (kWh/year)

D_e	Hypothetical return path of the earth current and is a function of both earth resistivity, ρ and frequency, f
D_{ij}	Distance between conductors i and j (per unit-length)
E_{prim}	Primary load served (kWh/year)
E_{def}	Deferrable load served (kWh/year)
$E_{grid,sales}$	Total grid sales (kWh/year)
f	System frequency (Hz)
$f(u)$	Wind speed distribution within the 10-minute period (Gaussian wind speeds, normally distributed about the mean)
GMR_i	Geometric Mean Radius of conductor i (per unit-length)
GMR_{cn}	Geometric Mean Radius of *bundled* conductor i (m)
h_a	Height of conductor a (m)
k	Shape factor (Weibull and Rayleigh distribution functions)
l_c	M*ixing (turbulence) length scale* in the canopy layer
$l_m(z)$	Matching region where a linear variation of turbulence mixing scale l_c is assumed
$L(z)$	Monin-Obukhov length (m)
P_{abs}	Average of individualised (6000) calculations of power over the observation window and represents the truest measure of generated power by the turbine (kW)
$\overline{P(u)}$	Ten minute average of measured power output

$\overline{P_{obs_{(TI)}}(u)}$ Simulated 10-minute average power output in terms of the measured wind speed and standard deviation (σ_{obs}). The σ_{obs} is used to derive a representative *TI*.

$P_{I=0}(u)$ Idealised wind turbine power curve, i.e. not inclusive of the affects of turbulence

$P_S(V)$ Momentary value of power (kW)

$\overline{P_{sim}(u)}$ Average simulated power (simulated by considering the variation of wind speed within a window of measurement (10 minutes)) (kW)

$\overline{P_{simTI}(u)}$ Simulated 10-minute average of measured power output in terms of the measured wind speed distribution (over 10 minutes) and an assumed *TI*

$\overline{P_{Normalised}(u)}$ Approximate power output based on consideration of how the turbine power curve is affected by turbulence

$\overline{P_{Normalised}(u,TI)}; P_{norml}$ The Albers' approximation of power output based through the observed wind speed and TI over the observation period

$P_{power-curve}(u)$ 10th order polynomial description, of the turbine power curve, in terms of wind speed, u

$\overline{P_{Weibull}(u,TI)}; P_{weib}$ Weibull approximation of power output based through the observed wind speed and TI over the observation period

R_i Resistance of conductor *i* (Ω/unit-length)

R_{proj} Project lifetime (years)

S_H Suburban High-platform wind observations

S_L Suburban Low-platform wind observations

TI_{obs}	Turbulence intensity based on observed/measured mean wind speed ($\overline{u_{obs}}$) and measured standard deviation (σ_{obs}) over an observation period (10 minutes)
TI_{sim}	Turbulence intensity based on observed/measured mean wind speed ($\overline{u_{obs}}$) and simulated standard deviation (σ_{sim}) calculated from an assumed *TI* over an observation period (10 minutes)
u	Wind speed (m/s)
u_{hub}	Wind speed at the hub height of the wind turbine (m/s)
u_{anem}	Wind speed at the anemometer height (m/s)
$\bar{u}$	Mean wind speed (m/s)
$\overline{u_{obs}}$	Measured mean wind speed over the observation window
$u(z)$	Wind speed variation with height (m/s)
u_*	Frictional velocity (m/s)
V	Wind velocity (m/s)
V_{mean}	Mean velocity of the wind over an observation period
S_{ij}	Distance between conductor *i* and image *j* (per unit-length)
z	Vertical distance (m)
z_{anem}	Anemometer height (m)
z_d	Displacement height (m)
z_{hub}	Hub height of the wind turbine (m)
z_{Hm}	Mean height of buildings (m)
z_{ii}	Self impedance of conductor *i* (Ω/unit-length)
z_{ij}	Mutual impedance between conductors *i* and *j* (Ω/unit-length)

z_0	Surface roughness (m)
$z*$	Wake diffusion height (m)
z_{UBL}	Urban boundary layer height (m)

Greek Symbols

κ	Von Karmann constant (m)
λ_p	Plan area density (m^2)
λ_f	Frontal area density (m^2)
σ_u	Standard deviation of the wind (over an observation period)
σ_{sim}	Standard deviation of the wind (over an observation period), based on an assumed *TI*
Φ_M	Dimensionless stability function (Momentum)
ρ_{air}	Density of air
ρ	Resistivity of earth (Ωm)
θ_{ij}	Angle between a pair of lines drawn from conductor i to its own image and to the image of conductor j (degrees)
σ_{obs}	Standard deviation of wind speed over 10 minute observation period
ω	Rotational speed of the rotor

Glossary of Terms

Urban Boundary Layer	The internal boundary layer formed when air flows over a city, the characteristics of which are affected by the nature of the urban surface.
Capacity Factor	The ratio of the actual energy produced by the generation technology to the energy that would be produced if operating at rated output over the same time period
Capital Cost	The initial cost of buying, installing and commissioning of the energy supply system
Central Generation	Production of energy on a large scale (MW) that is transmitted through the transmission/distribution network to a widely distributed group
Distribution Network	The electrical network infrastructure involved in the distribution of electricity from 230V to 20kV (AC)
Feed in Tariff	The price per unit of electricity that a utility/supplier pays for the renewable electricity
Generation capacity	The maximum rated power output of the wind generator under specific conditions designated by the manufacturer
Levelized Cost of Energy	The average cost per 1 kWh of useful electrical energy produced by a wind energy system
Low Voltage	Voltage band between 50V (AC) and 1kV (AC)
Medium Voltage	In Ireland, the distribution network operates at 10 and 20kV (AC)

Micro Generation	EN50438 defines microgeneration as generation at a maximum of 25A/phase ($5.75kW_e$) when the distribution network connection to the distribution network is at single-phase and 16A/phase when the connection is three-phase ($11kW_e$).
Power Flow	Power flow (also known as load-flow) is the analysis of a power system in normal steady-state operation with the goal of obtaining a complete voltage angle and magnitude description for each bus in the power system; for specified load and generator real power and voltage conditions. Also considered in such analyses is the magnitude of real and reactive power flows in the system lines. Power flow studies are important for planning future expansion of power systems as well as in determining the best operation of existing systems
Renewable Energy Sources	Energy resources that are naturally replenishing but flow limited, in that the amount of energy that is available per unit of time is limited. Renewable energy resources include: biomass, waste energy, hydro, wind, geothermal, solar, wave and tidal energy
Replacement cost	This is the cost of replacing components of a wind energy system before completion of the lifetime of the system.
Surface Roughness	The roughness length is used in numerical models to express the r*oughness* of the surface. It affects the intensity of mechanical turbulence above the surface and is a parameter in the description of some vertical wind profile equations. A lower roughness length z_o, implies less exchange between the surface and the atmosphere. Whilst not a physical length, it can be

	considered as a length-scale or a representation of the roughness of the surface, which is particularly relevant in the field of urban climatology
Transmission Network	The electrical network infrastructure involved in the distribution of electricity from 110 – 400kV
Turbulence Intensity	The ratio of wind speed standard deviation to the mean wind speed, determined from the same set of measured data samples of wind speed, and taken over a specified time
Voltage Unbalance	The IEEE definition of voltage unbalance, also known as the phase voltage unbalance rate (PVUR), is given by the ratio of the maximum voltage deviation from the average phase voltage to the average phase voltage. This definition only deals with magnitudes (and does not consider phase). So a true definition of voltage unbalance is the ratio of the negative sequence voltage component to the positive sequence voltage component.

Table of Contents

List of Figures

List of Tables

Chapter 1: Introduction

1.1 Chapter outline

The aim of this Chapter is to set out the context for the research presented in the subsequent chapters. The case for micro wind energy systems as part of the urban energy infrastructure is initially established by considering existing electricity distribution network systems and how there is a trend towards increased distributed generation. The emphasis on the urban environment is as a consequence of where energy will be needed most and as global populations increasingly reside in cities, all forms of renewable energy must have a place in these locations

For small/micro energy systems to become a constituent part of this new paradigm, holistic improvements in understanding of the electricity generation technologies, as well as the limitations of the available distribution networks, are required. As opposed to prioritising these alone however, this research focuses on acquiring a better understanding of the associated primary energy, the urban wind resource. This is not a trivial task as the urban environment represents a significant challenge in this regard by virtue of building morphology and geographic heterogeneity.

This Chapter subsequently lays out the aims and objectives of the work and how the thesis is structured to convey the significant contributions to knowledge as well as the associated research outcomes.

1.2 Background

The demand for electricity worldwide is increasing year-on-year and consumption of electricity has increased by c350% in the period 1973 – 2010 [1]. This growth has been interrupted recently by recession, but will be re-established as economic cycle's worldwide return to relative stability and growth thereafter. Electricity - for the most part – is generated in centralised systems. Central Generation is the electric power production by central station power plants using large gas, oil, coal or nuclear boilers to provide bulk electrical power. These generators supply a high-voltage transmission network that feeds power in one direction – down through distribution networks at lower voltage stages to a large number of end-users. These end-users can be connected to the grid at different voltage stages depending on their demand, but in terms of customer numbers, the largest category is low-voltage end-users such as households [2]. Burt *et al* [3] argue that power networks were developed over many years on the premise of "many loads - few sources". Patterson goes on to suggest that while this made sense during much of the network's long development, it is less justifiable now [2], or as Burt *et al* asserts, novel solutions are required to support the operation and management of a "many loads - many sources" based electricity supply industry [3].

The limitations to this type of energy supply, in terms of efficiency and environmental impact as well as stability to sustain them, is further giving rise to increased distributed and renewable energy resource option considerations [4]. Historically, the prioritisation of a centralised generation paradigm was due to a number of drivers [5]:

- Economies of scale facilitating minimal marginal cost of electricity production; derived mainly through the advent of steam turbines
- Larger generation facilities leading to higher energy efficiency
- The employment of alternating current (over direct current) deriving a reduction in associated losses in transmission
- Larger generation plants facilitating the potential for increased reliability at the customer's end, particularly in the context of generation pooling
- Environmental considerations. The development of transmission/distribution networks meant that the associated generation could be located outside the urban centres thereby reducing pollution caused by exhausts.

However, the main drawbacks associated with centralised generation are similarly related and include transmission/distribution system costs, investment in transmission and distribution networks (e.g. rural electrification), security/reliability of supply and energy efficiency as well as environmental impact.

Transmission/distribution losses can account for 30% of the cost of delivered electricity, with the highest costs attributable to customers utilising electricity at low voltage [6]. The high costs come from losses in the transmission and distribution lines and associated conversion losses. Rural electrification is a significant issue – particularly in terms of developing countries. As large capital costs are required in connecting remote areas (due primarily to the distances involved), connecting remote areas with lower power consumption may be uneconomical [5]. Related to this point and with respect to the developed world, investment costs associated with large centralised energy supply in the form of maintenance and expansion systems are very high.

Energy efficiency is limited by the pressures that steam can operate within the centralised power stations. Attempts to offset this issue by encouraging the use of

cogeneration plant are resulting in plant that is predominantly heat driven. But difficulties associated with transpiration of heat and steam is leading to the justification of locating distributed generation closer to points of consumption [5]. Centralised generation systems do not readily diversify away from the dominant forms of fossil fuel leading to security and reliability concerns. Associated with these fossil fuels, the environmental impact of centralised energy is significant due to its reliance on natural gas, oil and coal (particularly in developing countries). Furthermore, the lack of indigenous fossil fuels in some countries is leading to a form of primary energy poverty which in turn creates an economic burden as well as energy security concerns in such countries. Indeed, as these traditional forms of primary energy deplete, these economic pressures will be further exasperated. In terms of the current energy supply paradigm, decoupling the economy from how electricity energy is being utilised is difficult to realise. Patterson [7] supports this position. He argues that electricity is first and foremost a function of infrastructure; it can be generated without fuel, but not without infrastructure and it is the latter where focus – in terms of generators, transmission/distribution network and load – should be prioritised.

In summary, the main issues identified are: the depletion of primary energy sources, insecurity affecting the energy transportation infrastructure, the associated climate change impact and the high-risk nature of large-scale plant investments. Given these issues, there is an increased impetus internationally towards an alternative form of energy supply and network infrastructure [8]. It is unlikely that on a global scale, more efficient use of fossil fuels will address these problems. Instead, an energy generation/transmission paradigm with a priority towards renewable distributed

generation is increasingly being recognised by policy makers as the direction to take if economic/energy decoupling is to be achieved [9, 10].

Figure 1.1 presents a model to provide an energy supply perspective, which describes the transition from the historically prevalent centralised supply paradigm towards a decoupled energy context that incorporates the benefits of both. The red circles represent the energy supply sources, whereas the blue crosses represents consumer demand. Pre-electrification homes were essentially self-sufficient (distributed) with fossil fuels as the source for all energy requirements. These homes were eventually afforded electricity through centralised, large power plants. Currently, there is an increased impetus (driven by Governmental policy and the green agenda) to maximise energy efficiencies and alleviate reliance on fossil fuels, towards increased distributed and renewable electricity generation to facilitate demand. In the context of Figure 1.1 however, most distributed generation is autonomous and not centrally controlled, and there is a disjointed approach with difficulties associated with dispatching of the associated plant. In the context of population demographics, in the future, said populations will reside in cities and as centralised load centres, the distributed generation needs to facilitate this type of load. The future energy paradigm therefore needs to be a compromise of these approaches where distributed generation can operate in harmony with centralised power systems (smart grids) with an emphasis away from fossil fuels towards more renewable energy supply.

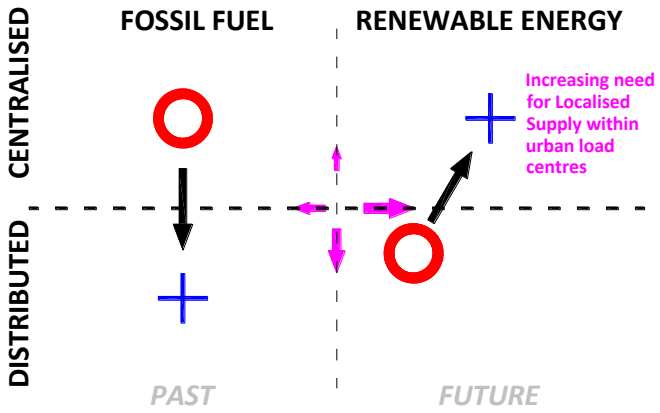

Figure 1.1 Evolution towards the future electrical energy supply paradigm

1.2.1 Distributed Generation

Distributed generation (DG) is not a new concept. It mainly depends upon the installation and operation of a portfolio of small size, compact, and clean electric power generating units at or near an electrical load (consumer) [11]. The main driving forces towards increased distributed generation are electricity market liberalisation and environmental concerns. The developments in distribution technologies have been around for a long time, but were as such not capable of pushing the "economy as scale" out of the system [12]. However, with the disadvantages identified in centralised generation and supply, a distributed approach is becoming increasingly more prevalent internationally. This will facilitate the integration of increased renewable forms of energy that can integrate into distribution networks at different entry points all the way down to end consumers becoming part of an evolved distribution network.

1.2.2 Small Scale Embedded Generation

A developing aspect of distributed generation is small scale embedded generation (SSEG) or microgeneration. Microgeneration is small scale heat or electricity

generation in or around individual buildings (or groups of buildings) [13]. Increasingly these technologies form part of the energy mix in many economies and represent an important component of environmental strategies aimed at reducing Carbon Dioxide emissions. This form of energy production involves small businesses and communities to meet their own needs while having the potential to combat fuel poverty, add to the diversity of energy supply and offset shortfalls in centralised generating capacity [14]. In Europe, microgeneration is defined as a source of electrical energy and all associated equipment, rated up to and including 25A at low voltage (230V), single-phase and 16A at low voltage (400V), three-phase. In addition to the technical benefits that microgeneration can bring (electricity generation at point of use and the positive contribution to the carbon rating of a building [15, 16]), microgeneration can also promote energy usage reduction through behaviour change [17].

The (dis)advantage of these technologies is their size, which allows energy to be generated at multiple sites (close to the point of consumption) but makes it difficult to integrate with existing energy generation/distribution systems. While individually, microgeneration technologies have minimal impact on the distribution network, collectively - if widely adopted - these technologies could significantly impact the distribution network system operation and planning [18]. It is in such a context that microgeneration (including micro wind generation), could contribute towards energy sustainability. Such a goal involves incremental adoption of available technologies, practices and policies that may help to decrease the environmental impact of the energy sector, while providing an adequate standard of energy services [19]. This thesis will concentrate on micro wind electrical energy. Wind energy is the dominant European renewable energy resource [20], but within an urban environments, this renewable

energy source has yet to be embraced in any meaningful way. There are still relatively few examples of these systems within urban settings where demand is greatest and where they could provide an alternative to centralised generation using fossil fuels that generate carbon emissions [21].

Currently nearly half of the world's population resides in cities and within two decades, it is envisaged this figure will rise to about 60% [22]. In industrialised countries, the residential sector constitutes a significant portion of total energy use, accounting for 32.79% and 30.9% of final electricity consumption in the US [23] and EU-27 [24] respectively. So in the context of end consumer and where they are likely to reside, they have a role as a supplier that could lead to optimised efficiencies.

It is with respect to all these issues therefore, that detailed analysis is required to establish the optimal level of participation by smaller wind energy electricity generation. Such analysis needs to take account of the renewable energy resource, the technologies available and affects they have on the distribution grid in the locations within which they operate. The focus of this thesis will be small/micro wind generation and how increasing connections in the urban context affects the grids. This analysis is with respect to accurate wind speed considerations and how the heterogeneity of the urban environment diminishes and complicates the available wind resource. Figure 1.2 succinctly demonstrates the consequences of the wind resource complexity. Three identical wind turbines installed within metres of one another on the roof of an urban environment. Each wind turbine is facing a different direction, with turbine (c) facing (almost) completely opposite to turbines (b) and (c). This shows the consequences of turbulent wind manifesting different yawing reactions.

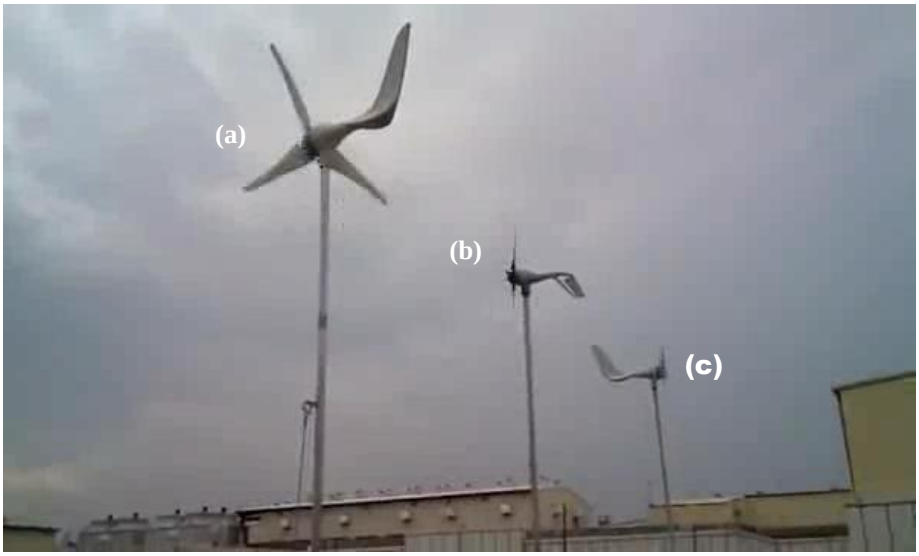

Figure 1.2 Example of micro wind turbine installations in an urban environment (*source:* http://www.youtube.com/watch?v=lQLLtrIvF_g&feature=relmfu)

1.3 Micro Wind Energy

Wind turbines extract kinetic energy from moving air, converting it into mechanical energy via the turbine rotor and then into electrical energy through the generator. Micro wind turbines can be either horizontal axis (HAWT) or vertical axis (VAWT). Their associated characteristics include blade diameter, cut-in/rated wind speed, and output power at rated wind speed. The two defining aspects of a wind turbines performance are the blade sweep area and the associated power curve for the turbine. The blade sweep area defines the amount of power that can be captured from the available wind whilst the power curve describes the turbines' performance against varying wind speeds. The mechanical energy captured by the wind rotor is defined by the Betz constant in the equation describing mechanical power through wind energy:

$$P_{Mech} = \frac{1}{2}.C_p.\rho_{air}.A_{rotor}.u^3 \qquad \textbf{(1.1)}$$

where

- C_p, is the power coefficient, defining how much wind power is captured and turned into mechanical power to subsequently generate electricity
- ρ_{air}, is the mass density of air;
- A_{rotor}, is the rotor area ($\pi.R^2$ where R is the length of the blades);
- u_0 is the free stream wind speed.

The micro wind sector is still at an early stage of development, but there is evidence of a growing market for micro wind systems [25]. Less complex approval processes, improved site identification and grid connection are contributing towards small and micro-wind energy being perceived (globally) as an attractive prospect to developers in the industry [26].

Several countries have introduced legislation and similar measures to encourage the growth of distributed renewable energy generation [27]. In the United States for instance, there is promising growth in the sector where some 9,800 new small and micro wind turbines were commissioned between 2008 and 2009 alone representing a 15% growth in the market [28]. Global sale trends are also positive and in 2009 there was an estimated increase of 21,000 small and micro wind turbines installations [28]. These figures include wind turbines ranging up to 100 kW, but nonetheless, they suggest an uprising of smaller distributed generation systems with regard to wind energy.

From an urban wind energy perspective, the majority of energy potential research is somewhat biased as the performance of wind turbines is prioritised [29, 30]. In the urban environment, the initial cost of micro wind turbines and the locations in which units are likely to be installed (i.e. where the wind speed and direction are very dependent on the site, proximity to potential obstacles etc.) serve to cloud perspectives. The wind resource is invariably not the focus in such research, but rather the energy

yield of the turbines. This can lead to the potential for inappropriate installation locations where the energy potential can never be realised.

There is therefore a deficiency in understanding concerning the potential energy that could be harnessed from micro wind energy systems as well as the viability of these systems to provide a cost effective power generation option [31]. Missing from the majority of the aforementioned research is the technology's primary energy source, the wind. There is significant research assessing the wind energy resource in 'rural' locations around the world [32-34], and in some research [35-37], such work has been extended to apply to the potential for wind energy conversion systems. But the available test studies that investigate the viability of micro wind generation in urban centres, are more generic and broad, suggesting that the technology can work *if* installed correctly and in appropriate locations [29, 30]. Prioritising better understanding of the wind resource therefore, could potentially lead to improved choices of installation locations and more realistic productivity expectations from this form of energy system. As global populations increasingly migrate towards urban centres, small wind energy systems, either for urban dwellings or for greenfield locations must be considered as a possible contribution towards renewable energy targets [21].

1.4 The Distribution Network

As outlined in the previous sections, micro energy systems will have a role in a new paradigm of increasing distributed generation. Their participation will, however, present technical issues for the distribution network operators. It is in this regard that there is an increased impetus to investigate distribution networks with particular focus on the Low Voltage (LV) consumer level. Actual issues that warrant consideration include voltage profile, voltage unbalance, loading levels and fault analysis. Such investigations will

inform network operators of any associated operational limitations and how future iterations of these networks may evolve. This research prioritises voltage concerns.

Power flow is used to determine the steady state operating condition of a power system and any associated solution methods should be fast, have low storage requirements, be reliable and versatile through an inherent simplicity [38]. In terms of the transmission networks, Power Flow is considered using Gauss-Seidal, Newton-Raphson and its decoupled versions [39]. Distribution networks, however are for the most part radial in structure and as a consequence of associated high R/X ratios, multi-phase unbalanced operation, unbalanced load (and generation) distribution, are ill-conditioned for these conventional power flow methodologies.

This thesis will explore the effects of increased micro wind energy systems connected to the grid through different options of power flow analysis. These models are to include wind energy systems connections driven from urban wind reference. Initially, the Irish position is discussed with respect to a generic but representative distribution network model. However, as these micro wind generators are coupled to the grid through a single-phase consumer interface, more complex 3-phase/4-wire systems are required. While distributed load/generation arrangements are standard considerations for the majority of power flow solutions, the additional consideration of systematic earthing systems, further exasperates the ill-conditioning for the standard power flow approaches. So the associated modelling is developed to facilitate accurate analysis that is representative of the LV distribution network from the substation transformer down to the consumer connection. To achieve this, a sample of an urban distribution network,

incorporating 74 customer connections and the associated cable details is made available by the Irish DSO, *ESB Networks*.

1.5 Statement of Research Problem

This thesis examines the proposition for an alternative energy model which is based upon integrating micro energy generation using the wind resource. Therefore the intent of this research has two aspects:

- *What are the implications for existing distribution networks in an alternative energy paradigm and how will these networks need to be planned and operated to accommodate appreciably higher level of small-scale embedded energy generation.*
    - This involves modelling of the urban distribution network at low voltage (LV) to take account of micro energy at neighbourhood/building scale. The majority of current research is with respect to generic Distribution Network Operator (DNO) models, but urbanised wind generation and network reaction needs to be cognisant of the specifics of the urban distribution networks. This research will consider an actual urban distribution network configuration as provided by the operator of the electricity distribution system in the Republic of Ireland (ESB Networks), with load flow analyses detailing how the network reacts to microgeneration connections
- *What is the nature of the wind resource in terms of its variability and reduction by the presence of the city itself and how does a city effect how usable energy can be extracted from the resource*
    - Current research in this area is predominantly based on *computational fluid dynamics* (CFD) analysis – a methodology which is very case-specific and consequently cannot be generalised to the required extent. The method proposed in this research facilitates accurate estimation of the urban wind resource through empirical analysis of wind observations cognisant of surface roughness parameterisation
    - Various wind data is employed in this regard, but the primary data is acquired from both high resolution (10Hz) and standard meteorological observations at high (relatively) and low platform positions within Dublin City, Ireland. These

observations are employed in conjunction with the synoptic meteorological station at Dublin Airport.

- Essentially overlapping the two main research themes, turbulence modelling is also a consideration of this research. But instead of modelling turbulent wind speed, modelling prioritises how it affects the productivity of a turbine. These models are subsequently to be integrated as the system generation for power flow analyses.

1.6 Research Aims and Objectives

The aim of this research is to develop novel modelling capability that can represent the complexities associated with urbanised small/micro wind generation in a holistic and accessible manner. This aim is predicated on the deficiencies in understanding concerning small/micro wind opportunities within urban distribution networks. This thesis presents applied research in which electrical engineering is informed by urban climate research. The thesis will present analysis considering how small/micro wind turbines interact with urban distribution networks and in urban environments. This associated work is based on urban climate research that has examined for the effects of varying surface roughness on the wind-fields accessible to these technologies. These goals require a synergy of urban wind resource and low voltage distribution network modelling. Clearer understanding of this electrical energy resource will facilitate improved and more efficient utilisation/deployment of said technologies leading towards meaningful contributions towards national renewable targets from both energy and sustainability perspectives. This modelling must therefore be cognisant of environments characterised by the prevalence of turbulence, where complex and heterogeneous morphologies directly inhibit the viability of the wind resource available. Also, the urban distribution network, which these technologies access, needs to be accurately considered so that associated power flow analyses are representative and inclusive of the network configuration complexities. Indeed, the context of micro wind

technologies is with respect to LV consumer connections. Therefore, the distribution network model needs to be capable of representing the unbalanced nature of multiple single-phase connections within a three-phase distribution system environment.

As well as the distribution network operator, this modelling will be useful to the energy regulator. Decisions pertaining to both network tolerances and smart-grid development will be better informed from the models developed in this research. Furthermore, if these technologies are to be incentivised in the future, both the network operator and the energy regulator require accurate modelling. Such modelling will facilitate understanding of the loading capabilities of the distribution network (including the distribution transformer), which depends on the installed renewable energy capacity. A further aim of the research relating to informing the energy regulator is to consider the cost of energy (COE) associated with small/micro wind turbine technology systems.

The means to accurately predict the wind speed over an urban terrain is useful on multiple levels. Architects, engineers and all professionals involved in urban planning will be interested in knowing the wind loads as presented by the wind resource within the urban landscape. Current approaches require specific computational solutions, which for the most part, use metrics developed within the urban landscape itself and as such is subject to compromises in accuracy. Where input parameters are remotely derived, the wind maps utilised have tolerances based on generic descriptions of terrain, most of which are not 'urban sensitive'. A simple model that can derive wind speed estimates to working tolerances of +/- (10-15) % is something that can be universally appreciated. The broader research synergy between the wind resource consideration and distribution network analyses is summarised in Figure 1.3.

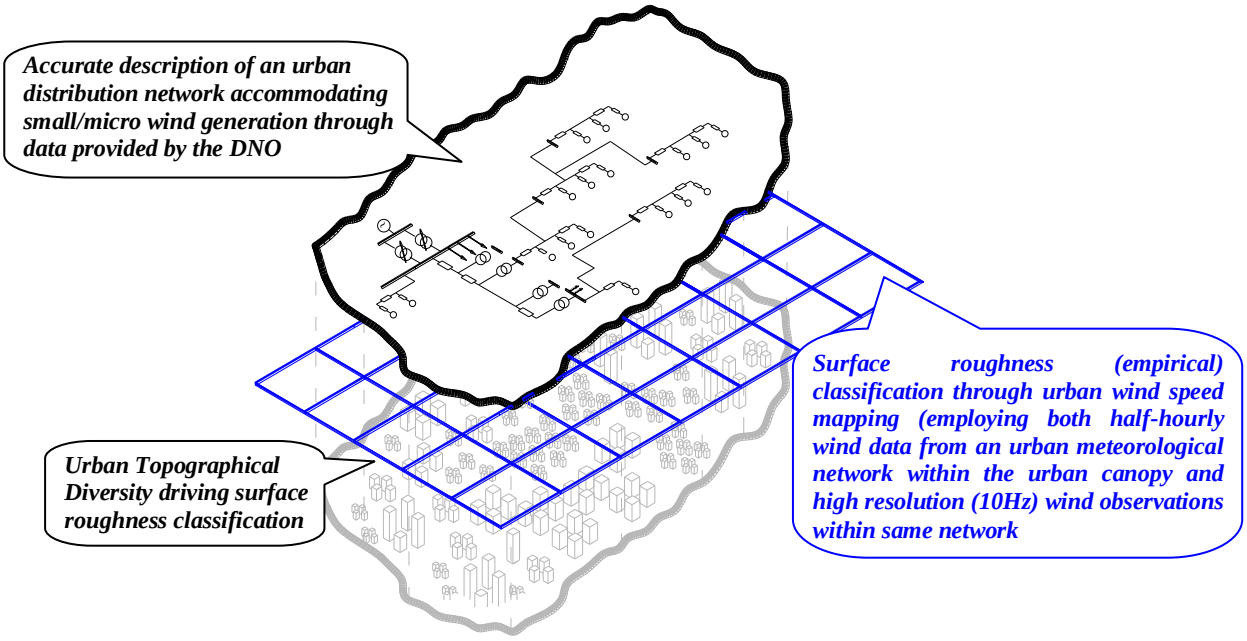

Figure 1.3 Rationale for a three stage urban wind/(electrical) distribution model encompassing the integration of wind speed modelling and urban distribution network analyses

Figure 1.3 contextualises how a predictable assessment of the urban wind resource, through appreciation of the urban topographical complexity, can be integrated into the operational capability of an urban distribution network.

1.6.1 Research Objectives

With respect to the aims of the research, a number of objectives are classified as follows:

1. To establish the state-of-the-art with respect to microgeneration and more specifically, micro wind generation
2. To develop a balanced distribution network model to perform power flow analyses in terms of base-line load implications and different wind speed models
3. To develop a simple and accurate wind speed model cognisant of a heterogeneous environment incorporating significant building morphology complexity
4. To develop a model that represents the influence of turbulence in the (power) performance of a small/micro wind turbine

5. To develop a 4-wire (unbalanced) power flow (urban) network that accurately includes the network configuration including LV consumer earthing. The model is to be capable of incorporating the derived urban wind speed modelling
6. To describe the performance of an urban distribution network incorporating significant wind generation with respect to the available wind resource within the urban environment
7. To consider the cost of small/micro energy of wind energy systems and present a comparison in terms of both rural and urban contexts

It is important to point out that this thesis will not consider the aesthetics of wind generation or other non-technical issues such as sound level(s). There are many challenges in respect of incorporating wind generation into urban areas. These include the nature and variability of the wind resource, planning constraints associated with urban installations, manufacturer inconsistencies and financial concerns (predominantly the associated capital outlay). Planning issues primarily relate to noise and visual impact as well as structural considerations and some planning legislation effectively places limitations on their deployment in residential areas [40]. In identifying the potential for this form of renewable energy, the context is technical performance based on the available wind resource. In this regard, the research will highlight cases where this form of energy could be beneficial.

Each section of the thesis contains a literature review to establish both the relevance of the proceeding modelling/analysis, but the first section serves to justify the consideration of wind energy in a small/micro context as the means to supplement distribution energy supply. These objectives are summarised in Table 1.1 in which further detail pertaining to how the research objectives are to be realised is presented.

Table 1.1: Research objective dissemination into component parts

Part	Chapter	*Detail*	Objectives: outline of the goals in the associated chapter
I	2	***Renewable energy: the potential for micro energy systems in a macro renewable energy context.***	• Identify the current position *vis-à-vis* renewable energy internationally, with a specific focus on wind energy • Investigate the state-of-the-art with respect to the potential for microgeneration and more specifically micro wind generation as a form of energy that accessible to the distribution network operators
	3	***Technical constraints associated with increased micro small energy connections***	• Establish international/national perspectives on Network tolerances, incentives and inhibitors to microgeneration • Establish the technical effects of micro wind energy systems as distributed energy sources as well as identifying the general technical concerns associated with microgeneration • Develop a generic Distribution Network Model representative of the 38/10/0.4kV context • Analyse (*Power Flow*) the developed Balanced Distribution network model incorporating micro wind turbines and synthetically derived wind speed
II	4	***Wind in Cities***	• Wind: constitution and complexities • Utilising boundary layer theory to consider wind speed profiling; prioritising the urban boundary layer • Investigate the state-of-the-art with respect to urban wind speed modelling
	5	***Urban wind observations: modelling& validation***	• Analyses (statistically) a network of weather stations within and directly above the urban canopy • Develop a wind speed model that extrapolates a rural reference wind speed into the urban environment utilising empirical analysis of wind observations cognisant of surface roughness parameterisation
III	6	***Turbulence: impact on the productivity of micro wind energy systems***	• Identify how the wind regime is affected by turbulence prevalent environments such as cities • Establish how the performance of (small) wind turbines is affected by turbulence and productivity in an inherently turbulent environment, namely a city (Dublin, Ireland), • Modelling to establish the effect of turbulence on small/micro wind turbine productivity
	7	***4-Wire unbalanced distribution network model incorporating micro wind energy generation systems (system also incorporating turbulence affected urbanised wind resource)***	• Develop a representative (urban) distribution network model incorporating accurate system parameter representation (including earthing and network cabling) • Analyse the performance of the distribution network model in terms of the configuration and the integration of the urban wind speed model o Network configuration considerations o LV consumer earthing o Power flow techniques o Load/generation integration • Analyse the effects on the distribution network model in terms of turbulence affected urban wind resource
IV	8	***The cost of energy associated with micro wind systems technologies***	• Case study considerations of the associated micro wind energy costs per unit of electricity generated from the perspective of both urban and rural locations • Implementation of Cost of Energy analyses to assess the viability of micro wind systems which can assist in decisions pertaining to suitable feed-in tariff rates for such systems.

1.7 Research Methodology

In order to realise all of the research objectives, a strategy detailing how they – in an applied research context - relate with one another is required. Figure 1.4 provides an overview of how each aspect of the bi-lateral approach works independent of the other while at the same time collectively leading towards the ultimate goal. For each of the main research objectives, a specific methodology is presented in each chapter.

1.7.1 Research Methodology Flow Chart

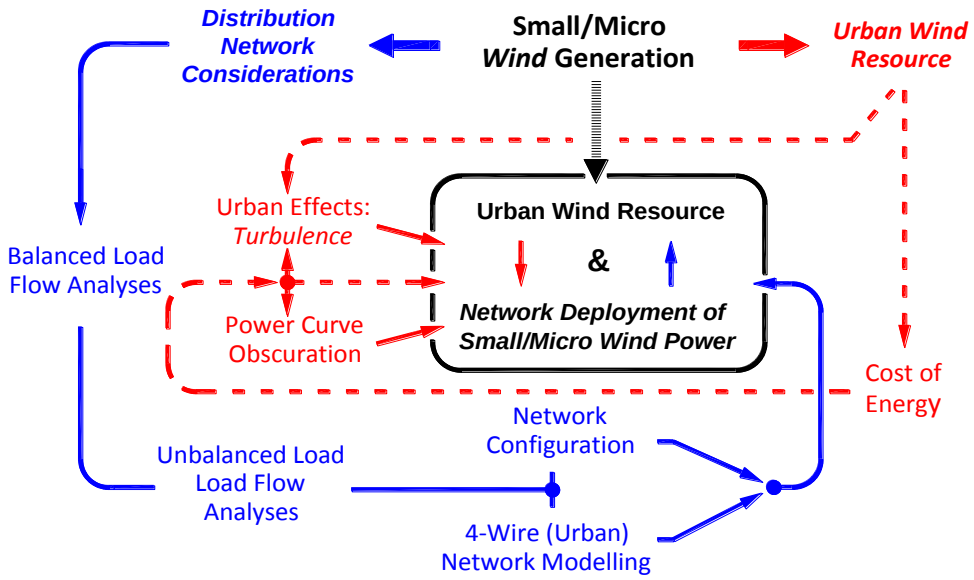

Figure 1.4: Research Methodology Flow Diagram

The flow chart illustrated above presents the overall goal: a model that facilitates accurate representation of how small/micro generation, cognisant of an urban wind regime as it is affected by the underlying surface complexities, impacts the urban distribution network; from both the perspectives of the DNO and the consumers it accommodates. In terms of its constituent, bi-lateral, considerations, the flow chart illustrates the inter-relationship of the research objectives and also how they contribute in the overall context.

1.8 Thesis structure

The thesis is divided into 4 Parts. In Part 1, chapters 2 and 3 outline the rationale for microgeneration from a justification perspective and present a balanced power flow analyses considering how micro wind generation impacts the distribution network generically. Part 2 presents how urban wind is considered using boundary layer theory. Chapters 4 and 5 present how this theory, in conjunction with an understanding of the surface form, is employed to develop a simple model that facilitates the logarithmic extrapolation of wind observations, at rural locations adjacent to cities (primarily Airports), into the urban landscape. This model is developed in Chapter 5 through empirical analyses of wind observations within Dublin city. Observations within the urban canopy from the Weather Information Network of Dublin (WIND) and high resolution wind/speed observations above the urban canopy (Dublin Urban Boundary Layer Experiment, *DUBLex*) are statistically analysed to formulate the effects of the surface roughness on the rural/urban wind resource linkage. Part 3 considers the effects of microgeneration on an accurate representation of a LV urban distribution network. In particular, detailed power flow analyses are presented cognisant of the urban wind resource and consumer load towards a more realistic representation of how small/micro wind generation integrates into distribution networks. Chapter 6 explicitly deals with the main manifestation of urban heterogeneity – namely, turbulence. The impact of turbulence on the productivity of small/micro generation technologies is considered in this chapter with novel models using the industry standard metric for quantifying turbulence, *turbulence intensity* (TI), representing said impact. Chapter 7 details accurate modelling of a 4 wire distribution network and the associated parameters involved including cabling and earthing. Part 4 (Chapter 8) considers the financial implications associated with micro wind generation systems by considering the cost of

energy (COE) per unit of electricity generated from the perspective of both urban and rural locations. This type of analysis is vital for decisions pertaining to suitable feed-in tariff rates for such a system. Finally, Chapter 9 provides conclusions to the work and outlines the limitations of the research as well as pointing towards where the research will be developed further.

1.9 Contributions to Knowledge

The outcomes from this research will facilitate an improved understanding of the technical performance of urban distribution networks with respect to small/micro wind generation based on accurate wind speed references. These can inform policy evaluation towards promoting the uptake of this form of renewable energy. In achieving the research goals and objectives, the following represents the main contributions to knowledge in this regard:

- Development of an empirical urban wind speed model using boundary layer theory that is cognisant of surface roughness through the employment of statistical analysis of a range of wind speed/direction observations
- Development of a novel approach towards the prediction of small/micro wind turbine productivity in turbulent environments (urban) in terms of two modelling algorithms
- Design and implementation of a 4-wire unbalanced distribution network power flow algorithm which is cognisant of system parameters and LV earthing requirements
- International case study consideration and comparisons of the cost of energy per unit of electricity generated from wind generation technologies positioned in both rural and urban locations

Chapter 2: Renewable Energy Sources: The Context for Small/Micro Wind Energy

2.1 Introduction

Moving towards a more renewable energy society is recognised internationally as a priority, with reduced fossil fuel dependency at its core. Such a move is even more important when one considers the fifth report of the *Intergovernmental Panel on Climate Change* (IPCC) [41]. The report concludes that it is extremely likely that human influence has been the dominant cause of the observed global warming since the mid 20th century, representing an increased probability from 90% in its previous report to 95%.

However, the depletion of the globally finite (primary) fossil-energy reserve, inevitably results in increasing energy price volatility and consequentially, this is forcing international economies to react. Some economies are exploring alternative forms of fossil fuels such as those being explored in the US and Japan ([42] and [43] respectively). Alternatively, a green agenda, supported by a green economy needs to become the mainstream for energy supply. It is important to note that irrespective of the development of such fuels, they still contribute negatively to GHG emissions. However and notwithstanding an increased global awareness of the detriments associated with energy production from fossil fuels, with the economic importance of energy supply,

alternatives to standard fossil fuels will be explored meaning that there will be a mix of both approaches going forward with one gaining prominence over the other at various times. Such cyclic variation was experienced in the 1970s and with larger global economies currently prioritising alternative fossil fuels, this cyclic behaviour will be prevalent once again.

From a renewable energy perspective, significant momentum is actively being achieved in an economic "greening" and in 2011 alone, there was a 17% increase in global investment in renewable energy representing $257 billion [44]. This same report outlines how renewable power accounted for 44% of new generation capacity added worldwide, which is up from 34% in 2010, compared to 10.3% back in 2004. The majority of this new capacity comes from larger plant (such as wind farms), but the residential sector's influence should not be neglected. The residential proportion of total electricity consumption accounts for 58.1% [45] and 30.9% [46] in the US and Euro zone respectively. Engagement by small and microgeneration at consumer level - or indeed in green community developments encapsulating domestic consumption - could therefore contribute positively in this regard.

Renewable energy at these capacities also assists in the reduction of Green House Gas (GHG) emissions. According to the *Approximated EU GHG inventory (early estimates)* report for 2011, the residential and commercial sectors contributed most to lower emissions in the EU-27 [47]. Micro/Small generation connections at these levels could therefore assist in sustaining this momentum.

The aim of this chapter is to review the literature pertaining to renewable forms of electrical energy. This review considers the case for smaller scale renewable energy sources and their potential vis-à-vis national and international energy policies. This consideration, therefore, is with regard to international uptake on renewable energy and more specifically, small wind energy, the drivers towards increasing the impact of such renewable energy and the Irish position where wind capacity is being prioritised. If micro (wind) generation is to be a participant in this green agenda, then there must be appreciation of how and where it can fit within the priorities of green policy.

2.2 Renewable Energy – Are There Alternatives?

The exploitation of non-conventional sources of oil and gas has increased significantly. There has been awareness of these non conventional reserves for years but rising prices for conventional crude oil coupled with advances in extraction technologies have only recently combined to justify their economic extraction. This is particularly the case in the United States where large scale exploitation of shale gas has revolutionised the gas market and now shale oil exploitation (of which the US has huge reserves) may do the same for oil [48], potentially making the USA independent of energy imports. The Organization of the Petroleum Exporting Countries (OPEC) had to cut its forecast of demand for its oil for 2013, citing growing production from U.S. shale deposits [42]. If these scaled-back forecasts prove correct, OPEC could be on track to have its lowest share of the global oil market for more than 10 years [42]. OPEC's move comes as industry experts increasingly question whether the producers' group, which has had a decisive influence on the oil market since the 1970s, can maintain its position amid a boom in U.S. oil production resulting from shale- rock drilling technology [48].

Outside of the US, shale gas and oil exploitation has not taken off to the same extent; partly due to uncertainty over reserves, partly due to environmental and regulatory concerns. In the US, these significant developments have happened so quickly that it is hard to get solid data to see what is going on and a lot of the evidence is anecdotal. Table 2.1 presents a perspective on the World Energy Council's Survey of Energy Resources 2010 using 2008 data (latest set of statistics), with Figure 2.1 providing a comparison of the global percentage associated with each fuel type.

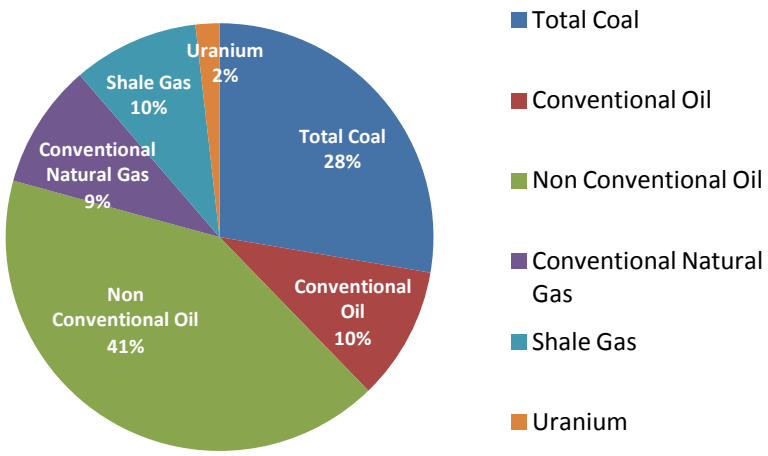

Figure 2.1 Provable Fossil Fuel Reserves
(Total Reserves at 7.5×10^{22} Joules in terms of Annual Production: 5.2×10^{20} Joules) [source: Extracted from [49], provided by [48]]

Looking at the reserve to production ratios in Table 2.1 (how many years it would take to exhaust known reserves at current rates of production), a simple extrapolation suggests that there are only decades remaining before exhausting conventional reserves of crude oils and natural gas (41.33 and 54.51 years respectively).

Table 2.1 Primary Energy 'Reserves to Production' Ratio [source: Extracted from [49], provided by [48]]

Resource	Units	Proved Recoverable Reserves (end of 2008)	2008 Annual Production	Reserves to Production Ratio	Energy Conversion Factor (to Joules)	Energy Reserves	Energy Production
Total Coal		860938	6739	127.8	2.4136×10^{16}	2.078×10^{22}	1.6266×10^{20}
Conventional Oil	Million Barrels	1238834	29974	41.33	6.119×10^{15}	7.5804×10^{21}	1.8341×10^{20}
Non-conventional Oil		5094934	2361	2157.7	6.119×10^{15}	3.1176×10^{22}	1.4449×10^{19}
Conventional Natural Gas	Billion (m^2)	185544	4304	54.51	3.8139×10^{16}	7.0765×10^{21}	1.2982×10^{20}
Shale Gas	Billion (m^3)	187514			3.8139×10^{16}	7.1516×10^{21}	
Uranium	ktonnes	2302	43.9	52.46	5.94×10^{17}	1.359×10^{21}	2.5907×10^{19}
TOTALS						7.5123×10^{22}	5.1624×10^{20}

From Table 2.1, it is apparent that known reserves of non-conventional oil (Shale, Bitumen and Heavy Oil) already dwarf known reserves of crude while known reserves of Shale Gas are comparable to known reserves of conventional gas. Shale gas is already being commercially exploited in the United States and has grown in a few short years to become more than 50% of their gas supply. By 2030, the U.S. is likely to import only 1% of its energy needs, compared to 30% in 2005 [50]. This comes as major emerging economies such as China and India are likely to be more reliant on energy imports. The development of non-conventional sources has revolutionised the gas market in the US.

On an even more speculative note some countries (notably China and Japan) are looking at another source of methane called Methane Hydrate which is methane trapped in a lattice of water and ice. This is found deep underground or under the ocean but the reserves are potentially enormous [43, 51].

From Table 2.1 it is clear that time is limited before conventional reserves of oil and gas is exhausted. It is also apparent, however, that there are substantial non-conventional

reserves which are more costly to extract and may also require technological advancements to develop. From an environmental perspective, these "bridge fuels" that can power nations during the transition from oil, coal and other alternatives, could be "a bridge from the coal-fired past to the coal-fired future" [43].

However, as conventional reserves deplete and associated prices rise, it is inconceivable to think that global economies will not endeavour to put off the inevitable by exploiting more and more non-conventional reserves. This should stabilise energy prices for a few years (at a higher level though because they are more expensive to extract). But these are still fossil fuels. The danger is that the focus on non-conventional sources will divert investment away from renewable energy technologies. This is in some ways a repeat of the situation in the 1970's oil crises which caused significant research and development in renewable energy. Subsequently oil markets settled down and the 1980's and 90's gave the world two decades of cheap oil and the removal of the drivers for the development of renewable energy.

The main point from this discussion is that these fossil fuels are essentially not 'game changers', but at best offer an interlude before a resumption of 'tightening-in' of the supply of fossil fuels. Or as suggested in the SEAI Embedded Sustainability report concerning the business case for small wind energy [52], the windfall derived from these alternative fossil fuels may be deployed to aid but not delay the transition to greater provisions of renewable energy forms. Indeed, these non-conventional fossil fuels will essentially defeat efforts to control GHG emissions.

2.3 Renewable Energy: An International Perspective

The *Renewables 2012: Global Status Report* [20], presented a very positive picture for 'sustainable' renewable energy development across the world. This report highlighted a number of key statistics, which are summarised below:

- Renewable Energy sources supplied 16.7% of global final energy consumption in 2010. This success is greatly facilitated by the power sector (nearly half of the 208GW additional electric capacity added in 2011 coming from renewable, with wind contributing 30%)
- In the EU, renewables account for 71% of total electric capacity additions, which brings the renewable share of total electricity capacity to 31.1% (contributing 19.8% towards total electricity consumption)
- Contrasting the European position, the US renewable energy sector made up nearly 39% of electrical capacity additions in 2011, contributing to the 11.8% TPEP coming from renewable forms of energy. China on the other hand by the end of 2011, was the country with the most renewable power capacity. Over the course of 2011 one third of the 90GW new electricity capacity came from renewable electrical power.

From a European perspective, there are a number of key European Legislative obligations as a result of the Kyoto Protocol which set legally binding targets for each signatory nation to limit its green house gas emissions to 8% above the 1990 baseline level. Ireland's obligation in this regard is to limit GHG to 13% above the 1990 baseline level. Looking forward from the commitments defined in the Kyoto protocol, at the United Nations Climate Change Conference (2012), the conference reified the 2011 Durban Platform, extending the scope of the Protocol to be developed by 2015 and implemented by 2020. Under guidelines agreed at the conference, richer nations could be financially responsible to other nations for their failure to reduce carbon emissions [53]. The European Environment Agency's *Greenhouse gas emission trends and projections* in its most recent report suggest that almost all European countries are on

track towards their Kyoto targets. Based on calculations from the *United Nations Framework Convention on Climate Change* (UNFCCC) Secretariat, Quantified Emission Limitation or Reduction Commitments (QELRCs) will lead to reduction by 2020 in the range of 25%-40% compared to 1990 levels [54]. Table 2.2 in this regard summarises the base line position (in terms of tonnes per CO2 equivalent and targets under burden sharing agreement) against the 2020 targets [54]. These obligations will influence the first world to further develop and embrace cleaner and more efficient energy.

Table 2.2 EU 15 Member baseline and 2020 targets (source: extracted from [54])

	Kyoto Protocol			Effort Sharing Decision Target (2020)	
	Base-year level of total national emissions as determined by the intial review (tonnes per CO_2 – equivalent)	Target under Burden Sharing Agreement (% of base year)	Individual target	(% non-ETS emissions 2005)	Participating in EU ETS
EU-15	***4265.5***		***-8.0%***		***x***
Austria	79.0	-13.0%		-16%	x
Belgium	145.7	-7.5%		-15%	x
Denmark	69.3	-21.0%		-20%	x
Finlan	71.0	0.0%		-16%	x
France	563.9	0.0%		-14%	x
Germany	1232.4	-21.0%		-14%	x
Greece	107.0	25.0%		-4%	x
Ireland	**55.6**	**13.0%**		**-20%**	**x**
Italy	516.9	-6.5%		-13%	x
Luxembourg	13.2	-28.0%		-20%	x
Netherlands	213.0	-6.0%		-16%	x
Portugal	60.1	27.0%		1%	x
Spain	289.8	15.0%		-10%	x
Seden	72.2	4.0%		-17%	x
UK	776.3	-12.5%		-16%	x

In 2009, the *Energy & Climate Package* (20-20-20) set ambitious energy and climate targets of 20% emissions reduction, 20% increase of renewable energy and 20% increase in energy efficiency by 2020. Under 406/2009/EC, EU member states are further committed to collectively reduce emissions of greenhouse gases by 30% by 2020 compared to 1990. From a RES-E perspective, 2009/28/EC established a common framework for the use of renewable energy within the European Union including a mandatory requirement for each nation to provide a *National Renewable Energy Action Plan* (NREAP). These plans set out how each member state plans to achieve its targets. Figure 2.2 illustrates the targets for each member states in terms of a 2005 baseline.

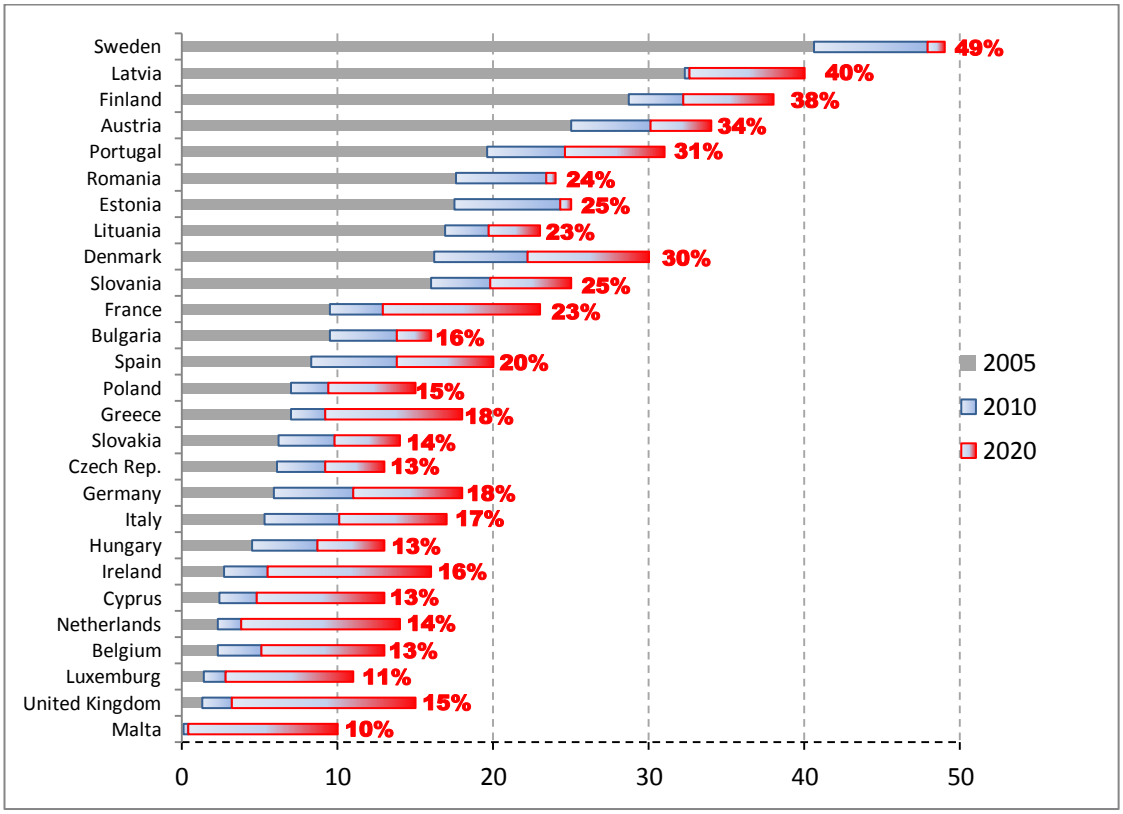

Figure 2.2 EU Renewable Shares of Final Energy, 2005 and 2010, with Targets for 2020 (Extracted from [55])

This legislation appears to be making some impact. According to the 2011 European Renewable Energy Council report [55], 25 out of the EU-27 countries expect to reach or

exceed their 2020 targets domestically and the share of renewable energy sources in electricity consumption is predicted (in terms of the NREAPs of the respective member states) to be 34.3%.

2.3.1 Global Wind Energy

There has been significant growth in the global wind power industry since 1996. The global wind capacity has grown from 6.1GW to 238GW [20] and since 2006, there has been 321.6% growth in capacity, representing an annual (average) growth of 26%. Wind power is also the most widely applied renewable energy with the EU representing 23% of the global market and accounting for 41% of total global capacity [20]. During 2011, and more than any other renewable technology, an estimated 40 GW of wind power capacity was put into operation increasing global wind capacity by 20% to approximately 238 GW, with China, the United States, India, Germany and the UK accounting for the majority of installations [20]. From a European perspective, the European Wind Energy Association further assert the positivity towards wind energy and point out that in 2012 a further 11.895GW of wind power was installed in the EU [56]. This actually suggests that the EU is lagging 1.5% behind its 27 National renewable energy action plan forecasts, but onshore capacity is 3% ahead of the EWEA forecast [56].

As illustrated in Figure 2.3, Ireland has one of the greatest wind energy resources in Europe [57], but this potential has yet to be translated into energy extraction. In terms of the EU 15, Figure 2.4, which summarises European installed wind capacity in terms of percentage contribution of wind energy towards electricity consumption (based on 2012 statistics), shows Ireland in 11th place with respect to wind capacity.

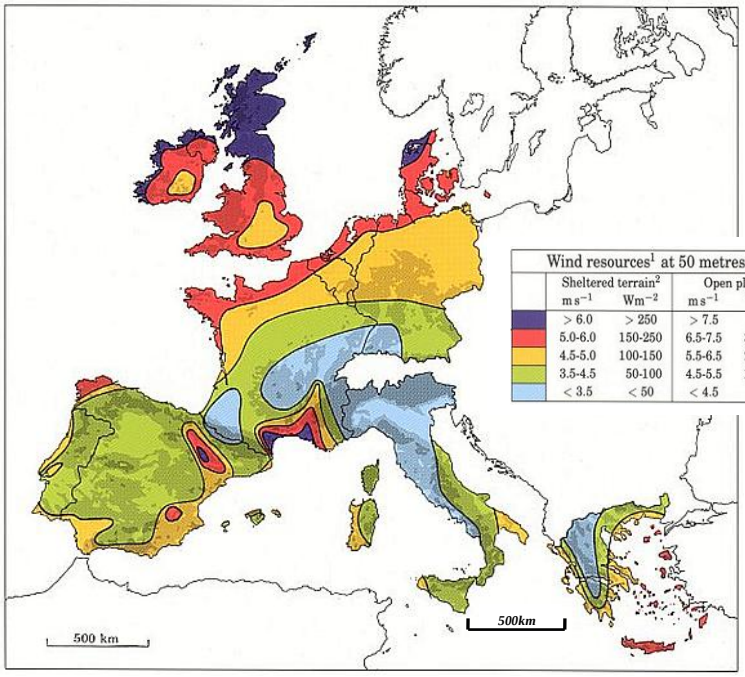

Wind resources[1] at 50 metres above ground level for five different topographic conditions

	Sheltered terrain[2]		Open plain[3]		At a sea coast[4]		Open sea[5]		Hills and ridges[6]	
	$m\,s^{-1}$	Wm^{-2}	$m\,s^{-1}$	Wm^{-2}	$m\,s^{-1}$	Wm^{-2}	$m\,s^{-1}$	Wm^{-2}	$m\,s^{-1}$	Wm^{-2}
	> 6.0	> 250	> 7.5	> 500	> 8.5	> 700	> 9.0	> 800	> 11.5	> 1800
	5.0-6.0	150-250	6.5-7.5	300-500	7.0-8.5	400-700	8.0-9.0	600-800	10.0-11.5	1200-1800
	4.5-5.0	100-150	5.5-6.5	200-300	6.0-7.0	250-400	7.0-8.0	400-600	8.5-10.0	700-1200
	3.5-4.5	50-100	4.5-5.5	100-200	5.0-6.0	150-250	5.5-7.0	200-400	7.0- 8.5	400- 700
	< 3.5	< 50	< 4.5	< 100	< 5.0	< 150	< 5.5	< 200	< 7.0	< 400

Figure 2.3 European Wind Resource at 50m (Extracted from [57])

Figure 2.4 further illustrates that Germany and Spain had by far the largest installed capacities in Europe (EU 15) with 33.3GW and 22.8GW capacities respectively. This is compared to the remaining leaders, the UK, Italy, France, Portugal and Denmark, which collectively had 32.8GW with capacities ranging from 4.2-8.5GW. That said, the significance that wind energy plays in Ireland is quite evident in Figure 2.4, where it is seen to account for 13% of total electricity consumption. Ireland ranks fourth in the EU15 in this regard.

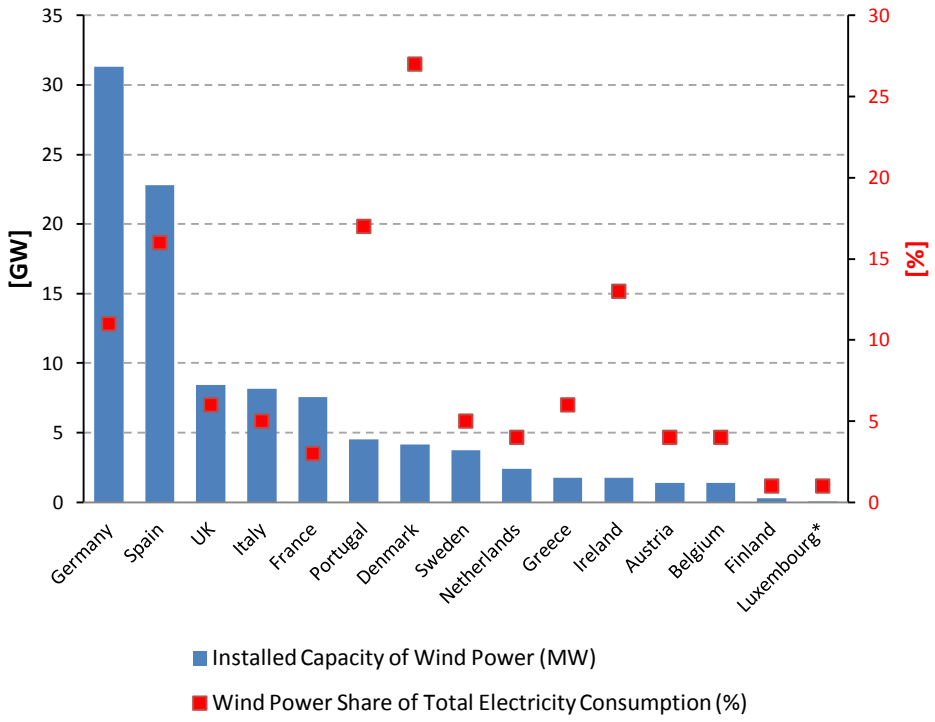

Figure 2.4: International Wind Capacity & % contribution to electrical consumption [source: interpreted from [56]]

2.3.2 Energy in Ireland

The Irish Government has set a target of 40% of national electricity to be generated through renewable energy by 2020 (the highest target in the EU for variable renewable electricity within a single electricity system [58]) and this will account for 16% of all energy consumed. It is envisaged that wind energy will play a significant role in achieving these goals and indeed in the Government's strategy for renewable energy (2012-2020) [59], the first key strategy is to facilitate more renewable electricity from onshore and offshore wind power for the domestic and export markets.

The contribution of renewable energy to overall energy demand in Ireland reached 6.5% in 2011 with a share of electricity generated from renewable energy sources being 17.6% (bearing in mind the target under the EU RES-E Directive being a 16% renewable energy penetration by 2020)[60]). Ireland remains however, very dependent

on energy imports. Even though renewable energy use actually increased by 395.3% from 1990 to 2011, fossil fuels – the majority of which are imported – are still the dominant form of primary energy [61]. In 2011, fossil fuels accounted for 94% of all energy used in Ireland and energy imports accounted for 88% of requirements [61]. This dependency ultimately leads to uncertainty and risk with regard to energy price volatility and Ireland faces significant challenges in this regard. Irish dependency on foreign energy imports with limited indigenous fuel resources, with the propensity to oil and then gas as primary energy supply sources (representing 49% and 30% respectively [61]), renders national security of energy supply a significant concern. Compounded with this dependency, Ireland's geographical location on the periphery of Europe - as well as the scale of the Irish market - further contributes to Ireland's vulnerability to supply disruption and economic volatility. The primary fuel mix for Ireland with specific regard for electricity generation is illustrated in Figure 2.5.

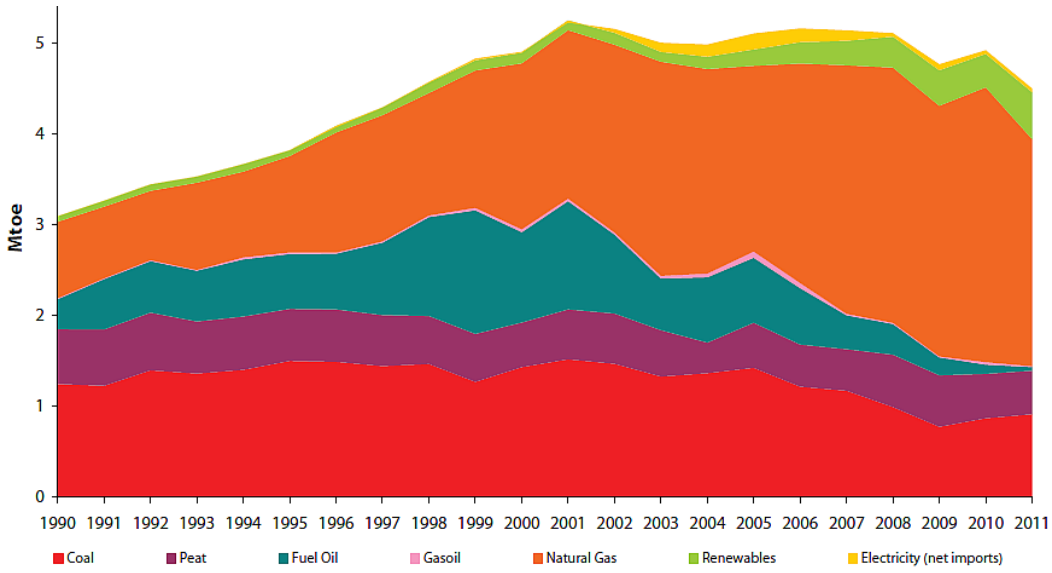

Figure 2.5 Primary fuel mix for electricity generation in Ireland 1990-2011 [61]

Of specific importance, Figure 2.5 illustrates that the primary fuel requirement for electricity generation grew by almost 69% from 1990 to 2011. It is further evident from Figure 2.5 that gas is the dominant fuel type and in 2011 it accounted for 55.5% of

(gross) generated electricity [61]. The fuel inputs to electricity generation were 33% of the total primary energy requirement in 2011 with electricity consumption as a share of total final consumption increasing from 14% to 19% between 1990 and 2011. Notwithstanding the increased demand for electricity experienced over this period of time, the impact of the economic recession is also evident in the sudden dip in energy demand evident from 2010 to 2011.

At the Distribution Network level and with respect to key statistics provided by the Distribution Network Operator (DNO), ESBN [62], there is year-on-year increase in the number of connections (and associated percentage of total demand) in relation to urban domestic consumers. This is mirrored by a reduction in rural domestic demand/number of connections (Figure 2.6). This supports the hypothesis that with increasing urban migration by the Irish population and the associated increasing demand being expected of suppliers, opportunities are being created for more distributed generation within urban environments.

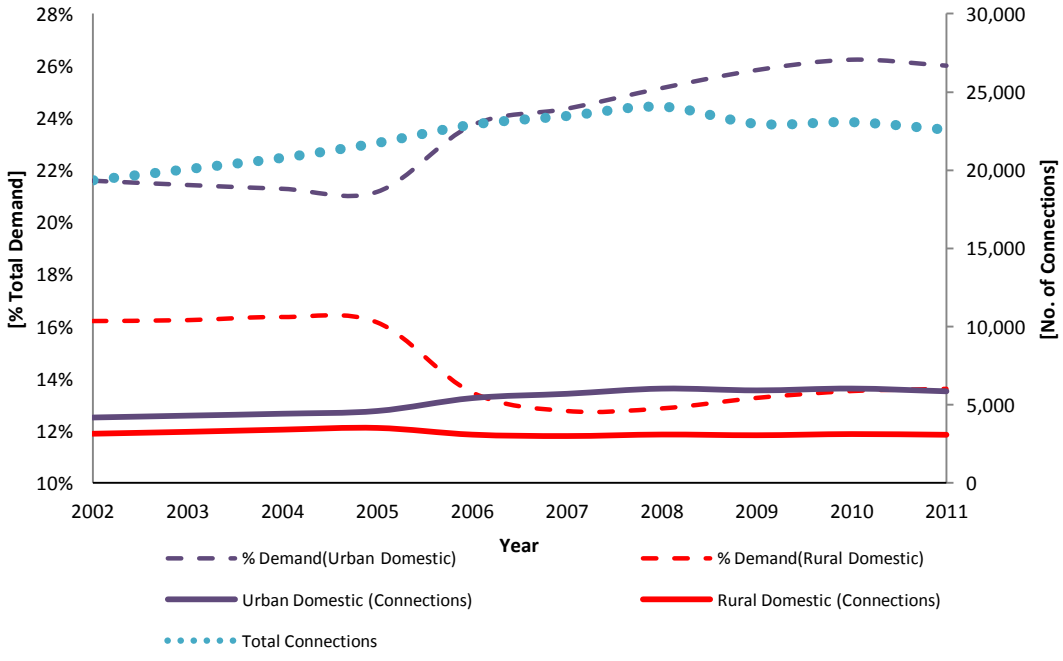

Figure 2.6 Number of urban/rural domestic (grid) connections with respect to demand [source: extracted from [62]]

Specific policy issues related to Ireland were identified in the Energy White Paper in 2007 [63], with the key energy policy being grouped under the three pillars of sustainable energy development; namely, security of energy supply, sustainability of energy supply and competitiveness of energy supply.

Cost of Energy is also a significant issue in Ireland. Domestic electricity prices have remained higher in comparison to other EU countries and countries with similar markets. In the January – June (2012) Euro household electricity charge comparison [64], for the two consumption bands with the largest share (DC and DD[1], which represent 80% of consumption) the price differential for Ireland stood at between 6% and 15% above their EU counterparts. The capacity for Ireland to deliver energy at a competitive cost is a critical consideration for both end consumers and for the nation itself if it is to attract foreign investment. Sustaining a favourable environment for all sectors of Irish industry to compete in export and domestic markets is *key* in this regard.

The development of renewable energy is a fundamental strategy in Ireland's sustainable energy objectives. The main Irish energy policy issues identified in the White Paper [63] include security of energy supply, competitiveness of energy supply, and sustainability of energy supply can all be addressed through significant grid contribution from renewable energy sources. As renewable energy in Ireland is facilitated through indigenous energy sources, an increased focus on these sources of energy – in a diversified context - could contribute to energy security. With increasing energy prices and market volatility, renewable energy can contribute to the cost competitiveness of the energy supply by reducing dependence on imported fossil fuels. With minimum

[1] Band DC (2,500 kWh < Consumption < 5,000 kWh); Band DD (5,000 kWh < Consumption < 15,000 kWh);

emissions compared to fossil fuel energy sources, renewable energy can further contribute to reducing GHG emissions and assist towards the decarbonisation of the Irish energy supply. Also, in order to fulfil objectives and address policy requirements detailed in the Energy White Paper 2007, EU Directives 2009/28/EC and the associated national climate change strategy in terms of the NREAP, the expansion of renewable energy becomes even more important.

The main renewable energy resource in Ireland is wind, with Ireland being one of the windiest countries in Europe. Wind energy accounted for over 13% of all electricity generation in 2011 [56, 65] and the grid connected and (operational) installed wind capacity on the island of Ireland as on the 11th of April 2012, was 2054.86MW [66]. However, it is estimated that Ireland will need a total installed wind capacity of between 3,500 and 4,000 MW by 2020 to meet its 40% renewables target [67]. Wind energy therefore presents an opportunity for further expansion in the development of micro/small-electricity via wind generation, something echoed in the World Wind Energy Association in its Small Wind World Report [68].

2.4 Small/Micro Wind Generation

The IEC define small wind energy in terms of rotor swept area and the current standard (IEC 61400-2) suggests rated power of 50kW. The discrepancy of the upper capacity limit of small wind ranges being between 15 and 100kW for 5 of the largest small wind countries [68]. The WWEA 2012 small wind report cites such confusion being prevalent in the UK, where the national wind energy association, Renewable UK and its MCS certification body all differ with respect to defining small wind. In Ireland microgeneration is defined by EN50438 [69] as generation at a maximum of 25A/phase (5.75kW$_e$) when the distribution network connection to the distribution network is at

single-phase and 16A/phase when the connection is three-phase ($11kW_e$). Micro wind energy systems are therefore limited to these specifications. In contrast, microgeneration in the UK is defined as generation connected to the Distribution Network having a capacity below 50kWe (UK Energy Act, 2004).

Globally, the use of small-scale wind turbines (SWT) (<100kW) is increasing; driven by the need for electricity in rural environments, the availability of lower-cost grid-connected inverters and the provision of Government incentives [70]. 'Small' wind was originally defined by its characteristics to produce a small amount of electricity for household appliances or to cover various household-based electricity demands. Depending on location, domestic consumption could warrant a 10kW turbine (USA) or a turbine with 1kW capacity (China) [68]. The capacity of these technologies is currently defined by IEC 61400-2 as having a rotor swept area of less than 200 m^2, equating to a rated power of up to 50 kW (approx.) [68] but there are different definitions used by different counties, ranging between 15 and 100kW [68, 71]. The World Wind Energy Association, in its 2012 Small Wind Report (which uses 100kW as a temporary reference for the upper capacity level) stated that there are more than 650,000 units representing 382GWh in annual energy production worldwide [68]. This contribution is in the context of the total existing wind power capacity which is an estimated 2-3% of global electricity consumption (year end, 2011) [20]. Figure 2.7 summarises the context of small capacity wind turbine with respect to the global number of installations and associated capacity. China has far more units installed than any other country, while the United States has a slight lead in capacity; the U.K., Germany, Canada, Spain, and Poland are also playing an increasing role in this market [20, 68].

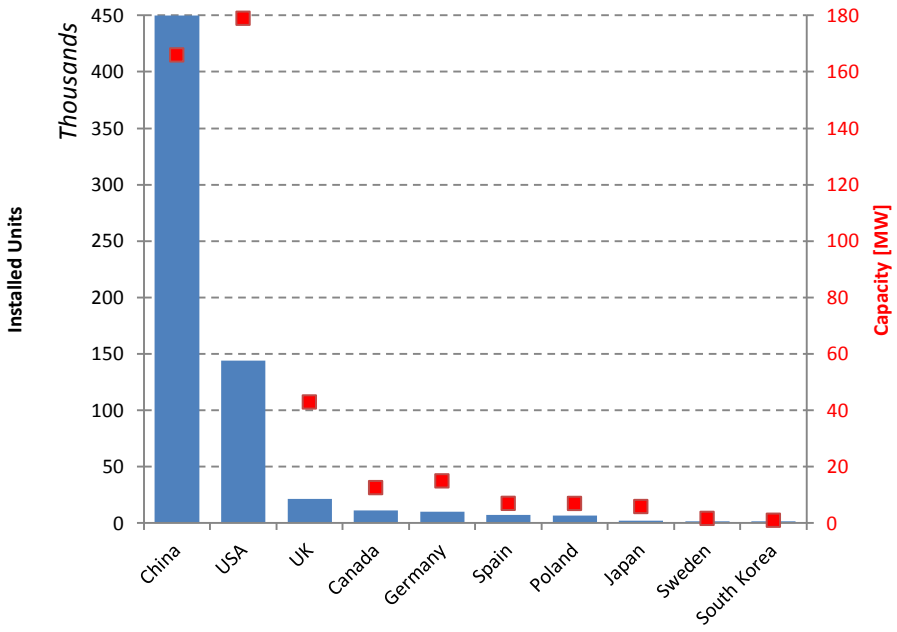

Figure 2.7 Small Wind Generation: Number of Installations and Associated Capacity (Extracted from [20, 68])

The blades of a wind turbine harness the kinetic energy in the wind and typically transfer this energy to a three-phase synchronous generator, which generates a form of A.C. (variable frequency and voltage – both of which are proportional to the blade rpm). A controller subsequently converts this variable A.C into variable D.C., which is still proportional to the blades rpm. This D.C. is eventually fed into a grid-tied inverter which synchronises to the network voltage/frequency to provide a proportional amount of power based on the supplied D.C. voltage. There are three types of wind turbine classification: horizontal axis (HAWT), vertical axis (VAWT) and building augmented wind turbines (BAWT), with the HAWT and VAWT being the most popular.

Mechanical power realisation in a wind turbine is manifested through either a drag-driven rotor or through a lift driven rotor or effectively through a combination of both [72]. A lift-driven wind turbine can be a horizontal axis wind turbine (Figure 2.8(a)) or

a vertical axis turbine (Figure 2.8(b)). Drag-driven turbines (Figure 2.8(c)) on the other hand are conventionally vertical axis turbines.

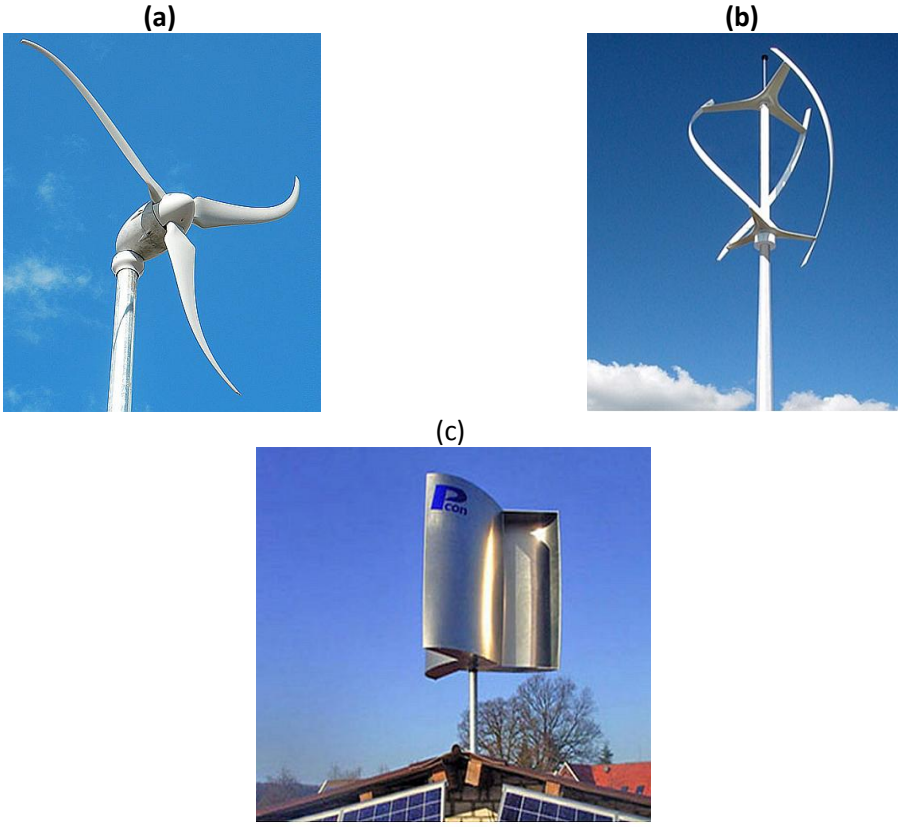

Figure 2.8 Lift-driven wind turbines ((a) and (b)) and a drag driven wind turbine (c)

Drag-based designs work on the principle that the turbine blade is dragged around by the force of the wind. In this regard, the maximum velocity for the blades of this turbine will be the same as the wind speed, or in other words, the tip speed ratio of these turbines is ≤1. The tip speed ratio (λ) is the ratio of the velocity of the tip of the turbine blade to the wind velocity. A tip speed ratio, λ, above 1 means some amount of lift, while λ below 1 means mostly drag. Lift based designs can usually output much more power, more efficiently. As Mertens explains [72], the rotor concept is an important factor in determining the efficiency of the energy conversion. This efficiency or power coefficient is defined as

$$C_p = \frac{P_{Mech}}{1/2\,\rho_{air}.A_{rotor}.u_0^{\,3}} \tag{2.1}$$

where P_{Mech}, is the mechanical power the rotor axis, A_{rotor} is the swept area of the rotor, $1/2\,\rho_{air}.A_{rotor}.u_0^{\,3}$ is the power of the incoming free stream wind per square metre rotor area, ρ_{air} is the density of the air and u_0 is the free stream wind speed. The non-dimensional power coefficient represents the fraction of the power in the wind that can be extracted by the rotor. The maximum performance of drag-driven wind turbines is ca12%, whereas for wind turbines based on the principle of lift is much greater; theoretically up to 59% due to the relatively high lift-to-drag ratio [72, 73].

The performance coefficient, C_p, of the turbine defines how much wind power is captured and turned into mechanical power to subsequently generate electricity. It defines the turbine's performance against varying wind speeds. For a given wind rotor, C_p depends on the pitch angle of the blades and on the tip speed ratio (λ) defined as:

$$\lambda = \frac{\omega.R}{u_0} \tag{2.2}$$

where ω (rads/s) is the rotational speed of the rotor, R (m) is the radius of the rotor blades and u_0 is the free stream velocity (m/s).

The maximum achievable power coefficient is determined by the Betz limit, 59.26%. In practice however, obtainable values of the power coefficient up to 40-45% are achievable for lift-driven turbines [74]. The difference between the achievable and the Betz limit is caused by the finite number of blades, the rotation in the wake and tip losses. Figure 2.9 depicts the Betz, ideal constant, and actual wind turbine power

coefficient as a function of λ, the tip speed ratio [74]. The figure illustrates that maximum power extraction occurs at the optimal tip-speed ratio where the difference between actual λ (blue curve) and the line defined by a constant λ is at a lowest. This difference represents the power in the wind that is not captured by the wind turbine. Frictional losses, finite wing size, and turbine design losses account for part of the un-captured wind power, and are supplemented by the fact that a wind turbine does not operate at the optimal TSR across its operating range of wind speeds [74]. A related concern associated with λ, is that if the wind speed is highly variable. The nature of the C_p/λ curve emphasises that optimal power extraction is only achieved at one value of lambda and hence if the wind speed is variable, optimal performance can only be achieved with a variable speed turbine a lower overall power coefficient will be realised.

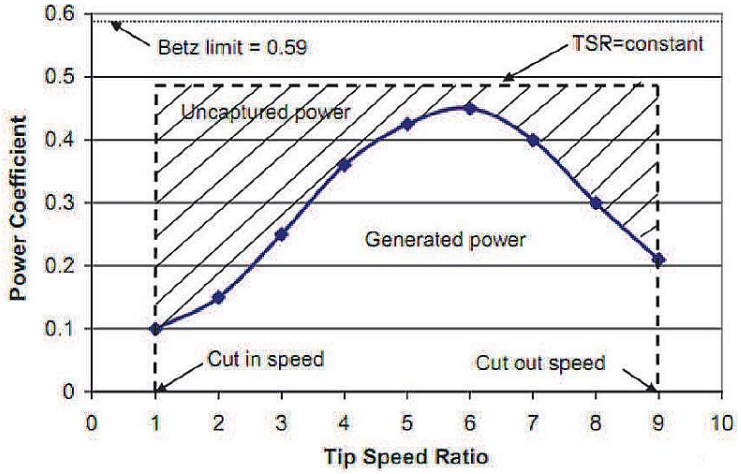

Figure 2.9 Power coefficient (C_p) as a function of tip speed ratio (λ) for a two-bladed rotor [74]

A further issue for wind turbines, particularly in the context of urban environments, is the turbines cut-in speed. Lift-type wind turbines have a relatively high cut-in wind speed. For example, the *Darrius* VAWT lift-driven turbine is not self starting [72] and requires auxiliary means to get up to generating speed, Whereas drag-driven turbines

have lower cut-in wind speeds making them more suitable for low wind speed environments, but they also have lower power coefficients.

The *Wind Energy Integration in the Urban Environment* (WINEUR) project (2005-2007) looked to identify the conditions that are needed to establish the integration of small wind turbines. As part of this project, 32 manufacturers (representing 57 wind turbine models, 65% HAWT and 35% VAWT) were surveyed. Table 2.3 identifies the recognised advantages and disadvantages of the three main designs of small wind turbines [75].

Table 2.3 Advantages and disadvantage of HAWTs, VAWTs and drag VAWTs [75]

	HAWTs	***Lift VAWTs***	***Drag VAWTs***
Advantages	1. Efficient 2. Proven product 3. Widely used 4. Most economic 5. Many products available 6. High cut-in wind speeds (relative to VAWT)	1. Wind direction immaterial 2. Less sensitive to turbulence than a HAWT 3. Create fewer vibrations 4. High cut-in wind speeds	1. Proven product globally 2. Silent 3. Reliable & robust 4. Wind direction immaterial 5. Can benefit from turbulent flows – less sensitive than HAWT 6. Create fewer vibrations 7. Low cut-in wind speeds
Disadvantages	1. Does not cope well with frequently changing wind direction 2. Does not cope well with buffeting	1. Not yet proven 2. More sensitive to turbulence than drag VAWT	3. Not efficient 4. Comparatively uneconomic

The HAWT is the most frequently used type of micro wind turbine and whilst being geometrically simple with aerodynamically complex operating regimes , the technology has a well-developed design offering the greatest performance at present [21]. The technology is well disposed to rural settings [17, 76, 77], or more importantly, in open areas free from shading and influence from adjacent structures. Indeed, the capacity factor (measured energy output as a percentage of the theoretical maximum rated output

of a turbine) increases significantly when a turbine is located in an open field with trees and buildings 10m away from the turbine (10.4% compared to 4% - 6.4% for roof-top turbines in the UK and USA respectively) [77]. International research prioritises the wind energy resource in 'rural' locations [32-34] and in this regard, the majority of literature suggests rural deployment of small/micro wind generation as being optimal [16, 78].

There are a number of issues with urban deployment of micro wind technologies. These issues include noise, visual impact, animal (bat) strike and also the impact of a profusion of turbines being deployed in one area [16]. These, along with the complex/diminished wind characteristics and associated difficulties in determining with accuracy the yield expected from a particular turbine at a particular location, present significant challenges to a micro wind turbine market [16]. The location of these technologies, in relation to adjacent buildings or other *shading* objects, as well as optimal hub-height positions, considerably affects performance. Indeed, Bahaj and Myers [76] acknowledge that in any analysis of device payback period, the key parameter in ensuring success of the technology. Bahaj and Myers further conclude that it is mainly the wind resource that will dictate turbine energy yields and the associated increase in wind speed with height above ground level can improve financial and carbon payback times. But if a renewable solution to increasing energy demand is to be achieved, energy conversion systems where populations are concentrated must be considered. In the UK for instance, micro wind turbines are recognised as an emerging technology driven by advances in design, increasing energy prices and the financial incentives offered to aid their uptake in buildings [76]. This focus must however be

based on achievable performance indicators, which means an understanding of the 'raw material' or primary energy utilised and not for '*greenwashing*' purposes [79].

Another issue for renewable technologies in general is their ability to directly replace the existing electric energy grid technologies; the latter are too established to abandon and the former not sufficiently developed to meet energy demands [80]. A sensible approach is to gradually infuse renewable energy sources into existing systems and transform said systems over time [80]. Such transformation could be expedited through smart grid evolution as they offer an upgraded electricity network enabling two-way information and power exchange between suppliers and consumers [81].

A challenge for the future smart grids will be in the control over how renewable energy sources are connected to the grid. If such distributed sources are not sufficiently controlled, the grid can become unstable and even fail [80]. In the smart grid, energy from diverse sources is combined to serve customer needs minimising the impact on the environment and maximising sustainability [82]. Such aspirations will support not only centralised large scale power plants and residential-scale, dispersed distributed energy sources. In this context, 'distribution producers' (including small wind) are not marginal players but highly influential and integral parts of the energy web and thereby increase the reliance of the grid in the face of widespread disturbance [82].

The Irish approach to smart grid development [58] is one encompassing smart networks, operations, generation and pricing. Microgeneration (including micro wind energy) is recognised as a core consideration in this vision. Such a vision will enable more renewable energy to be connected to the electricity system, helping to secure Ireland's

energy supply and reducing our carbon intensity [83]. In particular, as DeBlasio comments [83] from a smart grid perspective, small scale renewables' modularity offers benefits that central-station power plants and long-distance transmission alone cannot deliver because power is generated when and where it is needed. That said, as discussed by Gaviano *et al* in their discussion on the challenges faced by Wind and PV systems [84], in order for distributed/fragmented wind energy systems to enhance the smart grid of the future, standardised communication and certified products are required. A standardised communication protocol is vital to ensure security, safety and reliability in a diversified future grid infrastructure [84].

Table 2.4 provides a technical comparison of a sample of commercially available micro wind turbines available on the market. These three HAWT technologies are initially considered in the distribution network analyses (section 3.5.2), but primarily in an electrical context. The primary considerations in this regard are cut-in wind speed (u_{cut-in}), and rated wind speed (u_{rated}). Between these two boundary speeds, the respective turbine characteristics are modelled on the basis of the cubic fraction of the observed wind speed (u_i) and rated wind speed (u_{rated}), in terms of rated power ($P_{Wind\,Turbine}$), i.e., $(u_i/u_{rated})^3 \times P_{Wind\,Turbine}$. This desk-top survey illustrates the range of performances associated with these technologies. Figure 2.10 (a) illustrates the power characteristics for the three technologies in terms of this cubic relationship. Also included is a more representative power characteristic of the *Skystream 3.7* turbine. This power curve was acquired from HOMER^{TM} (Hybrid Optimisation Model for Electric Renewables (version 2.81) as developed by the US National Renewable Energy Laboratory (NREL) [85] and is indicative of a standard manufacturer's power curve. This more detailed representation of the performance of the Skystream 3.7 is employed in turbulence

modelling in Chapter 6 and subsequently employed in the analysis of how a distribution network might react with increasing wind generation engagement in Chapter 7.

Table 2.4 Sample of micro wind turbines available on the (Irish) market

Model	Diameter (m^2)	Swept Area (m^2)	u_{cut-in} (ms^{-1})	u_{rated} (ms^{-1})	$P_{u-rated}$ (W)
Skystream 3.7 [86]	3.8	11.38	3.5	13	2400
Whisper 200 [87]	2.7	5.73	3.0	11..6	1000
Proven 2.5 [88]	3.7	10.75	2.5	11	2500

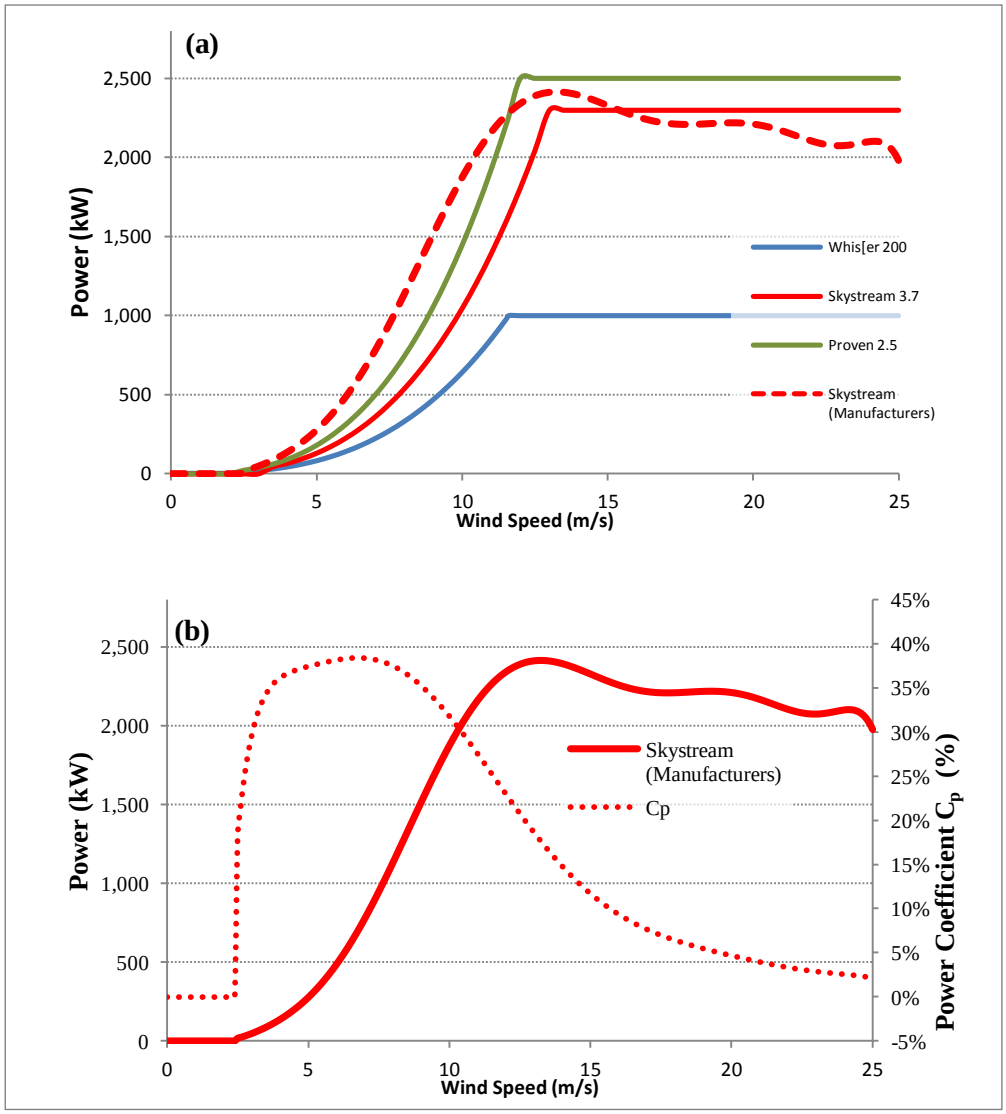

Figure 2.10 (a) Power curve comparison between the three primary technologies considered in this research; (b) Power coefficient (system efficiency) variation with wind speed

2.4.1 Micro Wind Energy and the wind resource in the urban environment

The flow of power conversion in a wind turbine system is illustrated in Figure 2.11 (in consideration of a HAWT) .

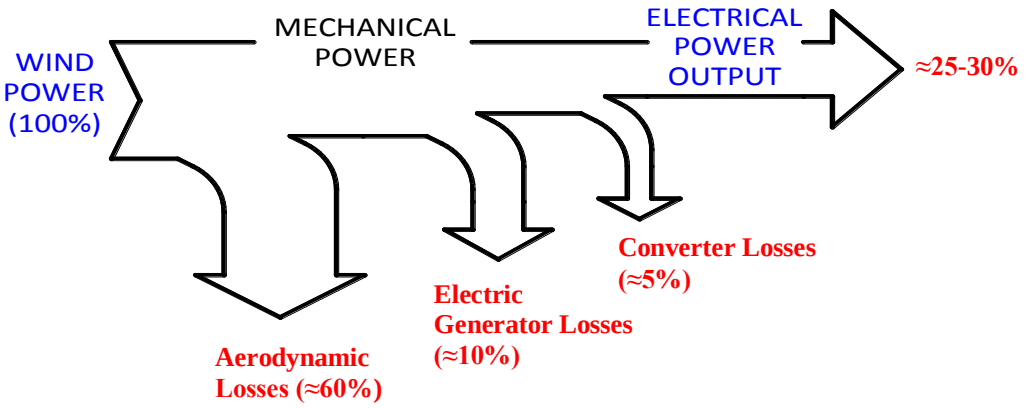

Figure 2.11 Flow of Power Conversion in a Horizontal Axis (Lift-driven) Wind Turbine System

Figure 2.11 represents the individual efficiencies of a wind rotor, generator and convertor. Most of commercially available wind turbines have overall efficiencies typically around 30% [89]. For instance, Figure 2.10 (b) (for the HOMER Skystream characteristic) illustrates the efficiency for the Skystream 3.7 in terms of the parameters provided in Table 2.4. The Power Coefficient/Tip Speed Ratio (C_p-λ) relationship for a typical wind turbine, as suggested Muljadi *et al* is around 42% [90]. On this basis, aerodynamic losses could be considered to be 58%. Typical generator efficiency is around 90% [91] so typical generator losses are in the order of 10%. Finally, with regard to the converter losses, Glass and Levermore in their analysis of micro wind turbine performance [92], observed the effect of converter efficiencies on the overall performance of the turbines that were considered. In particular, they observed how efficiency in this regard is more arduously affected at lower wind speeds. In general however, such converters are high efficiency devices so it is reasonable to attribute a loss in the order of 5% in this regard.

The *Building Research Establishment* (BRE) in its assessment of micro-wind turbines in urban environments [93] acknowledges the difficulties pertaining to wind assessment in urban environments. The study highlights that payback periods associated with micro wind turbine systems are highly sensitive to relatively small changes in parameters including:

- Local wind conditions
- The size of conurbation and the position within the urban terrain
- The type of building on which the turbine is mounted
- The proximity of surrounding buildings

Other than the BRE study, there have been some other field trials around the UK. The *Encraft Warwick Wind Trials Project* [30] covered 168,950 hours of operation of 26 building mounted wind turbines from five manufacturers across the UK during 2007-2008. These turbines were mounted on sites ranging from theoretically poor (single storey urban buildings) through to theoretically excellent (45m tall exposed flats in isolated settings on hilltops). This project's primary objective was to investigate how grid connected micro-wind turbines perform on a variety of building types in urban environments. It was also envisaged that the data collected could provide a helpful guide to potential purchasers, manufacturers and installers. This survey prioritised building mounted turbines and not freestanding wind of any size mounted on poles or masts well away from obstructions.

A summary of the results is as follows:

- The average energy generated per turbine per day across the sample set has been 214Wh (including times when turbines were switched off for maintenance or due to failures).

  - This is equivalent to an average of 78 kWh of energy produced per site per year and an average capacity factor of 0.85%[2].
  - If the results are adjusted to exclude data from periods when turbines were switched off or broken the average energy generated per turbine per day rises to 628 Wh (230kWh per year equivalent) and an average capacity factor of 4.15%.
- The best performing turbine in the trial generated an average of 2.382 kWh per day when in operation, equivalent to 869 kWh in a full year.
- The poorest site generated an average of 41Wh per day when in operation or 15 kWh per year, which is less than the energy it consumed to run the turbine's electronics. Energy consumption averages 80Wh per day per turbine (29kWh per year) which is significant on some sites.

The overall conclusion from the trial was that the microgeneration industry and technologies are still at development stage and are only likely to make a tangible contribution to energy and carbon saving in the most exposed sites and tallest buildings.

Another study that monitored the output from actual installations was the *Energy Saving Trust* (EST) field trial of household wind turbines [94], but it presented a somewhat opposing view to the *Warwick Wind Tri*als. The EST trials concluded that micro wind turbines do work but only when installed properly in appropriate locations. The EST trials further suggested that in the UK, there is potential for nearly 2 million tonnes of CO_2 savings from a potential of up to 3,500GWh electricity per annum from domestic small-scale wind turbines. The report did emphasise however, that wind speeds are difficult to predict and highly variable. Indeed, EST recommended that potential customers first utilise the best available wind speed estimation tools and then, where appropriate, install anemometry to determine the wind speed distribution(s). James *et al* [17] subsequently investigated the implications of this wind trial. Their analysis

[2] This compares to typical capacity factors of between 10% and 30% for larger turbines on free standing sites in good areas

highlighted, in particular, the inconsistencies with respect to site selection and indeed, how sites were selected to include as wide a range of manufacturers and wind regimes as possible. This could be interpreted that the trial had a lack of focus with respect to proper installations and locations that were cognisant of the available resource. Their analysis further pointed to the inconsistencies between manufacturers in terms of how "they chose to rate their turbines".

These relatively high profile field studies in illustrating that wind turbines (currently) installed in urban areas produce less energy raise doubts about their potential, both in the context of financial benefits to owners and with regard to decarbonising the energy sector [95].

2.5 Microgeneration in Ireland

From an Irish perspective, microgeneration integration into the distribution network is at an early stage of development. When one looks holistically, however, at Irish policy towards renewable technologies against its European commitments as contained in the RES Directive [96], there have been achievements. According to the Sustainability Authority of Ireland [60] report, the target of 13.2% RES-E by 2010 was exceeded (14.8%). This should however, be considered in context with the *aspirational* 40% target as set in the Strategy for Renewable Energy 2012-2020 [59].

Microgeneration technologies are identified in Irish legislation as options for alternative energy supply. The recently published Building Regulations (Part L Amendment) [97] stipulates that in new dwellings, "a reasonable proportion of the energy consumption to meet the energy performance of a dwelling is provided by renewable energy sources". However, in reality, microgeneration uptake has been relatively poor.

Micro generation systems in Ireland are regulated and since 2008 and in 2009, the Department of Communication Energy and Natural announced a payment scheme €0.19 for spill energy 'exported' onto the grid i.e. the excess energy than the demand of the installation. Since April of 2012 however, this scheme has been indefinitely suspended. As this scheme was based on two components, the first €0.09 being the price advocated by the regulator (CER) and the remaining €0.10 being a subsidy from *ESB Customer Supply* (now *Electric Ireland*). Currently, for every kWh exported to the (Irish) distribution network (defined as microgeneration capacity), a price of €0.09 is offered Even with a technical and fiscal infrastructure, microgeneration uptake to date has been relatively poor. Table 2.5 shows the total metered micro generation capacity in Ireland at the end of 2011[3] [98].

Table 2.5 Total Installed capacity of microgeneration technology (year end, 2011)

December 2012	kW Installed Capacity (kW)	*% increase on 2010*	Market Share by Capacity	*% increase on 2010*	No. of Inst.	*% increase on 2010*	Market Share by Installation	*% increase on 2010*
Micro CHP	7.00	*133.33%*	0.24%	*0.00%*	7	*66.67%*	1.13%	*38.57%*
Micro Hydro	38.65	*85.82%*	1.31%	*30.00%*	8	*75.00%*	1.29%	*35.00%*
Solar PV	291.83	*141.62%*	9.92%	*19.35%*	114	*41.82%*	18.39%	*14.96%*
Micro Wind	2602.85	*43.16%*	88.52%	*-1.77%*	491	*19.89%*	79.19%	*-3.02%*
TOTAL(S)	**2940.3kW**				**620 installations**			

There is nearly 3MW of micro generation grid connected, representing an increase of 49.8% capacity compared to 2010 (1962.73kW [99]), but there is long way to go before the sector can make an impact on renewable energy targets. A breakdown of the scale of microgeneration connections is provided in Figure 2.12, which illustrates

[3] This table being indicative of data from the microgeneration scheme and does not consider commercial installations outside of this scheme. (https://www.electricireland.ie/ei/residential/price-plans/micro-generation-scheme.jsp)

microgeneration technology connections in terms of capacity share and associated number of connections.

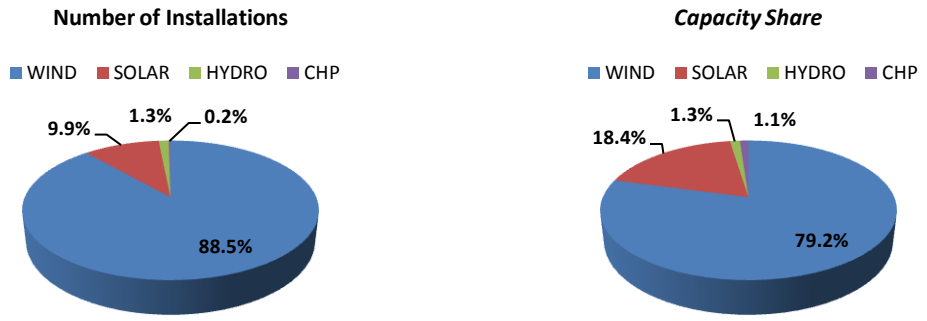

Figure 2.12 Irish Microgeneration connection and capacity statistics [98]

Wind generation is the most embraced microgeneration technology in Ireland with 79.2% of the 620 connections. The wind turbines involved have installed capacities ranging from 500W up to 17kW, although under the micro generation connection [69] criteria, only technologies with ratings up to 6kW are considered as micro generation. Figure 2.13 illustrates the range of micro wind turbine capacities connected to the Distribution Network [98].

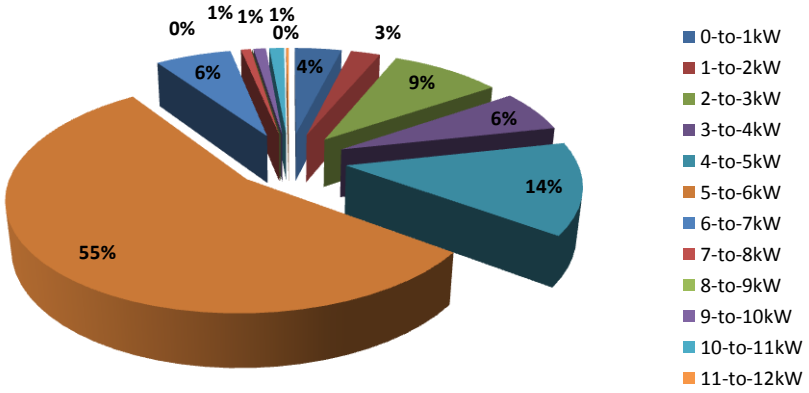

Figure 2.13 Breakdown of (small/micro) wind turbine installations by capacity

Figure 2.14 illustrates the cumulative energy outputs from solar PV and micro wind generation from Q1, 2009 until year end 2011 [98]. From Figure 2.14, the largest proportion of the Irish microgeneration capacity is through wind energy, with 6kW being the average rating of the technolgies.

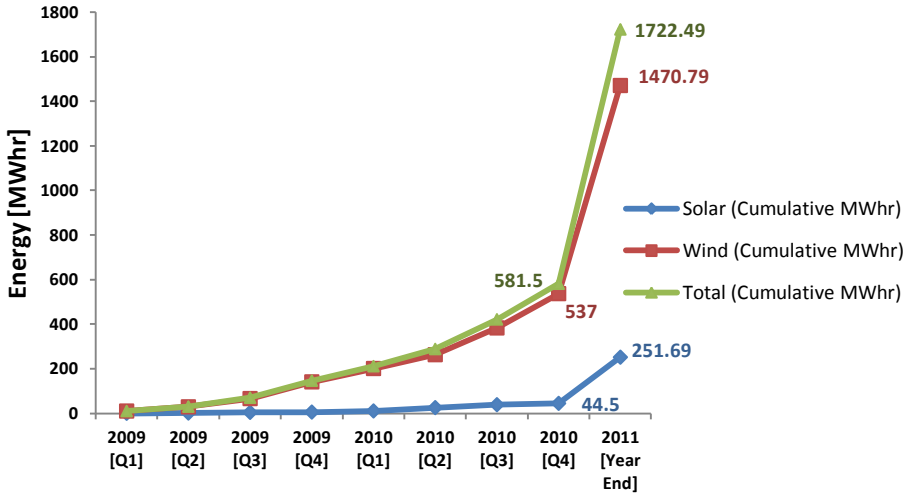

Figure 2.14 Cumulative Energy Exported by Microgeneration Technologies (2009 – 2011)

2.5.1 Microgeneration Regulatory Framework: Drivers/Inhibitors

In the context of increased efficiencies in the built environment, the Directive on Energy Performance of Buildings (Recast) has defined that minimum requirements pertaining to the energy performance of new and existing buildings are afforded and that "*alternative energy supply systems should be considered for new buildings, regardless of their size, pursuant to the principle of first ensuring that energy needs for heating and cooling are reduced to cost- optimal levels*" [100]. Micro generation technologies are identified as options for the alternative energy supply systems in this context, with building regulations – particularly for 'new builds' providing a focus for alternative green options [101]. According to the National Renewable Energy Action Plan (NREAP) [102], the introduction of a robust framework for the development of a

vibrant Micro generation sector is an important component of building societal acceptance of energy infrastructure and ownership of the national renewable energy targets. Indeed the NREAP acknowledges that microgeneration has the potential to create employment and enable participation by a wide section of the community.

It must be pointed out though, that while this is encouraging, it falls short of the UK NREAP (again for 2020), which proposes that 2% of national electricity demand will come from small-scale sources [103]. Since April 2010, 160.96 MWe of low carbon electricity generation has registered under the scheme (representing 44,460 installations) in the UK [3]. Table 2.6 illustrates the installed generation capacity in terms of the technologies considered under the scheme. Micro wind generation represents 14.2 % of this capacity (1,490 installations). A Comprehensive Review of the Feed-in Tariffs (FITs) scheme in the UK was undertaken lately and published in July, 2012 [104]. The tariff from December 2012 for all forms of (small) wind energy installations less than 100 kW is €0.263/kWh [23].

Table 2.6 Total Installed Capacity of Micro generation (UK, 30th June, 2011) [25]

	MW Installed Capacity (MWe)	Market Share by Capacity (%)	No. of Installations	Market Share by Installation (%)
Anaerobic Digestion	4.99	3.10%	5	0.01%
Micro CHP	0.16	0.10%	157	0.35%
Micro Hydro	12.75	7.92%	218	0.49%
Solar PV	120.16	74.65%	42590	95.79%
Micro Wind	22.90	14.23%	1490	3.35%
TOTAL	**160.96 MWe**		**44460 Installations**	

There are essentially two ways to think of the benefits derived from micro generation. There are the environmental considerations and an ability to derive financial benefits. Allen *et al* [105] in their energy analysis and life cycle assessment of an installed

micro-wind turbine for domestic (residential) electricity generation found that the micro wind turbine considered could have positive environmental effect in all but the poorest wind conditions. Their analysis considered the environmental performance of the turbine was assessed by assuming that each unit of electricity generated displaces (avoids the use of) a unit of grid electricity. The metric they employed in this regard was the *Energy Gain Ratio* (EGR), or the amount of energy developed by the turbine over its life time as a factor life cycle primary energy input. They found for a given primary energy investment, the electricity delivered by the turbine is an order of magnitude larger than for fossil or nuclear-based generation technologies and when the electricity generated by the turbine is valued as the quantity of primary energy that is displaced from the current grid, the gain ratios are increased significantly further [105].

An important component of the energy requirements of a wind turbine is the energy embodied in their manufacture, construction, installation, maintenance, and parts replacement. Embodied energy has been shown to account for a significant proportion of the life cycle energy requirements for particular products [106]. However, as concluded by Allen *et al*, this impact is not considered to be significant on a global scale and it has positive impacts if used in an open or rural environment, or if the maximum output is achieved in an urban environment [105].

From a financial perspective, the most important parameters in evaluating the economic viability of micro wind turbine systems are the initial cost and the value of potential energy generated. These parameters depend on the average wind speed, turbine type, size, mechanical design and the ability to optimise the generation output. The price per kW installed will vary per country, but a conservative estimate would be $3000-$5000/kW [107], though manufacturers estimate that once mass production starts, this

figure may drop to ≈1,500 $/kW. The actual value of 1 kWh of electricity produced by the turbine depends on the load profile, electricity tariff and whether a feed-in-tariff is applied. Chapter 8 presents analyses in this regard towards establishing the *levelised cost of energy* (LCOE) for small/micro wind energy systems.

2.6 Summary

This chapter reviewed the literature relating to renewable energy, focusing on an increasing international energy portfolio divergence towards non-fossil electricity generation and the opportunities for small/micro wind energy systems. Wind energy, as the most widely applied renewable energy, is globally considered the best option to serve this transition [20]. While there is global appreciation of the merits of such a green economy, alternative fuels such as shale gas/oil and potentially Methane Hydrate, may present an antagonistic position in the future [43, 50, 51]. Notwithstanding the immediate benefits that these fossil fuels present, the fact remains however, these are still fossil fuels and are not a sustainable energy resource and at best they offer a delay [52] to the inevitable time when all forms of fossil fuels are depleted.

The renewable energy context in Europe is underpinned by European regulatory statutes with said legislation imposing strict obligations on European states. Each state is obliged to outline national energy strategy in the form of NREAP. These policies are making a significant impact with 25 of the 27 EU members expecting to exceed their 2020 targets [55]. Indeed, Ireland with its own ambitious (and self-imposed) target of achieving 40% electricity generation from renewable resources, is currently ahead of the EU RES-E Directive for 2020 by over 1.5%.

Ireland with its reliance on energy imports and its geographically marginal position has even more to gain from increased embracement of renewable energy. These 'weaknesses' were addressed in the 2007 Energy White Paper where security of energy supply, competitiveness of energy supply, and sustainability of energy supply as the primary energy concerns could be addressed by significant grid contribution from renewable energy sources. The main renewable energy form in Ireland actually comes from the wind, with Ireland being one of the windiest countries in Europe. Wind energy accounted for over 13% of all electricity generation in 2011 [56, 65]. Indeed, a report compiled by Erigrid in junction with SONI (the Irish and northern Irish TSO respectively), suggest that wind energy needs to increase by 100% in order to meet its 40% renewable energy target [67]. Wind energy therefore presents an opportunity for further expansion in the development of micro/small-electricity via wind generation, something echoed in the World Wind Energy Association in its Small Wind World Report [68].

Small wind energy systems can contribute towards this wind energy deficit. Globally, the use of small-scale wind turbines (SWT) (<100kW) is increasing, with an estimated 650,000 units providing an estimated 382GWh in annual energy production worldwide [68]. This contribution is in the context of the total existing wind power capacity which is an estimated 2-3% of global electricity consumption (year end, 2011) [20].

However, deployment of small/micro wind energy systems where they are required most as alternative sources of energy in the load centres defined by population, have yet to make a meaningful impact. UK studies investigating performance of these technologies have suggested that urban environments present insurmountable

difficulties as media to capture the wind energy [30]. That said, there are studies [94] that suggest that with emphasis on understanding the wind resource, they could be a viable green option – even in urban environments.

Chapter 3: Technical Considerations & Distribution Network Integration of Micro/Small (Electricity) Generation Systems

3.1 Introduction

This Chapter reviews the technical implications associated with small/microgeneration for the electrical distribution network. The focus is on the associated effects, particularly with respect to network voltage concerns that arise from increased microgeneration capacity proliferation. Analysis in this area suggests that there is scope for considerable participation of these technologies in distribution networks. As these networks become 'smarter', the context of small scale embedded generation (SSEG) will become increasingly relevant particularly with regard to the discussions in Chapter 2.

The technical limitations are subsequently tested using a representative (Irish) Distribution Network model [108, 109]. Detailed description of the component parts of the network are provided as well as detail pertaining to how the model that was developed in MATLAB^{TM}. The associated analysis is presented in the context of a two stage process. *Stage 1* involves the genesis of the network including the ability to incorporate fixed levels of load and generation; *Stage 2* investigates the model's performance in terms of variable load and generation as derived from a variable wind resource. Power flow analyses are performed on the basis of DISTFLOW as this

algorithm offers an optimal and computationally efficient method for distribution networks with respect to the specific characteristics of predominantly radial networks with high R/X ratios.

3.2 Microgeneration Characteristics

Holistically, microgeneration can be thought of in terms of heat generation, electricity generation and combined heat and power. Heat generation incorporates solar water heating, ground source heat pumps, air source heat pumps, biomass stoves and boilers (e.g. wood and energy crops e.g. willow). Electricity generation is facilitated through solar photovoltaic (PV) systems, micro-wind turbines and micro-hydro systems (in hilly areas or river valleys). Micro CHP provides heat and electricity together. While one of the most notable features of renewable forms of energy is the diversity of technologies and resources [110], from a domestic prospective, Figure 3.1 illustrates the main forms of microgeneration as domestic electricity producers.

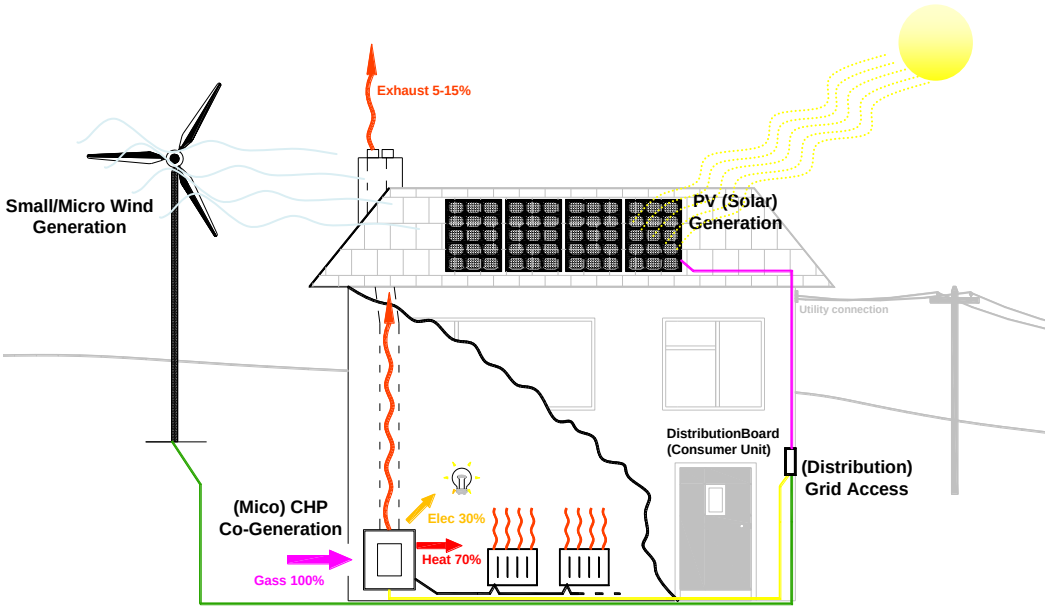

Figure 3.1 Examples of Microgeneration Technologies (Domestic Context)

Micro generation, in the context of distributed generation (DG) connected to the electrical (distribution) network, is not a universally defined concept. Microgeneration in the UK is defined as generation connected to the Distribution Network having a capacity below 50kWe (as per the UK Energy Act, 2004 and further supported in the Climate Change and Sustainable Energy Act 2006). Indeed, in the UK, microgeneration is often referred to as small scale embedded generation (SSEG) and is defined by *Ofgem*, the Energy Regulator in the UK as "... a source of electrical energy rated up to and including 16A per phase, single or multiphase, 230/400V a.c.". In Ireland microgeneration is defined as per EN50438 [69] as generation at a maximum of 25A/phase (5.75kW$_e$) when the distribution network connection is at single-phase and 16A/phase when the connection is three-phase (11kW$_e$). There is however, no universally accepted definition for microgeneration (internationally) as the application of these technologies is dependent not only on national policy but also on the arrangements and technical requirements of Distribution Network Operators (DNOs) within respective countries. There is also the difficulty in the decisions surrounding when generators can operate on or off-grid. The common theme associated with all microgeneration is that no central dispatch is employed controlling output.

The DNO governs the connection protocol(s) and in the majority of European countries (including Ireland), these protocols are implemented through EN50438 [69]. A block diagram description of how these technologies connect in parallel with the distribution network (in Ireland) is illustrated in Figure 3.2.

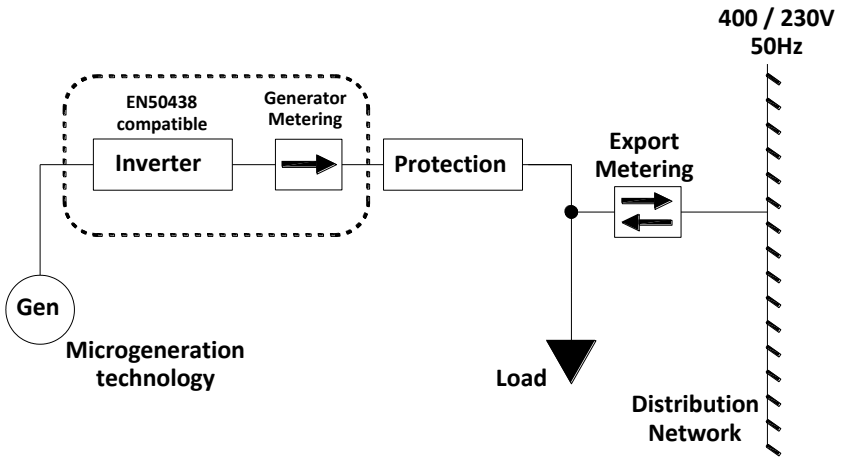

Figure 3.2 Block Diagram of Grid Tie logistics for Microgeneration Technologies

The technical constraints for parallel connection of these technologies to the distribution network are prescribed by this standard and Table 3.1 outlines the interface protection for all microgeneration technologies.

Table 3.1 Interface Protection Requirement (EN50438)

Parameter	**Trip setting**	**Clearance time**
Over voltage	230V +10%	0.5sec
Under voltage	230V -10%	0.5sec
Over frequency	50Hz +1%	0.5sec
Under frequency	50Hz -4%	0.5sec
All explicit Loss of Mains (LOM) functionality must be included (e.g. Change of frequency, Vector Shift or Source Impedance (through purely passive means) Measurement. ***Note:*** *any implementation which involves the injection of pulses on to the (Distribution Service Operator(DSO) network shall not be permitted*		
ROCOF (where used)	0.4Hz/sec	0.5sec
Vector shift (where used)	6 degrees	0.5sec

In Ireland, the Energy Regulator (Commission for Energy Regulation, CER) defines the regulatory logistics involved in the connection of microgeneration to the grid as an

"inform, consent and fit" process [111]. Owners must inform the DNO[4] of any planned installation and follow the formal application process as prescribed by CER.

Figure 3.3 outlines a particular concern that both the Regulator and DNO have with respect to connecting microgeneration in parallel with the Distribution Network. *Islanding*, or autonomous operation of the microgeneration technology on a disconnected network, is something that could lead to significant safety implications. The diagram (extracted from [112]), illustrates how in the event of a network fault, without anti-islanding (loss of mains (LOM) protection), the fault can be exasperated through contribution from the embedded microgeneration. This contribution could even be such that the network customer cut-out device does not operate, thereby presenting a health & safety concern for network technical personnel

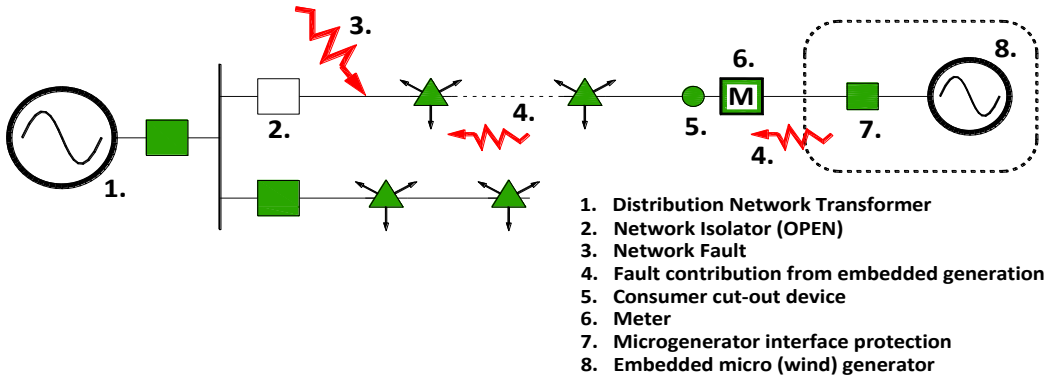

Figure 3.3 Distribution Network in terms of a Network fault and islanding (interpreted from [112])

Installing micro wind turbines in Ireland is subject to planning considerations but some exemptions were introduced by the Department of Environment, Heritage and local Government in January 2007 [113]. These exemptions are on condition that:

- The turbine must not be fixed to a building/house
- The total height of the turbine cannot exceed 13 metres.

[4] The Irish DSO is ESB Networks (http://www.esb.ie/esbnetworks/en/home/index.jsp)

- The rotor diameter shall cannot exceed 6 metres.
- The minimum clearance between the lower tip of the rotor and ground level shall not be less than 3 metres.
- The supporting tower shall be a distance of not less than the total structure height (including the blade of the turbine at the highest point of its arc) plus one metre from any party boundary.
- Noise levels must not exceed 43db(A) during normal operation, or in excess of 5db(A) above the background noise, from the perspective of nearest neighbouring inhabited dwelling.
- In domestic installations, there can not be more than one turbine instalations

Building mounted wind turbines are not exempted from planning and therefore full planning permission for such installations is required.

3.2.1 Distribution Networks & Microgeneration Connection: General Technical Constraints

In any examination of microgeneration, two factors need to be clearly understood. Firstly, electricity networks were originally designed with relatively few centralised power stations providing the electrical energy through high voltage (HV), medium voltage (MV) and low voltage (LV) networks to supply the (total) electrical load demand. In this generation/transmission/distribution paradigm, the electricity is generated in large generation plants, usually located in non-populated areas and geographically remote from load centres so as to avail of the economics of size and avoid environmental issues. The electricity is transported through transformers, transmission line systems and other transmission equipment, with the distribution voltage level(s) affording connection to the consumption or load centres. These uni-directional original networks were never designed for bi-directional flows of electrical energy. Secondly, in the context of such networks, the technical connection of appreciable amounts of embedded generation has consequences (technical/socio-economic) as a whole and for all users connected to it at all voltage levels.

With increases in technology efficiencies and changes in environmental policies, as well as an associated expansion of the finance and electrical markets, the modern distribution network paradigm is one that promotes new conditions in the sector of electricity supply. Figure 3.4 contextualises this paradigm shift towards more distributed generation participation as a consequence of an increasing prevalence of smaller capacity plant in conjunction with an increasing use of renewable sources.

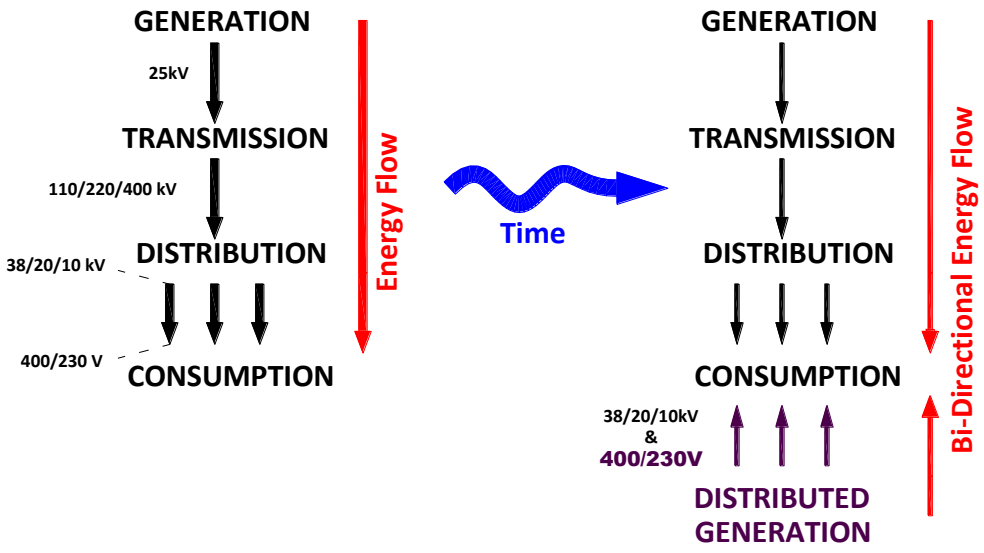

Figure 3.4 Transitioning from a central energy systems paradigm to one that includes increased penetration of distributed generation at consumption connections

Thomson in his discussion on microgeneration [114], suggests that as the quantity of grid-connected distributed generation (DG) increases, the associated affects on the system will be become more appreciable and may even push upwards through the distribution/transmission infrastructure from the LV into the MV networks and even into the HV networks. Such logic could apply with microgeneration – but would require a massive adaptation of these technologies. DG may impact on a distribution system and associated equipment significantly in terms of steady-state operation, reliability, power quality, stability and safety and affect both suppliers and customers alike [115,

116]. The impact may be positive or negative and depends on the distribution network itself and the characteristics of the connected DG and load. According to Van Gerwent [117] and Bloem [118], some typical technical implications of increased DG include:

- High voltage profiles along the network (as depicted in Figure 3.5), which depending on the ratio between produced/consumed power could result in network voltage tolerances being breached
- Extenuation of voltage transients with the connection/disconnection of generation
- Increased short-circuit potential
- Variable losses as a function of the production and load levels
- Network congestion issues
- Power quality (PQ) issues - as well as reliability may be affected.
- Prevalence of *Islanding* where SSEG/microgeneration in autonomous operation could present health and safety concerns on disconnected networks
- Network protection issues; utility protection and DG protection measures must be co-ordinated.

Vu Van *et al* [116] also observed that with many DG technologies being connected to the grid via power converters (rectifier/inverter systems), there will be an increased prevalence of harmonic current/voltage distortion manifestations.

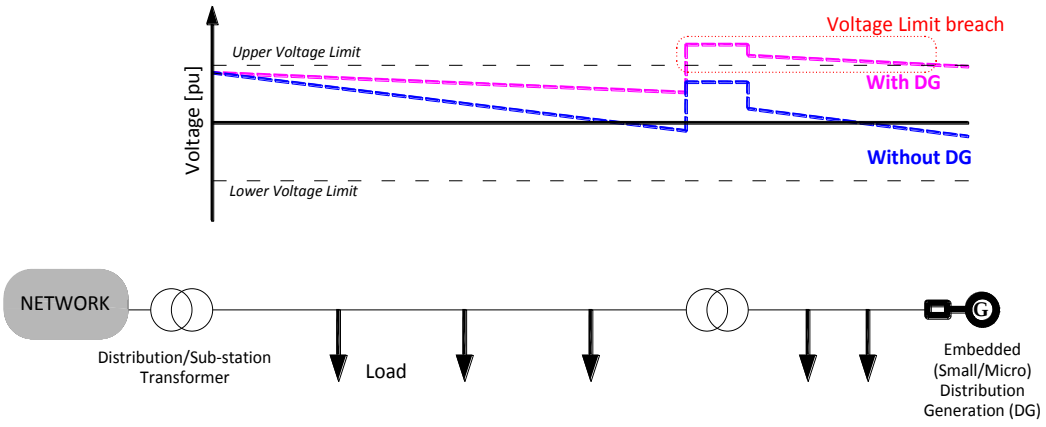

Figure 3.5 Voltage rise along a Distribution Network – with DG (modified from [118])

However, as suggested by Barker and de Mello in their consideration of the impact of DG on power systems [115], positive manifestations (or as they put them – 'system support benefits') resulting from increased DG include:

- Voltage support and improved power quality
- Loss reduction
- Transmission and distribution capacity release
- Deferment of Transmission/Distribution network infrastructural development
- Improvement in utility system reliability

Vu Van *et al* [116], also cite the potential for carbon savings through renewable DG as a benefit of increased DG.

Infield [18], discusses how the UK Government recognises a significant potential for microgeneration as a viable alternative to large scale renewables. As observed by Peacock *et al* [16], the UK have a comprehensive approach towards micro renewable energy and the industry is expanding with institutional support and UK legislation and the number of installations nationally (at 44,460 installed in 2012) support this [25]. For instance, the UK Government's Low Carbon Buildings Programme provided grants over the period of 2006-2011 to householders to purchase micro wind turbines for domestic applications. The modern evolution from the Low Carbon Buildings programme is the '*Green Deal*', facilitated by the Energy Saving Trust. This initiative supports the installation of 'green' technologies on the basis of viability assessment - without the burden of upfront costs. Instead, the costs are paid through the associated energy bill over a period of time [119]. The Energy Saving Trust further estimate that micro generation could meet 30-40 % of UK electricity demand in the UK by 2050 [120]. According to the UK Department of Energy and Climate Change (DECC), by

2020, the Feed-in Tariff (FiT) scheme currently available since April 2010 could support over 750,000 small-scale, low carbon electricity installations and save 7 million tonnes of carbon dioxide [25]. A further example of the progressive nature of the UK micro generation embracement is the *Micro generation Government-Industry Contact Group*, which provides a single point of contact with Government to discuss and tackle the non-financial barriers facing mass deployment of micro generation [121]. Technically, the microgeneration sector in the UK is underpinned by the *Microgeneration Certification Scheme* (MCS)[122].

In a report commissioned by the Energy Savings Trust [123], the Department of Trade and Industry, through *Element Energy*, found that microgeneration could also deliver significant efficiency and CO_2 benefits. The same report however, also points to the fact that for microgeneration to have a significant impact on the UK electricity system and its markets, units would need to be installed by consumers in their millions. Infield [18] considered both the potential from microgeneration and also the impacts of microgeneration. The benefits to the distribution networks would be the reduction in loading levels. Such reductions could delay or defer network reinforcement and possibly extend network assets service life.

Mott McDonald in the SIAM report ("*System Integration of Additional Micro-generation*"), presented a detailed report that considered not only the technical impacts of microgeneration but also the economic and fiscal considerations as well [124]. This report followed on from the report by P.B Power [109], which considered explicitly the technical aspects associated with microgeneration. The P.B. Power report, which was commissioned by the Department of Trade and Industry in the UK looked at three

scenarios of microgeneration up to 2020 (with an upper bound of 17GW to 2023) and modelled DSO data based on three load densities. The Mott McDonald report [124] incorporated the technical aspects of [108]. The conclusions of the Mott McDonalds work suggest that the economic cost of accepting more than 17GW of microgeneration onto UK networks would be comparatively small, and substantially less than the wider benefits of micro-generation. The report further concluded that existing LV networks can, under most circumstances, accept up to 100% penetration of microgeneration with regard to the rating of the distribution transformer, provided that certain steps to reconfigure the networks are taken (principally modifying network transformer tap settings). In other words, the total wind generation capacity on a feeder is at 100% if that total equals the MVA or MW rating of the transformer supplying the feeder. The report further testifies that the costs of accommodating large levels of micro-generation are considerably outweighed by the ability to defer reinforcement costs and reductions in distribution losses.

Thomson [114], considered the effects of high density microgeneration connection including reverse power flows as well as voltage rise manifestations and concluded that there were no major obstacles to the installation of microgeneration in distribution networks. In the study undertaken by Douglas, Andrews and Roscoe [125], an examination of the need for the distribution network to change and develop with respect to the evolution towards the smart grid, was undertaken. This study presented different scenarios with respect to the development of the UK network to 2020. The biggest concern identified in that work was the management of the variable output from renewable technologies, driven principally by weather patterns rather than demand as with conventional generation.

The Network described in [109] was analysed [126] in the context of the Irish Energy Regulator's (CER) decision paper where a 40% capacity limit was to be mandated for microgeneration connection [127]. Those analyses provided an overview of the situation pertaining to microgeneration in Ireland, focusing on micro-wind and the technical aspects of SSEG [126]. An exemplary distribution network, consistent with the Irish context, was modelled (under balanced conditions) for power flows using both Excel^{TM} and MATLAB^{TM} in terms of various generation scenarios. Conclusions suggested that the modelled network can accept almost 100% of customers with 1.1kVA micro-generation at minimum load of 0.16kVA per customer (which is considered a pessimistic loading level) without exceeding the maximum voltage excess of +10%.

Similar analysis was undertaken by Keane and Richardson [128], where network modelling, based on data from a real network in suburban Dublin, was instigated. The micro-generation units in that analyses were rated at 1.2kWe and this generation was positioned at each house i.e. 100% penetration. In the paper, the test network is radial consisting of two 10kV/400V transformers supplying a total of 307 (400/230V) domestic loads on two separate sections of LV network. The conclusion there was that voltage levels could breach the network constraints, but only under extreme conditions of minimum load and maximum generation. In addition, when the network is operating under *n-1* contingency situations, Richardson and Keane's analysis suggests that there would be a significant drop in the number of houses that could accommodate a microgeneration system while the network maintained tolerable voltage constraints.

From a non-technical perspective, behavioural aspects and public opinions concerning microgeneration are also significant issues. With respect to people's attitudes towards

microgeneration, the *Hub Research Consultants*, on behalf of the Sustainable Consumption Roundtable [129], published qualitative research which examined people's attitudes to SSEG in different socio-economic groups in the general population as well teachers and students within three schools. The study concluded that energy conservation and energy efficiency were not considered important by the mainstream sample, but with regard to post technology installation reflections, there was a widespread – but not universal – behavioural change in the area of energy efficiency. Comparing these results with the analysis performed by Claudy *et al* [130], which investigated why the uptake of microgeneration in most European countries remains low, Claudy's empirical analysis took a closer look at awareness of microgeneration. Employing a nationally representative study conducted in the Republic of Ireland (in the form of a survey), Claudy's analysis showed a lack of knowledge in relation to the renewable forms of energy. Analysis in this regard illustrated that awareness among the Irish population for the individual technologies differs significantly, but that there is scope to raise awareness in urban areas.

With regard specifically to micro wind generation, Cipcigan *et al* [131] describe research into the effects derived from large scale integration of small scale wind turbines on LV distribution networks and more specifically towards increasing the value of small scale wind turbines (SSWTs) on the quality of LV distribution networks. In that work, a dynamic electrical model is used to investigate the connected generation (micro wind) capacity level to breach the voltage tolerances (+/- 10%). Interestingly, it is claimed that initial steady state modelling, 40% wind turbine penetration will result in the upper voltage tolerance being breached, whereas when a dynamic simulation is considered, with even slight variations in the wind regimes, the limit would only be met at higher penetrations.

Cipcigan *et al* in both [131] and [132] employ a *small scale energy zone* (SSEZ). A SSEZ, as a controllable section of LV network containing a mixture of small scale electric generators (SSEGs), distributed storage and load, facilitates different levels of analysis into technical effects and said effects as these technologies are aggregated. In [132] the value of SSEG can be determined by the following factors:

i) The revenue streams that can be achieved;
ii) The degree to which they can participate in ancillary services markets;
iii) The environmental impact that can be achieved
iv) The ability to contribute to deferral/avoidance of network reinforcement

In both papers ([131] and [132]), the wind turbines and the wind resource are modelled, with the latter including a turbulence component. The conclusions of [131] confirm the potentially negative effect of dispersed generation on voltage profile and how steady-state voltage rise could be a major limiting factor in the integration of large amounts of SSEG. Indeed [131] illustrated that for the connection of individual SSEGs, a threshold occurs for approximately 100% penetration under load conditions before voltage violations are manifested. In [132] however, the employment of a SSEZ network paradigm facilitates controlled aggregation of wind turbine technologies towards a more predictable and less variable energy source than could be derived from individual technologies acting autonomously. The associated results [132] even suggest that benefits would increase with increased number of turbines spread across wider geographical areas particularly in a context of mixed generation sources within multiple SSEZ. So power production in this regard could also assist the DNO with network voltage control and, from a commercial perspective, facilitate groups of SSWT owners to negotiate improved contracts with electricity supply companies.

The SSEZ as considered by researchers such as Cipcigan *et al* [131] and [132], will assist in identifying issues associated with small/micro wind capacity as distributed generation within future smart grids. In terms of prerogatives and benefits associated with DG connected to the smart grid, [133] highlights that a key challenge facing the evolution of this network infrastructure will be in the provision for the transmission/distribution of electricity derived from the full spectrum of energy sources efficiently.

Figure 3.6 illustrates the Irish approach to smart grid development [58] and from an embedded generation perspective, it involves a synergy between five pillars of 'smart' networks, operations, generation and pricing. Figure 3.6 further illustrates that in the move towards a smart grid such a synergy needs to be a staged process with each individual pillar being achieved through research, development, demonstration to deployment.

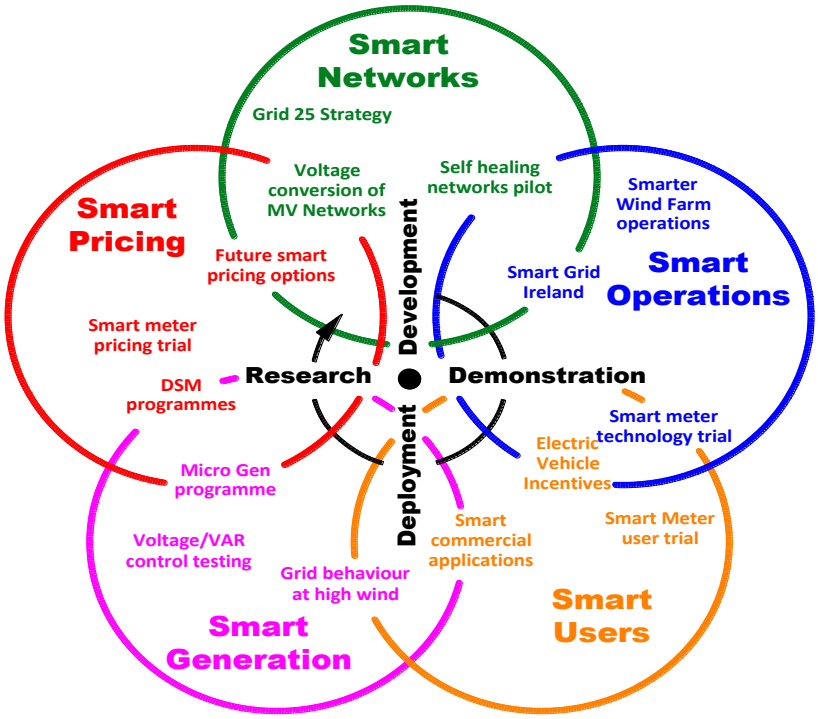

Figure 3.6 The Irish Approach to the *Smart Grid* (source: interpreted from [55])

This following sections will describe analyses of a representative (Irish) Distribution Network model and its make-up as defined in the SEAI commissioned report [109]. An addendum to this report provided the context for microgeneration consideration with respect to the network model. Indeed this report served as the rationale for the Irish Regulator (CER) to impose an initial limit on the installation of microgeneration at 40% of the local transformer capacity [127].

For the purposes of this thesis, a power flow programme based on the *DISTFLOW* algorithm was developed in MATLAB^{TM} to replicate the analysis carried out in [109] and the analyses therein were employed to validate results for fixed levels of load and generation (Stage 1) [126]. Stage 2 extends this work by incorporating variable levels of load and generation so that voltage variation against time over the period of a day, week, month, etc. could be determined.

3.3 Power Flow

Power flow is one of the basic problems in the field of power system engineering but is considered to be the most fundamental algorithm for power systems analysis [134]. The development of numerical methods to solve the matrix of power flow equations has been continuing for 40 years. This work has not only improved the techniques for power flow analysis, but has also influenced the developments in other areas such as contingency analysis and voltage stability [135].

Power flow analysis involves the calculation of currents and voltages throughout a transmission network for specified generation dispatch. Power flow analysis provides the detailed steady-state solution for an electrical network under specific conditions of

load and generation. Load flow analysis also provides the initial conditions for any subsequent electromechanical dynamic analysis of an electrical system or network.

Such calculations are required for the analysis of steady state as well as dynamic performance of systems. When integrated over a very short period of time, the power delivered to a system must be equal to the power consumed by demand. If a mismatch persists, the system becomes unstable [136]. Power flow analysis helps to pinpoint problems in an existing system and determines the effects of additions and upgrades before they are implemented. Its results allow engineers to confidently plan improvements to a system and justify the decisions made. Solution methods should be fast, have low storage requirements, be reliable and versatile through an inherent simplicity [38]. The system of equations which describe electrical power flow on transmission systems are solved by iterative approaches including Gauss-Seidel and Newton-Raphson techniques [137]. Iterative approaches are required as the load is typically defined as a constant power quantity (active and reactive) which inherently involves the product of the voltage and current variables in the representation. Direct solutions can be used if the load can be used if the load can be represented as a constant impedance, constant current or constant voltage. Transmission systems are generally relatively highly meshed and have low values of line R/X (resistance to reactance of lines). In contrast, distribution networks are generally radial and high values of R/X and present computational difficulties for standard power flow approaches.

3.3.1 DISTFLOW Algorithm

DISTFLOW was employed as the optimal methodology to derive the power flow results for the representative Irish network. In particular, as this initial analysis is with respect to a balanced load configuration, the methodology defined in the series of papers

outlined by Das, Gosh, Kathari and Nagi was employed [138], which was developed from the methodology proposed by Baran and Wu [139]. The *DISTFLOW* voltage equation (3.3) is derived in terms of Figure 3.7 and equations (3.1) and (3.2) to describe the voltage derived by the power flow solution [138, 139].

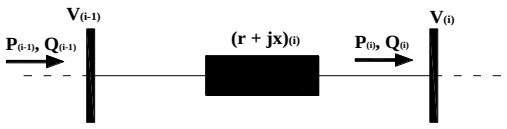

Figure 3.7 Radial Feeder Consideration (DISTFLOW Power flow)

Figure 3.7 shows that the voltage derived at a bus ($V_{(i)}$), depends on the voltage of the preceding bus ($V_{(i)}$) and any losses incurred in the line $(r+jx)_{(i)}$ connecting both buses as a consequence of power flowing through the line ($P_{(i)}$, $Q_{(i)}$). $(r+jx)_{(i)}$ is the series impedance (resistance and reactance) of the line connecting node (i-1) to node (i).

The Power flow and associated loss respectively can be derived in terms of Figure 3.7. From Figure 3.7., it is apparent that the active /reactive power flowing into node *(i)* from the connecting line to node *(i-1)* is equal to the power (active and reactive) leaving node *(i-1)* plus the line loss:

$$P_{(i)} = P_{(i-1)} + P_{(loss)};\ \ Q_{(i)} = Q_{(i-1)} + Q_{(loss)} \qquad \textbf{(3.1)}$$

With the associated active and reactive losses described as

$$P_{(loss)} = \frac{P_{(i)}^{2} + Q_{(i)}^{2}}{V_{(i)}} \times r\,; \qquad Q_{(loss)} = \frac{P_{(i)}^{2} + Q_{(i)}^{2}}{V_{(i)}} \times x \qquad \textbf{(3.2)}$$

If (3.1) and (3.2) are considered in terms of the current flowing into node *(i)* from the connecting line to node *(i-1)*, the voltage at node *(i-1)* can be derived from:

$$V_{(i)} = \sqrt{\frac{\left\{2.\left(P_{(i)}.r_{(i-1)} + Q_{(i)}.x_{(i-1)}\right) - V_{(i-1)}{}^{2}\right\}}{2} + \frac{\sqrt{\left\{2.\left(P_{(i)}.r_{(i-1)} + Q_{(i)}.x_{(i-1)}\right) - V_{(i-1)}{}^{2}\right\}^{2} - 4.\left(P_{(i)}{}^{2} + Q_{(i)}{}^{2}\right).\left(r_{(i-1)}{}^{2} + .x_{(i-1)}{}^{2}\right)}}{2}}$$

(3.3)

Equation (3.3) is the means through which the voltage on each bus of the Distribution Network is derived. **Appendix A1** provides a full derivation of (3.3).

The Power Flow for the system was derived by applying a similar algorithm as described in [138] and is outlined by the chart contained in Figure 3.8. Power Flow is based on Equation (3.4).

$$P_{(i)} = TP_{(L)} - PS_{(L)} - SPL_{(L)}$$

(3.4)

where

***P*$_{(i)}$** is the power flowing into the specific bus being evaluated

***TP*$_{(L)}$** is the total power flowing into the specific lateral containing the bus being investigated

***PS*$_{(L)}$** is the total power of associated laterals connected to the specific lateral prior to the bus being investigated

***SPL*$_{(L)}$** is the actual load and associated losses attributable to branches prior to the bus in question.

Figure 3.8 Illustrates a flow-chart describing the DISTFLOW power flow methodology as described in [138].

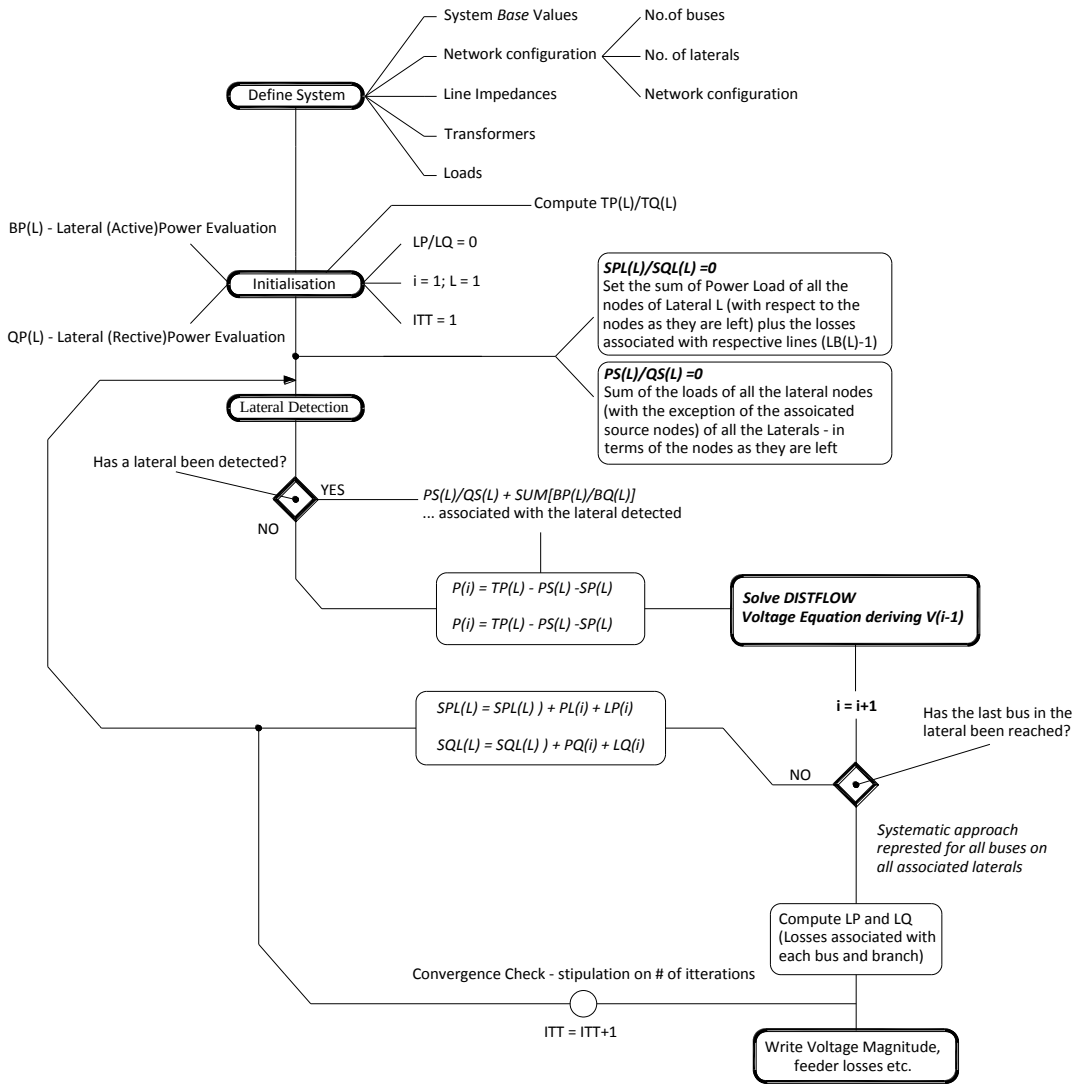

Figure 3.8 The DISTFLOW Algorithm as applied to the Representative Distribution Network (source: interpreted from [138])

The methodology described in Figure 3.8 is particularly applicable to radial networks. As explained by Das *et al* [138], R/X ratios in such networks are generally high and with the networks being ill conditioned, conventional Newton Raphson and fast decoupled power flow methods as described by Tinny *et al*, Stott and Nagrath *et al* [140, 141] are respectively inefficient in deriving solutions for said networks. The method described by Das *et al* in [138] involves only the evaluation of simple voltage comparisons without any trigonometric functions – thereby providing an efficient

methodology requiring little computational resources. As explained in 3.3, an iterative approach is required as the load is defined as a constant power quantity (active and reactive) which inherently involves the product of the voltage and current variables in the representation. The next section will present the analysis to consider the network described in [109] through a two stage process: the first replicating the analysis in [109] with stage 2 developing the analysis to be inclusive of variable load and generation. In this regard, Figure 3.11 and Figure 3.18 respectively present a context for the application of the DISTFLOW algorithm as summarised in Figure 3.8 above.

3.4 Power Flow Solution for a *Representative* Irish Network

The analysis in both stages 1 and 2 uses the SEAI commissioned P.B. Power report [109]. Stage 1 will consider a generic distribution network and how system voltage is affected as a consequence of consumer load and generation. Here minimum and maximum consumer load and generation are specified. The PB Power report [109] considered voltage regulation limits to be +10%/-6% (1.1-0.94 pu) across the LV network and +/-10% (1.1-0.9 pu) across the MV network. Similarly, for stage 1 (section 3.4.1), the analysis presented here considers the same voltage tolerances. The analyses presented for Stage 1 is carried out to validate the network developed in MATLAB for fixed levels of load and generation.

With regard to Stage 2, which will be detailed in section 3.5, the same network structure (as described in section 3.4.1) is employed, but the analyses for stage 2 are with respect to variable load and generation and the current standard adopted in Ireland (EN50160). The standard stipulates that with regard to voltage magnitude variations, for LV and MV +-10% for 95% of the week (mean 10 minute rms values) is applicable [142].While the analysis here does not analyse to this level of accuracy (hourly values of load and

wind speed), it does present a context of how often as a percentage that these limits are breached. With regard to voltage and voltage regulation in general terms, the distribution network in Ireland (ESB Networks), operates to the DNO code of practice [143].

3.4.1 Network Development: Stage 1

A model based on the *Micro generation Addendum* contained in [109], which itself is predicated on a report pertaining to the impact of small scale embedded generation on the operating parameters of distribution networks [108], was developed in MATLAB™. Whilst more technical analysis is performed in the latter, as it is in the context of the UK distribution network, the former has been used as the basis for analysis in this section. The model is comprised of two 38/10kV transformers fed from a 500MVA source. The transformers are connected in parallel feeding a network containing five distribution feeders (10.5kV). One of these feeders is modeled in detail. Each 10.kV feeder has 10 substations (400KVA) each servicing 4 LV (400V) cables from a 10/0.433kV transformer to supply 78 customer connections across three phases per line. The total length of the detailed 10/0.4kV network line is 3.3km. The model developed in this section considers balanced load conditions only. In this context, the generation is connected across the three-phases connected proportionately along the length of the detailed LV feeder (300m). The primary goal in this regard is to investigate voltage rise scenarios from a network integration perspective.

Appendix A2 provides further detail of how the network and Figure 3.9 shows an overview of the configuration.

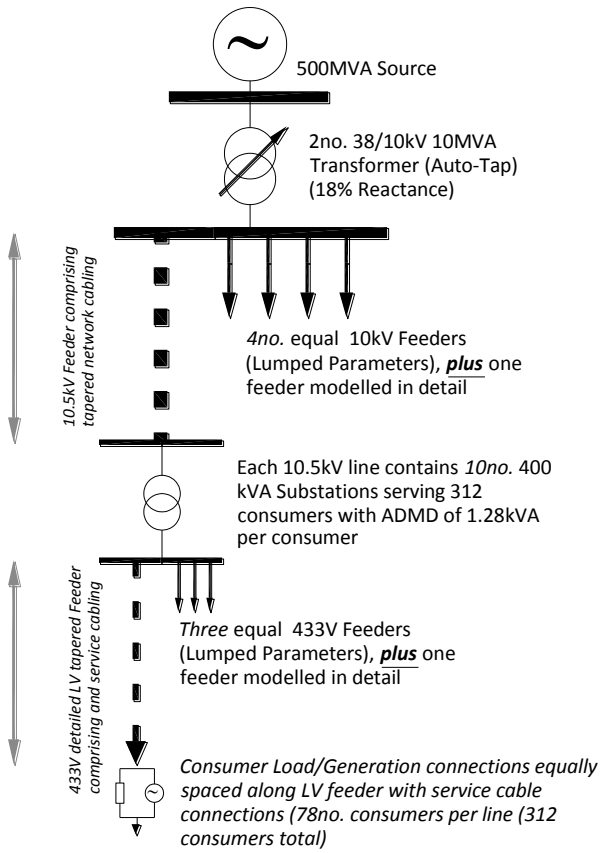

Figure 3.9 38/10/0.4kV Power System Model (Stage 1) [109]

Table 3.2 summarises the Network Max/Min Loading for Stage 1 of the Representative Distribution Network. The PB Power report [109] stipulated that consumer load could be 0.16kW minimum or 1.28kW maximum (After Diversified Maximum Demand (ADMD) at unity power factor in both scenarios). For system planning, consumer loads are often diversified based load consumption and consumption patterns. A diversity factor takes into consideration that not all connected load in an installation will consume power simultaneously. Therefore, for the detailed LV feeder under minimum load, for the 78 customers, there will be a demand of 12.48kW. Including the other 3 lines per 10/0.433kV substation, this implies a load of 49.92kW in total for the 312 customers per substation. There are 10 substations per 10kV line, which implies that there will be a load of 499.2kW per 10kV line and with 5 such lines, this implies a system load of

1248kW. Similarly, for customers consuming an ADMD of 1.28kW, the total system load will be 9984kW.

Table 3.2 Network Max/Min Loading (at unity power factor)

		Network Capacity [kW]			
		Minimum		Maximum	
Network Component	Quantity	Load	ADMD Min	Load	ADMD Max
38/10.5 kV [10MVA] Transformer	2	2496	1248	19968	9984
10kV Line(s)	5	2496		19968	
10/0.433kV Substation	***10***	***499.2***		***3993.6***	
400V Line(s)	4	49.92		399.36	
Consumer Load/Line	78	12.48		99.84	
Consumer Load	1	0.16		1.28	

Based on the description of load allocation across the network, Table 3.3 illustrates how for the detailed LV line, the load is allocated along its 3km length (Stage 1). The model developed in MATLAB compiled the network [109] (Figure 3.9 (with a more detailed description provided in **Appendix A2**)), in which aggregate LV-line/substation/10kV-line loading are apportioned. **Appendix A5** illustrates how the load, as presented in Table 3.2 and Table 3.3 are apportioned (depending on whether the system is considering minimum or maximum consumer loads throughout).

Table 3.3 Load Allocation per LV Line *Representative Distribution Network* (4 no.) (maximum loading): Stage 1

Load Customer connections

kW	kVA	kVAr	p.f.
1.28	1.28	0.00	1.00

	Generator allocation per Phase			*Load $_{TOT}$*
	L_1	L_2	L_3	*(kW)*
1	2	2	2	7.68
2	2	2	2	7.68
3	2	2	2	7.68
4	2	2	2	7.68
5	3	3	3	11.52
6	3	3	3	11.52
7	3	3	3	11.52
8	3	3	3	11.52
9	3	3	3	11.52
10	3	3	3	11.52
	26	*26*	*26*	**99.84**

	78	per line
(No. of customers)	**312**	per substation

Susbstation Load

	Load (kW)
LV (400V) Feeder	99.84
Substataion Load	**399.36**

System Load

	Load (kW)
MV (10kV) Feeder	3993.6
Transformer Load	**19968.00**

Model initialising is facilitated by defining each of the following (with the associated impedance (and load) parameters acquired from [109]):

- The Bus/Node designation
- The Line/branch impedances
- The Transformer impedances and transformer ratios
- The Load allocation

Bus/Node designation: Figure 3.10 illustrates the identification scheme that was developed in MATLAB for the representative Irish Network, as required in employing *DISTFLOW* [138, 139]. The model was developed as having 43 buses and 20 branches (laterals). To evaluate the power flow solution, detail pertaining to transformer identification and rating, distribution line impedance, load connection and generator injection was required.

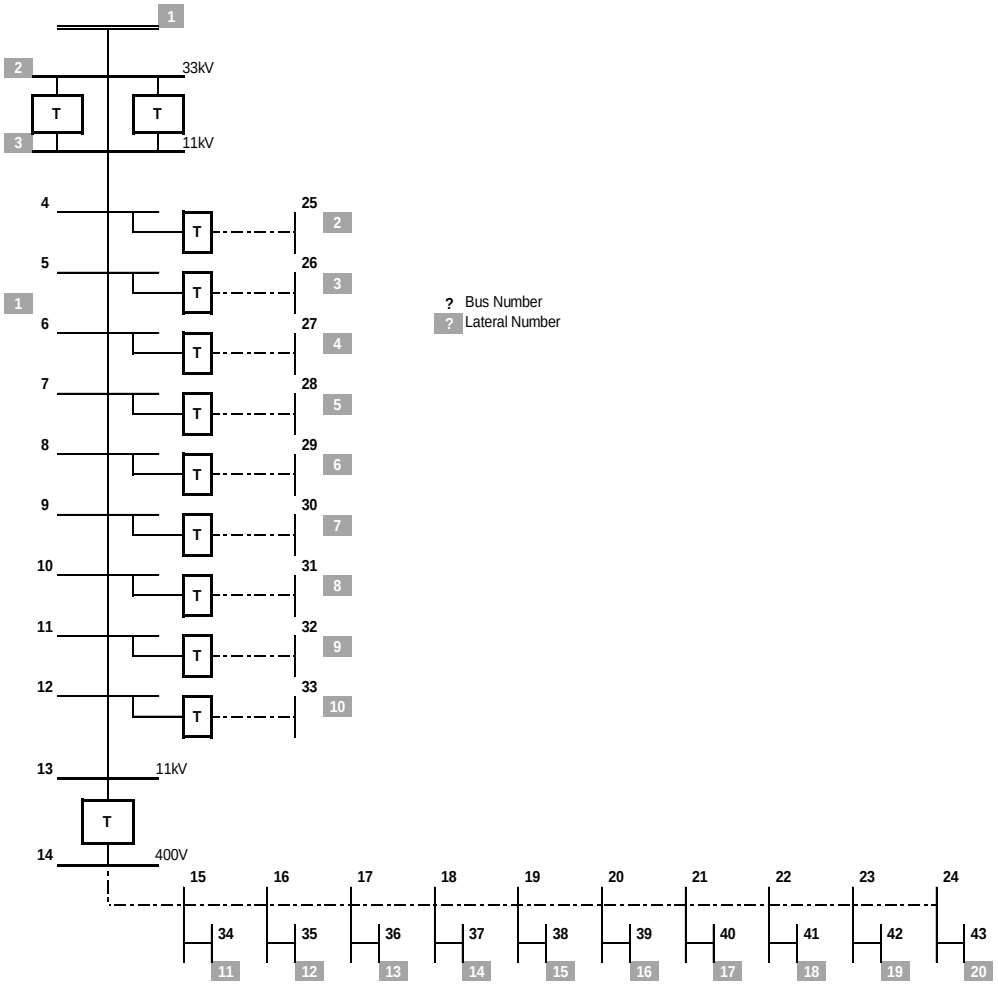

Figure 3.10 Bus/Node designation of representative Irish Network

Line Impedances (including transformer impedances): **Appendix A3** details the pu line impedances applicable to the model. Ohmic values were contained within [109]). The system base power (MVA) is 1MVA.

Transformers: **Appendix A4** details the pu values applicable to the distribution Network Transformers (calculated on the basis of information provided in [109]). There are two types of transformers with the following transformer ratios:

- ***38/10.5kV:***
    - -20/+10% tap changer with 1.67% tap steps

- Transformers within these substations are normally configured with Automatic Voltage Regulation (AVC), through transformer taps. The AVC scheme described by P.B. Power [109]with bandwidth (BW) of 2.5%

  In the analyses that will be presented here (for both stages 1 and 2), the distribution transformer (38/10.kV) ratio was manually set for each model simulation and results collated for multiple sweeps of BW setting. In other words, the network was considered for each tap setting available to the AVC but fixed for each simulation so as to capture the effect for a specific transformer setting.

- ***10/0.433kV:***
  - For the PB Power model, The transformer taps were set at Taps set at -2.5% on HV side

    For the analysis presented here, the transformer ratio (10/0.433kV) was fixed at 1.085 pu. As per the PB Power analysis, these transformers did not facilitate variable tap settings.

Load: A sign convention is employed with respect to connected load and generation:

- Load → *positive*
- Generation → *negative*

Micro generator connections are specifically considered for the detailed LV feeder. The model developed for Stage 1 generically considers micro generators and does not (at this stage) specifically model micro wind turbines. Therefore, the load/generator balance is considered in terms of:

- 312 consumer connections on one detailed LV feeder. There are 10 connection points per LV line at which either 6 or 9 consumer connections (balanced load) are modelled
- The load on the other three lines per (10/0.433kV substation) is represented as an aggregation based on the detailed LV line load.
- The remaining 9no. 10kV substations (per 10kV line) are aggregated based on the previous step to provide for a total 20kV loading

- There are 5 10kV lines and the load per line is as the previous step, with the total aggregate connected to the relevant network section.

.

3.4.1.1 Detailed LV Feeder

There are ten consumer (lumped) connection points along the detailed feeder. These connections are facilitated as balanced three-phase connections. There are 78 customers connected on the detailed LV feeders. The allocation of customer connection/load is assigned evenly along the line as depicted in Table 3.4. The load on the other three LV feeders is lumped on to the outgoing side of the substation distribution transformer. The network load allocation (for maximum demand) is described in **Appendix A5**. Table 3.4 shows the allocation for maximum-load/100%-Generation for the detailed 400V feeder.

Table 3.4 Load allocation across the three phases of the (detailed) LV feeder

Load/Gen Customer connections		kW	kVA	kVAr	p.f.
Load:	Max	1.28	1.28	0.00	1.00
	Min	0.16	0.16	0.00	
	Generator:	1.05	1.10	0.34	0.95

Phase allocation	L_1	L_2	L_3	Min Load (kW/point)	Max Load (kW/point)	Gen (kW/point)	(*Min*) NET (kW/point)	(*Max*) NET (kW/point)
1	2	2	2	0.96	7.68	6.27	-5.31	1.41
2	2	2	2	0.96	7.68	6.27	-5.31	1.41
3	2	2	2	0.96	7.68	6.27	-5.31	1.41
4	2	2	2	0.96	7.68	6.27	-5.31	1.41
5	3	3	3	1.44	11.52	9.405	-7.965	2.115
6	3	3	3	1.44	11.52	9.405	-7.965	2.115
7	3	3	3	1.44	11.52	9.405	-7.965	2.115
8	3	3	3	1.44	11.52	9.405	-7.965	2.115
9	3	3	3	1.44	11.52	9.405	-7.965	2.115
10	3	3	3	1.44	11.52	9.405	-7.965	2.115
	26	*26*	*26*	**12.48**	**99.84**	**81.51**	**-69.03**	**18.33**

	Min Load (kW)	Max Load (kW)	Generation (kW)
LV (400V) Feeder Load:	12.48	99.84	81.51
Substataion Load	49.92	399.36	326.04

	Min Load (kW)	Max Load (kW)	Generation (kW)
MV (10kV) Feeder Load:	499.2	3993.6	3260.4
Transformer Load	2496	19968	16302

Table 3.4 shows how net load in the system (based n the algebraic sum) of Load (positive power) and generation (negative constant power) is calculated. System loading is extrapolated based on individual customer demand/generation with max(min) load of 0.16kW(1.28kW) respectively and generation capacity of 1.1kVA operating at a power factor of 0.95 (as detailed in [109]).

3.4.1.2 Model Implementation

The model is developed in MATLAB^{TM} and the power flow solution is solved iteratively. The sequence involved in the acquisition of the solution is summarised by the sequence depicted in the flow chart contained in Figure 3.11, with Figure 3.8 providing explicit detail on how the power flow solution is derived.

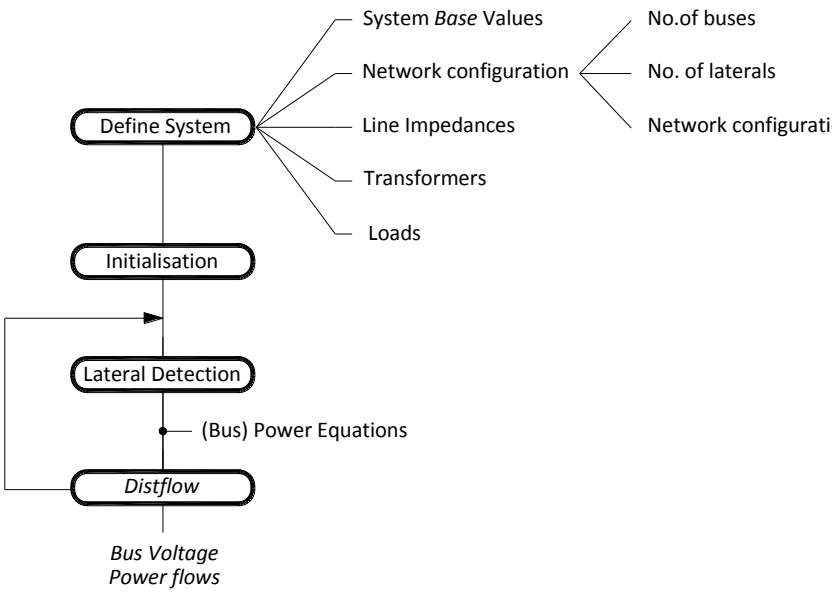

Figure 3.11 Flow chart of Power Flow solution (Stage 1)

3.4.2 Stage 1 Model Analysis

The results for stage 1 are consistent with the voltage profiling considered in [108, 109], but the model was primarily developed to acquire a technical context for the distribution network capability to accommodate consumer micro wind generation (as presented in Stage 2). Stage 1 is therefore considered in advance of considerations pertaining to micro wind generation and network tolerances.

With respect to voltage rise, the following studies were investigated:

1. Maximum Load, zero generation
2. Minimum load, zero generation
3. Maximum Load, maximum generation
4. Minimum load, maximum generation

In particular, studies 1 and 4 represent the extremes of operation of the network and in particular, the fourth study was of interest with regard to the position of CER in curtailing micro generation integration to maximum of 40% of local substation capacity [144].

The figures presented in 3.4.2.1 to 3.4.2.4 illustrate the network profile voltages along the network for each of the scenarios as considered in [126]. From a 10kV perspective, these voltage considerations included the source and both the primary and secondary of the 38kV transformers as well as each of the 10 substation transformers of the detailed 10kV line. From a 400V perspective, the voltages along the 300m of the detailed 400V line at 10 positions are considered. Unlike the results presented in [109], detail pertaining to the specific 38kV transformer tap arrangements are provided.

3.4.2.1 Scenario 1: Maximum Load, zero generation:

The model is loaded with all customers on the detailed LV feeder requiring 1.28kVA (unity pf). No micro generation is included. This loading is replicated and lumped for the other three LV lines, for each of the ten substations on each of the five 10kV lines supplied by the two 10MVA transformers. The model derived a power flow solution with the distribution transformer (38/10.5kV) requiring six positive tap steps (maximum +10%). The voltage profile across the modelled network resulting from this scenario is illustrated in Figure 3.12. Clearly visible – and consistent with the subsequent illustrations - is the 38/10.5kV distribution transformer tapping and the voltage ramp in secondary voltage resulting from the fixed-tap 10/0.433kV substation transformer.

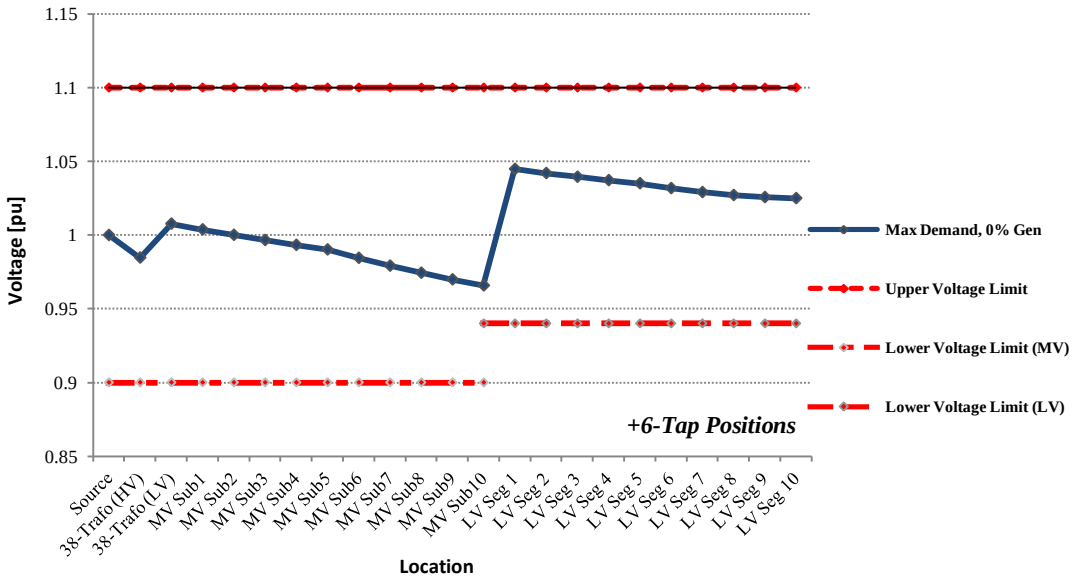

Figure 3.12 Network Profile (Stage 1) - ***Maximum Demand, Zero Generation***

3.4.2.2 Scenario 2: Minimum Load, minimum generation:

The model is loaded with all customers on the detailed LV feeder allocated 0.16kVA (unity pf). No micro generation is included. This loading is replicated and lumped for

the other three LV lines, for each of the ten substations on each of the five 10kV lines supplied by the two 10MVA transformers.

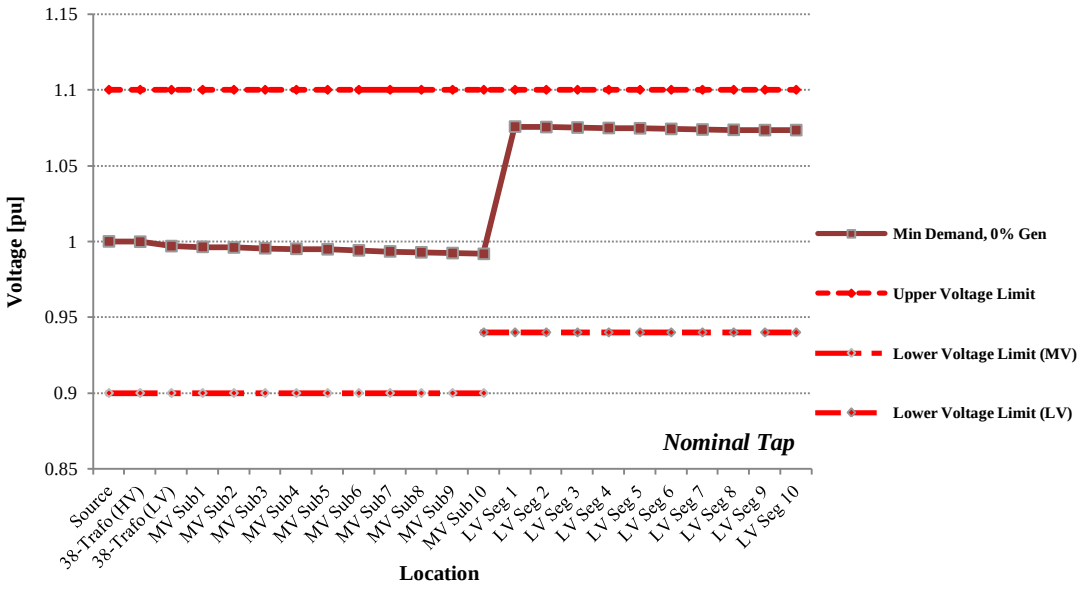

Figure 3.13 Network Profile (Stage 1) - Minimum Demand, Zero Generation

The model derived a power flow solution with the distribution transformer (38/10.5kV) requiring no tap steps (Figure 3.13)

3.4.2.3 Scenario 3: ~Maximum Load, maximum generation:

The model is loaded with all customers on the detailed LV feeder allocated 1.28kVA (unity pf) load and 1.1kVA (0.95 pf), 1.045kW, generation. This loading is replicated and lumped for the other three LV lines, for each of the ten substations on each of the five 10kV lines supplied by the two 10MVA transformers. The model derived a power flow solution with the distribution transformer (38/10.5kV) requiring four negative tap steps (-6.68%), and the results are illustrated in Figure 3.14)

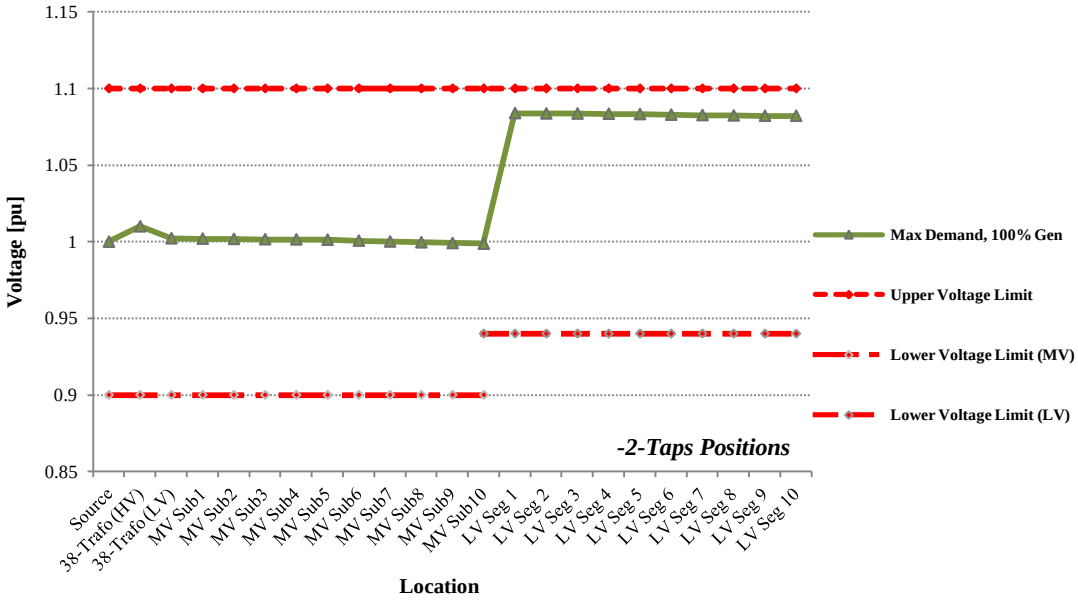

Figure 3.14 Network Profile (Stage 1) - Maximum Demand, Maximum Generation

3.4.2.4 Scenario 4: Minimum Load, maximum generation:

The model is loaded with all customers on the detailed LV feeder allocated 0.16kVA (unity pf) load and 1.1kVA (0.95 pf), 1.045kW, generation. This loading is replicated and lumped for the other three LV lines, for each of the ten substations on each of the five 10kV lines supplied by the two 10MVA transformers. The model derived a power flow solution (Figure 3.15) with the distribution transformer (38/10.5kV) requiring six negative tap steps (-10%)

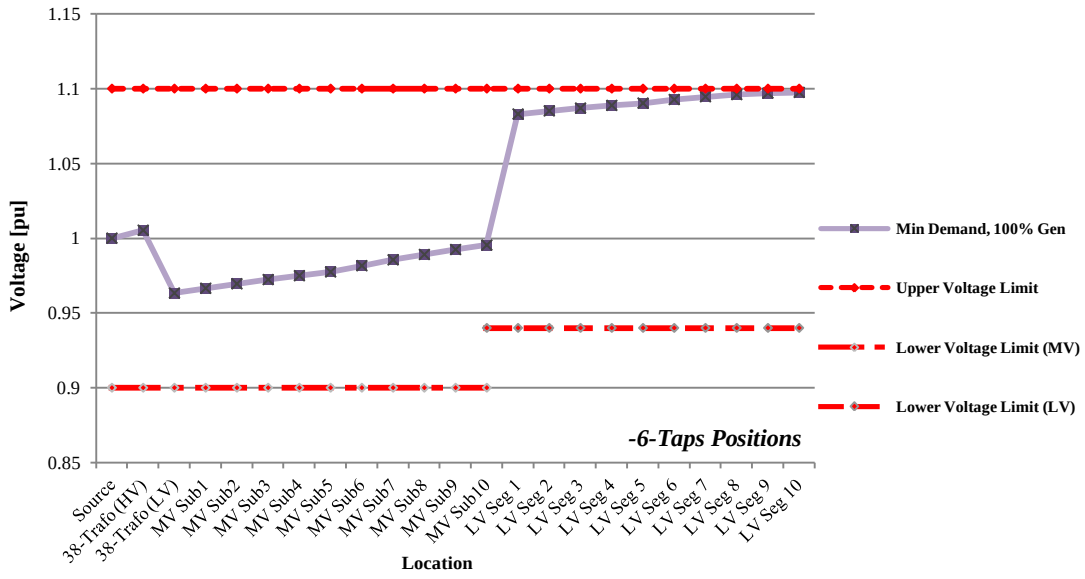

Figure 3.15 Network Profile (Stage 1) - Maximum Demand, Maximum Generation

Figure 3.16 collates the results of the different scenarios and shows that for the two worst case scenarios (maximum demand, zero generation and minimum demand and maximum generation) there are no breaches of the network constraints.

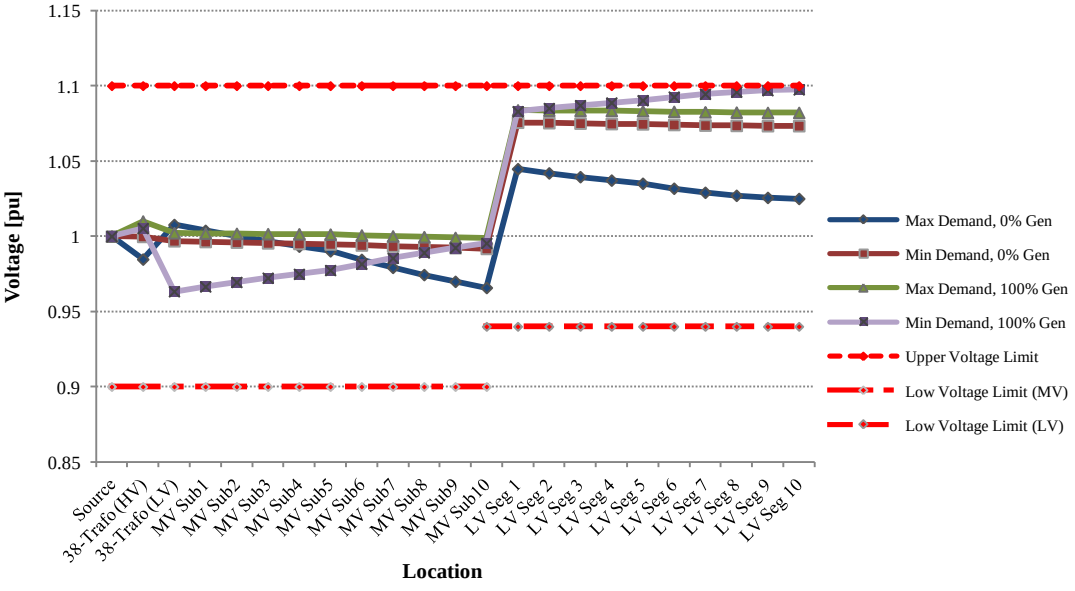

Figure 3.16 Voltage Profile Results for the Representative Irish Network (Stage 1)

3.5 Network Development: Stage 2

The model was modified to facilitate more practical wind generator connections (Table 2.4). From a network operability perspective, the goal was to establish the effect(s) as a consequence of a market available technology and to ascertain the associated network voltage tolerances with increased technology proliferation.

Stage 2 in developing the Network Model considers the integration of variable consumer load and (modelled) micro wind generation as illustrated in Figure 3.17.

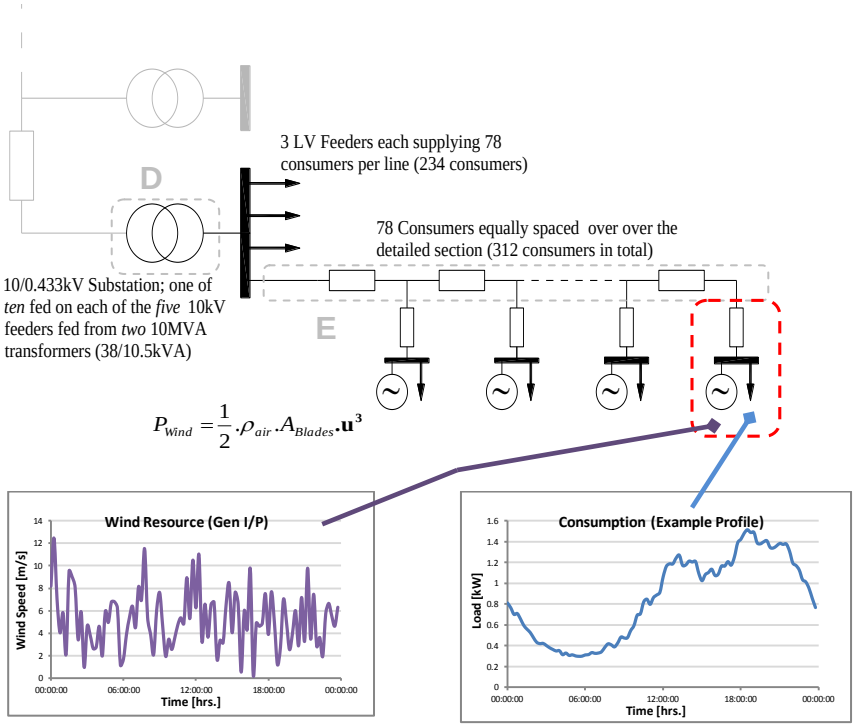

Figure 3.17 38/10/0.4kV Power System Model (Stage 2)

3.5.1 Load

The Standard Load Profiles are developed by *Retail Market Design Service* (RMDS) who are commissioned by CER to develop them for the Irish Market [145]. The profile data is collected and processed annually. The profile data is then unitised, so that all

Demand Energy Coefficients (DECs), for each *Quarter Hour* (QH) interval, sum to 1.0 for each *Standard Load Profile* (SLP). It was envisaged that the SLPs could be used for *Distribution Use of System* (DUoS) and *Public Electricity Supplier* (PES) tariff formulation. The data acquired from [145] was then organised in MATLAB™ into hourly readings representative of the domestic sector.

Figure 3.18 illustrates a flow chart of how the model is developed in stage 2. The analysis is based on the Dublin Airport recorded wind speed with respect to the generators identified in Table 2.4 over the year of 2008. It is important to note that the wind resource at Dublin Airport would be considered a good resource and as such the analysis and generator contribution could be considered as somewhat overly optimistic.

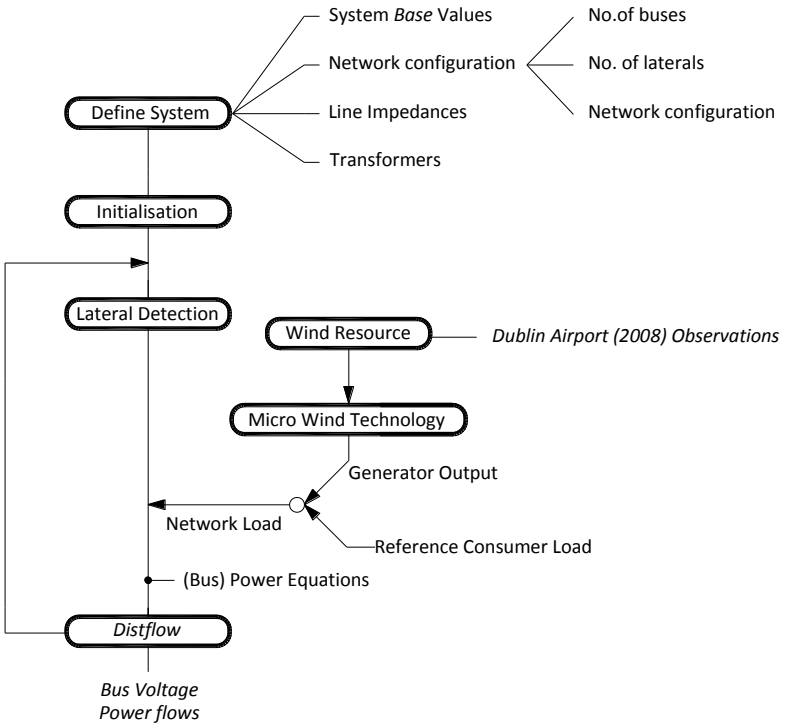

Figure 3.18 Flow chart of Power Flow solution (Stage 2)

3.5.2 Micro wind Turbine Performance

The technologies in Table 2.4 are used for investigative purposes to analyse respective performance comparisons. Table 3.5 illustrates these comparisons as derived through MATLAB^{TM} (in association with the hourly consumer load [145]) and more specifically with respect to:

- How much energy can be produced from over the year (2008),
- The average output power for the technologies and,
- The capacity factor of the technologies for the period, which describes the ratio of actual power produced over a period of time and its output if it had operated at full capacity over the entire period.

Table 3.5 Summary of selected wind turbines with respect to the Airport wind resource selection (and consumer load)

Technology	u_{Mean} [m/s]	u_{STD} Deviation	Energy Demand [kWh]	Energy Produced [kWh]	Net Energy [kWh]	Average Output [kW]	Capacity Factor [%]
Skystream 3.7	5.97	3.01	5979.04	3499.67	-2479.37	0.40	16.65
Whisper 200				1948.19	-4030.85	0.22	22.24
Proven 2.53				5394.69	-584.35	0.62	27.99

To put Table 3.5 into context, Drew *et al* in their analysis looking at the potential for wind turbines across the Greater London area [95], which involved a consideration of 30 turbines (9 VAWT and 21 HAWT), estimated that the average capacity factor of 4.4%for the VAWTs and 10.6% for the HAWTs. The figures derived in Table 3.5, on the basis of Airport observations, are more representative of a rural context.

A summary of the *Skystream 3.7* and *Whisper 200* characteristics and performance (based on consideration of the representative Dublin Airport wind speed) in conjunction with the consumer load are generators with respect to **Appendix A6**. These two

generators represent the opposite ends of generator output potential for the sample load and wind speed considered.

It is obvious that for the wind data, which is more indicative of a rural environment and could therefore be considered as representing a *good* wind resource, there will a marked performance difference depending on the ratings of the respective technologies ($u_{cut\text{-}in}$ and also P_{rated} at u_{rated}). The *Proven 2.5* has the capability of generating the requirement of the consumer load to the point of being able to marginally export some energy. That said however, the *Skystream 3.7* – which has a performance rating comparable to the *Proven 2.5,* does not perform as well (based on the detail included in Table 2.4), suggesting that the poorer rated operational efficiency associated with the *Skystream 3.7,* has a detrimental effect on the potential for electricity generation. Furthermore, the lower rated (power) wind speed associated with the *Proven 2.5* will have a considerable influence on the energy harnessing capabilities of the technology. The capacity factors of each technology are more a testimony to the wind resource than the technologies themselves, which for the purposes of this specific analysis employed Dublin Airport hourly data.

3.5.3 Stage 2 Model Analysis

With respect to the selection of micro wind generators identified in Table 2.4, the analysis (in the context of the hourly observations of the wind speed recorded at Dublin Airport as well as the CER (representative) Load data for the same period (2008) [145]) was performed through the following scenarios: zero generation, 50% generation capacity (for each generator) and 100% generation capacity. The representative annual load was allocated (on the basis of load allocation as defined in stage 1) with each consumer on the detailed feeder being incurring hourly demand based on [145]. All

other feeders/substations being allocated the representative *lumped* load on an hourly basis. The sample/representative load had a maximum demand of 1.64kW [145]. This implied that with respect to the model, there was the possibility of 26MVA demand on the Network (as per Table 3.6 below, which in turn is scaled on the same basis of Table 3.2), compared to a maximum demand per customer of 1.28kW.

Table 3.6 System loading worst case scenario – undiversified

Customer Generator connections

kW	kVA	kVAr	p.f.
1.67	1.67	0.00	1.00

	Generator allocation per Phase			*Gen $_{TOT}$*
	L_1	L_2	L_3	*(kW)*
1	2	2	2	10.02
2	2	2	2	10.02
3	2	2	2	10.02
4	2	2	2	10.02
5	3	3	3	15.03
6	3	3	3	15.03
7	3	3	3	15.03
8	3	3	3	15.03
9	3	3	3	15.03
10	3	3	3	15.03
	26	*26*	*26*	**130.26**

	78	per line
(No. of customers)	**312**	per substation

Susbstation Load

	Load (kW)
LV (400V) Feeder	130.26
Substataion Load	**521.04**

System Load

	Load (kW)
MV (10kV) Feeder	5210.4
Transformer Load	**26052.00**

With this level of load being applied to each consumer for any time step through the year, the transformer would be overloaded by 30%. In order to avoid this, consumer load was diversified by a factor of 0.7659, which would limit maximum loading to be within the transformer capacity. This level of diversity factor is deemed appropriate on the basis that the probability that every consumer on the network would have such a demand at the same time, is negligible,

Figure 3.19 illustrates network profile results based on (hourly) consumer load and and zero-generation. As previously explained, transformer tapping was fixed for each simulation until an optimal voltage profile – that prioritises the detailed LV line – was

achieved. Figure 3.19 provides a context for how the system profile can be varied with transformer tap settings. For the remaining analysis within this section, all associated voltage profile illustrations prioritise the physical network structure presented in Figure 3.9 and the electrical modelling structure presented in Figure 3.10. In particular, a section of 10kV line and the associated MV substation at the end of this line section (*MV-Sub*) is considered With respect to Figure 3.10, the last substation of the detailed 10kV line is node 13. The detailed LV line and in particular the end of the line segment (*LV-Seg*) is prioritised. The last consumer connection position in terms of Figure 3.10is identifiable as node 43. In this way, the associated results present a voltage profile from the distribution transformer through the last of the 10/0.433kV substation and with regard to the last load connection at the end of the LV line is achieveable.

Figure 3.19 is divided into two: (a) considers the network reaction based on a nominal (38/10.5kV) transformer tap arrangement and (b) the network voltage profile with the (38/10.5kV) transformer fixed at +6-tap settings. Figure 3.19 (a) (i) and (b) (i) presents network voltage frequency distribution, whereas Figure 3.19 (a) (ii) and (b) (ii) present the worst case scenarios (over the same demand and wind speed considerations) for the network. In particular (and with reference to Figure 3.10, which describes the electrical modelling (numbering) structure of the physical network), nodes 13 and 43 are highlighted. These represent the last 10/0.433 substation transformer along the detailed feeder transmission line and the last consumer on the detailed 400V feeder respectively. Figure 3.19 (a) (ii) illustrates the network voltage as a result of minimum load whereas Figure 3.19 (b) (ii) shows the network voltage profile as a consequence of maximum load (a diversified 1.674kW (0.766) being applied to all consumer connections). Both figures illustrate the system (38/10.5kV) transformer tapping effects with increasing

taps causing network voltage (110%) breaches. These results are consistent with the analysis carried out in section 3.4.2.

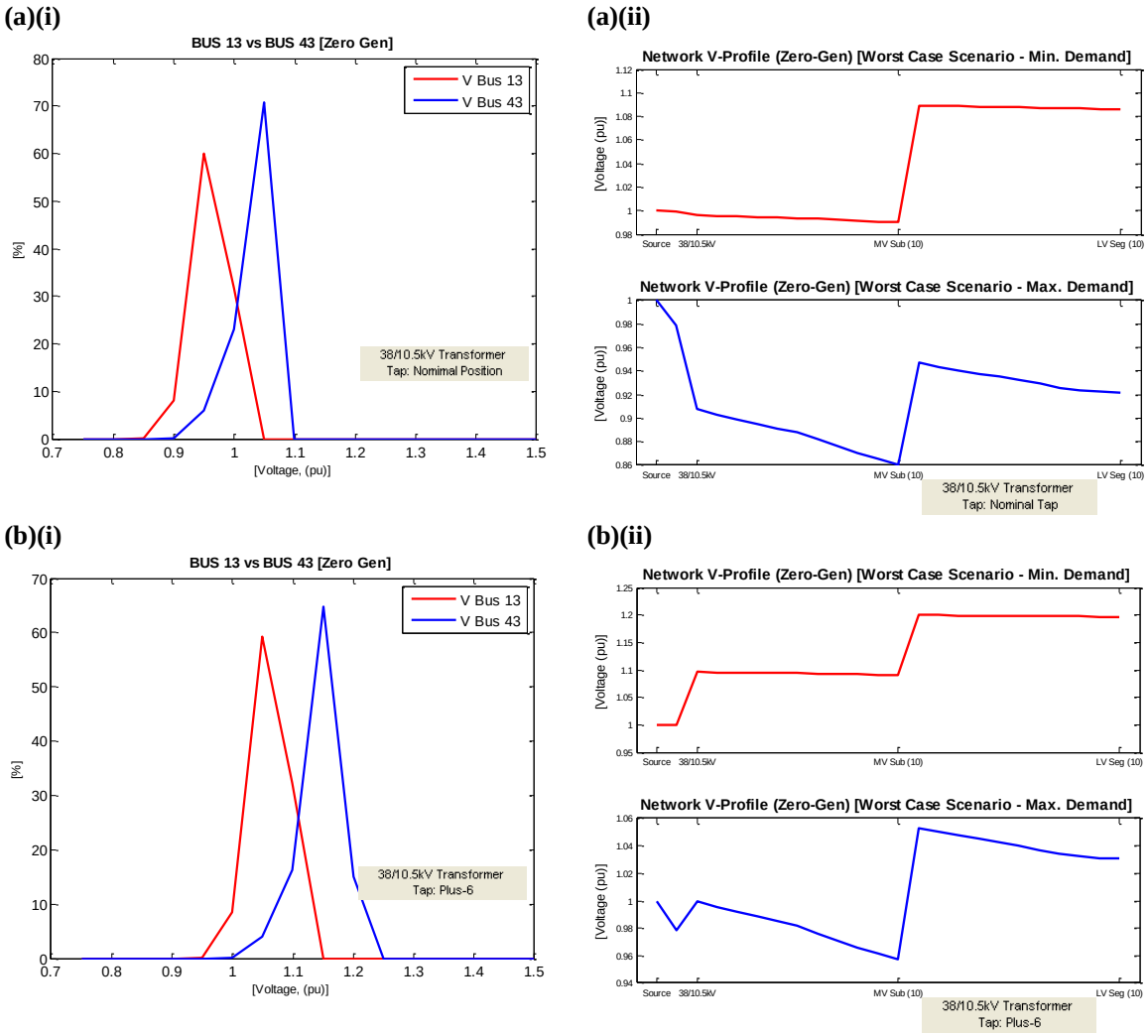

Figure 3.19 System Analysis for Zero Gen & Variable Load in terms of Variable 38.5/10.5kV Tap

Figure 3.20 and Figure 3.21 further consider Figure 3.19 (a) (i) and Figure 3.19 (b) (ii) in terms of the level of voltage tolerances (+/-10%) at node 13 (MV Sub (10)) and node 43 (LV Seg (10)) under the network operational constraints as considered in Figure 3.19. Positive breaches (i.e. >110% V) are presented by positively displaced bars and represent minimal load demanded over the annual demand being considered, whereas

negative breaches (i.e. <90% V) are illustrated by negatively displaced bars and represent maximum load requirements across the network.

(a)

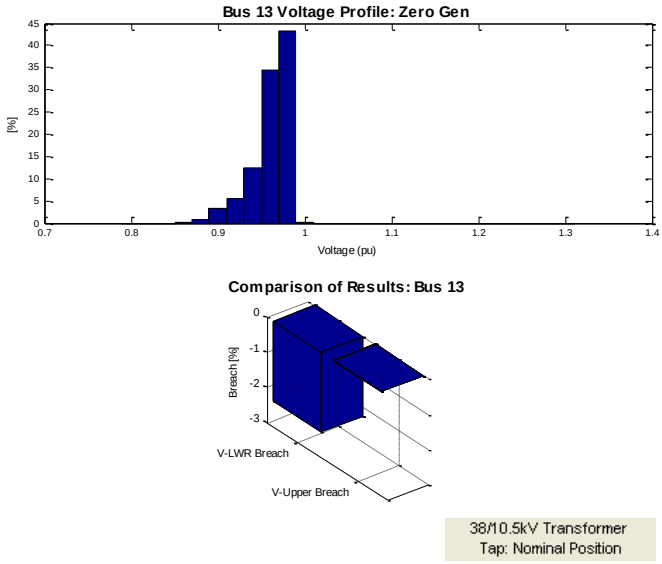

(b)

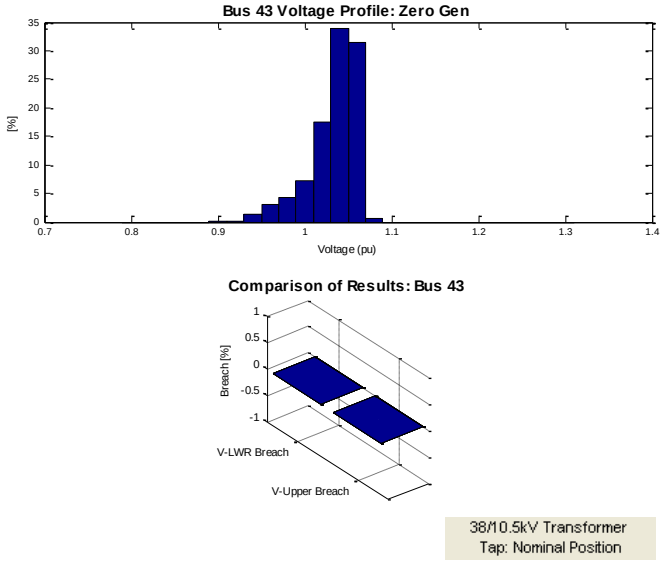

Figure 3.20: Voltage Tolerance Breach Analysis (Zero Gen); 38.5/10.5kV Nominal Tap and Variable Load

Both Figure 3.20 and Figure 3.21 illustrate the effect of varying the 38/10.5kV tap has on the operational voltage across the network depending on consumer demand, particularly when considering the full range of control available to the AVC.

(a)

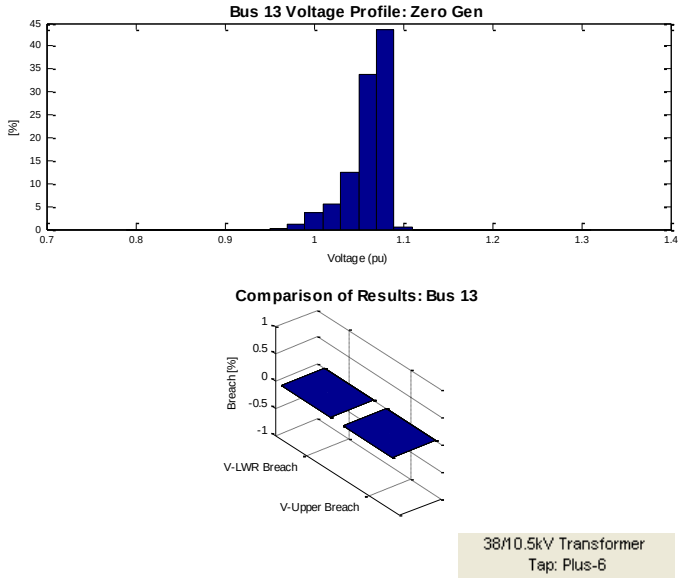

(b)

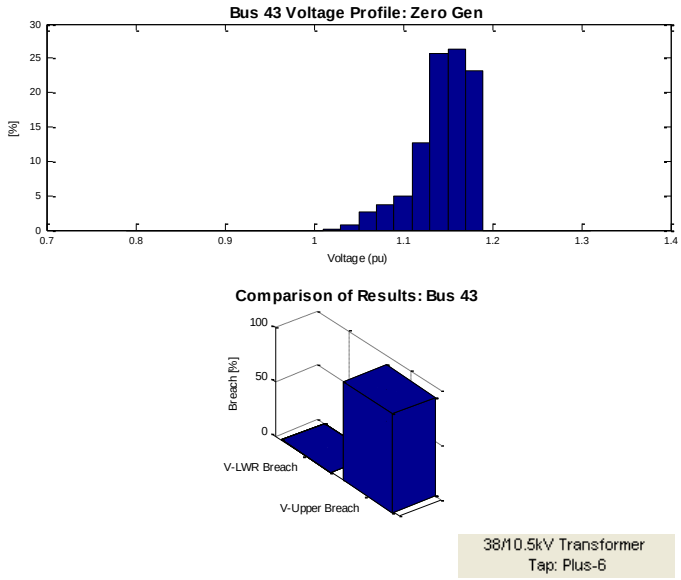

Figure 3.21: Voltage Tolerance Breach Analysis (Zero Gen); 38.5/10.5kV Plus-6 Tap and Variable Load

Looking closer at Figure 3.20, the consumer demand required is such that over the year, the minimum voltage level at Bus-13 (MV-Sub (10)) will be breached for 2.5% of the year for the nominal 38/10.5kV transformer tap. Similarly in Figure 3.21 (b), with the 38/10.5kV transformer on plus-6 tap, node 43 is within voltage tolerances, where as node 13 breaches the upper-most voltage tolerance in excess of 75% of the year. The

justification for this is as a consequence of the 38/10.5kV transformer tap setting and by virtue of the occurrences in the consumer load profile when consumer demand is at a minimum, thereby resulting in significant voltage increases across the system.

Figure 3.22 illustrates how the system voltage varies with respect to both the 10kV and 400V lines respectively for minimum and maximum loading (and zero generation).

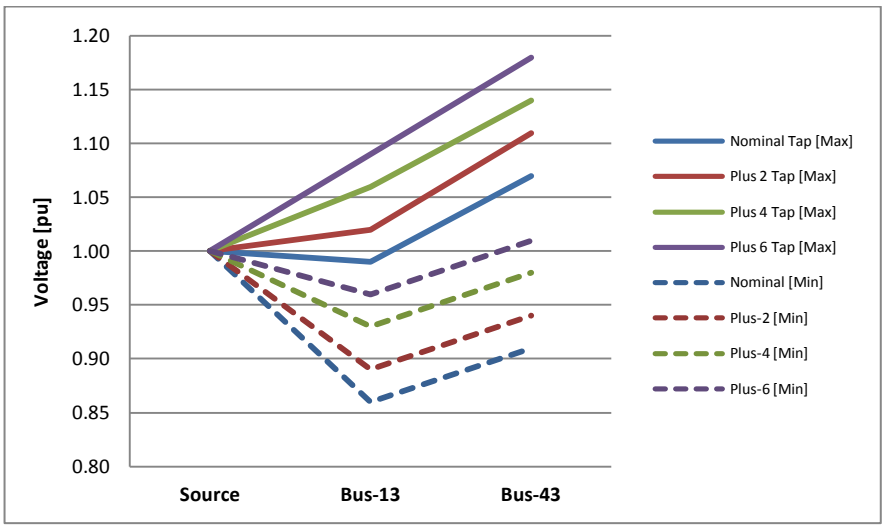

Figure 3.22 Network Voltage (maximum/minimum profile) with respect to varying the 38/10.5kV transformer tap (zero generation)

Similar analysis was then instigated with respect to the application of micro generation. The micro generation applied to the system included:

1. *Skystream 3.7*
2. *Whisper 200*
3. *Proven 2.5*

With regard to the representative distribution network, the criterion for analysing the voltage reaction of the representative distribution network is based on the following:

- The analysis was performed in terms of 50% and 100% generation capacity application onto the network in parallel with the consumer load. The performance of the network and the resulting voltage results were recorded and compared.
- As with the zero generation analysis, voltage breaches above and below the 10% constraints were also compared and for the worse case scenarios for the network (i.e. instances of maximum and minimum load conditions), the system voltage profile was plotted.

Figure 3.23 illustrates the network voltage profile for maximum and minimum load contingencies (worst case scenarios) with regard to the three generators and wind speed observations for the year in question (2008), including the respective annual consumer demand. Here generation capacity has been limited to 50% (i.e. 50% of the ratings of each of the wind turbines), with an associated operational power factor of 0.95 for each technology (as suggested in the PB Power analysis [109]). As a consequence of this power factor and with regard to a 50% generation capacity integration, 0.33kVAr, 0.79kVAr and 0.82kVAr would be delivered from the Whisper, Skystream and Proven technologies respectively per customer.

Again, the voltage at the end of the detailed 10kV line (MV Seg (10)) and 400V kine (LV Seg (10)) are highlighted for consideration. Figure 3.24 contextualises Figure 3.23 in terms of occurrences over the year when voltage levels breach the network high/low tolerances. Figure 3.24 further illustrates a comparison between the micro wind turbines in that as the *Whisper 200* is only a 1kW device, its contribution towards any over voltage issues will be substantially less than the other two technologies. Similarly, the *Skystream 3.7* has a lower capacity than the *Proven 2.5* so once again, the level of overvoltage prevalence is less, albeit not significantly less. Indeed, at consumer connection level (node 43), for a minus 4 tap on the 38/10.5kV transformer, an over-

voltage situation occur on 3.77%, 0% and 10.55% of the time (over the year in question) for the *Skystream 3.7*, *Whisper 200* and *Proven 2.5* devices respectively.

(a)

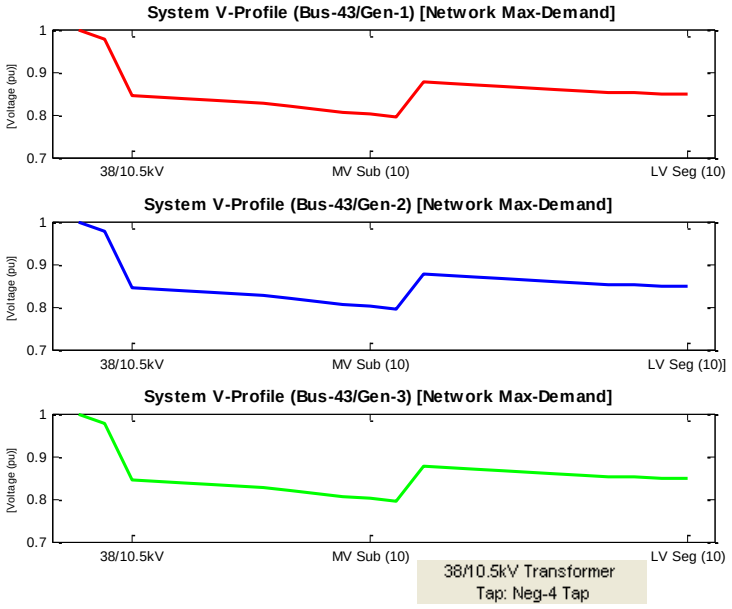

(b)

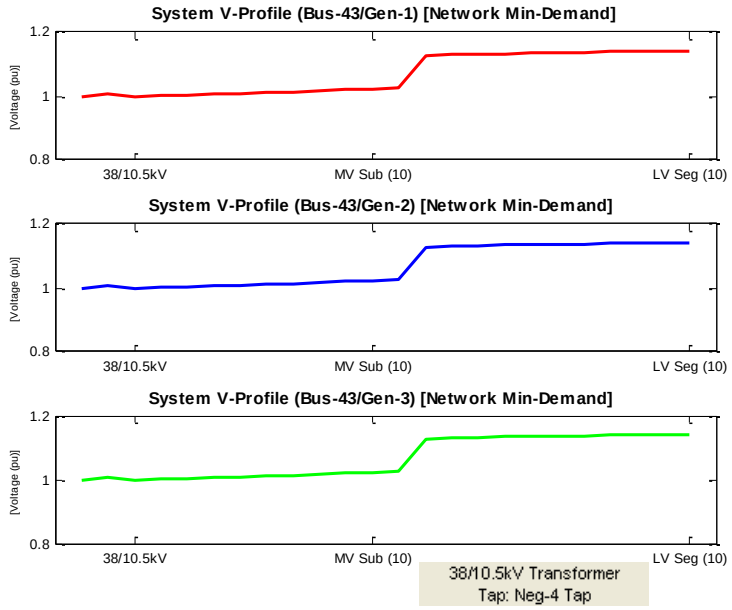

Figure 3.23 Network Voltage with respect to (a) Bus 13 (MV Seg (10)) and (b) Bus 43 (LV Seg (10)), (micro wind generators operating at 50% capacity)

(a)

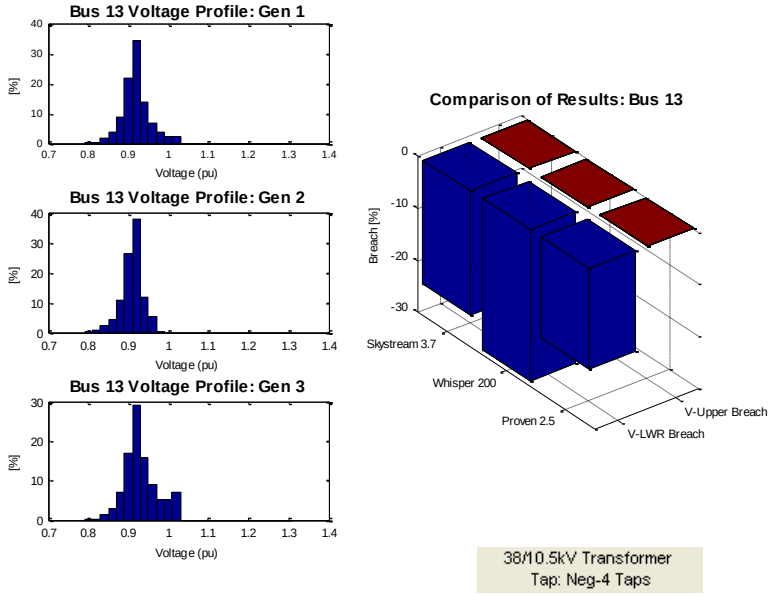

(b)

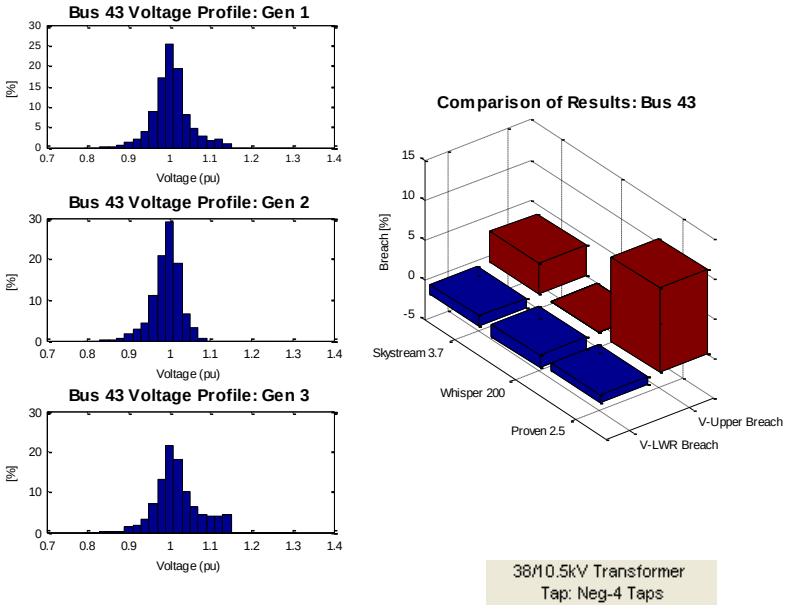

Figure 3.24: Voltage breach analysis for (a) Bus 13 (MV Seg (10)) and (b) Bus 43 (LV Seg (10)) (micro-generators operating at 50% capacity)

The minus-4 tap position is a sensible tap configuration in consideration of the generation capacity on the Network. Looking closer at Figure 3.23 and Figure 3.24 and with respect to maximum loading on the system, there is an issue with under-voltage primarily for a 10kV line and the last associated substation on the detailed line (MV Seg (10), or node 13). Here under-voltage occurs between 19.22% and 23.77% of the time

over the year for the Proven and Whisper technologies respectively. This is as a consequence of the negative tap setting applied to the 38/10.5kV network and more specifically with regard to the consumer at maximum demand and generation at 50% capacity. Table 3.7 summarises the network voltage profile including breaches for 50% generation capacity, with **Appendix A7** providing detail on network voltage levels for 0% and 100% generation capacities respectively. Figure 3.25 further emphasises the influence of the tap changer and over-voltage by considering the consumer connection voltage at the end of the 400V line (node 43) in terms of the three generation technologies.

Table 3.7 Variable Consumer Load and variable generation capacity (50%) and Network voltage

V_{BUS}[13]

		Gen-1				*Gen-2*				*Gen3*			
		V_{max}	V_{min}			V_{max}	V_{min}			V_{max}	V_{min}		
50% Generation	**Neg-6**	0.99	0.76	75.13	<90% V	0.94	0.76	85.98	<90% V	0.99	0.76	62.29	<90% V
				0.00	>110% V			0.00	>110% V			0.00	>110% V
	Neg-4	1.02	0.80	23.77	<90% V	0.97	0.80	29.05	<90% V	1.03	0.80	19.22	<90% V
				0.00	>110% V			0.00	>110% V			0.00	>110% V
	Neg-2	1.06	0.83	5.34	<90% V	1.01	0.83	6.46	<90% V	1.06	0.83	4.27	<90% V
				0.00	>110% V			0.00	>110% V			0.00	>110% V
	Nominal	1.09	0.86	0.74	<90% V	1.04	0.86	0.92	<90% V	1.09	0.86	0.59	<90% V
				0.00	>110% V			0.00	>110% V			0.00	>110% V
	Plus-2	1.13	0.89	0.10	<90% V	1.07	0.89	0.01	<90% V	1.13	0.89	0.01	<90% V
				3.87	>110% V			0.00	>110% V			10.81	>110% V
	Plus-4	1.16	0.93	0.00	<90% V	1.11	0.93	0.00	<90% V	1.16	0.93	0.00	<90% V
				10.50	>110% V			1.32	>110% V			20.31	>110% V

V_{BUS-43}

		Gen-1				*Gen-2*				*Gen3*			
		V_{max}	V_{min}			V_{max}	V_{min}			V_{max}	V_{min}		
50% Generation	**Neg-6**	1.10	0.81	5.78	<90% V	1.04	0.81	6.88	<90% V	1.11	0.81	4.59	<90% V
				0.23	>110% V			0.00	>110% V			1.22	>110% V
	Neg-4	1.14	0.85	1.19	<90% V	1.07	0.85	1.55	<90% V	1.14	0.85	0.89	<90% V
				3.77	>110% V			0.00	>110% V			10.55	>110% V
	Neg-2	1.18	0.88	0.05	<90% V	1.11	0.88	0.05	<90% V	1.18	0.88	0.05	<90% V
				9.46	>110% V			1.12	>110% V			19.01	>110% V
	Nominal	1.21	0.92	0.00	<90% V	1.15	0.92	0.00	<90% V	1.22	0.92	0.00	<90% V
				23.90	>110% V			12.97	>110% V			36.48	>110% V
	Plus-2	1.25	0.96	0.00	<90% V	1.19	0.96	0.00	<90% V	1.26	0.96	0.00	<90% V
				67.63	>110% V			60.59	>110% V			74.52	>110% V
	Plus-4	1.29	0.99	0.00	<90% V	1.22	0.99	0.00	<90% V	1.29	0.99	0.00	<90% V
				91.45	>110% V			89.79	>110% V			93.06	>110% V

Figure 3.25 illustrates the voltage derived at node 43 with respect to variation of the 38/10kV transformer tap settings.

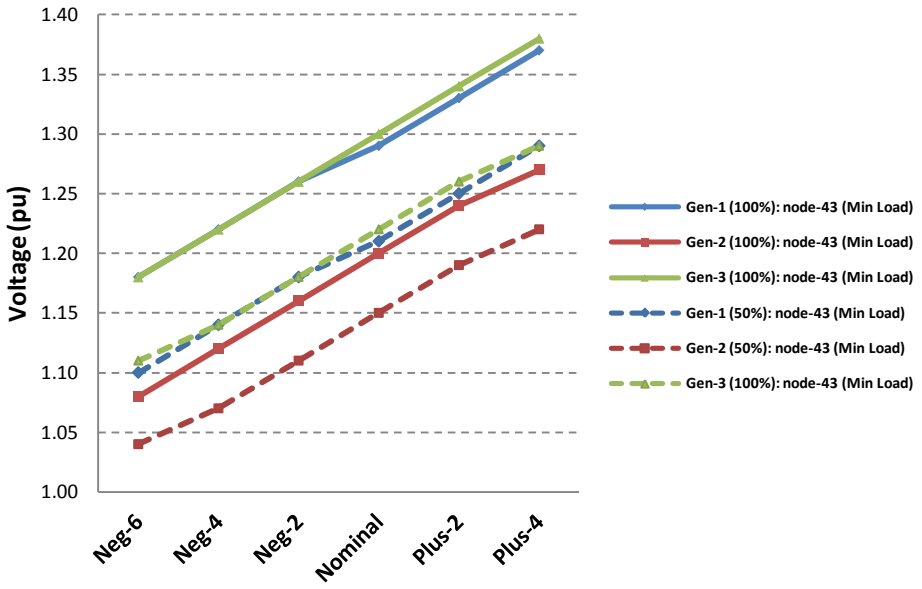

Figure 3.25 Voltage profile for the consumer connection at the end of the detailed 400V line

Figure 3.25 confirms that with respect to node 43, the final consumer connection location at the end of the detailed 400V line, even with generation at 50% capacity, network over-voltage tolerances will be breached for both the *Skystream* 3.7 and *Proven 2.5* technologies.

3.6 Conclusions

As distribution networks evolve, increased embedded generation will become more main-stream with microgeneration potentially participating in this regard. While the inclusion of this form of generation will derive benefits in the context of voltage support, reduced losses, distribution capacity release, infrastructural development deferral and ultimately, reliability improvements [117], there will also be detrimental implications; particularly in the form of high voltage proliferations [118].

The literature points towards a range of concerns including network congestion, power quality induced reliability issues, exasperations of voltage transients and network

capacity as well as health and safety concerns arising if islanding occurs. But the greatest concern would appear to be with regard to voltage rise as a consequence of increased proliferations of micro generation connection. There are control measures in place. For instance, CER and Ofgem, the energy regulators in Ireland and UK respectively, enforce connection logistics through respective parallel connection standards (EN50438 and G83).

A number of Government commissioned studies [108, 109, 124] have found that current distribution networks could accommodate this form of embedded generation at every consumer connection to the grid, even in contingency analyses considering minimum load and maximum generation (and vice versa), but many of these reports prioritise standard representations of both load and generation capacity and the associated analyses is based on defined circumstances. The issue with these circumstances is that the diversity of technologies and consumer freedom to source them reduces the control available to DNOs in ascertaining the capacity of the microgeneration technology installed – particularly as this microgeneration is non-dispatchable. In particular, the intermittency of microgeneration output could present capacity stress on the distribution network (especially with respect to wind generation). Cipcigan *et al* [131, 132] present a dichotomy between steady state and dynamic wind generation modelling/representation and micro wind generation integration into an SSEZ. In their analysis, they found the latter would contrive only marginal probabilities for voltage tolerance breaches, whereas the former would incur such breaches potentially with as little as 40% generation capacity integration.

A representative Irish distribution network was subsequently utilised to instigate preliminary investigations into micro wind generation integration. While representative consumer load and wind generation (incorporating wind observations) were utilised, the focus was on a balanced load perspective and specifically with regard to voltage rise contingencies. The network, while representative, did not facilitate single-phase load interrogation nor were network parameters including cabling and grounding considered.

Generation capacity was varied from zero to 100% (50% steps) and it was ascertained that for the range of technologies considered, network voltage rise could be an issue for two of the technologies (Proven and Skystream 3.7 with capacities of 2.5kW and 2.4kW respectively) even with the associated network transformers tapped at minus-6 with the generation at 50% capacity. The analysis considered the implications for the entire network with respect to the supply transformer (38/10.5kV) tap configuration.

The analysis leads towards investigating a more detailed network model and in the context of an urban environment, the incorporation of a representative wind resource. Chapter 7 will consider these issues holistically with the inclusion of a model for urban wind speed derived in Chapter 5 and the implications of turbulence as discussed in Chapter 6. The model will facilitate granular investigations down to end consumer level.

Chapter 4: Wind in Cities

4.1 Introduction

General adjectives that describe the wind resource include variability and unpredictability. Indeed a full understanding of the resource is further complicated due to the fact that these characteristics are geographically and temporarily interdependent. As Burton [146] describes the variability of the wind preserves over an extensive range of scales, both in space and time. This property is enhanced in built environments where airflow is highly disturbed.

There are many challenges in respect of incorporating wind generation into urban areas. These include the nature and variability of the wind resource, planning constraints associated with urban installations, manufacturer inconsistencies and financial concerns (predominantly the associated capital outlay). Planning issues primarily relate to noise and visual impact and some planning legislation effectively prohibits their deployment in residential areas [40] while elsewhere planning law is more permissive [147]. This inconsistency has undermined confidence in the market for urban based micro wind generation. Moreover, technical inconsistencies have not helped. For example there are disparities between the claims of manufacturers regarding the energy yield and the actual yields derived in the field [79]. The economic viability of this resource is linked to the rate of return on the capital investment, which partly depends on the financial

incentives available. These come in the form of Feed-in-Tariffs or grant schemes such as the '*Green Deal*' as outlined in Chapter 3. However, there are inconsistencies in the type of support provided. Despite these challenges, the overriding issue is our poor understanding of the available wind resource in the urban area that will allow us to assess the variability of the current technology.

Wind turbines are most efficient when air flow is strong and steady, that is high mean wind speeds with little variability in speed or direction. Urban areas disturb the airflow (reducing the mean wind speed and increasing variability) and produce sub-optimal environments for turbines. However, little is known of the actual wind resource in urban areas and a major (technical) barrier to the effective deployment of wind turbines in these areas is due to a lack of accurate methods for estimating wind speeds and energy yields at potential urban sites [148]. This is because cities are aerodynamically *rough* and heterogeneous and have a highly localised and complex wind environment. In contrast, there is significant research assessing the wind energy resource in non-urban or 'rural' locations around the world [32-34] where the resource is relatively predictable. That research has fed into assessing the potential for wind energy conversion systems using micro/small-turbines [35, 36]. There is no equivalent research on urban environments so that estimates of wind energy conversion are often based on arbitrary – even opportunistic – installations. Nevertheless as the global population becomes increasingly concentrated in urban areas [22], the potential for accessing the available wind resource cannot be dismissed without study.

This chapter will explore the complexities associated with the urban wind resource. Wind modelling and the available methodologies to acquire urban wind speed

references are also discussed. Two urban wind speed analytical models are prioritised and considered within the context of urban climatology. The first model was developed by Macdonald [149], in his work on modelling the mean wind velocity profile in urban environments. The second model developed by Fisher *et al* in the COST 715 Action Report [150] applies micro (urban) meteorology methods originally developed to considered air pollution. These modelling techniques contextualise the significant complexities associated with urban wind profiling in the range of optimal mounting positions relevant to micro wind turbine installations.

4.2 The Wind Resource

Wind velocity (V) is a vector with a magnitude (speed) and direction. For convenience, we often decompose the vector into movement along three perpendicular axes (x, y and z) such that

$$\mathbf{V} = u(\hat{\mathbf{a}}_{\mathbf{x}}) + v(\hat{\mathbf{a}}_{\mathbf{y}}) + w(\hat{\mathbf{a}}_{\mathbf{z}}) \tag{4.1}$$

where u, v and w represent speed along the *x*, *y* and *z* axis respectively (shown in (4.1) as unit vectors along the respective axes, $\hat{\mathbf{a}}_{\mathbf{x}}, \hat{\mathbf{a}}_{\mathbf{y}}$ and $\hat{\mathbf{a}}_{\mathbf{z}}$ respectively). Prioritising the horizontal flow (in the *x*-*y* plane) and consequently ignoring the '*w*' component, the magnitude of the polar horizontal velocity at any instant (i), is given by (4.2)

$$\left|V_{(i)}\right| = \sqrt{(u_{(i)})^2 + (v_{(i)})^2} \tag{4.2}$$

The mean is provided in (4.4) and the standard deviation in (4.3)

$$\overline{V} = \frac{1}{N_s}\sum_{i=1}^{N_s}(\left|V_{(i)}\right|) \tag{4.3}$$

$$\sigma_V = \sqrt{\frac{1}{N_{s-1}} \sum_{i=1}^{N_s} (|V_{(i)}| - \overline{V})^2}$$

(4.4)

where N_s is the number of samples and $V_{(i)}$ and $\overline{V}$ are the wind observation and mean wind speed respectively.

Wind is a highly variable property of the atmosphere both in space and time. The available wind resource at a place depends on global/local geographical conditions, the height above the Earth's surface and weather conditions. Temporal variations of wind speed can be divided into categories of inter-annual, annual, seasonal, diurnal and short-term [151]. Figure 4.1 (extracted from [151]), summarises the time and space variations of atmospheric motion as applied to wind energy. With regard to micro wind turbines, as will be discussed more specifically in Chapter 5, the spatial detail has a significant role to play, particularly with respect to the sensitivities these technologies have to the variability of the wind resource.

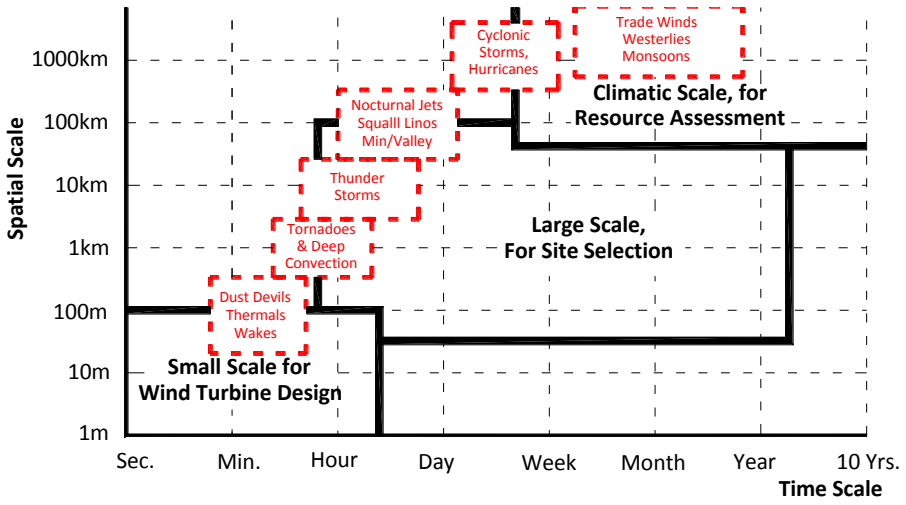

Figure 4.1 Spatial and temporal variation in the wind resource (interpreted from [152])

Wind speed variations can be annual and seasonal at any particular location. Annual variations in the wind resource are not simple to estimate, particularly if the wind speed is subject to a slow long term variation. From a wind engineering perspective, probability distribution analysis using established probability density functions (PDFs) such as the Rayleigh and Weibull PDFs, are commonly employed to more accurately characterise annual wind speeds [32-34, 36, 37]. However, as Chapter 5 (section 5.3) will illustrate, these tried and tested approaches are complicated in urban environments.

Wind speed variations over shorter timescales other than annual and seasonal variances, while containing definite patterns, are still difficult to estimate or predict [146]. The characteristics of the wind speeds over these shorter timesales may be considered in terms of their kinetic energy distribution in the frequency domain (described by the *van der Hoven spectrum* [153]). Van der Hoven described the power spectrum of horizontal wind speed by analysing wind speed observations at the upper three levels of a 125m meteorological tower (Brookhaven New York), He found two distinct energy peaks in the observed spectrum at approximately 4 days and 1 minute. The former corresponds to the movement of synoptic scale pressure systems while the latter reflected micro scale turbulence driven by mechanical and convective processes. Other work on wind spectra identified an additional peak at 24 hours, which corresponds to the diurnal cycle of heating [146].

Depending on the period of examination, we can decompose the wind field into a mean and fluctuating component.

$$V_{(i)} = \overline{V} + dV_{(i)} \tag{4.5}$$

where $\overline{V}$ is the mean wind speed and *dV* is a fluctuating or turbulent wind component.

In a wind turbine productivity context (as will be discussed in detail in Chapter 6), the averaging period is chosen as 10 min [154], which is representative of the macro meteorological changes in wind speed manifested as slow fluctuations of the mean wind speed - whereas the *dV* term denotes the turbulent wind speed component. Optimal conditions for turbine productivity are when the wind velocity is strong and steady (high mean wind speed and small fluctuating component). Conversely, low wind speeds and turbulence reduce turbine productivity [92, 105, 155]. One measure of the relative importance of turbulence is Turbulence Intensity (TI) [146], which may be defined as "*the ratio of wind speed standard deviation to the mean wind speed, determined from the same set of measured data samples of wind speed, and taken over a specified time"* [154]. Specifically, for a set of wind observations in the horizontal plane it is the standard deviation of the wind speed σ normalised by the mean.

$$T.I. = \frac{\sigma_{\mathrm{V}}}{\overline{V}} \tag{4.6}$$

where in (4.6) $T.I.$ is a longitudinally defined turbulence intensity and σ is the standard deviation of the observed wind in the horizontal plane (as defined in (4.4)).

Turbulence is driven by two processes, which can often act together. Forced (or mechanical) turbulence is generated by friction with the Earth's surface, which acts as a momentum sink. The effect of the surface extends vertically through the atmosphere as momentum is transferred to the surface. The depth of this effect depends on both the ambient wind-speed and the roughness of the surface. Roughness describes the 'texture' of the surface and accounts both for the individual roughness elements and how they

interact: an urban surface that consists of large obstacles is very rough by comparison with a short grass surface. Free (or thermal) turbulence is a result of differences in atmospheric density caused by surface heating. The intensity of turbulence from this source is a function of atmospheric stability [156]: a stable atmosphere impedes vertical motion and dampens free convection whereas an unstable atmosphere encourages it. The effect of instability is to transfer the effects of the surface momentum sink to a deeper layer of the overlying atmosphere (which is explained in section 4.3).

4.2.1 Wind Turbines and Capacity Factor

Wind turbines extract kinetic energy from moving air, converting it into mechanical energy via the turbine rotor and then into electrical energy through the generator. The two factors that regulate power then are the turbine technology and the wind resource. The power generated is proportional to the cube of the wind-speed, so that small variations in wind speed will have a significant impact on the wind turbines productivity.

The two properties that distinguish a specific turbine technology are its blade sweep area and its power curve. The former governs the amount of power that can be captured from the available wind on site while the latter describes performance with varying wind speed. Evaluating the power curves have come a long way from a time where little or no validation was undertaken [16]. This is particularly, for example, in the UK, where the Microgeneration Certification Scheme has been introduced [89]. The UK MCS defines its own power curve based on site assessment and as the regulating body, this is the only power curve that can be used for marketing purposes. That said, wind turbines are not tested on a large amount of sites and power curves are defined by averaging results from multiple sites of varying conditions.

The cumulative energy output of a generator is often presented as a capacity factor: the ratio of the measured turbine yield to the maximum output over a given time period. Establishing the capacity factor *a priori* is essential for calculating the economic return on investment in wind turbine technology. For example, in the UK the measured capacity factor ranges from 24% in Durham to 33% in Caithness, or an average capacity factor of 28.4% for network scale on-shore wind [16]. To evaluate the capacity factor accurately, knowledge of the wind resource is critical. Broadly speaking, there are two approaches to acquiring this knowledge: detailed modelling of the atmospheric physics (Computational Fluid Dynamics) and; empirical estimation based on boundary layer theory and surface descriptions.

Computational Fluid Dynamics (CFD) tools are ideally suited to evaluating the wind resource at specific locations. However, as they resolve the detailed physics of atmospheric processes they require a great deal of information at each site and are therefore very computationally resource intensive. Some researchers have used CFD modelling to ascertain the potential of building mounted turbines [21, 157, 158]. This work has shown the sensitivity of energy output to turbine position and mounting height with regard to the building, such that small changes in location can have dramatic impacts on performance. However, this approach is of limited value for routine site evaluation, which commonly estimates the wind resource at a site of interest from observations made at a nearby location, which are subsequently adjusted for the location of interest. Employment of CFD simulation provides useful guidance as to the best location for small wind turbines above a given specific building or within a given street. However, due to cost and time constraints, it is not possible to apply this method to

consider the wind speed across a wide spatially heterogeneous location such as an urban area [95].

Empirical tools employ our acquired knowledge of the atmospheric boundary layer to estimate the properties of near surface airflow from standard observations adjusted for local considerations (e.g. variations in the roughness of surface cover and terrain). These schemes derive vertical profiles of the horizontal wind. For example, the μ-wind modelling software uses data from a number of sites across the UK to characterise the wind potential for wind turbine [76]. The tool accounts for terrain roughness and height of turbine. There are also wind atlases which have been developed based using air flow models that account for the effects of topography and provide estimated wind speed at 10m (and higher) above the surface at a horizontal scale of $1km^2$ [158]. These wind atlases estimate the mean wind speeds over an area as a function of height by employing both the regional wind climate and the roughness characteristics of the surface [159]. For example, the small scale wind resource study [160], was later developed into a freely available tool by the Carbon Trust (*Wind Estimator*) [148]. A modern form of wind speed estimation, as suggested by Drew *et al* [95] is through the *Department of Energy and Climate Change* (DECC) database [17, 161]. These types of wind speed profiling tools/databases generally employ transfer functions to transfer the properties of regional scale wind climates to an area of interest.

The empirical techniques have proved useful in evaluating locations for wind farms where turbines are located in an exposed setting at a considerable height above extensive surfaces that are relatively homogenous (grass, crops or shrub). However, they are of limited use for microgeneration in cities where buildings generate considerable turbulence and the urban terrain is heterogeneous. Millward-Hopkins *et al*

[162]) employed large-scale wind speed climatology data bases such as the *Numerical Objective Analysis of Boundary Layer* (NOABL) database to predict wind speeds in typical urban and suburban areas using heterogeneous block arrays to estimate the effects of urban roughness. In other research deWit *et al* [163] used a scaling factor to estimate wind close to rooftops based on observations taken at a standard meteorological site, located at a nearby Airport. Nevertheless, there remains a need for observations of wind speed close to urban rooftops to provide validation for model results [157].

4.2.2 Wind Resource Complexity

The frictional aspect affecting the wind resource is manifested at heights relatively close to the ground and by how rough the surface is. Above a certain height, air flow is considered to be independent of surface influences, and is dependent on large-scale synoptic pressure differences and the rotation of the earth. However, closer to the ground, the effect of the earth's surface can be recognised and experienced. This 'layer' near the surface in which the velocity changes from zero at the surface to the free stream value away from the surface is described as the *boundary layer*. As wind moves past the ground the wind speed is reduced due to the friction related to ground surface. The magnitude of this friction is dependent on the texture of the surface. The farther one moves away from the surface, the less affected the wind becomes by the object surface. The influence of the surface is effectively limited to the lowest 10km of the Atmosphere in the troposphere and over the period of a day, this influence is restricted to a much shallower zone known as the planetary or atmospheric boundary layer [156]. This layer is characterised by well developed mixing (turbulence) generated by the aforementioned frictional drag and by air parcels deriving momentum from the heated surface [156].

The boundary layer height varies with time and depends on the strength of the surface-generated mixing and this thermal mixing (convection) facilitates a boundary layer which is generally below 2-3km during the day [164-166]. With respect to air flow, or wind within this height range, the surface characteristics or *roughness* effectively defines both the magnitude and nature of the wind resource, with friction causing the wind speed to be slowest near the ground [165]. The *surface roughness* of the earth's surface refers to how homogeneous or heterogeneous the surface characteristics are that define the particular area. These areas can consist of grassland, high-rise buildings and even water sources. Urban surfaces, for instance, are aerodynamically very rough and the individual roughness elements (i.e. buildings and trees) are often arranged into patterns that may generate organised motions both between and above buildings. Variations at building and street scales have the net effect of either channelling or retarding airflows so that at the height of roof tops an intense shear layer forms where wind-speed and direction change rapidly with height.

However, depending upon the scale one considers, all surface roughness characteristics are analogous to blades of grass in a field. The influence that the grass has on the wind resource is limited to heights very close to the ground. In a similar way, high-rise buildings, while they obviously affect the wind resource, eventually at some height this influence is effectively removed. In other words, heterogeneity in landscape can be considered as homogeneity if the height above the surface is sufficient. In this way, surface roughness characteristics (z_0) are grouped into classifications or *lengths* describing how fractious or rough a particular landscape might be [156, 167]. The next level above the surface roughness length, z_0, is the zero-plane displacement height, which is the effective zero wind speed height or the height above the ground at which

the wind speed has zero magnitude as a consequence of flow obstacles such as buildings or trees.

As Stull explains, if individual roughness elements, such as houses in a city, are packed close enough together, then the average roof-top level begins to act on air flow like a displaced surface [165]. Table 4.1 extracted from [156], details the aerodynamic properties of natural surfaces.

Table 4.1 Aerodynamic properties of natural surfaces [156]

Surface	**Remarks**	z_0 Roughness length [m])	***d***, Zero-plane displacement [m]
Water	Still – open sea	$0.1 – 10.0 \times 10^{-5}$	-
Ice	Smooth	0.1×10^{-4}	-
Snow		$0.5 – 10.0 \times 10^{-4}$	-
Sand, desert		0.0003	-
Soils		0.001 – 0.01	-
Grass	0.02 – 0.1m	0.003 – 0.01	≤0.07
	0.25 – 1.0m	0.04 – 0.10	≤0.66
Agricultural crops		0.04 – 0.20	≤3.0
Orchards		0.5 – 1.0	≤4.0
Forests	Deciduous	1.0 – 6.0	≤20.0
	Coniferous	1.0 – 6.0	≤30.0

Wind flows encountering significant changes in such surface classifications (e.g. boundaries between a rural and urban environment), have to adjust to the new surface characteristic and as Elliot (1958) and Panofsky and Dutton (1984) showed, the new surfaces causes a new boundary layer to grow called an *Internal Boundary Layer* (IBL) [95]. Internal boundary layers are significantly developed disturbance layers in the near-surface layer, which are generated by horizontal advection over discontinuities of the surface properties (roughness, thermal properties, etc.) [168]. In these circumstances the local surface characteristics govern the wind profile, but above the height of the newly created IBL, the wind profile remains characteristic of the upwind surface [95]. Figure 4.2 describes such a *step change* in surface roughness and how it affects both the wind

and turbulence profiles. The figure illustrates how a deviation in surface roughness results in a zone of turbulent mixing and the consequence is that the boundary layer depth increases as does the height above the zone of deviated surface roughness before the resultant wind speed profile acquires equilibrium. Ultimately the modified wind speed profile - with an associated decreased mean wind speed - extends deeper into the zone of altered surface roughness before said equilibrium is achieved. This extension is known as fetch. Fetch describes the distance involved where post interaction with an obstacle, the wind regime retains uniformity. In urban environments, non uniform fetch in conjunction with local advection, give rise to variable internal boundary layer development.

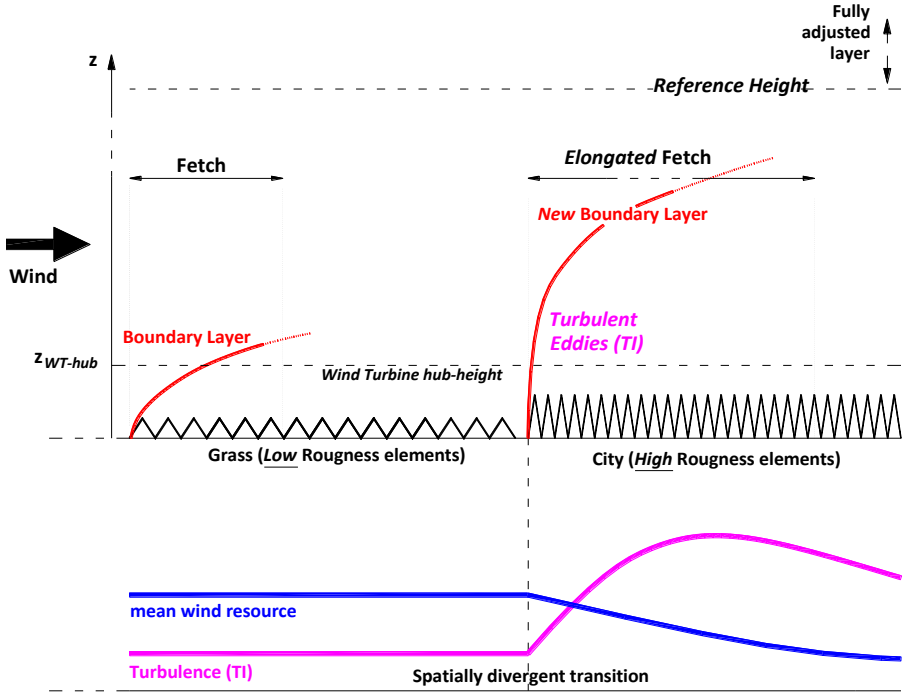

Figure 4.2: Change in wind resource as a consequence of step-change in roughness.

The influence of surface roughness in the context of a wind profile is discussed further in Section 4.3, which considers boundary layer theory more specifically.

4.3 Boundary Layer Theory

Section 4.2 introduced the concept of atmospheric boundary layers to describe the effects on air flow as it encounters surface form. This section will develop this concept further to describe how urban (morphometric) complexity affects the urban wind resource. The concept of a 'boundary layer' arises where a moving fluid meets a solid boundary. The layer of air near the ground responds to spatial and temporal changes in the properties of the surface. The surface essentially influences transport processes such as the transfer of heat, mass and momentum so as to modify the properties of the lowest couple of kilometres of the atmosphere. Closer to the ground, the surface influences the boundary layer by friction and by heat fluxes at the ground. In this way, wind shear and temperature gradients can either generate or suppress turbulence.

The dominant process climatologically, in the lower atmosphere, governed by the vertical air temperature, is convection and it is defined as *free, forced* and *fixed* convection or more specifically, how air (or eddies) transport energy and mass from one location to another. *Free convection* or natural convection is where heat itself causes air (parcel) motion via expansion and a buoyancy force. *Forced convection* depends on the roughness and depends on the speed of the horizontal flow. In this regard forced convection is derived when heat is carried passively (heat advection). *Mixed convection* occurs due to free and forced convection coexisting.

The type of convective activity, as described in Oke's work on boundary layer climatology, is also influenced by the vertical temperature structure as expressed by *stability* [156]. Stability is described in [156] in terms of the relative tendency for an air parcel to move vertically. It can be evaluated (in a dry atmosphere) by comparing values

of *environment lapse rate* (ELR), which is a measure of the actual temperature structure as sensed by thermometers above a given location, to the dry adiabatic lapse rate (Γ), which describes how an air parcel will warm/cool as it is moved vertically through the atmosphere. This ratio has three possibilities. *Unstable Atmospheres (*ELR > Γ), arise when there is a considerable amount of surface heating causing warm air near to the surface to ascend. As the air rises it will eventually cool but if the associated cooling is insufficient to facilitate cooling of the air to form thermal equilibrium, said air will continue to rise manifesting large-scale eddies. Restrained stratification occurs if the cooling effect causes the rising air to become cooler than the existing air results in *Stable Atmosphere* (ELR < Γ). Stable conditions occur on cooler nights when the ground surface is cool. Turbulent eddies created in this context are as a consequence of the frictional relationship the air as flows over the ground. Finally, *Neutral Atmospheres* (ELR = Γ) are derived in the boundary layer under cloudy, windy conditions where cloud restricts surface heating/cooling thereby minimizing the development of horizontal temperature stratification and the wind helps to homogenize the temperature structure through vigorous mechanical convection. Figure 4.3 [156] explains how urban wind profile is a function of (i) surface and (ii) thermal structure.

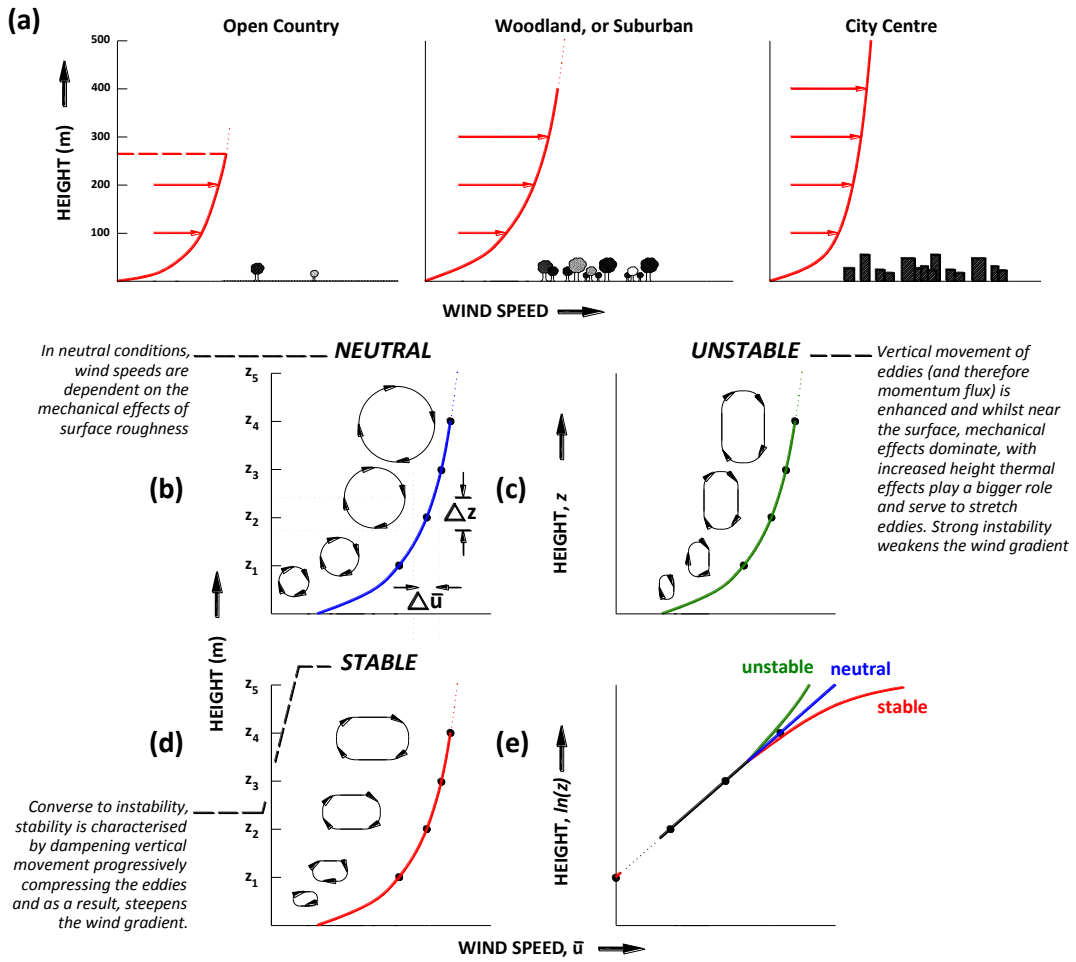

Figure 4.3 Wind Speed profile development close to the ground
(a) the effect of terrain roughness, with (b) to (e) illustrating the effect of stability on the profile shape and eddy structure (*Source:* interpreted from [156])

Figure 4.3 (a) shows that the effect of increasing surface roughness is to deepen the atmosphere that is affected. The horizontal wind speed depends on the roughness of the surface with the vertical gradient of mean wind speed, $\partial u/\partial z$ being greatest over smooth terrain. Figure 4.3 (b) to (d) illustrate the influence of thermal structure. The relationship between the surface roughness and the atmosphere is essentially modulated by the thermal atmospheric structure.

The actual form of the wind variation under neutral stability is described by a logarithmic decay curve which provides the basis for the logarithmic wind profile (4.7).

In neutral conditions buoyancy, which is sensitive to temperature stratification, is less influential and cloudy skies and strong winds are prevalent. Cloud reduces radiative heating and cooling of the surface with strong winds promoting mixing without strong temperature stratification.

$$u(z) = \frac{u_*}{\kappa} \ln\left(\frac{z - z_d}{z_0}\right) \quad \textbf{(4.7)}$$

where, z_o is the roughness length and z_d is the displacement height; the roughness length is a measure of the drag exerted on the wind by the underlying surface – higher values indicating more drag [169]. The displacement height (z_d) is the effective zero wind speed height. In this way, this "effective ground level" is not the base of the buildings but some point within the vertical plane of the urban canopy and represents the level at which the log relationship might produce zero wind (obtained from (4.7)), whereas, varying z_d changes the effective origin from which height is measured. The frictional velocity (u_*) is a measure of the shearing stress that drives the flux of momentum to the Earth's surface, $u_* = \sqrt{\tau / \rho}$ (τ being the turbulent shear stress and ρ being the density of air). Finally, κ is the *Von Karmans constant* and is approximated to 0.4. A topic of considerable research is the application of (4.7) outside of urban environments.

This relationship (4.7) describes wind-speed in the direction of airflow within a boundary layer where airflow has adjusted to the underlying surface. It is properly applied to extensive homogeneous surfaces (such as grass) under neutral atmospheric conditions and is valid under these circumstances to heights (z) above ($z_d + z_o$). Typical values for the roughness length are listed in Table 4.2.

Table 4.2 Davenport classification of effective terrain roughness [170]

Roughness Class	Roughness length (z_0) [m]	Description of landscape
Approx. Open	0.1	Moderately open country with occasional obstacles (e.g. Isolated low buildings or trees) at relative horizontal separations of at least 20 obstacle heights
Rough	0.25	Scattered obstacles (buildings) at relative distances of 8 to 12 obstacle heights for low sold objects (e.g. buildings)
Very rough	0.5	Area moderately covered by low buildings at relative separations of 3 to 7 obstacle heights and no high tress.
Skimming	1.0	Densely built-up area without much building height variation.
Chaotic	2.0	City centres with mix of low and high-rise buildings (Analysis by wind tunnel advised)

The MET Office report compiled by Best *et al* [160] explains that the displacement height quantifies flow blocking effects [160]. To use (4.7) requires values for the friction velocity, the displacement height and the roughness length. These can be obtained from standard wind observations where instruments are positioned above an extensive short grass surface ($z_0 \approx 0.1$ m) in neutral conditions. In these circumstances, wind speed plotted against the log of height will be described by a straight line with an intercept at z_0 and u_* can be obtained from its slope. The profile is not sensitive to the value for z_d, which is approximately equal to 2/3 the average height of the surface roughness elements (essentially 0 m in the case of short grass).

The logarithmic wind profile is a topic of considerable research outside of the urban environment, but the highly heterogeneous morphologies associated with the roughness elements within cities will significantly impact its applicability within the urban SL.

4.4 The Urban Boundary Layer

The vertical structure of the *urban boundary layer* (UBL) has been outlined by Oke and Grimmond [156, 167] based on observations. As described by Rotach *et al* (2002), the urban boundary layer has a complicated three dimensional structure making it difficult

to comprehensively describe [150]. Figure 4.4 provides an (idealised) sketch of the structure. The urban boundary layer is characterised by the exceptionally large surface elements such as buildings and trees and indeed, the aerodynamic 'stiffness' of the buildings therein, presents increased complexity compared to environments characterised by trees, bushes and grass [150].

In a horizontal plane, the distinctive changes in the roughness properties within a city, particularly at a city's edge, lead to the formation of an internal boundary layer. At the lee side of a city, a new urban boundary layer will grow upwards as the wind transitions into the city so flow in this regard will extend downwind as a plume (Figure 4.4 (a)). Such internal boundary layers will also be developed in transitions from suburban to urban environments and potentially between zones of significantly differing surface characteristics, each transition deriving individual plumes.

In the vertical plane and again described in Figure 4.4 (a), the UBL is composed of two distinctive atmospheric layers, the mixing layer (ML) and surface layer (SL). In the SL, the air is in contact with the surface and there are strong vertical gradients in both temperature and wind and the associated atmosphere responds to surface forcing on an hourly time scale. The SL is further described in terms of three distinctive atmospheric layers. The lowest of these is the *urban canopy layer* (UCL). The UCL extends from ground level to the approximate height of the surrounding roof level (z_{Hm}) and is characterised by micro-scale effects (Figure 4.4 (c)). Here, processes are dynamic and dictated by the immediate locality resulting in extremely complex flow. The UCL is part of the roughness sub-layer (RSL). The RSL extends from up to 2 - 4 times the height of the local buildings [167, 171] to the *wake diffusion height*, z* and is

mechanically and thermally influenced by length-scales associated with the roughness of the environment [172]. Observations here will measure contributions from a great variety of distinct urban surfaces (buildings, roofs, trees, gardens, etc.), which may be difficult to attribute. Above the RSL is the inertial sublayer (ISL). The effects of the individual surface types are 'blended' in this region (Figure 4.4 (b)), and momentum and turbulence fluxes are constant therein with height.

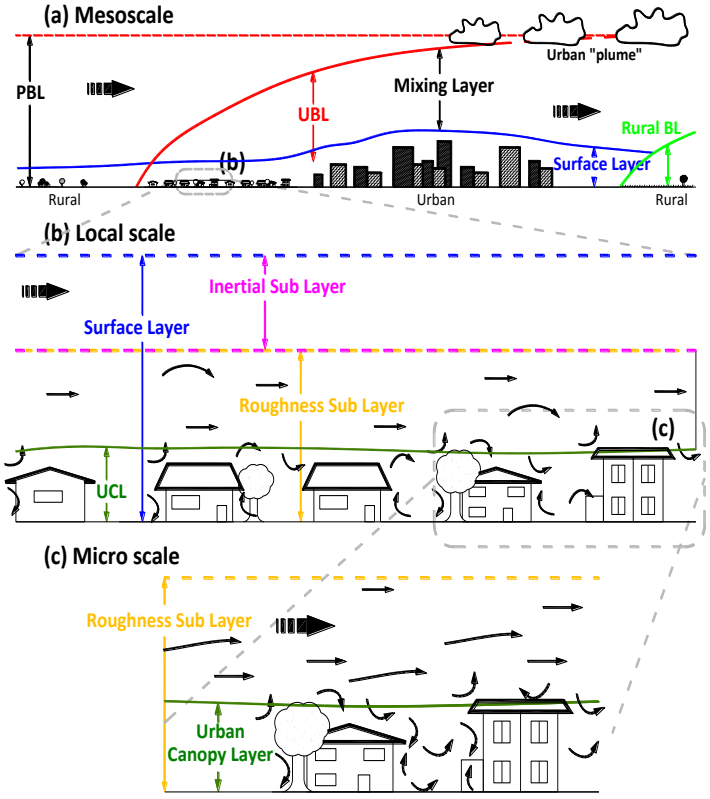

Figure 4.4 The atmospheric layers describing the urban boundary layer (UBL) (source: interpreted from) [160]

In the context of small/micro wind energy systems, the roughness and inertial sub-layers are the most relevant in terms of potential for harnessing the wind resource in the urban setting. In the inertial sub layer (down to the roughness sub layer), the wind shear is represented by the logarithmic expression as described by (4.7), but the complexity of the wind environment below the inertial sub layer (within the roughness sublayer) makes for difficult surface roughness parameterisation. In this regard, the application of

the logarithmic profile therein (i.e. $z < z*$) is also difficult. Work by Cheng and Castro [173] has shown however, that a single log-law spatially averaged mean velocity in the roughness sublayer is however achievable, provided an appropriate u_* for the surface is known.

Ricciardelli's work on the characteristics of the wind in the lower boundary layer suggests that the flow in the roughness layer is dictated by the uniformity of the building height and the building aspect ratio (ratio of the average building height to the average street width), H/W [174]. In the UCL, the flow is almost completely governed by street geometry and building height distribution. Therefore the flow is aerodynamically separated by the characteristics in the upper layers; especially in the case in which the buildings are closely spaced [174]. With respect to urban wind applications and their installation, the mean wind speed and surface stress within the SL are the most significant considerations. The surface stress, in particular, characterises the turbulence levels and mean wind speeds within the UCL and RSL [160].

As a consequence of heat output from the city, urban climates tend to be more unstable than neutral [175], however, in climates such as the Irish climate, the characteristically high wind speeds, neutral stabilities dominate (which will be discussed further in section 5.4.1). Therefore, for a given wind direction, in conjunction with enhanced mixing and decreased thermal stratification, a neutral urban boundary layer is promoted. The research carried out by Metzger and McKeon [176] demonstrates that in neutrally stable environments, surface roughness dominates turbulence production. From a wind resource perspective the associated building morphology as well as the roughness length

of the urban surface, z_0, are the significant parameters to be considered when assessing the turbulent structure of air masses [161, 176, 177].

4.4.1 Building Morphology and Roughness

The complex morphology experienced in an urban environment results in a modified flow and turbulence structure in the urban atmosphere in contrast to the flow over 'ideal or homogenous' surfaces [171]. Mertens [72] proposes that TI can be linked to the surface roughness parameter in (4.7).

$$T.I. = \frac{1}{\left| \frac{z - z_d}{z_0} \right|} \tag{4.8}$$

This equation, (4.8), is predicated on z (the observation height) being greater than the wake diffusion height (z*), which is above the surface roughness sub layer and into the inertial sub layer (Figure 4.4). Equation (4.8) further suggests that there will be an increasing level of turbulence with increasing roughness and decreasing height relative to the earth's surface.

Studying the UBL is particularly complicated by the difficulties associated with the diversity of surface elements. In their analyses of urban air flow, Fernando *et al* [178] discuss the sensitivity to building morphology as well as the direction of approach winds. Grimmond and Oke [167] considered how urban air flow is affected by the *packing* of roughness elements. In their consideration of of the surface roughness parameters (z_0, z_d), two classes of approach are available: 1) morphometric (or geometric) methods that use algorithms that relate aerodynamic parameters to measures of morphometry; and 2) methods that employ field observations of wind or turbulence

[167]. Morphometric methods are based on empirical relations derived from wind tunnel work that concern idealised over simplified arrays of roughness elements.

Figure 4.5 illustrates flow regimes common in 2D obstacle clusters with approach flow normal to the leading edge [160].

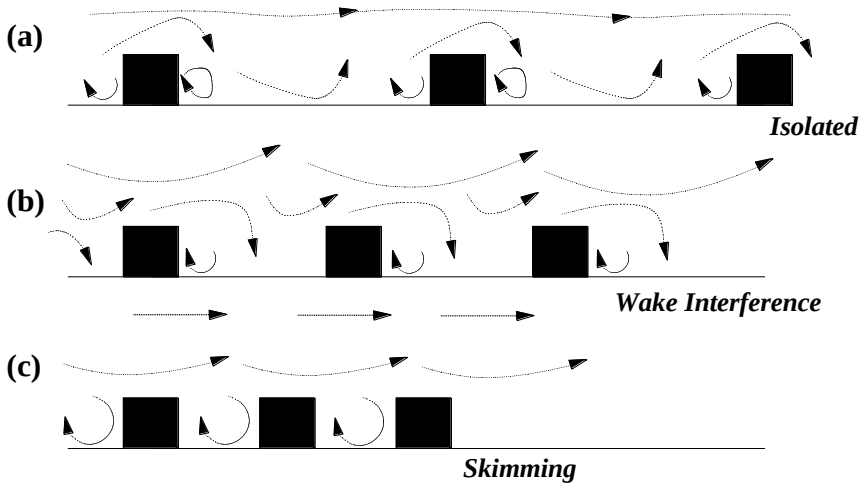

Figure 4.5 Flow regimes with respect to 2D obstacles (source: interpreted from [160])

Three types of flow are identified in Figure 4.5 and are described as *isolated*, *wake interference* and *skimming* flows. When roughness-element density is low and the roughness elements are *isolated*, in the sense that each is outside the main wake area of the element upwind; an isolated flow regime is derived. Associated with this regime are low magnitudes of z_0 and z_d, which increase with increasing density. Conversely, w*ake interference* is the resultant of the wind not having space to recover its undisturbed profile between one roughness element and the next and this is manifested at intermediate densities. In this regime there is also an increase in z_0 and z_d as the density of the surface increases, until at a certain density, z_0 reaches a characteristic peak [179]. Skimming flow regimes are such that the roughness elements block the wind at canopy

level resulting in a displacement of the origin of the wind profile upwards to near the top of the canopy.

In this regime mutual sheltering of the obstacles increases with surface density, leading to a reduction in the drag and a decrease in z_0. The displacement height, z_d, however continues to increase with density, but the rate of increase gradually slows. However, as Millward Hopkins demonstrates [179], height heterogeneity within urban environments means that it is possible for the flows illustrated in Figure 4.5 to be mixed. Figure 4.6 explains this point in that for a simple staggered height arrangement, flow can be characterised by a mixing of skimming flows (within the dense canopy) and wake interference flows (around the sparser tops of the larger blocks).

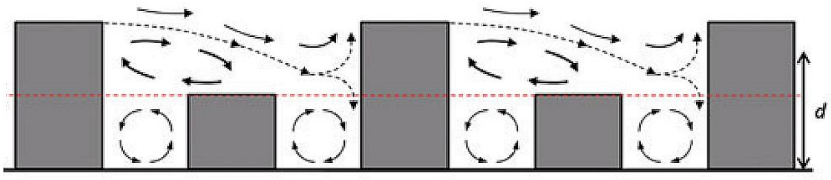

Figure 4.6 2D flow regimes within height heterogeneous blocks (extracted from [179])

The practicalities of cities mean however, that rather than 2D blocks of equal height as illustrated in Figure 4.5 (or indeed staggered blocks with varying height in Figure 4.6), the urban boundary layer has a complicated three dimensional structure [150]. In that regard, morphometric descriptions are often considered in terms of the plan air density (λ_p) and the frontal area density (λ_f) of block arrays as illustrated in Figure 4.7 [167].

$$\lambda_p = A_P / A_T \qquad \lambda_f = A_F / A_T \tag{4.9}$$

where A_P is the total plan area of the roughness element(s) as seen from above and A_T is the total surface area and where A_F is the total frontal area.

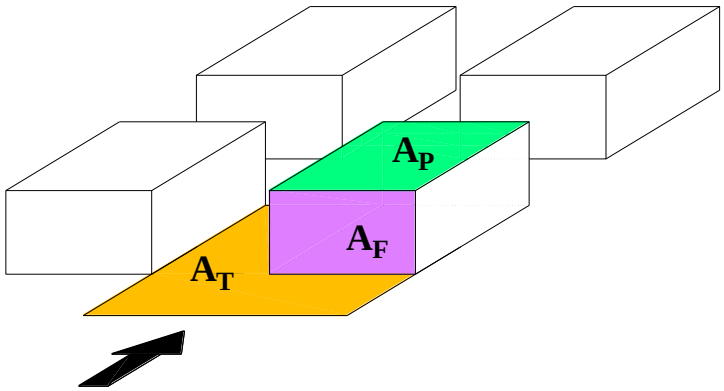

Figure 4.7 Illustration of the areas considered when calculating the different area densities Originally based on work carried out by Grimmond & Oke [167] (*Source:* interpreted from [160])

Cities, however, cannot be represented by staggered block arrays, as presented in Figure 4.7, as this is not an accurate representation of the complexity of roughness elements prevalent within these environments. Grimmond and Oke [167] consider Figure 4.7 in terms of flow regimes but further presented heuristic arguments in attempt to explain the effects if extra roughness elements are included (Figure 4.8). Figure 4.8 attempts to contextualise the realities for cities in terms of the flow regimes described in Figure 4.5. Figure 4.8 illustrates that isolated flow occurs when $\lambda_p \approx 0.1$. Wake interference will occur for plan air densities in the range of $0.1 < \lambda_p < 0.4$, whereas skimming flow will occur for a plan air density, $\lambda_p > 0.4$. Eventually, at $\lambda_p = 1$, a new surface is formed of height z_{hm}, implying that z_d is now equal to z_{hm}. Figure 4.8 further suggests the urban roughness element densities for real cities (shaded envelopes).

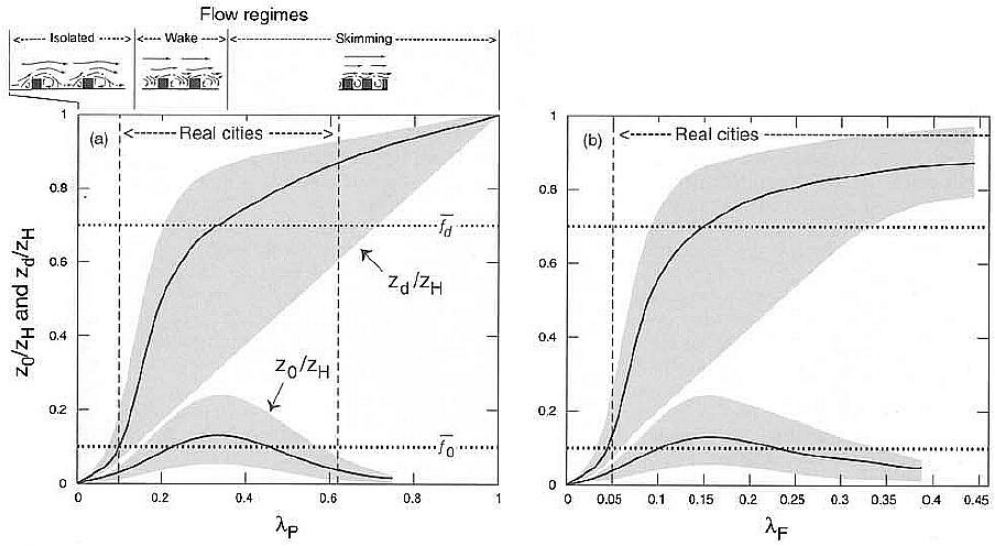

Figure 4.8 Relationship between height-normalised values of zero-plane displacement (z_d/z_H) and roughness length (z_0/z_H) and the packing density of roughness elements using λ_p (a) and λ_f (b) to describe density(source extracted from [167])

However, in considering Figure 4.8 in the context of real urban environments and their heterogeneous characteristics, two characteristics of cities are not included. Firstly, as reported by Millward-Hopkins [179] variation of building heights may prevent skimming flow from occurring. This has the effect of *softening* the characteristic z_0 peak found at the transition from wake interference flow to skimming flow, causing it to become shifted towards higher densities [180]. Secondly, the upper limit for uniform arrays of $z_d/z_{hm} = 1$ is no longer valid, and indeed, for heterogeneous arrays z_d/z_{hm} can exceed unity [173, 180, 181].

Grimmond and Oke [167] employ the plan density (λ_p) and the frontal area density (λ_f) in estimating the surface roughness parameters (z_0 and z_d). These surface parameters can subsequently be employed in urban wind speed estimation through the logarithmic profile (4.7) or approximations involving the logarithmic profile [182]. Alternative approaches, include, for instance, the method developed by Weekes and

Tomlin [183], where they employed a method developed by Raupach [184], as illustrated in (4.10) and (4.11)

$$\frac{z_d}{z_{Hm}} = 1 - \frac{1 - \exp(-\sqrt{15\lambda_f}}{\sqrt{15\lambda_f}}$$

(4.10)

$$\frac{z_0}{z_{Hm}} = 1 - \frac{z_0}{z_{Hm}} \exp\left(\frac{\kappa}{\min\left(\sqrt{0.003 + 0.3\lambda_f}.0.3\right)} + 0.193 \right)$$

(4.11)

There, estimates of z_{Hm} and λ_f are based on typical values found in UK cities as described in reference [160]. Drew *et al* [95] considered an alternative morphometric approach as derived by MacDonald [185] and described in (4.12) and (4.13)

$$\frac{z_d}{z_{Hm}} = 1 + A^{\lambda_p}\left(\lambda_p - 1\right)$$

(4.12

$$\frac{z_0}{z_{Hm}} = \left(1 - \frac{z_d}{z_{Hm}}\right) \exp\left(-\left[0.5\beta \frac{C_D}{\kappa^2} \left(1 - \frac{z_d}{z_{Hm}}\right) \lambda_f \right]^{0.5} \right)$$

(4.13)

where C_D is the drag coefficient of a single obstacle (C_D=1.2 as recommended in ESDU (1980)). A is a coefficient derived from experimental evidence and β is a parameter which modifies the drag coefficient to a value more appropriate to the particular configuration of obstacles [185]. More general classifications of surface roughness are also available. Davenport provides general classifications for the surface parameters (Table 4.2, [170]). The more morphometric approaches, as described in [167, 183, 185] consider specifically the three dimensional nature of the urban surface parameters.

These models lack consideration of both spatial and vertical surface element heterogeneity; geometrical factors that can significantly affect wind profiles above urban surfaces [179], which include oblique approaching winds [180], the addition of pitched roofs to buildings [186], and variations in building height [173, 180, 181] and are the reality of cities. Of these factors, Millward-Hopkins [179] further contends that height variability may be one of the most significant factors influencing surface parameters.

An alternative, but more simplistic alternative, to surface roughness parameterisation instead considers zones of roughness classification is presented by Stewart and Oke in [187]. In that research, categorisation of urban 'neighbourhoods' in terms of their significant climatic effects on the overlying atmosphere (Figure 4.9) led towards a *local climate zone* (LCZ) classification system.

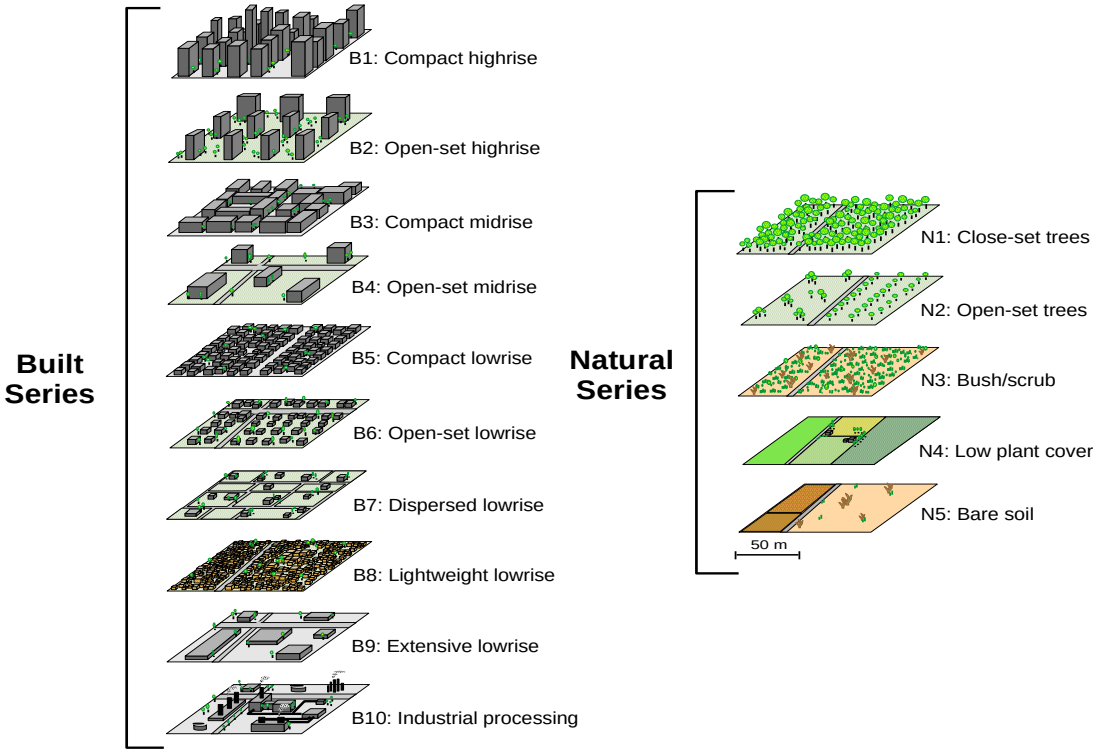

Figure 4.9 Categorisation of types of urban 'neighbourhoods' (source: extracted from [188])

While this type of classification is primarily employed in consideration of the urban heat island, each zone has specific surface roughness attributes and these can be utilised in the consideration of urban wind profiles.

With regard to wind energy applications and the morphometric influence of the urban roughness elements in the horizontal plane, isolated and skimming flow regimes offer optimal installation criteria. Wake interference flows, on the other hand, should be avoided. However, the vertical urban wind profile is also complicated. As part of the *Basel Urban Boundary Layer Experiment* (BUBBLE) [189] (a year-long experimental effort investigated the boundary layer structure in the city of Basel, Switzerland), the vertical wind profile of the urban wind resource was also considered. Figure 4.10 illustrates mean annual wind profiles at three (sub) urban sites contained within the experiment representing the characteristics for the whole observation period including different wind directions and stabilities. Here *z* denotes the local height where the variable is evaluated. The horizontal error bars represent run-to-run variability (25 and 75% quartiles respectively). The figure illustrates that the available wind resource is increasingly depleted into the UCL and at z_{Hm} there is an inflection point.

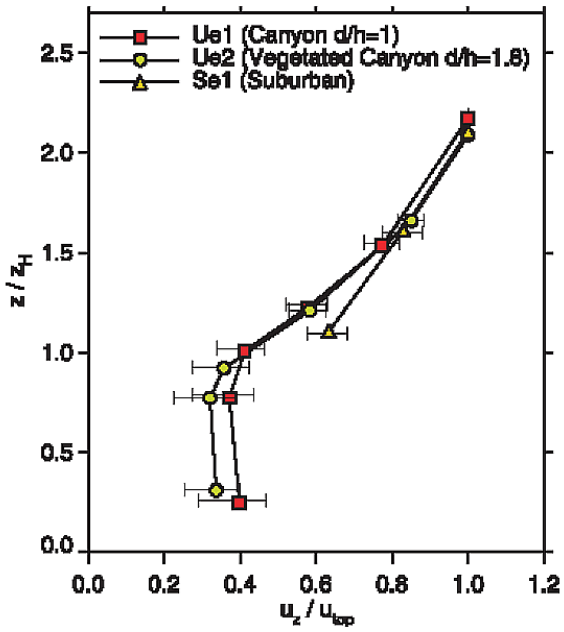

Figure 4.10 Mean annual profiles at three (sub)urban sites with horizontal mean wind speed scaled by wind speed at z/z_H, (source: extracted from [189])

The surface roughness parameters previously identified in conjunction with the morphometric considerations are commonly applied to the logarithmic profile (4.7) in the consideration of analytical urban wind speed modelling [95, 148, 183]. Indeed, as discussed in the COST 715 Action [150], "urban modifications" in meso-scale numerical models are often restricted to modifying the roughness length. The big question however, is the range of viability for (4.7) and what profile(s) are employable outside of this range. Section 4.5 will explore these concepts further.

4.5 Urban Wind Modelling

Best *et al* in [160] discuss, in general terms, the range of approaches to urban wind profiling within the UBL applicable to wind energy (Figure 4.11, which is an interpretative flow diagram of [160]). The diagram further shows modelling considerations within the different atmospheric sub layers in terms of the associated parameterisation required for wind speed estimation.

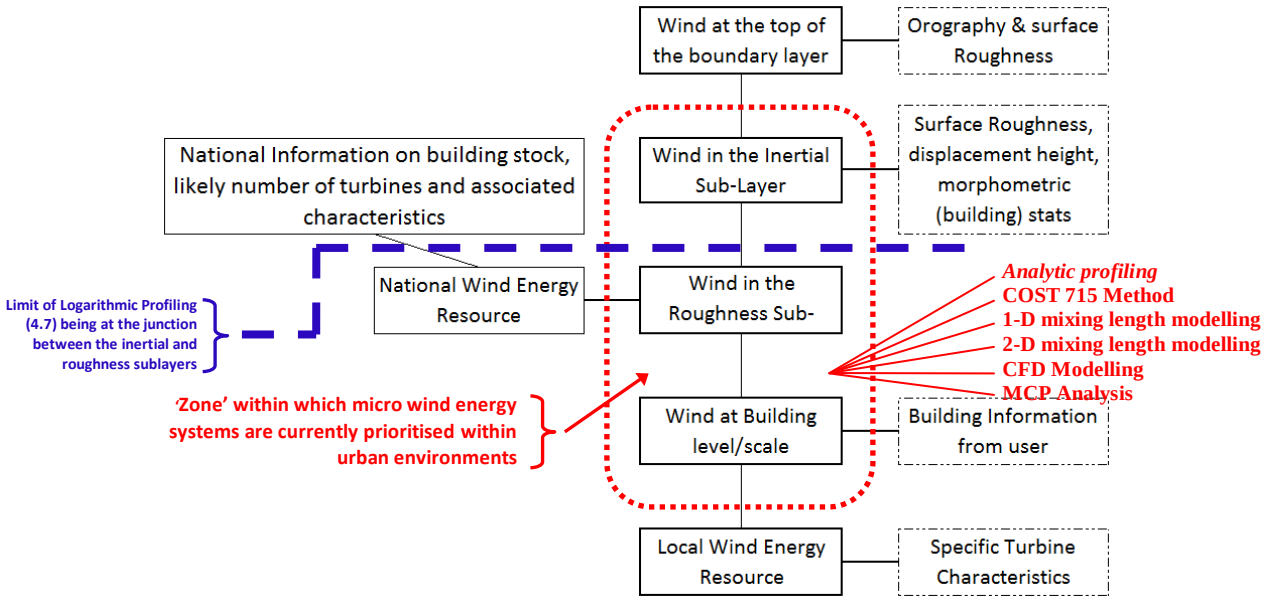

Figure 4.11 Generic Methodologies for Estimating Urban Wind Energy in a boundary layer context (source: adapted from [160])

This section prioritises analytical urban wind profiling, which relates a variation of the standard log law (4.7) to wind flow above the UCL in conjunction with a reference profile. Oke's '*Initial guidance to obtain representative meteorological observations at urban sites'* [170] a methodology, derived by Wieringa [182] is proposed that the log profile could be employed to estimate wind at a site of interest (site B), based on observations made at a nearby reference site (site A),

$$u_{zA} = u_{zB}\left(\frac{\ln\left(z_r/z_{0B}\right).\ln\left(z_A/z_{0A}\right)}{\ln\left(z_B/z_{0B}\right).\ln\left(z_r/z_{0A}\right)}\right) \qquad \textbf{(4.14)}$$

Mertens in his work relating to the energy yield of roof mounted wind turbines [72, 190], presents a similar methodology to extrapolate a rural wind into an urban setting in terms of a step change which was further developed by Heath [157]. These formulations require information on the roughness lengths at the respective sites and at a reference height (z_r), which is sufficiently distant from the underlying surfaces that their distinct aerodynamic effects have been erased.

4.5.1 Analytical Wind Modelling

Two analytical wind profiling methods are considered here for detailed consideration: 1) MacDonald employs a simple model that was originally developed for vegetative canopy flows [149] and 2) an applied meteorological methodology, conceived primarily to consider air pollution [150].

MacDonald [149], modified a vegetative canopy flow model for application to arrays of three-dimensional surface obstacles. The basic premise is to consider the flow within the RSL in three distinct layers. The uppermost layer is defined in terms of a logarithmic profile, the lowest is defined by an exponential relation and finally, the paper presents an approach for understanding the 'mid-range' 'transition-ary' layer. Heath [157] employs a similar extrapolation method to Mertens in analysing the energy potential of micro wind energy systems. His approach employs a computational fluid dynamics model to simulate the wind flow around a simple pitched roof building and investigate the potential energy yield of a micro wind turbine installed at optimal heights within an urban canopy. Watson, Harding and Infield in their work on predicting the performance of small wind turbines in the roof-top environment [149], synopsise the work by both Mertens and Heath by initially using a Wind Atlas to identify a local mean speed to investigate - based on local building geometries - the temporal and spatial averaged wind profile in the roof-top environment. A CFD analysis was subsequently employed to model the flow as it passes through different arrays of simple houses in order to develop an appropriate Weibull wind speed distribution to calculate micro wind turbine yield and capacity factor.

The applied methodology, conceived primarily to consider air pollution, is described in the COST 715 Action [150]. This approach applies meteorology to urban air pollution problems in which particular attention is paid to estimating airflow in the layer between the displacement height (z_d) and the top of the RSL, at z*. This method involves integrating the inertial sub layer flux-gradient relation using the local flux at each height together with an analytic description of the flux profile. A simplification or recipe for estimating the urban wind speed is based on an urban reference wind speed. The approach was evaluated using wind observations acquired as part of the Basel UrBan Boundary Layer Experiment (BUBBLE) [189], which included instruments located within both urban and rural settings.

4.5.2 Method 1: MacDonald Approach [149]

MacDonald [149] investigated the hypothesis that in the modelling of urban wind speed, it is fundamentally incorrect to extrapolate the logarithmic profile into the (urban) roughness sub layer. Indeed, MacDonald's work asserts that in the estimation of urban wind speed, the log law profile is applied outside its range of validity by extrapolating it down to $z = z_0 + z_d$ (the theoretical zero-velocity level). MacDonald proposes in his analysis that the extent of the inertial sub layer lies between $z = 2(z_{Hm})$ and $z = 0.25(z_{UBL})$ with z_{UBL} being the height of the boundary layer.

MacDonald's consideration of the UBL is in terms of three distinct sections:

1. $z_d < z < z_{Hm}$, defined by an ***exponential profile***
2. $z_{Hm} < z < \{z = (2 \to 4).z_{Hm}\}$, a ***'transition-ary' stage*** where an explicit model is currently undefined, but MacDonald suggests that this transition is 'matched' by assuming a simple turbulence length parameterization between z_{Hm} and. z*
3. $z^* < z < z_{UBL}$, defined by the ***logarithmic profile***

Macdonald's research [149] is based on work that considered mean wind speed profiles for vegetative canopies. In his application to an urban setting he treats obstacles as two-dimensional cylinders with sectional drag of $C_D(z)$ with the assumption that at each cross section there is local equilibrium, i.e. balance between obstacle drag force and local shear stress. On that basis, the wind resource is estimated by adapting a *Prandtl mixing length* (gradient-diffusion) model for momentum transport in the canopy and making the further assumption that the mixing length scale and the sectional drag within the canopy are constant. *Mixing length theory* is used to calculate the turbulent shear stress.

4.5.2.1 UCL Considerations

MacDonald's research led to a description of the wind profile below the mean building height z_{Hm}. This exponential profile is described by (4.15).

$$u(z) = u(z_{Hm}) e^{\left\{a\left(z/z_{H_m} - 1\right)\right\}} \tag{4.15}$$

where, $u(z_{Hm})$ is the mean velocity measured at the top of the obstacles ($z = z_{Hm}$), a is a constant (also referred to as an attenuating factor) dependent on the building morphology (similar to that outlined in Figure 4.7) and is described by both MacDonald [149] and Heath [157] as:

$$a = 9.6\,\lambda f \tag{4.16}$$

For crude calculations, the attenuator factor, a, can be approximated by a straight line in terms of the frontal density with $\lambda f \leq 0.3$ (4.16).

4.5.2.2 Integrating the UCL and RSL: The 'Transition-ary' Sub layer

Above the wake diffusion height, z*, the wind speed velocity profile follows the semi-logarithmic profile and some means of matching between the exponential and semi-logarithmic profile is required (in the range $z_{Hm} < z < z*$). This may be achieved by assuming a linear variation of the turbulent mixing length, l_c in this matching region (l_m).

$$l_m = l_c + \left(\frac{z - z_{Hm}}{z_0 - z_{Hm}} \right) \left(\kappa \left(z* - z_d \right) - l_c \right) \tag{4.17}$$

where in (4.17), l_c is the *mixing length* in the canopy layer and in this context refers to the Prandtl mixing-length (gradient-diffusion model) describing air parcel momentum transport in the canopy.

The methodology proposed by Heath in [157] is to assume that u_* is constant in the shear layer above the obstacle canopy and

$$\frac{\partial u}{\partial z} = \frac{u_*}{l_m} = \frac{u_*}{A + Bz} \tag{4.18}$$

where in this equation,

$$A = l_c - \left(\frac{z_{Hm}}{z* - z_H} \right) \left(\kappa \left(z* - z_d \right) - l_c \right); \qquad B = \left(\frac{1}{z* - z_{Hm}} \right) \left(\kappa \left(z* - z_d \right) - l_c \right)$$

Integrating (4.18), $\left(\int \frac{\partial u}{\partial z} = u(z) \right)$, and considering the boundary condition $u = u(z_{Hm})$ at $z = z_{Hm}$,

$$u(z) = \frac{u_*}{B} \ln \left(\frac{A + Bz}{A + Bz_{Hm}} \right) + u(z_{Hm}) \tag{4.19}$$

Equation (4.19) facilitates a means to ascertain the mean wind speed values at heights,

($z_{Hm} < z < z*$). Above this height ($z > z*$), the semi-logarithmic profile is employable.

4.5.2.3 MacDonald's Urban Wind Speed Parameters

Whilst (4.19) is solvable [149], this solution requires considerable input data:

a) $u(z_{Hm})$, the wind speed at mean building height
b) l_c, the mixing length scale
c) z_0, the surface roughness, z_d, the displacement height and $z*$, for the wake diffusion height
d) u_*, the friction velocity at the *building* height.

MacDonald [149] considers acquiring values for (a), $u(z_{Hm})$ (c), l_c and (f), u_*, as representing the biggest challenges.

a) $u_{(z_{Hm})}$, the wind speed at mean building height

MacDonald's approach requires observed wind speeds at (roughly) the mean building height at the location(s) in question so that extrapolation up/down is achievable.

b) l_c, the mixing length scale

MacDonald [149] considers two methods. The first ascertains the drag coefficient, $\overline{C_{DH}}$, on the basis of height-averaged mean square velocity over the face of the obstacles

$$\frac{l_c}{z_{Hm}} = \left(\frac{\overline{C_{DH}} . \lambda_f \left(1 - e^{-2a}\right)}{4a^3} \right)^{0.5} \quad \textbf{(4.20)}$$

where $\overline{C_{DH}}$, the mean drag coefficient (surface mounted cubes) in a shear flow = 1.2 [191] and a is established from (4.16). The second approach expresses l_c from the boundary condition at the top of the canopy, by estimation based on the mean wind speed (as observed at the top of the building(s)).

$$\frac{l_c}{z_{Hm}} = a^{-1}\frac{u_*}{u(z_{Hm})} \tag{4.21}$$

c) Surface roughness parameterisation (z_0 and z_d) and wake Diffusion Height (z*)

As discussed in section 4.4.1(and described in [167]), the surface roughness parameters can be evaluated through morphometric methods (as described in Section 4.4.1) or by micrometeorological (or anemometric) methods that use filed observations of wind turbulence to solve for the aerodynamic parameters.

The wake diffusion height (z*) is a poorly defined parameter. Grimmond and Oke in [167] cite a number of references for this parameter in the range of $2.5z_{Hm} < z^* < 4.5z_{Hm}$ where z_{Hm} is the average building height. Raupach *et al* in [192] recommends $z^* = z_{Hm} + 1.5(W)$, in which W is the building width. An alternative to the description for z* in the context of the prevalence of turbulence within the urban sub layer, z*, is described in terms of the height where maximum Reynolds stress occurs. This implies considering the height where the influence of individual roughness elements (buildings) on mean wind and turbulence profiles and where said influence vanishes. Accordingly, Rotach in his work simulating urban-scale dispersion using a lagrangian stochastic dispersion model [193], suggests $z^* \geq 2z_{Hm}$.

The displacement height, z_d, can be estimated in terms of the distribution and density of buildings (the roughness elements). The simplest method as proposed by [167] suggests that $z_d = (0.7).z_{Hm}$.This however, is very much a simplification. Section 4.4.1 Illustrated how, in the context of building height heterogeneity can cause z_d/z_{hm} to exceed unity [173, 180, 181]. Indeed, in this regard, z_d/z_{hm} varies between 0.5 and 1.5 with λ.

Millward-Hopkins [179] developed a model to derive a height normalized zero-plane displacement height by dividing the canopy into sufficiently many distinct, horizontal layers, n, so that each layer is of uniform height with different flow patterns occurring within each layer. When these layers are stacked vertically to obtain the original heterogeneous array, z_d is approximated by taking the height normalized zero-plane displacement of each layer multiplied by the layers thickness and summing over all the layers.

d) u_* the friction velocity at the building height.

Bottema, in his work investigating aerodynamic roughness parameters for homogeneous building groups [194], estimated the frictional velocity (at a height, $z = z*$) based on

$$\left(\frac{z_{0_{URBAN}}}{z_{0_{RURAL}}} \right)^{\beta} = \frac{u_*(z^*)_{URBAN}}{u_{*RURAL}} \qquad \textbf{(4.22)}$$

where β = 0.0706.

A basic criticism applicable to MacDonald's approach, is that both methods are based on wind tunnel data from arrays of buildings within homogeneous heights. More recent work is investigating the affect of three-dimensional heterogeneity on the aerodynamic surface properties [179-181]. Understanding this heterogeneity can be applied towards estimating spatially-averaged vertical profile, such as the models proposed by Cheng and Castro [173], or Millward-Hopkins *et al* [179].

The semi-logarithmic profile can also be utilised to derive a value for $u_*(z^*)$ in a rural context so that values $u_*(z^*)$ can be estimated on the basis of z_0. A flow chart that holistically describes the implementation of MacDonald's approach is illustrated in Figure 4.12.

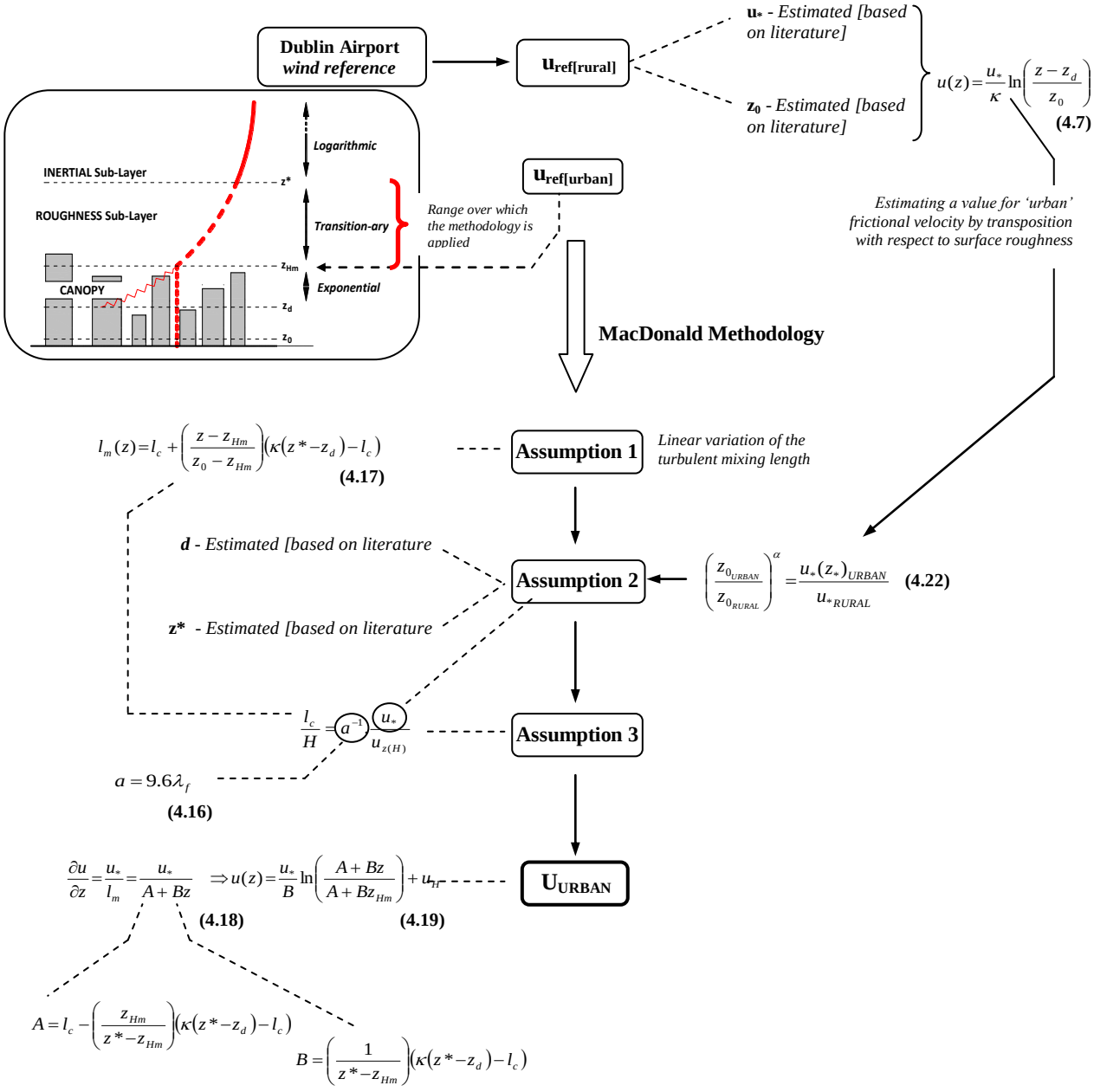

Figure 4.12 MacDonald Urban Wind Resource Estimation Methodology

4.5.3 Method 2: COST Approximation

In the COST 715 Action report compiled by Fisher *et al* in [150], a methodology for estimating the wind speed in the urban roughness sub layer using observations at other sites is developed. The COST approach was evaluated using wind observations acquired as part of the *Basel UrBan Boundary Layer Experiment* (BUBBLE) [189], which included instruments located within both urban and rural settings. BUBBLE is one of

the most spatially detailed urban boundary layer experiments and working group 1 of COST 715 investigated practical methods for obtaining appropriate meteorological data for undertaking urban air pollution calculations. A 'recipe' for estimating urban wind speed was derived based on three steps:

a) Step 1: Estimating the surface roughness parameters (z and z_d)*

This is estimated as per the analytical approach described in 4.5.2.3.

b) Step 2: Estimating u_*

The basis of this step is that the Reynolds stress varies with height within the roughness sub layer. Above the height of the urban roughness (in this context above z*), the logarithmic wind speed profile is employed, but below z* an allowance for variation of friction velocity with height (i.e. within the roughness surface sub layer) as proposed by Rotach [193]:

$$\left(\frac{u_*(z)}{u_*(z^*)}\right)^b = \sin\left(\frac{\pi}{2}.Z\right)^a \qquad \textbf{(4.23)}$$

where, in (4.23), z* represents the height of the urban roughness sub layer and z_d represents the displacement height and $Z = \frac{z - z_d}{z^* - z_d}$, where $0 \le Z \le 1$ and the relation is plotted for *a= 1.28 & b= 3.0*

c) Step 3: Estimating the wind speed

Step 3 of the COST approach uses a reference speed at z* to extrapolate into the UCL. This reference wind speed as described by Wieringa [182] is acquirable through a rural/urban wind speed step, which is also endorsed by Mertens [190] and Heath [157].

Figure 4.13 illustrates the rationale for such an extrapolation. By segmenting the 'stepped' approach, the logarithmic profile (4.7) is utilised to acquire, a value for $u_*(z^*)$ so that through (4.23) values for $u_*(z)$ at any height, z, in the range $z^* \geq z \geq z_d$ is attainable.

A rural wind speed reference (u_1) is logarithmically extrapolated to a height, z_1 in the inertial sub layer that can be assumed to be in equilibrium over a long fetch of constant roughness z_{01}. The urban inertial sub layer wind profile as a function of fetch from the edge of a roughness change from rural to urban environment(s) is established. This (urban) inertial sub layer wind profile is then employed to derive the upstream surface friction velocity in terms of $u(z_1)$, z_1 and z_{01}. If one assumes neutral conditions the frictional velocity, u_*, can be considered constant within the boundaries of the inertial sub layer. From the inertial sub layer, the wind speed can be related back down to a height within the urban environment.

Mertens, Heath and Watson in [190], [157] and [158] respectively, employ a wind atlas to ascertain the reference wind speed u_1 at height z_1 and surface roughness z_{01} upstream of the step while the urban wind speed downstream is given by (which is relatable to the Wieringa approach [182]):

$$u(z) = \frac{\ln \frac{(z - z_d)}{z_{02}}}{\ln \frac{(z_{UBL} - z_d)}{z_{02}}} \times \frac{\ln \frac{(z_{UBL})}{z_{01}}}{\ln \frac{(z_1)}{z_{01}}} u_{REF} \qquad \textbf{(4.24)}$$

In (4.24) z_{UBL} is the height of the internal boundary layer and Watson *et al* in their work [158] uses:

$$z_{UBL} = m \times z_0 \left(\frac{x}{z_0} \right)^{0.8}$$

(4.25)

In (4.25) Taylor and Lee suggest $m = 0.75$ [195] for a local surface length z_0 and x, is the fetch down-stream of the roughness change and for instance Heath[5] in [157] uses x = 1000m.

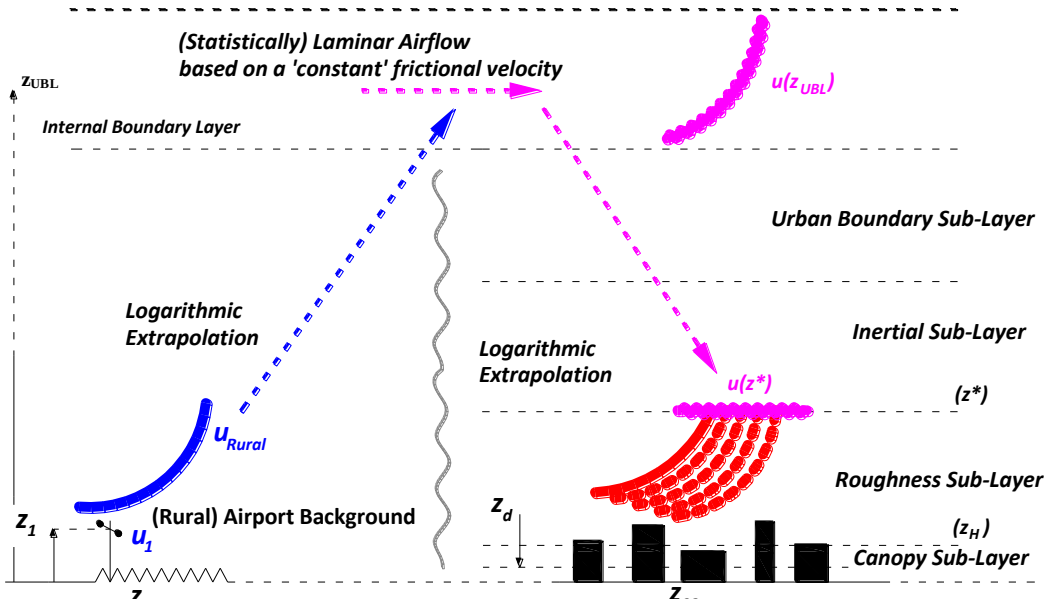

Figure 4.13 Rural/Urban Wind Speed 'Step-Change prioritising the Logarithmic Profile (4.7)

The velocity gradient can be parameterized in terms of the local friction velocity with stability effects being represented by using a local Monin-Obukhov length, L is defined using the net sensible heat flux from the surface (i.e. a single value independent of height which as suggested by Best *et al* in [160] can be obtained from the energy balance) and the friction velocity:

$$\frac{\delta u}{\delta z} = \frac{u_*(z)}{\kappa(z - z_d)} \Phi_m \left(\frac{z}{L} \right)$$

(4.26)

[5] The distance of 1km appears somewhat unrealistic if one is to use a reference wind speed based on rural measurement to be applicable in an urban setting – but according to Heath *et al* (2007) , larger values of x have little effect

The Monin-Obukhov length, is a parameter with dimension of length that provides a relation between parameters characterizing dynamic, thermal, and buoyant processes [196]. It is defined by

$$L = \frac{-u_*^{\,3} T_v}{\kappa g Q_{vo}} \tag{4.27}$$

where u_* is the frictional velocity, g is the gravitational acceleration, T_v is virtual temperature and Q_{vo} is a kinematic virtual temperature flux at the surface.

Φ_m is an unknown function known as the Monin-Obukhov stability function for momentum and varies in accordance to

$$\Phi_m = \left(1 - 19.3\left\{\frac{z - z_d}{L(z)}\right\}\right) \qquad \text{(L(z)<0 (Unstable))}$$

$$\Phi_m = \left(1 + 6\left\{\frac{z - z_d}{L(z)}\right\}\right) \qquad \text{(L(z)>0 (Stable))}$$

$$\Phi_m = 1 \qquad \text{(for neutral atmospheres)}$$

Therefore, for the neutral atmosphere,

$$\frac{\partial u}{\partial z} = \frac{u_*(z)}{\kappa(z - z_d)}.1dz, \Rightarrow \int \frac{\partial u}{\partial z} dz = \int_{z_d}^{z^*} \left\{\frac{u_*(z)}{\kappa(z - z_d)}\right\} dz \tag{4.28}$$

Considering (4.28) in terms of (4.23)

$$\Rightarrow \; u(z) = \frac{u_*(z^*)}{\kappa} \times \int_{z_0 + d}^{z^*} \left[\frac{\sqrt[3]{\sin\left(\frac{\pi}{2} \cdot \frac{z - z_d}{z^* - z_d}\right)^{1.28}}}{(z - z_d)}\right] dz \tag{4.29}$$

Numerically integrating (4.29) up or down – with respect to the conditions prevalent in the atmosphere (neutral, stable or unstable) – will derive the mean wind speed at the desired height. Figure 4.14 illustrates a 'context' for both the MacDonald and COST methodologies. The schematic relates the different heights within the RSL and emphasises the vertical linkages required in employing the methodologies. The MacDonald utilises a linear approximation (based on a turbulence mixing scale within the 'transition-ary zone') from z* to z_{Hm} and and then the exponential profile z_{Hm} (theoretically) down to z_d. The COST methodology on the other hand presents a single wind speed profile estimation from z* into the UCL (matching to the wind profile within the RSL).

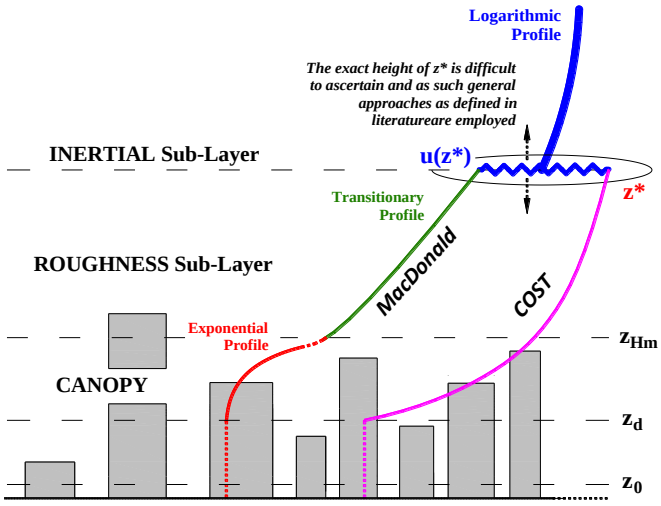

Figure 4.14 Contextualisation of MacDonald's proposals [149] and the COST method [150] considered in terms of the logarithmic model (4 7)

The experiments carried out in the BUBBLE project [189] showed through vertical profile investigations deep into the UCL, that the available wind resource is significantly retarded with reduced height within the RSL (Figure 4.10). The BUBBLE experiments informed the COST 715 Action.

Figure 4.15 illustrates a flow chart that holistically describes the COST methodology for urban wind speed profiling [150].

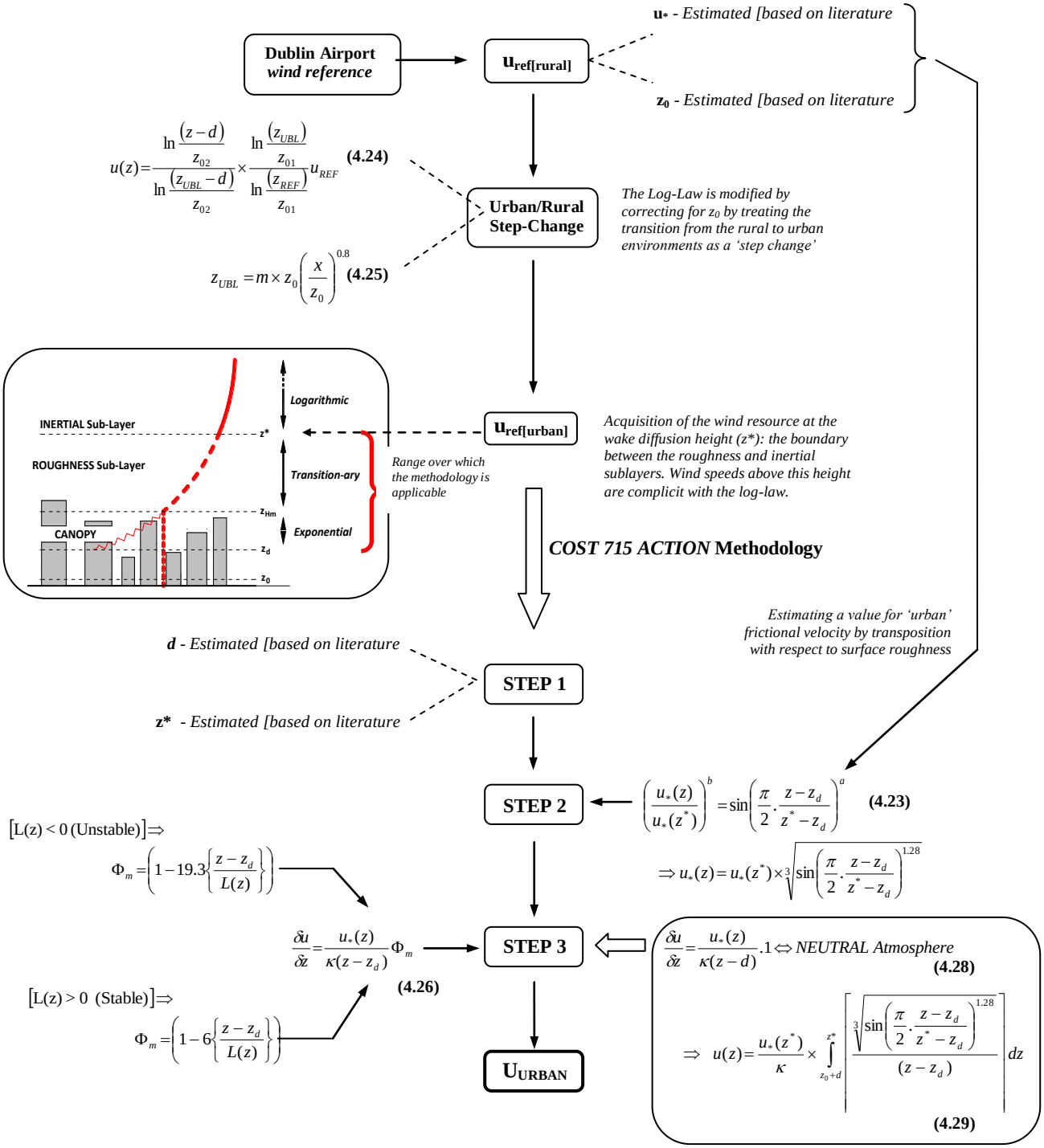

Figure 4.15 COST Urban Wind Resource Estimation Methodology

4.6 Discussion

The wind estimation methodologies that have been described here have limitations that need to be addressed. Firstly, the most basic analytical wind speed modelling that employs the Wieranga formulation (and indeed the Mertens approach), which employs the logarithmic profile, is overly simplistic. Although the log profile can estimate wind speed to the level of z_d+z_0 Homogenous surfaces), studies suggest that it is not applicable to a layer that extends above rooftop height where flow is not adjusted. Wind observations and modelling studies indicate that the roughness sub layer (RSL) in cities extends from the ground to between two and four times the heights of buildings (i.e. 2.z_{Hm} to 4.z_{Hm}).

Furthermore, the Wieranga approach suggests that the friction velocities for the two sites (in the rural/urban extrapolation) are identical. So the difference in wind-speeds at any given height can be attributed to the effects of surface roughness (z_0, z_d). However, where the differences in z_0 between the sites is very large, as is the case when urban sites are compared to most rural sites, the value of u_* must be adjusted. Bottema [197] in (4.22) suggests that the urban value of u_* can be estimated from the ratio of the urban to rural roughness lengths, but that research is based on using an urban surface created from homogeneous building groups. However, wind observations and u_{RSL} modelling studies indicate that the friction velocity (u_*) in the roughness sub layer (RSL) is no longer constant.

Secondly, the MacDonald approach is predicated on morphometric approaches that are based on staggered cubes of equal height. However, the dominant features of urban surfaces are the very heterogeneous roughness elements (buildings and other man-made

structures) that are relatively large and usually irregularly arranged [173], with differing geometrical properties. As Cheng and Castro [173] further point out, MacDonald's work [149] did not consider a spatially averaged vertical profile [149]; a general vertical profile. In this regard, Chen and Castro [149] considered more practical urban-like representations and employed staggered and random blocks as illustrated in Figure ?? below.

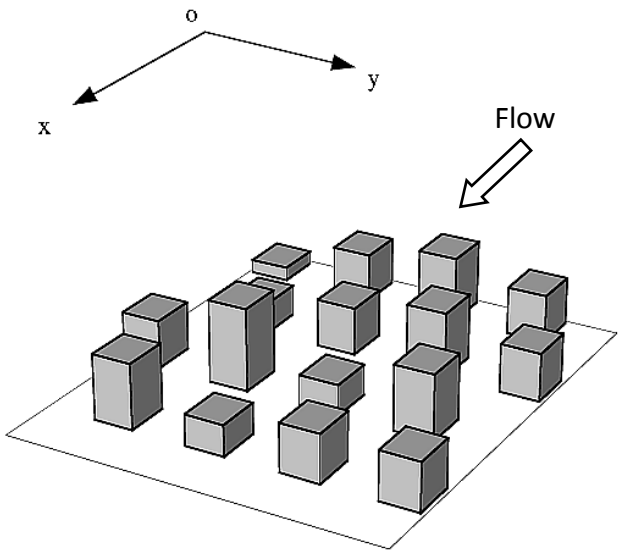

Figure 4.16 Experimental layout (3D view) illustrating the random arrays employed by Cheng and Castro [149]

The exponential profile as discussed in (4.15) from a wind energy perspective is of limited application to wind turbine installation where the objective is to normally install said technologies *above* local obstructions. At an installation height most conducive for wind turbines (i.e. $z_{Hm} < z < \left[z = (2 \rightarrow 4).z_{Hm}\right]$), MacDonald estimates wind speed based on observations at the building height (z_{Hm}), which at best, will have questionable reliability in a practical sense.

The COST methodology (third approach considered here) was evaluated using wind observations acquired as part of the Basel UrBan Boundary Layer Experiment (BUBBLE) [189]. This investigation showed that (4.23) yields good results (±10%) for estimates of airflow at z* (that is, the top of the RSL) using friction velocity values obtained from urban observations. The results were markedly poorer when u_* is estimated from rural observations using (4.22), chiefly as a result of systematic underestimation. This is perhaps not surprising as this formulation assumes well adjusted profiles over two extensive surfaces of different roughness where the wind at the top of the boundary layer is constant [194]. In reality, the urban surface may consist of discrete 'patches' of land-cover subtypes such as residential suburbs, commercial warehouses, parks, business districts, etc. each of which has distinct roughness properties. Depending on wind direction the wind profile at a site will reflect the different surfaces airflow encountered on its passage.

As a means to perform preliminary analysis on the MacDonald and COST wind profiling methodologies (Sections 4.5.2 and 4.5.3), a tool was developed using EXCEL^{TM} [198] (see **Appendix A8** for details on this preliminary analysis). The tool in facilitating short term wind profile comparisons allowed investigations of each analytical methodology, where the concerns expressed above were evident.

A further alternative analytical method commonly employed in wind energy applications is to estimate the wind speed within the RSL is the power law,

$$\frac{u(z)}{u(z^*)} = \left(\frac{z - z_d}{z^* - z_d} \right)^{\alpha} \qquad \textbf{(4.30)}$$

where, α is the wind shear exponent. Millward-Hopkins *et al* [162] suggest that the value for α could be obtained by matching the log- and power-law profiles at a reference height (z*).

4.7 Conclusion

This Chapter considered the complexities associated with wind profiling and more specifically, *urban* wind profiling. Meteorological Boundary layer theory facilitates wind analysis by recognising distinct layers of atmosphere where different processes dominate. Wind speed modelling is an inherently complex task and is even more complex when the morphological complexities associated with urban environments are considered. Indeed, unlike the rural wind resource, the effect of the city both diminishes and complicates the flow of the wind resource, with building morphology and associated landscape heterogeneity contributing to the increased fetch and turbulent characteristic of the resource.

Analytical wind speed modelling based on boundary layer theory, was considered in detail. Two analytical modelling techniques were considered in detail [149, 150]. Both methodologies employ rural/urban linkages based on a surface roughness step transition from rural to urban environments. Preliminary analysis of the analytical profile modelling techniques, while deriving inconclusive results, did facilitate investigation of the inter-relationships between rural/urban surface roughness and frictional velocity [198]. Indeed the preliminary analysis suggested that more consideration is required with respect to the wind speed modelling parameters and more specifically the surface roughness parameters as it was observed that both models are highly sensitive to variations in z_0.

Chapter 5 will use high resolution wind speed/direction observations within a suburban and an urban location to address the issues identified here and to consider more holistically, the potential for micro wind turbines in terms of an urban wind resource derived from empirically fitting the logarithmic profile in terms of the surface roughness parameters.

Chapter 5: Urban Wind Resource: Observations and Modelling Analysis

5.1 Introduction

This chapter continues from Chapter 4 and focuses initially on analysing the nature of the wind within the RSL, particularly the UCL and subsequently investigates the analytical modelling as discussed in Chapter 4. The analysis and analytical modelling presented here is facilitated by wind speed observations made at three locations across Dublin City, Ireland.

A reference site is located at the Airport (A), which is located on the margins of the city, 10 km from the city centre (Figure 5.1). The site conforms to the WMO standards for synoptic weather stations and is managed by Met Eireann, the Irish Meteorological Service. The wind records are used to represent the wind climate that would be present across the Dublin area in the absence of the city itself. These observations are typical of information that is commonly available to wind engineers throughout the world and from which extrapolations are made to a site of interest.

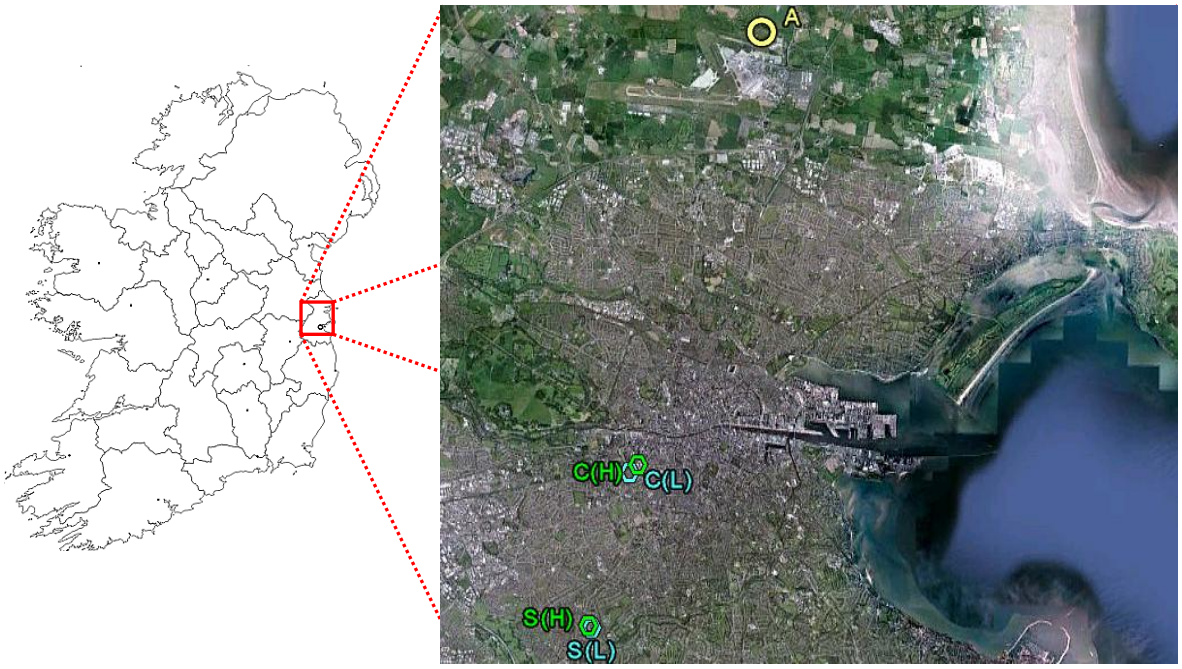

Figure 5.1 Relative positions of the observation locations across Dublin City
Dublin Airport (A), Suburban Upper-platform (S_H), Suburban Low-platform (S_L), Urban Upper-platform (C_H) & Urban lower-platform (C_L).
("Dublin", 53020'22.80''N and 6017'02.11''W; source: GOOGLE EARTH [199])

Initially, the wind resource within the UCL is compared to the available resource within the RSL. The applicability of the Rayleigh/Weibull distributions as standard tools in a wind energy systems context is subsequently considered.

Following on from this observational analysis, the analytical modelling discussed in Chapter 4 is considered in reaction to the issues raised, namely their over-simplified application and their limitations in urban environments. Here, the observed resource at 2-4 times the average building height at the respective observation locations is prioritised. Analysis of the wind resource below the recognised lower limit of the logarithmic profile is also carried out.

The objective of the analysis is to assess a renewable energy context by considering the productivity of a commercially available wind generator on the basis of the wind

resource available. The question of economical viability, particularly with respect to installation height variation is also considered.

5.2 Wind Observations

There are two observation sites prioritised in this research and they represent two distinct urban landscapes. The first is located close to the city centre in an area that has mixed residential, industrial and commercial uses. The buildings vary considerably in dimensions and there is comparatively little green space. The other is located in a mature, vegetated suburb, where the dimensions of the buildings are nearly uniform and the land use is residential in character. At each site there are two measurement platforms at different heights with regard to the urban surface. The high platform is at least 1.5 times the average height of buildings (as suggested by the BUBBLE experiment [189]) and the low platform is close to the rooftop height. Each of the stations is positioned within a broadly defined 'homogenous' landscape in the sense that the character of the surrounding urban morphology is similar in all directions. These sites are benchmarked against a reference site located at the Airport (A), (Figure 5.1).

The suburban site (S) is located within an extensive residential area consisting of area of two-storey houses with pitched roofs (6-7 m tall), significant green space and mature trees (Figure 5.2). The observation site is a one storey, flat-roofed school building. The high platform (S_H) is mounted on a mast on the roof at a height of 12m. The low platform (S_L) is less than 30 m distant and is positioned at 5m. The city centre site (C) is located within a mixed commercial/residential/industrial area. The buildings vary in size but are generally 2-3 storeys in height and there is little green space. Here, the high platform (C_H) is positioned on an antenna on the roof of a three storey building at an elevation of 17m. Its higher position is consistent with the higher mean building height

(z_{Hm}) in the surrounding area. The low platform (C_L) observations are made some 300m away at an elevation of 8m at the gable-end of a two-storey tserraced house.

The observations at C_H and S_H are used here to represent the wind resource available near the top of the Roughness Sub layer (RSL), that is, at z*. Those at the lower platforms (C_L and S_L) represent winds within the RSL.

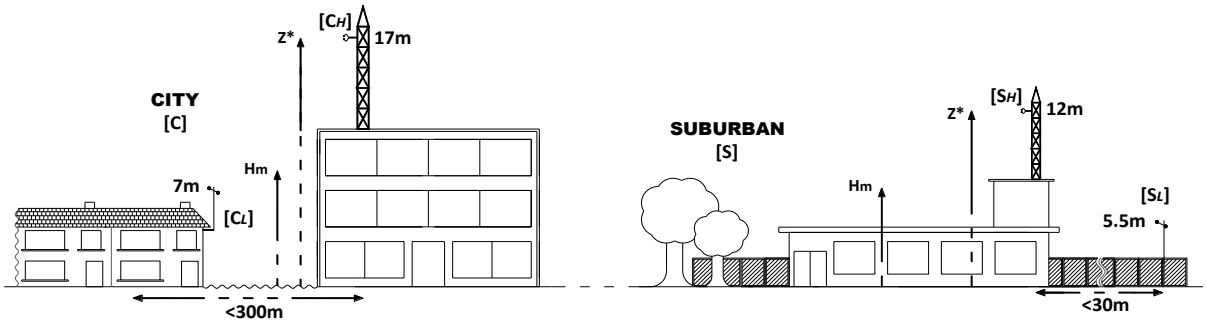

Figure 5.2 Relative context of wind observation locations.

The diagram further illustrates the relative position of the observation platforms and a z* estimation for both the urban and suburban locations**.**

Wind observations at the high platform for each site were made by *Campbell Scientific* sonic anemometers (CSAT 3D). These instruments record wind speed along three orthogonal axes at resolution of less than 1 mm/s [200] and in this deployment were interrogated at 10 Hz. The data was subsequently averaged to generate observations that were compatible with the Airport data.

Figure 5.3 and Figure 5.4 illustrate the installations at C_H and S_H. with Figure 5.5 summarising the range of instrumentation at both high-platform sites.

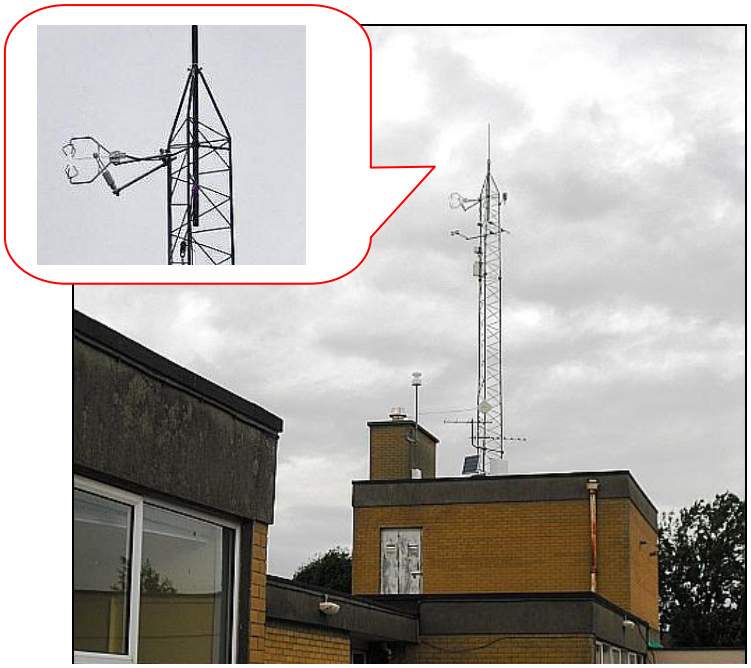

Figure 5.3 High-Resolution (CSAT 3D anemometers) Station – *St. Pius X* (S_H)

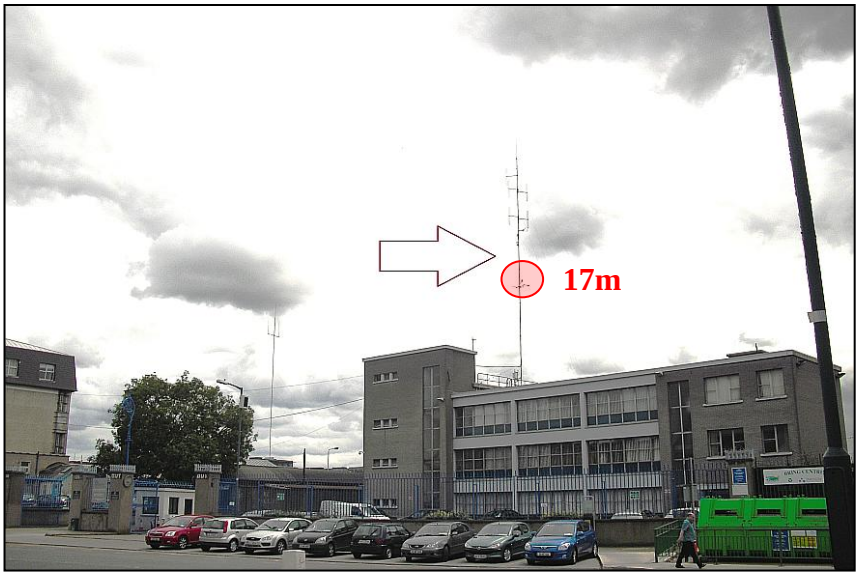

Figure 5.4 High-Resolution (CSAT 3D anemometry) Station – Marrowbone (CH))

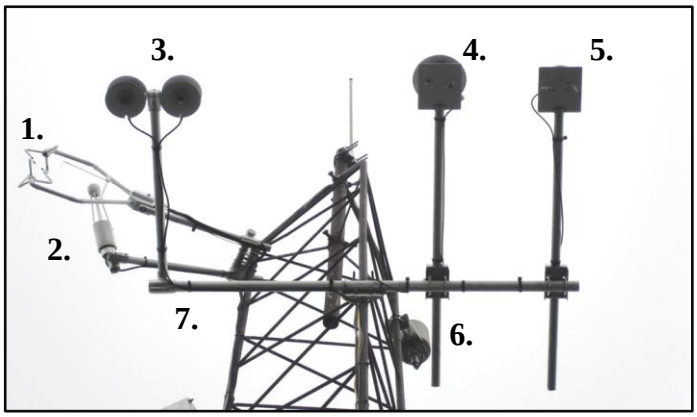

1. **3D Sonic Anemometer (CSAT 3)**
2. **Open Gas Analyser**
3. **Net Radiation Sensor**
4. **Pyranometer**
5. **Photosynthetic active radiation sensor**
6. **Temperature and humidity probe**
7. **Instrument mast**

Figure 5.5 Range of instrumentation at both C_H and S_H sites [201]

Observations at the lower platforms were made using inexpensive weather stations (DavisTM Vantage Vue) that utilise robust cup anemometers and simple vanes. The wind speed resolution is 0.1 m/s and wind direction is recorded at 22.5° wide sectors [202]. These instruments are interrogated every 15 minutes and the data was processed to yield half-hourly observations. Figure 5.6 illustrates the low platform instrumentation at the city centre location (C_L)

Figure 5.6 C_L, low platform observation within UCL at the city centre location

Hourly airport data for the period November 2010 – December 2011 was used in these analyses. These observation platforms are part of the *Dublin Boundary Layer Experiment (DUBLex)* research collaboration[6]. This collaboration is primarily engaged in urban heat island and micro-climate investigations as well as investigations into energy momentum and carbon fluxes. Whereas the low platform installations are specifically located to provide the parameters of climate in a micro-scale environment the high platform installations facilitate a three-dimensional description of the wind resource. While wind energy was not initially a priority in the rationale for this project, the experimental set-up is optimal for investigating the influence of the urban surface roughness on the wind resource. Furthermore, the set-up facilitates testing of analytical wind profiling. Figure 5.7 illustrates the context and interrelationship between the distinct research themes.

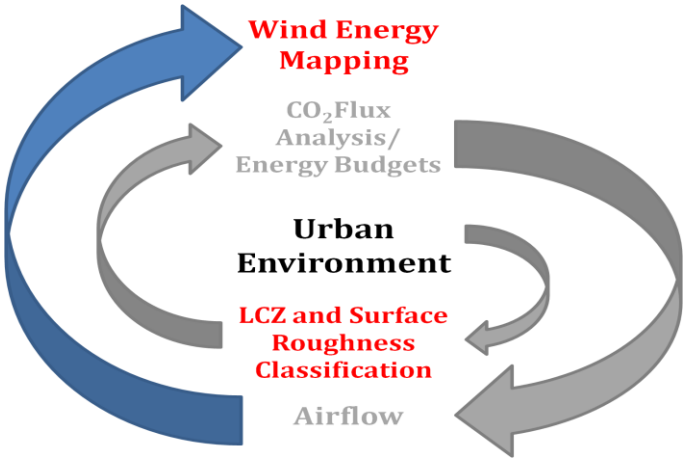

Figure 5.7 The basis of the *DUBlex* research collaboration

5.3 Urban wind observations: *A statistical consideration*

This section considers the observation platforms at each location from a resource (power density) perspective. In spatially homogenous locations, such as rural

[6] A cross-collaborative research initiative involving *University College Dublin* (UCD), *National University of Ireland, Maynooth* (NUIM) and *Dublin Institute of Technology* (DIT)

environments, it is common to consider wind energy applications in terms of the Weibull and Rayleigh probability distributions. The questions arises: how good are these distributions at representing the wind resource in heterogeneous surface conditions such as those in cities? Therefore while considering the wind resource at the respective platform elevations, analyses of the applicability of the Weibull/Rayleigh distributions in this regard is also considered.

At the high platforms, once erroneous or missing data was processed, there are 8603 and 7515 hours of wind speed/direction at S_H and S_C respectively. At both low platforms, 718 hours of observations were considered.

5.3.1 Frequency distribution

The Weibull distribution is commonly used to describe wind [32-34, 36, 37] and this function has been shown to give a good fit to measured wind speed data [203]. The Weibull distribution function is described in (5.1).

$$P(u < u_i < (u + du)) = P(u > 0)\left(\frac{k}{c}\right)\left(\frac{u_i}{c}\right)^{k-1} e^{\left[-\left(\frac{u_i}{c}\right)^k\right]} du_i \quad \textbf{(5.1)}$$

The Weibull scaling factor, *c*, has the same units describing wind speed, *k*, represents the Weibull shape parameter, u_i is a particular wind speed, *du* is an incremental wind speed. $P(u < u_i < (u + du))$ is the probability that the wind speed is between u and $(u + du)$ [204]. The Rayleigh distribution is a special case of the Weibull distribution in which the shape parameter, *k*, has a value of 2.0 [204]. From (5.1), the Rayleigh distribution function is described in (5.2).

$$P(u < u_i < u + du) = P(u > 0)\left(\frac{2.u_i}{c^2}\right)^{k-1} e^{\left[-\left(\frac{u_i}{c}\right)^k\right]} dv_i \quad \textbf{(5.2)}$$

The Weibull parameters are used to describe the mean wind speed in (5.3)

$$u_m = c.\Gamma\left(1+\frac{1}{k}\right) \quad \textbf{(5.3)}$$

where u_m is the average wind speed and $\Gamma()$ is the gamma function. The Weibull parameters can be derived in a number of ways, but in practically all of the approaches, a search is made for an estimator which, based on the sample data, gives rise to a single-valued estimation of the value of the parameters [205]. The approach employed here is to employ the *maximum likelihood method* [204] to compile fitted Weibull distributions of the WIND (and MET) weather stations.

5.3.2 Wind power density

The power contained within the wind flowing at a speed, *u*, per unit area, *A*, is discussed by Chang *et al* in [206] and expressed by (5.4), whereas (5.5) contextualizes how this power is translated mechanically for a wind energy system.

$$P(u) = \frac{1}{2}.\rho_{air.}.u^3.A \quad \textbf{(5.4)}$$

$$P_{Mech} = \frac{1}{2}.C_p\rho_{air.}.u^3.A_{rotor} \quad \textbf{(5.5)}$$

where ρ_{air} is the air density, which at sea level and mean temperature, 15^0C at 1atm is 1.225kg.m^3 and *Cp* is power coefficient, defining how much wind power is captured and turned into mechanical power to subsequently generate electricity. A_{rotor} in this regard is the rotor area ($\pi.R^2$ where *R* is the length of the blades). The average power

density per period of time can be calculated by using the probability density function of the measured wind data using (5.6).

$$P_{Measured} = \sum_{j=1}^{n} \frac{1}{2} . \rho . u_{m.j}{}^{3} . f(u_j)$$

(5.6)

where j represents the bin reference, u_j the bin range, u_{mj} the mid-point (or mean) of each bin (j=1:n) and $f(u_j)$ the frequency of observations within each bin range as a percentage of the overall observations.

Tsang in [206], as discussed by Jamil *et al* in [207], further describes how wind power density can be described by a Weibull probability density function (5.7).

$$P_{Weibull} = \frac{1}{2} . \rho . c^{3} . \Gamma\left(1 + \frac{3}{k}\right)$$

(5.7)

The wind power density can also be described by the Rayleigh probability distribution, where k=2 resulting in (5.1) being reduced to

$$u_m = c\sqrt{\pi/4}$$

(5.8)

Therefore the Rayleigh probability distribution describing the wind power density as described by Celik [208], is obtained by (5.9)

$$P_{Raylleigh} = \frac{3}{\pi} . \rho . u^{3}{}_{m}$$

(5.9)

The average error factor in calculating the power density ((5.7), (5.9)) by both the Weibull and Rayleigh function is found using (5.10).

$$Error\,(\%) = \left[\frac{P_{Weibull/\,Rayleigh} - P_{Measured}}{P_{Measured}} \right]$$

(5.10)

5.3.2.1 Evaluation of the Weibull and Rayleigh distributions

The Weibull/Rayleigh distribution performances over the respective high platform and low platform observations are evaluated through equations (5.11) to (5.13) on the basis of 1m/s bin widths from 0 to 20m/s:

- Mean root-square error (RMSE)

$$RMSE = \left\{ \frac{\sum_{i=1}^{N} (y_i - x_i)^2}{N} \right\}^{0.5} \tag{5.11}$$

- Chi-square Test (χ^2)

$$\chi^2 = \frac{\sum_{i=1}^{N} (y_i - x_i)^2}{N - n} \tag{5.12}$$

- The correlation coefficient (R^2)

$$R^2 = \left\{ \frac{\sum_{i=1}^{N} (y_i - \bar{y})(x_i - \bar{x})}{\sqrt{\sum_{i=1}^{N} (x_i - \bar{x})^2 (y_i - \bar{y})^2}} \right\}^2 \tag{5.13}$$

Where y_i is the i-th measured data and x_i is the i-th predicted data associated with the Rayleigh or Weibull distribution with $\bar{y}$ and $\bar{x}$ representing the mean of the measured and modelled data respectively. N is the number of observations and n the number of constants.

5.3.3 Wind powered density comparisons

The wind speed probability distributions at the high platform (S_H and C_H) low platform (S_L and C_L) were benchmarked against the Airport (background reference) and Weibull and Rayleigh probability wind speed distributions derived using the *maximum likelihood method*[204]. Figure 5.8 illustrates these comparisons.

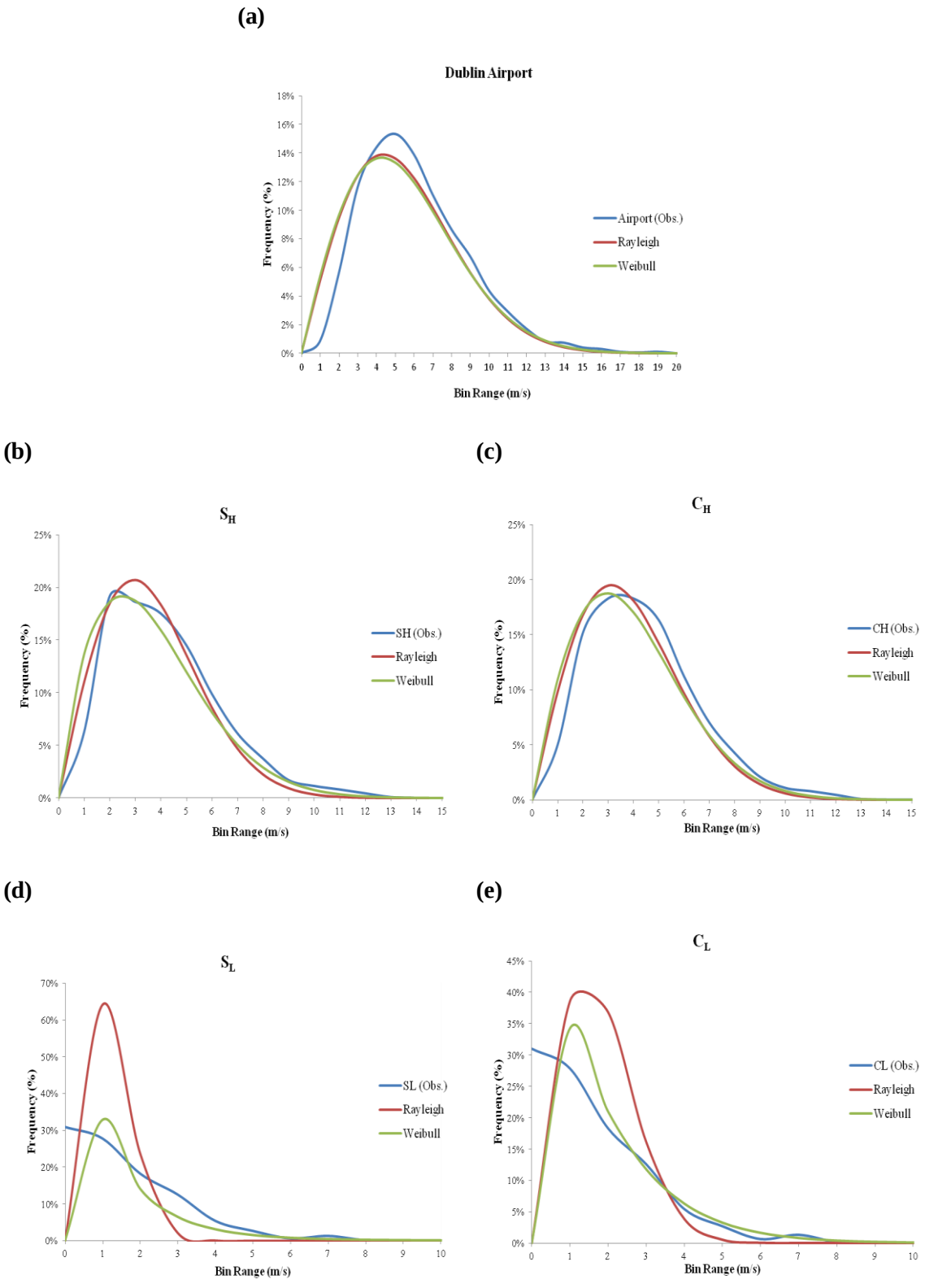

Figure 5.8 Wind Speed Probability Density Comparisons at the high/low platforms in terms of Weibull and Rayleigh representations
(a) Airport, (b) & (c) S_H & C_H respectively and (d) & (e) S_L and C_L respectively

Figure 5.8(a) illustrates the wind speed probability density (for all three considerations), with Figure 5.8(b) & Figure 5.8(c) facilitating a high-platform comparison between S_H

and C_H respectively. Figure 5.8(d) & Figure 5.8(e) provide a similar comparison at the low platform elevations. Immediately apparent is the reducing mean as the wind speed profile is compared from the Airport to the high platform observations until the profiles at the low platforms contain a significant proportion of null wind speeds. Also apparent is that while the Weibull and Rayleigh representations perform well in the high platform considerations, they do not statistically represent the low platform observations sufficiently well. This is further supported in the comparisons of the wind power densities at all sites as illustrated in Table 5.1. The correlation coefficient (R^2), chi-square (χ^2) and the Root-Mean-Square-Error (RMSE) techniques were employed to make the statistical comparisons on how well the observed frequency distributions are approximated by Weibull/Rayleigh fitting. The best comparisons are according to the highest values of R^2 and the lowest values of χ^2 and RMSE.

Table 5.1 Wind Speed and Power Density Observations at each platform compared to Rayleigh & Weibull representations (resolution: wind speed bin-width of 1m/s)

	Recorded Data			*Rayleigh PDF*					*Weibull PDF*					
Station	U_m $[ms^{-1}]$	U_S $[ms^{-1}]$	U_{PD} $[Wm^{-2}]$	*c*	$U_{PD\text{-}R}$ $[Wm^{-2}]$	R^2	χ^2	*RMSE*	*k*	*c*	$U_{PD\text{-}W}$ $[Wm^{-2}]$	R^2	χ^2	*RMSE*
Airport	5.47	2.88	196.32	6.18	191.78	0.92921	0.00024	0.01464	1.95	6.17	196.32	0.91704	0.00028	0.01585
S_H	3.67	2.16	67.81	4.14	57.95	0.96599	0.00020	0.01352	1.74	4.12	67.81	0.92721	0.00038	0.01858
S_L	3.90	2.13	8.06	1.33	1.92	0.42915	0.01365	0.11084	0.90	1.12	8.06	0.47198	0.00582	0.07237
C_H	1.71	1.41	74.09	4.41	69.43	0.96019	0.00021	0.01380	1.88	4.39	74.09	0.94023	0.00031	0.01663
C_L	2.03	1.58	15.36	1.79	6.65	0.47863	0.00799	0.08478	1.14	1.87	15.36	0.49227	0.00798	0.08477

Clearly evident in Table 5.1 is the good correlation between the Weibull/Rayleigh frequency distribution representations of the high-platform observations. However, within the canopy, such statistical correlations are less evident; likely caused by the mixture of calms and highly turbulent flow. Furthermore, the coarse binning of the data could be a cause of poor fits at the lower wind speed sites where the Weibull peak is likely to be steeper and could even be within the lowest wind speed bin.

5.4 Improved urban wind modelling and analysis

This section presents detailed analysis as described in [209] to investigate the limitations as discussed in Chapter 4 and the applicability of the associated modelling to small wind energy system deployment within the urban environment.

5.4.1 Methodology

The observations at the airport site (A) are used to derive estimates of the wind resource at both urban sites (C and S) and specifically with respect to the high-platform observations, three methods are considered:

1. A step response (as suggested by Wierenga [182]), based on the background wind reference at the Airport, on the basis of the guidance documentation for obtaining representative meteorological observations at urban sites [170]. In this formulation (5.15), the friction velocity (u_*) is treated as constant over all sites and the wind speed at C_H and S_H uses u_* from the Airport and the estimated roughness lengths for city centre and suburban landscapes, respectively [170].
2. A two-stage rural-urban logarithmic extrapolation which uses a regional classification of the urban surface roughness. This approach employs the Bottema rural/urban frictional velocity (u_*), which is adjusted according to (5.16) (hereafter, this is referred to as the *Bottema* approximation).
3. Again a two-stage rural-urban logarithmic profile is considered except in this *log-fitting* approach, z_0 at each urban site is estimated by numerically fitting (5.14) to the observed data at C_H and S_H, using the established values for *u* at a reference height of 200 m as an upper boundary condition (consistent with Figure 4.3). Hereafter, this approach is referred to as the *log-fitting* approach.

The relevant equations employed in the extrapolation of the rural/background wind reference into the urban environment, as established in chapter 4, are illustrated in Table 5.2.

Table 5.2 Cross-reference of equations employed in Chapter 4 to ascertain the urban wind speed

Chapter 5 reference	*Chapter 4 reference*
$u(z)=\frac{u_*}{\kappa}\ln\left(\frac{z-z_d}{z_0}\right)$ (5.14)	(4.7); Logarithmic profile equation; employed as a means to extrapolate the available wind at a rural site to an urban site by modification of its associated parameters
$u_{zA}=u_{zB}\left(\frac{\ln(z_r/z_{0B}).\ln(z_A/z_{0A})}{\ln(z_B/z_{0B}).\ln(z_r/z_{0A})}\right)$ (5.15)	(4.14); Wieringa [182] proposed that the log profile could be employed to estimate wind at a site of interest (site B), based on observations made at a reference site (site A),
$\left(\frac{z_{0_{URBAN}}}{z_{0_{RURAL}}}\right)^{\beta}=\frac{u_*(z^*)_{URBAN}}{u_{*RURAL}}$ (5.16)	(4.22); Bottema [197] suggested this formula so that the urban value of u_* could be estimated from a urban/ rural roughness length ratio.
$\left(\frac{u_*(z)}{u_*(z^*)}\right)^{b}=\sin\left(\frac{\pi}{2}.Z\right)^{a}$ (5.17)	(4.23); Rotach *et al* [189] suggested that the friction velocity at any height ($u_*(z)$) within the RSL above the displacement height (that is, from d to z*) may be parameterised against the value at the top of the RSL (which may be obtained from the log profile)
$\frac{u_{(z)}}{u_{(z^*)}}=\left(\frac{z-z_d}{z^*-z_d}\right)^{\alpha}$ (5.18)	(4.30); Estimation of the wind speed within the RSL using a power law formulation

These estimates were then tested against the measured data at *C* and *S*. The primary focus of this work is on wind at the top of the RSL (u_{z^*}) where turbine losses due to unsteady winds are minimized. The instrument at C_H and S_H are positioned at, or near, this level and may be used to evaluate different approaches. A secondary focus is on the loss of the wind resource within the RSL. For this analysis, the winds at z^* are employed to estimate the winds reported at C_L and S_L and to infer the wind profile of the RSL between z^* and close to rooftop height.

Again hourly airport data for the period November 2010 to December 2011 was used in these analyses. However, as each of the approaches used to estimate the wind resource is premised on the *neutral atmosphere* log wind profile, those days classified as predominantly neutral (more than 15 hours categorised as D, according to the *Pasquill-Gifford* stability index) were included. The dominant wind direction at the airport under

these conditions was south-westerly and wind directions varying from 120° and 300° from North on 82% of occasions were prioritised for analysis. Once gaps in data and erroneous records were considered, 6812 hours and 5905 hours of observational data respectively, were available at S_H and C_H. A shorter period of just 718 hours was used for the comparisons of estimates with measured winds at C_L and S_L.

For methods 2 and 3 (the *Bottema* and *log-fitted* approaches respectively), the background wind condition for all the observation sites (A, C and S) is established by extrapolation, using (5.14) from the airport site upwards to a reference height, well above the surface roughness elements (z_r), at which the influences of the underlying surface variations are assumed to be negligible. In [148, 183], Millward-Hopkins *et al* and Weekes & Tomlin respectively employ wind resource extrapolation techniques in which 200m blending height was chosen on the basis that at this height, the flow could considered independent of the local and regional surface roughness. This is also consistent with suggestions in the UK Met Office Small Scale Wind Energy Technical Report [160]. For this research, the blending height is also set at 200 m. The wind at this level (u_{zr}) is then used to estimate the wind resource at the top of the RSL (u_{z*}), which is situated close to observations at C_H and S_H and then within the RSL, where we have observations at C_L and S_L.

The results of these procedures are compared with the observations at both sites. Within the RSL (that is, $z < z^*$), the wind profile is estimated using *u(z*)* obtained from the log wind profile as the upper boundary condition. Two techniques are used to generate wind estimates at the heights of the lower platforms (C_L and S_L) for which observations are available. In the first, the power law (5.18) is used and following Willard-Hopkins *et al*

(2011), the wind shear exponent (α) is obtained by matching the gradients of the power and logarithmic profiles at z* through (5.19)

$$\alpha = \left(\ln\left(\frac{z - z_d}{z_0} \right) \right)^{-1} \quad \textbf{(5.19)}$$

The second technique is based on COST, (5.17), which allows the friction velocity to vary in the layer between the displacement height and the top of the RSL (that is, $z_d \leq z \leq z^*$). Inserting this into the log wind profile, (5.14) yields

$$u(z) = \frac{u_{*(z^*)}}{k} \int_{z=d}^{z=z^*} \frac{\sqrt[3]{\sin\left(\frac{\pi}{2} . \frac{z - z_d}{z^* - z_d} \right)^{1.28}}}{(z - z_d)} dz \quad \textbf{(5.20)}$$

A third technique is also presented in which the fitted logarithmic profile is utilised to establish $u_*(z^*)$ and then by variation of the parameters in (5.17), the COST profile is essentially locked into the logarithmic profile at z*. Figure 5.9 illustrates the profiles derived using these techniques and matching both the *Power* and *Cost* models to the logarithmic profile[7].

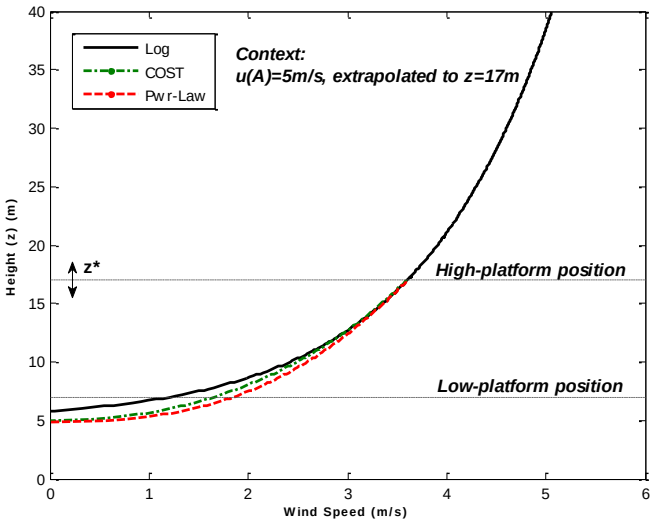

Figure 5.9 Roughness layer wind speed modelling (extrapolated from a 5m/s airport reference)

[7] The illustration is with respect to a background wind reference (A) of 5m/s

5.4.2 Results

Table 5.5 shows the wind climate over the study period for the Airport site. The statistics on the mean wind speed and direction (and their variability) are decomposed into 30° sectors of the compass. The predominant direction of the airflow is south-westerly (over 80% of wind originates in the 120° to 300° part of the compass). The mean wind speed is 5.2 m/s but the winds from south-west are closer to 6.0 m/s. The strongest winds (7.4 m/s), which occur on 24% of occasions have a mean direction of 260°. The recorded wind is generally strong and steady: the standard deviations are less than 25% the value of the mean. Figure 5.12 shows the frequency distribution of the recorded wind speed in the sector 120° to 300°, which is where the bulk of the wind resource lies. For each 30^0 sector, surface roughness was estimated by varying z_0 iteratively until the best fit was achieved so as to minimise the error between the predicted wind speed, based on the background climate, and the observed wind speed. Table 5.3 below illustrates the variation in surface roughness length as affected by upwind fetch for the prioritised directions.

Table 5.3 Surface roughness length (z_0) variation within the wind direction range of 120^0-300^0

	S_H						C_H					
Dir.[deg.]	Obs. Freq. [%]	u_M [m/s]	u_S [m/s]	Dir_M [deg.]	Dir_S [deg.]	**z_0 [m]**	Obs. Freq. [%]	u_M [m/s]	u_S [m/s]	Dir_M [deg.]	Dir_S [deg.]	**z_0 [m]**
0-30	1.8%	1.9	0.9	104	86		1.9%	2.3	1.0	82	86	
30-60	2.9%	2.4	1.0	91	47		3.0%	3.3	1.5	76	46	
60-90	3.5%	3.0	1.3	103	42		3.8%	4.1	1.8	91	34	
90-120	4.6%	2.8	1.6	127	51		3.9%	3.3	1.8	113	42	
120-150	12.1%	3.4	1.9	151	49	***0.924***	10.1%	3.6	1.8	139	42	***1.145***
150-180	5.8%	3.7	1.8	179	37	***0.395***	4.4%	3.4	1.7	167	39	***0.870***
180-210	10.1%	5.2	2.4	218	27	***0.180***	9.0%	4.9	2.2	211	26	***0.640***
210-240	21.2%	5.0	2.2	244	23	***0.342***	22.0%	5.0	2.2	239	18	***0.791***
240-270	22.4%	4.8	2.1	268	18	***0.660***	24.3%	5.1	2.1	263	14	***1.0575***
270-300	10.1%	3.4	1.6	281	30	***0.602***	11.3%	3.9	1.8	282	17	***0.724***
300-330	3.7%	2.6	1.4	286	55		4.0%	3.0	1.6	287	45	
330-360	2.0%	2.1	1.1	219	115		2.2%	2.2	0.9	231	117	
						$z_{0(average)}$ **0.5171**						$z_{0(average)}$ **0.8713**

Figure 5.10 and Figure 5.11 illustrate the context for the stability filtering and directional filtering for the urban and suburban (C and S) sites respectively.

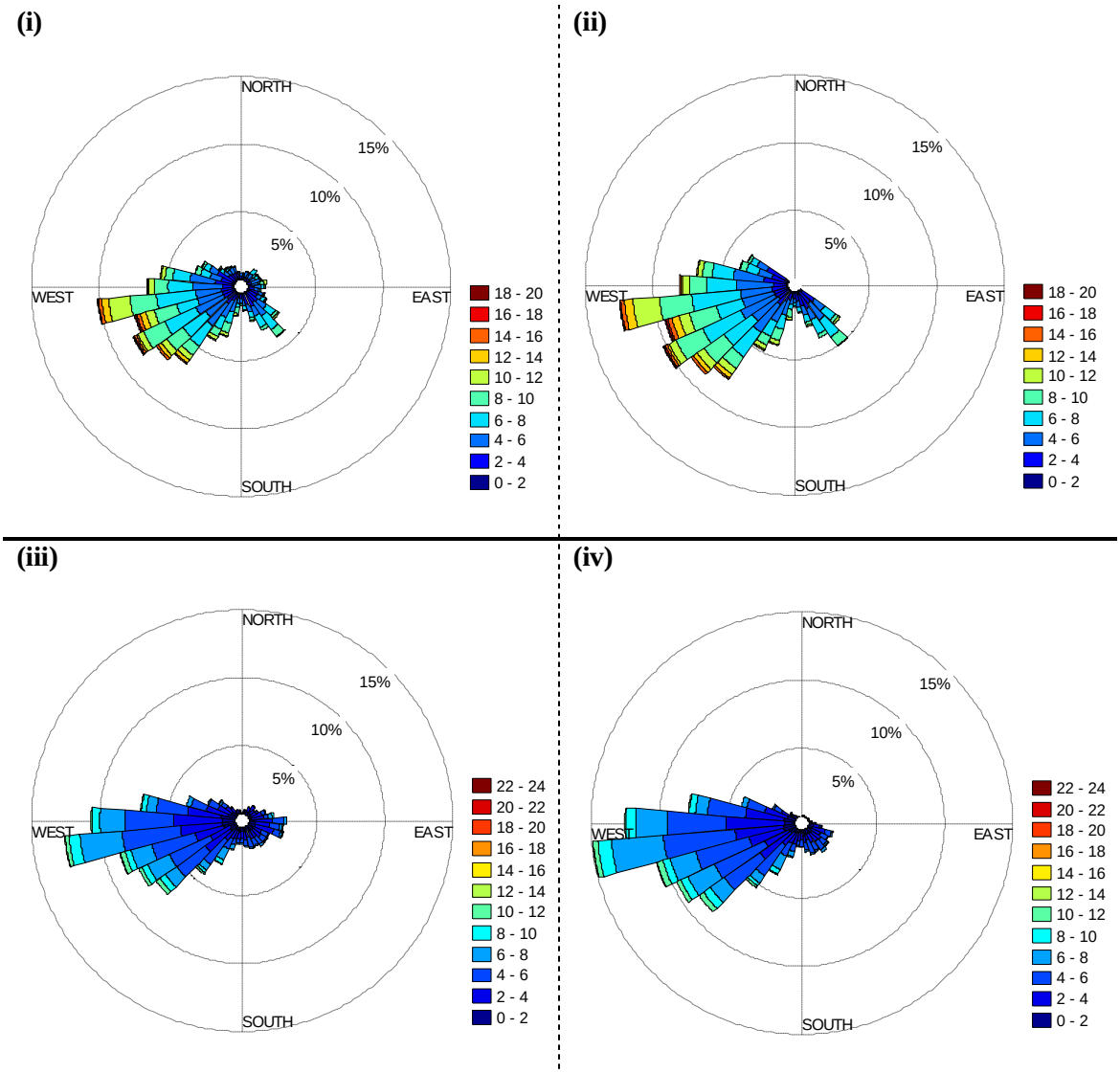

Figure 5.10 Wind Speed Data processing for the City Location, (C)
(i) Airport data stability processed; (ii) Airport data filtered directionally (120°-300°); (iii) CH stability processed; (iv) CH filtered directionally (120°-300°)

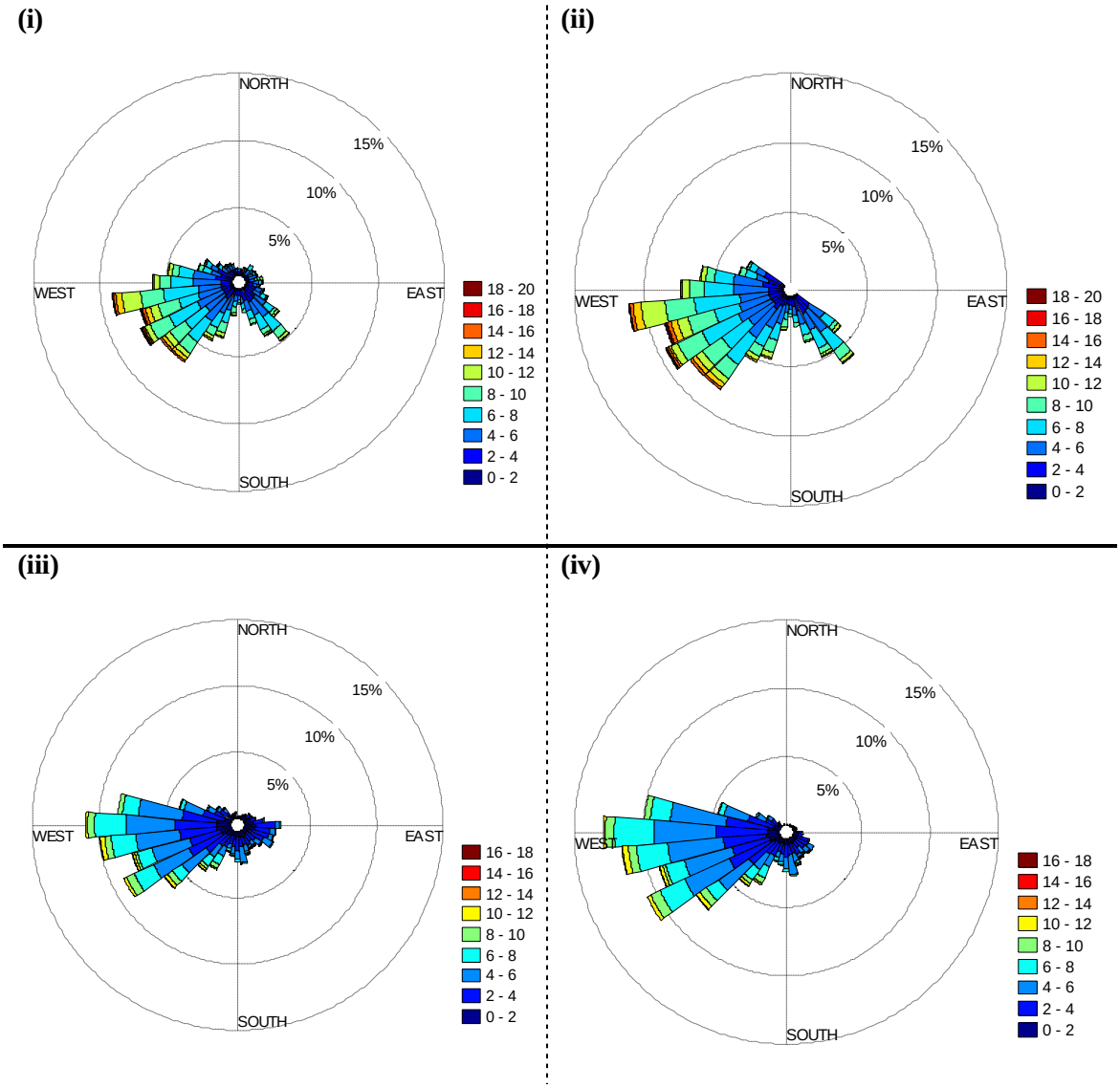

Figure 5.11 Wind Speed Data processing for the Suburban Location, (S)
(i) Airport wind data stability filtered; (ii) Airport data filtered directionally (120°-300°); (iii) SH stability processed; (iv) SH filtered directionally (120°-300°)

On the vast majority of occasions the atmosphere at the Airport is neutral (86%) or slightly stable/unstable according to the *Pasquill-Gifford* index. The *Pasquill Stability Indices* are used to calculate a stability category ranging from *A* to *F* that can help predict how well pollution will disperse, and are available for *Met Eireann* synoptic weather stations. The *Pasquill-Turner Stability Index* is summarised in the Table 5.4.

Table 5.4 Pasquill-Turner Stability Index; employed at the Dublin Airport Synoptic weather station

A	*Extremely Unstable*
B	*Unstable*
C	*Slightly unstable*
D	*Neutral stability*
E	*Slightly stable*
F	*Stable*
G	*Extremely Stable*

The Pasquill Index is always neutral (D) for overcast conditions with a cloud ceiling that is less than 2.1km. For the observations considered at Dublin Airport, on less than 4% of occasions is the atmosphere either stable or unstable. Consequently, the use of the log wind profile (5.14) without adjustment for stability is valid and as such, only wind speeds classified as D (Table 5.4) are employed in the ensuing analyses. To provide a context for what follows, the estimated wind speed (u_z) at a height (z) of 12 m and 17 m was obtained using (5.21).

$$u_z = u_{obs.}\left(\frac{\ln(z/z_0)}{\ln(z_{obs.}/z_0)}\right) \quad \textbf{(5.21)}$$

where u_{obs} and z_{obs} are the wind speed and measurement height at the observation station [170]. This will provide a basis for evaluating the loss of wind resource in urban areas.

Table 5.5 presents statistics for the wind speed and direction observed at the background reference site – Dublin Airport. Measurements are made at a height of 10 m above a grass surface and reported for each hour. The statistics include the mean and standard deviation of speed (u_M and u_S, respectively) and direction (Dir_M and Dir_S). These statistics are provided for the entire dataset and for 30° intervals of the compass direction (360° is north). The final two columns represent estimated wind speed at 17 m and at 12 m at this site using the log wind profile.

Figure 5.12 subsequently illustrates the urban (C) and suburban (S) wind speed frequency distribution as observed at the respective high platforms with respect to the background airport (A) wind speed. Evident here is the diminished mean wind speeds presented at both C and S and the consistency in distribution presented at both locations

Table 5.5 Wind speed (u) and wind direction (Dir) at the Airport (A) background climate site

		$A_{(10m)}$				$A_{(17m)}$	$A_{(12m)}$
Direction	Freq.	u_M (m/s)	u_S (m/s)	Dir_M (deg)	Dir_S (deg)	u_M (m/s)	u_S (m/s)
0-30	1.9%	4.157	1.836	20.893	8.004	4.512	4.279
30-60	3.0%	5.024	1.887	49.611	8.348	5.453	5.172
60-90	3.8%	5.189	2.323	80.676	7.902	5.631	5.341
90-120	3.9%	4.054	2.133	111.552	8.016	4.400	4.172
120-150	10.1%	5.341	2.228	140.151	7.729	5.800	5.500
150-180	4.4%	4.746	2.275	167.088	7.890	5.152	4.890
180-210	9.0%	6.418	2.640	202.467	7.532	6.970	6.606
210-240	22.0%	6.848	2.869	230.824	8.172	7.433	7.049
240-270	24.3%	7.378	3.118	259.513	7.617	8.008	7.595
270-300	11.3%	5.191	2.406	287.545	8.193	5.634	5.343
300-330	4.0%	4.462	2.247	318.912	8.229	4.843	4.593
330-360	2.2%	3.519	1.576	347.710	8.187	3.819	3.622
Summary (data set)		*5.194*	*2.295*	*184.745*	*7.985*	*5.638*	*5.347*
*Summary (120-300°)**		*5.987*	*2.589*	*214.598*	*7.856*	*6.500*	*6.164*

120-300° = 81.1% of data
** 27th of November 2010 to 9th of December 2011*

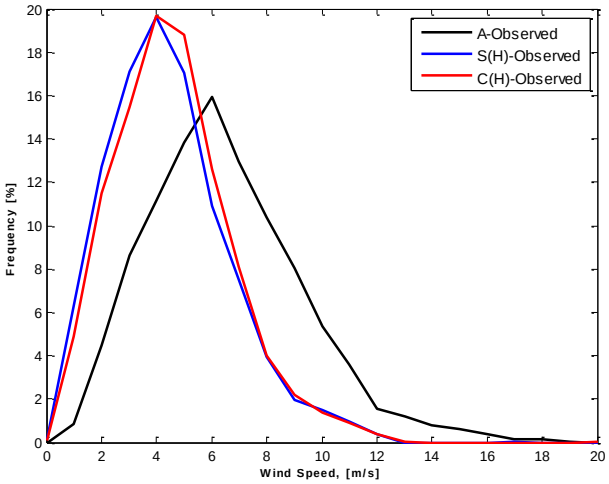

Figure 5.12 Urban (C) and Suburban (S) wind speed frequency distribution

5.4.2.1 Wind observations at urban sites

Table 5.6 presents the wind statistics for the high platform observations at C_H and S_H over the period corresponding to Airport data. The statistics are decomposed according to the 30° sectors used for the Airport data in

Table 5.5, to illustrate the urban effect on both wind speed and direction. Firstly, the wind speed is diminished at both sites: by comparison with the estimated speed at the same height at the Airport, the mean wind speed at C_H and S_H is 65% and 62%. While the standard deviations are also smaller, the ratio to wind speed is higher than at the Airport. In other words, the wind speed is both lower in magnitude and proportionately more variable. The effect of urban roughness is also clear in the direction statistics, especially when the wind is from the less frequently occurring northerly sectors. Within the south-westerly sector (120° to 300°) the mean wind direction at the Airport is 215°, while it is 217° and 223° at the two urban sites however, while the standard deviation at the Airport is 7.9°, the respective values for the urban sites are 25.9° and 30.7°. Thus,

while the average airflow direction at urban sites is broadly similar to that at the Airport in the sector where the wind resource is concentrated, it is less consistent. Figure 5.12 shows overall impact of urban roughness on the frequency distributions of measured wind at C_H and S_H. Note that the effect is similar at both sites.

Table 5.6 Wind speed (u) & wind direction (Dir) at the city (C) and suburban (S) high platforms

Direction	$C_{H(17m)}$				$S_{H(12m)}$			
	u_M (m/s)	u_S (m/s)	Dir_M (deg)	Dir_S (deg)	u_M (m/s)	u_S (m/s)	Dir_M (deg)	Dir_S (deg)
0-30	2.253	1.002	81.805	86.141	1.909	0.934	103.701	86.009
30-60	3.260	1.527	75.999	45.857	2.434	1.045	91.338	47.388
60-90	4.120	1.753	90.856	34.358	3.009	1.313	103.208	42.498
90-120	3.331	1.835	113.245	41.832	2.846	1.624	127.011	50.533
120-150	3.620	1.798	138.836	41.625	3.386	1.860	151.121	48.828
150-180	3.411	1.662	166.984	38.715	3.713	1.792	179.452	36.993
180-210	4.875	2.204	211.382	26.120	5.166	2.427	217.531	26.852
210-240	5.011	2.167	239.409	17.843	5.031	2.173	243.527	23.180
240-270	5.091	2.114	263.330	14.392	4.759	2.086	267.632	18.382
270-300	3.860	1.762	281.550	16.689	3.442	1.615	281.440	30.160
300-330	3.044	1.613	286.764	45.008	2.650	1.395	286.359	55.358
330-360	2.214	0.928	231.193	117.284	2.105	1.082	218.875	114.950
Summary (data set)	3.674	1.697	181.779	43.822	3.371	1.612	189.266	48.427
Summary (120-300°)*	4.311	1.951	216.915	25.897	4.250	1.992	223.450	30.732

120-300° = 81.1% of data
***** 27th of November 2010 to 9th of December 2011

Figure 5.13 shows a series of scattergrams representing the relationship between wind speed at each of the observation sites (Airport (A), C_H, C_L, S_H, S_L). The data shown here represent a shorter period (28th November 2010 to 16th January 2011) and is used here to show the strong relationship between the Airport and C_H and S_H sites. The relationship is considerably poorer at the lower level platforms which are positioned at near-roof height. While there is a strong correspondence between S_H and S_L, that between C_H and C_L is quite weak. One can speculate that the reason for this difference

is due to the distance between sites (circa 500 m in the City) and the placement of the instrument at the gable end of a house with a hipped roof, which is likely to generate considerable turbulence. The majority of the focus in the following discussion is on the wind resource well above roof height (C_H and S_H)

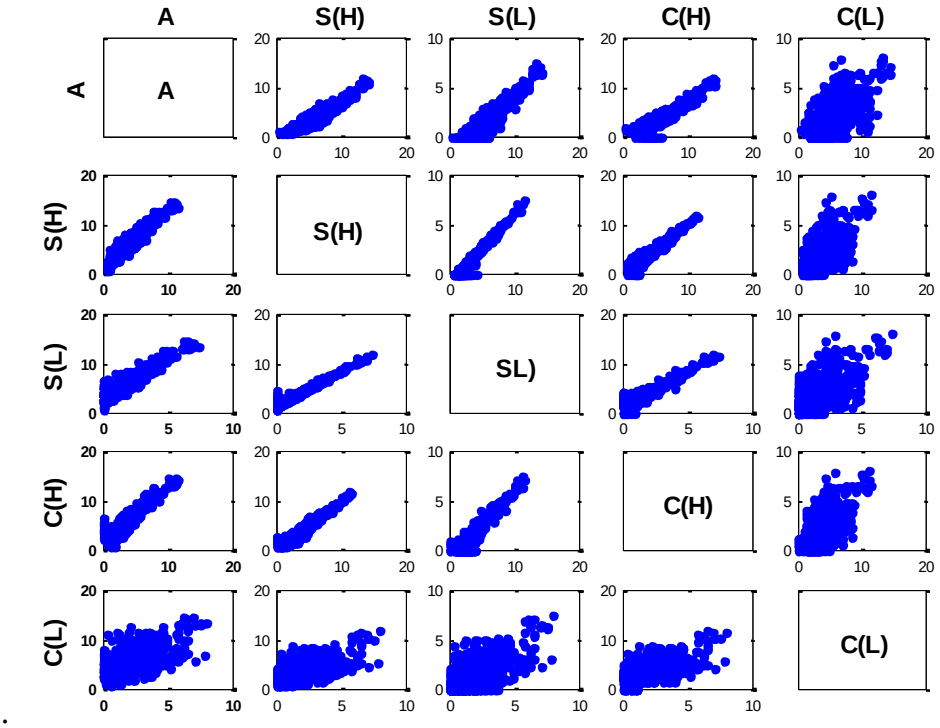

Figure 5.13 Relationships between observed wind speeds at upper and lower platform positions at both the suburban (S) and urban (C) locations with respect to the Airport (background)

5.4.2.2 Estimating urban wind speed

Table 5.7 illustrates the results of the three methods (Wieranga, Bottema and Log) used here to estimate wind speed at the high platform urban sites, that is above the urban RSL ($z \geq z^*$). Each method requires knowledge of the roughness length (z_0), which in the case of applying Wieranga and Bottema was obtained from on Davenport's classification [170]. The selected values of 0.55 and 1.15m representing the suburban and city sites respectively are the average values for that landscape. The friction velocity (u_*) in the Bottema approach is based on the ratio of urban to rural values (β in

(5.16)). Finally in the log model, both z_0 and u_* are determined by fitting the log profile to the measured wind at the urban sites. Overall, Wieranga overestimates the mean wind speed (by 8% at C_H and 12% at S_H) while Bottema underestimates (by 29% and 20%). Two measures of model fit are presented: the Mean Absolute Error (MAE) and the Root Mean Square Error (RMSE). The value of each was smaller for Wieranga at both sites and the difference was most pronounced for the city location.

Table 5.7 Estimated wind-speed at the high platform at the City (CH) and Suburban (SH) sites employing the logarithmic wind profile adjusted according to Wieranga (5.15), Bottema (5.16) and fitted to observed data.

	C_H				S_H			
	Observed	***Wieranga Model***	***Bottema Model***	***Log-Model***	***Observed***	***Wieranga Model***	***Bottema Model***	***Log-Model***
Roughness length (z_0)[m]	--	1.15	1.15	0.8713	--	0.55	0.55	0.5171
Friction velocity ratio	--	1.0	1.3312	1.7022	--	1.0	1.2636	1.5512
u_M [m/s]	4.5992	4.9728	3.2281	4.6165	4.4401	4.9804	3.5795	4.3940
u_S [m/s]	2.1288	2.2497	1.4604	2.0885	2.1712	2.2269	1.6005	1.9647
MAE [m/s]	--	0.7113	1.4248	0.6133	--	0.9392	1.0635	0.7594
RMSE[m/s]	--	0.9790	1.6878	0.8651	--	1.2202	1.3873	1.0479

Not surprisingly the fitted Log model provided the best overall fit. The model parameters are estimated using observed Airport winds between 120° and 300°, which contains 81% of the records. The estimated z_0 at the city and suburb sites is 0.87 and 0.52m. Both of these values are within the range of roughness associated with each landscape [170], but are on the low end (especially for the city site). This z_0 value represents an average for the urban landscape, weighted by the frequency of wind from a given direction. The ratio of the friction velocity at the urban sites, when compared to the rural site, was 1.70 and 1.55, respectively. These values are higher than that suggested by Bottema however, this may be expected given that the value of β in (5.16) was acquired from wind tunnel experiments using block like obstacles. In the city, the great variation in roughness elements and their placement is likely to exert a stronger

drag on the overlying atmosphere. These results indicate that, in the absence of measured values of surface roughness, the existing models produce significant errors in the mean wind speed and in assessing the potential wind resource.

Table 5.8 presents the comparison of the observations at S_L and C_L (over the shorter period from the 28th November 2010 to 16th January) to modelled wind speed using the Power Law (5.18), the COST approach (5.17) using Bottema's adjustment for friction velocity (5.16) and, the COST approach using the friction velocity obtained from the fitted Log model above. The results for the low platform City site are especially poor with the mean and standard deviation values consistently underestimated. The results for S_L are somewhat better but the error terms are also large compared to the measured wind resource and the measured coefficient of variation (u_M/u_S) is 0.9 for the observations, but is over 2.0 for the estimates. These results do not provide any confidence in our ability data to assess the wind resource at this level.

Table 5.8 Estimated wind-speed at the low platform at the City (CL) and Suburban (SL) sites using the Power Law (5.18) and COST (5.17) methods. The measures of goodness of fit are the Mean Absolute Error (MAE) and the Root Mean Square Error (RMSE).

	C_L				**S_L**			
	Observed	***Power Law***	***COST***	***COST (Fitted)***	***Observed***	***Power Law***	***COST***	***COST (Fitted)***
a	--	--	1.28	1.65	--	--	1.28	1.6025
b	--	--	3.00	3.00	--	--	3.00	3.00
u_M *[m/s]*	2.03	2.0043	1.5151	1.3731	1.37	1.9590	1.5150	1.4094
u_S *[m/s]*	1.63	0.9573	0.7309	0.6624	1.52	0.9431	0.7293	0.6785
MAE [m/s]	--	*0.9487*	*1.0373*	0.0919	--	*0.8016*	*0.7561*	0.7660
RMSE[m/s]	--	*1.2562*	*1.3949*	1.4697	--	*0.9579*	*0.9108*	1.5933

5.4.3 Discussion

Ideally, in assessing the potential wind resource at different urban sites, one could make use of observations made at a standard meteorological station and adjust these to suit a

selected site. Work on the urban wind field, completed primarily for the purpose of air quality modelling, has shown that this adjustment is not straight-forward owing to the rough nature of the urban surface that creates a deep Roughness Sub layer that is between 1.5 and 4 times the mean height of the roughness elements. This is echoed in the comparison of wind power densities for the weather stations positioned within the UCL in Figure 5.8 and more specifically in consideration of the quantity of associated null wind speeds.

Observations above the RSL may be transferred to other sites using the log-wind profile, once the surface roughness length is known. However, employing standard tabulated values is likely to result in significant over (under)estimation of the wind-speed. Moreover, the results here suggest that the friction velocity also cannot be taken as constant between the two sites. Using the existing techniques of Wieranga and Bottema and employing tabled roughness values produced biased estimates indicating that site specific knowledge of the surrounding urban morphology is needed. Here, the parameters of the log profile (z_0 and u_*) were obtained by fitting the profile to observed wind-speed at the level of the measurement platforms (z*). This profile was constrained by establishing a boundary condition at a level well above the roughness elements, based on extrapolating the measurements made at an Airport site using a log profile. The resulting model describes the observations closely.

The logarithmically fitted profile extrapolation methodology as a means to model the urban wind speed and its applicability for micro wind turbine performance was initially evaluated in terms of the Wilcoxon Rank-Sum Test (non-parametric statistical hypothesis test). The *WES(5) Tulipo* wind turbine was utilized as an appropriate

generator choice. It has a cut-in wind speed of 3m/s (ideal for urban locations) and can produce 2.5kW from its associated 5m (diameter) blades at a rated wind speed of 9m/s [210]. This turbine, in comparison to the technologies illustrated in Table 2.4 benefits from a lower rated wind speed thereby presenting the most optimistic basis for analysis. The sums of rank for both power output as derived from the modeled speeds and modeled wind speeds are presented in Table 5.9 In this analysis, the accuracy of the wind model is ascertained by how closely aligned the modeled turbine output is with respect to the turbine output as derived through the observed wind speed. It is clear from the results that the modeled wind speeds are accurate and appropriate for use as inputs into (micro) generator models.

Table 5.9 Validation of the wind speed Model in terms of generator output using the Wilcoxon Rank-Sum Test

Hourly wind speed is denoted by μ_2

Test the hypothesis, H_o: $\mu_1 = \mu_2$

S(H)

Bin range (kW)	Average generator output for bin ranges (0 – 2.5kW) based on ***observed*** wind speed	Average generator output for bin ranges (0 – 2.5kW) based on ***modelled*** wind speed	Ranking of Generator output with respect to bin ranges				
0.00 – 0.25	0.07	**0.11**	0.07	1	**1.16**	11	
0.25 – 0.50	0.36	**0.36**	**0.11**	2	1.37	12	
0.50 – 0.75	0.61	**0.57**	0.36	3	**1.41**	13	
0.75 – 1.00	0.87	**0.76**	**0.36**	4	**1.41**	14	
1.00 – 1.25	1.112	**0.97**	**0.57**	5	**1.47**	15	
1.25 – 1.50	1.37	**1.16**	0.61	6	1.6	16	
1.50 – 1.75	1.6	**1.41**	**0.76**	7	1.87	17	
1.75 – 2.00	1.87	**1.41**	0.87	8	**2.01**	18	
2.00 – 2.25	2.11	**1.47**	**0.97**	9	2.11	19	
2.25 – 2.50	2.48	**2.01**	1.12	10	2.48	20	

Sum of the ranks assigned to power output obtained from measured hourly wind speeds: 112

Sum of the ranks assigned to power output obtained from modelled hourly wind speeds: 98

Critical value for Wilcoxon Rank-Sum Test (5% two-tailed values) corresponding to sample sizes 10 and 10 78

Neither rank sum is less than (or equal to) the critical value, therefore the null hypothesis at the 5% level of significance cannot be rejected

C(H)

Bin range (kW)	Average generator output for bin ranges (0 – 2.5kW) based on **observed** wind speed	Average generator output for bin ranges (0 – 2.5kW) based on ***modelled*** wind speed	Ranking of Generator output with respect to bin ranges				
0.00 – 0.25	0.08	**0.1**	0.08	1	**1.3**	11	
0.25 – 0.50	0.36	**0.37**	**0.1**	2	1.36	12	
0.50 – 0.75	0.61	**0.61**	0.36	3	**1.48**	13	
0.75 – 1.00	0.86	**0.88**	**0.37**	4	1.61	14	
1.00 – 1.25	1.12	**1.08**	**0.61**	5	**1.71**	15	
1.25 – 1.50	1.36	**1.3**	0.61	6	1.88	16	
1.50 – 1.75	1.61	**1.48**	0.86	7	**1.9**	17	
1.75 – 2.00	1.88	**1.71**	**0.88**	8	2.13	18	
2.00 – 2.25	2.13	**1.9**	**1.08**	9	**2.28**	19	
2.25 – 2.50	2.48	**2.28**	1.12	10	2.48	20	

Sum of the ranks assigned to power output obtained from measured hourly wind speeds: 107

Sum of the ranks assigned to power output obtained from modelled hourly wind speeds: **103**

Critical value for Wilcoxon Rank-Sum Test (5% two-tailed values) corresponding to sample sizes 10 and 10 78

Neither rank sum is less than (or equal to) the critical value, therefore the null hypothesis at the 5% level of significance cannot be rejected

Further validation is presented in Figure 5.14, which compares the (hourly) observed wind speeds against the estimated (hourly) wind-speed at both the urban and suburban

sites – the coefficients of determination (r^2) are 0.92 and 0.88, respectively. Note that the scatter of points is consistent across the range of observations.

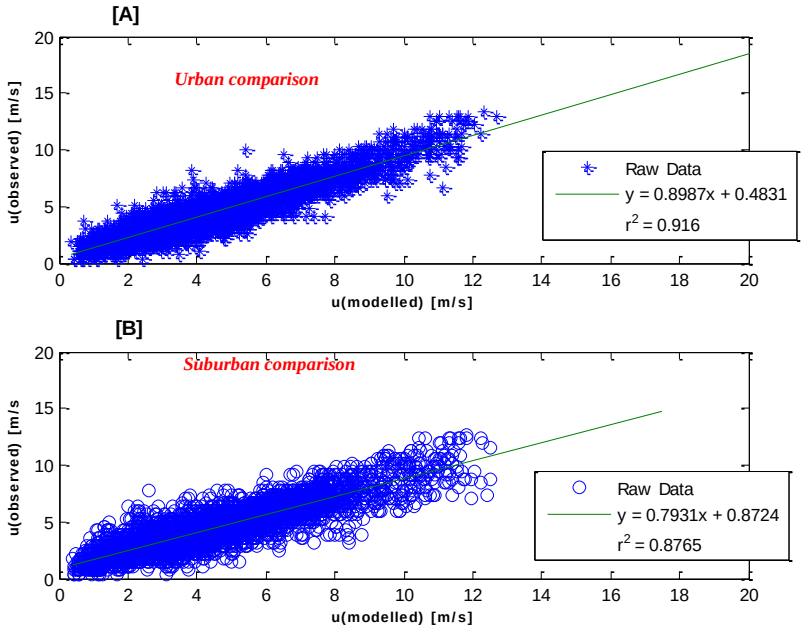

Figure 5.14 Scatter-grams comparing the (high-platform) observed and modelled hourly wind speeds (28th November 2010 to 16th January 2011).

An objective of this research is to determine if there is a predictable wind resource in an urban area that is worth harnessing. To evaluate this, the output of a micro wind turbine positioned at the level of the high platforms at the urban (17 m) and suburban (12 m) sites is estimated. The Wind Energy Solutions' (WES5) Tulipo turbine is again used as an appropriate (comparative) technology. The results based on observations are shown in Table 5.10. At the Airport site, the turbine averages 1.06 kW and over the period, the capacity factor was observed to be 42%. Over the course of a year, it could generate in excess of 5892 kWh, which exceeds the average domestic (electrical) energy demand in Ireland (approx. 5000 kWh). At the city and suburban site, the lower mean wind-speeds results in a reduced output: 2445 kWh and 2672 kWh, respectively. Moreover, for both sites the capacity factor was halved to 20%. Nevertheless, these values still represent potentially half of the domestic energy demand. In Table 5.11, the frequency

distribution of energy generation is shown for all three observation sites based on the recorded hourly wind-speeds. Not surprisingly, the urban sites have higher frequencies at the lower end of energy output, which shows the effects of surface roughness (see Figure 5.13). The slowing of wind has a non-linear and significant impact on energy generation. Allen *et al* [105] in their analysis of the performance of a wind turbine located in varying geographical locations (urban and rural) also observed that the height positioning of the turbine, by virtue of the cubic relationship associated with wind speed, significantly affects the energy harnessing of such technologies.

Table 5.10: Micro wind turbine potential at the Airport, City (CH) and Suburb (SH) sites based on observations and employing the WES(5) Tulipo, which has a rated speed at 9 m/s when it generates 2.5 kW.

Property	Airport	C_H	S_H
u_M [m/s]	6.43	4.60	4.44
u_S [m/s]	2.87	2.13	2.17
Energy [kWh]	5892.13	2445.53	2672.70
$Power_{(average)}$ [kW]	1.06	0.51	0.48
Capacity Factor [%]	42.42	20.43	19.24

As a test of the model developed, the energy generated by the *Tulipo* turbine using observed and estimated wind at the City and Suburb sites was calculated. Although the wind-speeds are well matched (Figure 5.14), the cubic relationship with power as described in (5.15) means that comparing estimates of energy generation based on observed and predicted winds is less straight-forward. Here the ability of the modeled winds to match the observed frequency distributions presented in Table 5.11 is assessed. At the suburban site, the model predicted the correct power category 59% of the time and on 27% of occasions was one category higher or lower. In other words, the model can predict the energy output with a precision of +/-0.25kW, with 86% confidence. At the city site the model correctly predicted the power category on 63% of occasions and its predictions were correct within a band of +/-0.25kW, with 90% confidence. In

summary then, the log-wind model can provide an accurate assessment of the wind resource above roof height once its parameters are known with sufficient precision.

Table 5.11: Average turbine generator output (kW) using observed and modelled wind speed at the City (CH) and Suburb (SH) sites. Turbine output has been categorised into 10 ranges and the average output at each site is tabulated.

Turbine output	Airport		City high platform		Suburb high platform	
Bin range (kW)	N	Measured	N	Measured	N	Measured
0.00 – 0.25	1391	0.11	2145	0.07	2722	0.08
0.25 – 0.50	771	0.40	1050	0.36	1135	0.36
0.50 – 0.75	462	0.62	518	0.61	534	0.61
0.75 – 1.00	422	0.81	307	0.87	332	0.86
1.00 – 1.25	377	1.03	229	1.11	213	1.12
1.25 – 1.50	345	0.00	130	1.37	159	1.36
1.50 – 1.75	309	1.58	91	1.60	102	1.61
1.75 – 2.00	277	1.91	65	1.87	67	1.88
2.00 – 2.25	0*	0.00	47	2.11	51	2.13
2.25 – 2.50	1201	2.46	207	2.48	241	2.48

*Airport wind speeds are in knots and normalized to m/s.

Finally, consideration is provided to how the wind resource becomes depleted as the turbine is moved downwards, closer to roof level. The observation data utilised does not allow exploration into this region so a reliance on the available models to extrapolate from the predicted wind at the high platform levels (z*) into this zone, is required. Figure 5.15 shows how generator productivity diminishes with height: at 0.7z* the energy capture capability has dropped by almost half at both sites. The primary axes of Figure 5.15 show, for the respective locations in Dublin, the decreasing energy yield for the micro generator with reduction of turbine hub height into the UCL. The secondary axes instead present the affect on capacity factor as the turbine hub height is lowered.

This demonstrates the sensitivity of the wind resource in this region. This result can be translated into economic terms using rudimentary information on the cost of the turbine system and the expected income that arises (either by offsetting external energy sources or by export to a grid) from energy generation. Assuming that the cost for wind turbine

system, such as that described above, is about €14,500 [211] and the energy income rate is €0.25 per kWh. Using (modeled) annualized wind speeds at z* (that is, the height of C_H (17 m) and S_H (12 m)) and sample consumer load [145], facilitates the estimation that the turbine cost is recovered within 13.8 and 14.3 years, respectively (simple payback). However, at 0.7z* (that is, about 5.1 m and 3.6 m lower than C_H and S_H), the time taken to recover the initial investment is doubled. Clearly, the vertical placement of the turbine within the urban environment is critical. Superimposed on to Figure 5.15 for both sites is the variation in simple payback with reducing turbine hub height.

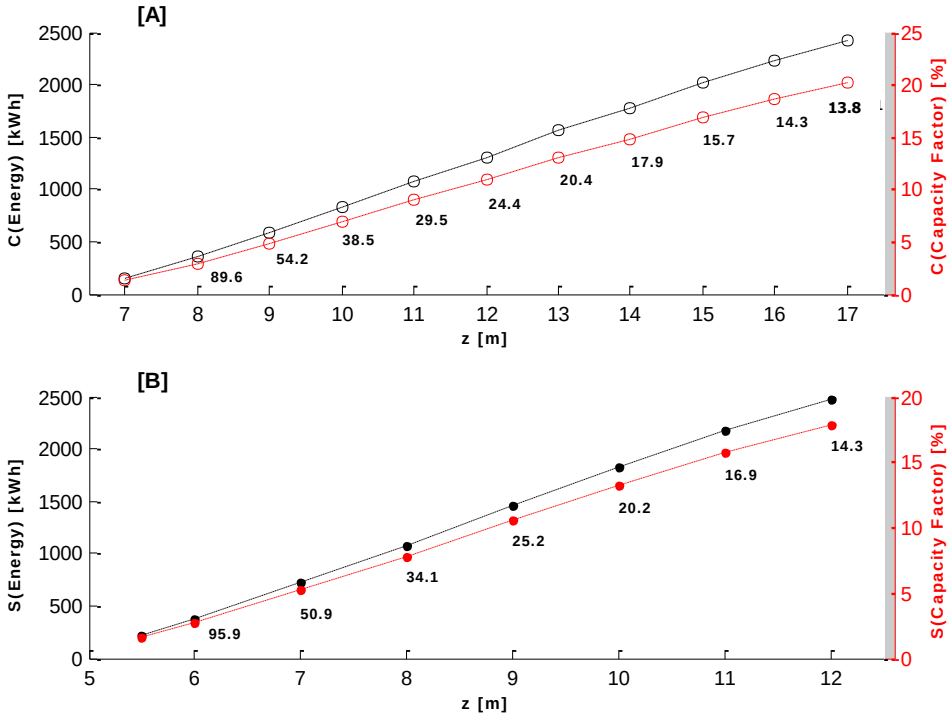

Figure 5.15 The energy implications with respect to height variation for a wind generator at both the urban [A] and suburban [B] locations.

5.5 Conclusions

The goals in this chapter were to investigate the nature of the wind resource (particularly within the UCL) and to assess whether the wind resource above a city surface can be predicted from wind observations made at a nearby site, such as those

available at conventional meteorological weather station. Initial considerations were with respect to how valid wind speed observations within the UCL are in terms of their applicability to wind energy systems. To this end, the Weibull and Rayleigh probability distributions were employed. It was apparent from the analysis that the nature of the UCL in supporting very low wind speeds (with a prevalence of calm periods), means that there is very little by way of wind resource. Furthermore, as illustrated in Table 5.1, traditional means of wind power/engineering, such as the Weibull and Rayleigh distributions, have limited application. In general for both the Airport and high platform observations, the Weibull and Rayleigh distributions underestimate slightly and with the exception of the Rayleigh description for S_H (-7%), the underestimation of wind power density is less than 3.5% This is in stark contrast with the low platforms where in general, there is a significant over estimation (for instance, the Weibull distribution over estimates the resource by 41% at S_L)

In terms of improved modelling capability, the availability of high quality wind observations in Dublin allowed testing of several different approaches to transferring data gathered at an Airport site to two urban locations representing a city centre and a suburban site. Both urban sites are positioned at between 1.5 to 2 times the mean height of buildings and are taken to be above the roughness sub layer (z*). The results indicate that a simple log-profile model performs very well but that the selection of parameter values (roughness length and friction velocity) is critical. In the case reported here, using tabled values without a detailed examination of the urban landscape around the observation sites resulted in significant errors of bias. The availability of wind observations facilitated the acquisition of the values for the parameters precisely. Future

research will focus on obtaining these parameters by urban morphological analysis, independently of wind measurements.

A suitably parameterised log model has been shown to provide consistently good predictions of the urban wind resource at z* and of the energy potential at this level. However, this would place the turbine well above the height of the buildings which is unacceptable in many current planning environments (although this may change). Unfortunately, there are few studies on the wind profile in the layer between roof-height and z* and the observations at near roof level do not provide a basis for evaluating existing models, which have been developed primarily for air quality purposes. Using the estimated wind speed at z*, these models indicate a rapid decline in the energy generation capacity and a corresponding increase in the time taken to recover the initial investment. This work indicates that it is possible to provide guidelines for the correct placement of micro-turbines in urban environments and that their potential for energy generation and cost recovery are predictable.

Chapter 6: Turbulence & Wind Turbine Productivity within Urban Environments

6.1 Introduction

As explained in Chapter 4 and demonstrated in Chapter 5, profiling the urban wind resource is a complex task; particularly in the context of wind energy systems. That profiling prioritised the *mean* wind energy potential over a half-hourly/hourly observation period, so it does not consider implicitly the gusting or turbulence within those observations. What does turbulence mean for the wind turbine? From a wind energy harnessing perspective, there is a lack of understanding concerning the turbulent component of the resource and how it affects turbine productivity; further leading to existing scepticism concerning the technologies viability. Current wind turbine power output measurements (particularly for small/micro wind turbines) are based on an average wind speed over an observation period; with limited accountability of the variability of wind speed within the observation time frame. To account for this variability some researchers have employed computational fluid dynamic modelling to ascertain the potential of building mounted turbines [21, 157, 158]. These works demonstrate the significance of turbine position and mounting height *vis-a-vis* the building, such that small changes in location can have dramatic effects on the power generated. Such analyses is very (computationally) resource intensive and validation of

results is very difficult to achieve. A number of studies have indicated that turbines installed in urban environments are subject to high levels of turbulence. These installations appear to underperform when compared to installations in non-turbulent environments. For example, both the Warwick Field trials [30] and the Energy Savings Trust monitoring programme [29], concluded that problems such as the development of localised turbulence could reduce generation output considerably. The Energy Savings Trust monitoring programme found that turbine outputs in urban locations corresponded to a load factor of less than 3%. Vertical Axis Wind Turbines (VAWT) have been shown to be less affected by turbulent wind streams and it is deduced that this is due to the fact that there is no yawing mechanism associated with these turbines (i.e. turbines do not have to turn to face the wind). However they are still subjected to pulsating wind speeds due to eddies/gusts etc.

The objective of this Chapter is to consider *simple* means to understand the effect on electrical power output of a wind turbine in a turbulent environment. Two mathematical models are proposed that respectively utilise Gaussian statistics and the Weibull distribution to accurately model the consequences on turbine productivity within turbulent environments. These models are facilitated through look-up table(s) that describe the turbulence affected turbine electrical power in terms of *wind speed* and calculated *TI*. In this way, turbine output on the basis of mean wind speed and standard deviation over an observation period (10 minutes) is achieved; both of which are standard parameters within the measurement spectrum of practical wind turbines. The work presented here is based on the analyses presented in [212].

Wind turbine productivity is also affected by mechanical constraints such as how quickly the turbine can react to changing wind directions (yawing). The hypotheses presented here consider an idealised electrical performance of the turbine and doesn't include the inertia associated with the wind energy systems. Notwithstanding this omission, the analyses presented facilitate modelling that can be subsequently applied to a distribution network model to establish an improved understanding of how small wind energy systems can affect the voltage levels. This consolidation will be explored in Chapter 7.

The turbulence models presented in this chapter are tested at the two locations within Dublin City utilised in Chapter 5. At both locations, the high resolution (sonic) anemometry samples the wind resource at 10Hz at a height of about 1.5-2 times the average building height. As these sites are selected as being representative of a specific urban landscape, the paper uses the analysis as a basis for discussion considering how surface roughness might be linked to the models developed.

6.2 The Urban Wind Resource and Energy Harnessing in a Turbulent Context

Research has shown that the lower mean speeds are linked to the higher surface roughness lengths z_0 prevalent in urban environments [159, 161]. The manifestation of turbulence however, is less well understood. Turbulent flows can be described as those in which the fluid velocity varies significantly and irregularly in both position and time [213]. As discussed in section 4.2.2, turbulent flows impact both on the design of wind turbines as well the productivity of power within the turbines – particularly in areas of complex morphologies. Turbulence Intensity (*TI*) is the most common metric to explain the turbulent effect [146], and is defined in (4.6) as the standard deviation of the wind speed σ_u normalised with the mean wind speed (flowing in the horizontal plane) [154]

As discussed in section 4.4.1, a modified flow is manifested in an urban environment resulting with a turbulent structure. Mertens [72] attempts to link *TI* to the surface roughness parameter in (4.8). However, in linking *TI* to z_0, equation (4.6), is predicated on $z >> z*$.

With respect to the impact on the power output of wind turbines subjected to turbulence, the majority of the available research considers utility scale systems with capacities in the MW ranges [214-216]. Cochran, [217], considered empirically linking surface roughness and the power law wind shear coefficient to turbulence manifestation. Cochran further presented a description for turbulence intensity within the lower portion of atmospheric boundary layer also based on surface roughness. His conclusions were that the (kinetic) energy available at the turbine hub height can vary by as much as 20% depending on the level of *TI* present at a site. In references [215, 216, 218], a consensus regarding how a wind turbines power curve is affected by *TI* is reported. Higher *TI* tends to exaggerate the potential output power from a turbine at moderate wind speeds (cut-in), whereas low *TI* undermines the potential output power at rated wind speed (as summarised in Figure 6.1).

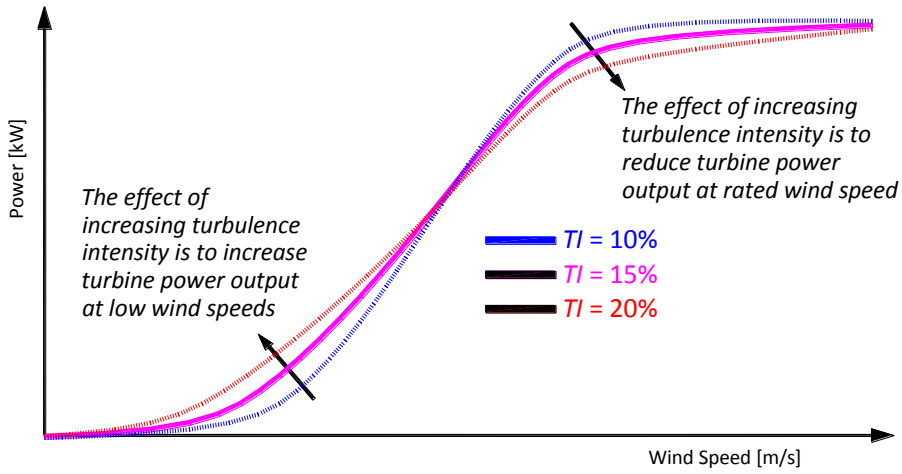

Figure 6.1 The effect of TI on Turbine Power Curves (interpreted from [215])

Lubitz [155], considered the influence of turbulence on energy production from a Bergey XL.1 (small wind turbine). His 1Hz observations were also in agreement with [215, 216, 218]. More specifically, his analysis found that low *TI* consistently results in reduced power output (-2%) between 4m/s and 7m/s, whereas high *TI* contributes to increased power output (up to +4%), over the same speed range. Available studies utilise measured data to provide a description of the turbulent effect and these studies are often in rural locations. However, in urban environments, unbiased high resolution wind data is difficult to acquire for wind speeds – and similarly, reliable and unbiased data for wind turbines (*vis- à-vis* localised building morphologies) in such environments is practically non-existent.

6.2.1 IEC 61400-2

The design requirements for small wind turbines in urban environments are defined by IEC 61400-2 [154]. The standard considers four different small wind turbine classes (SWT) classes (I-IV), which describe the external conditions at various sites. These external conditions relate to wind conditions as being normal or extreme. Normal wind conditions are the dominant experiences during the operation of the SWT. Turbulence and turbulence intensity in the standard is described in terms of a *Normal Turbulence Model* (NTM) and is utilised within the standard in deciding the suitability of a given turbine to the particular urban location. It is generally accepted that with respect to turbulence, there are two components (gusting and change of direction) that affect the performance of micro wind turbines. The gusting component is currently classified by means of the longitudinal turbulence intensity as described in [154, 219]. In ascertaining the impact of the longitudinal turbulence intensity, cosine-corrected longitudinal wind speed along the mean wind direction, is employed. Here the wind speed vector in the horizontal plane, $\mathbf{V}$, is corrected against the mean wind direction of the observations

within the 10-minute time frame ($\mathbf{u} = |\mathbf{V}|.Cos\vartheta$, with ϑ as the angular difference between the angle of $\mathbf{V}$ and the mean direction over the observation period that is employed to correct the individual wind directions in the horizontal plane). Figure 6.2 illustrates the basis for this cosine correction of wind speed observations. In line with common notation, the variable *u* is used to represent the cosine corrected (longitudinal) wind speed in subsequent performance assessment of turbulence (indicated by the red lines in Figure 6.2 below, with the black lines illustrating $|\mathbf{V}|$).

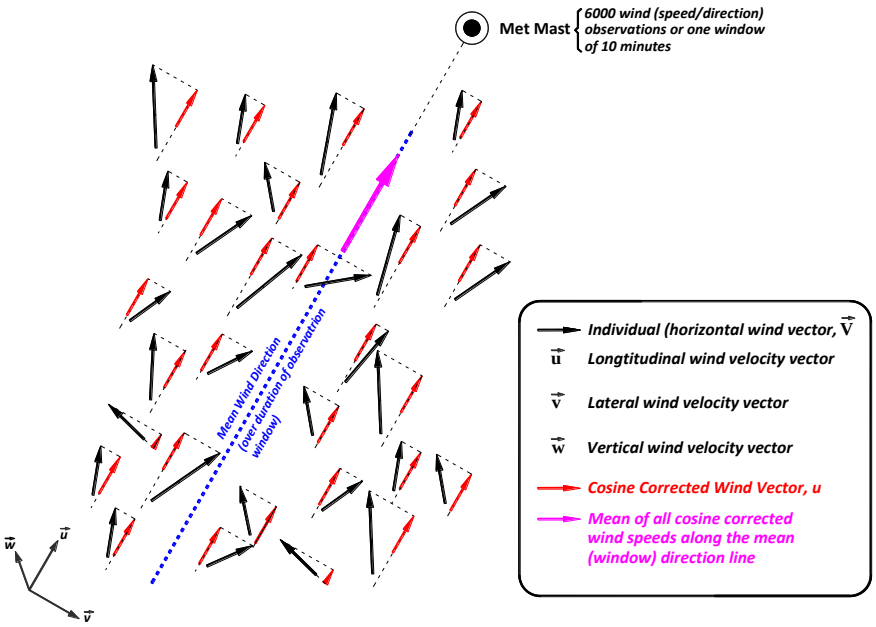

Figure 6.2 Cosine Correction of longitudinal wind speed observations in the horizontal plane

The IEC standard specifies the requirements for an NTM. These requirements include the characteristic value of standard deviation of the longitudinal wind velocity and a means to describe the power spectral density of the longitudinal component of turbulence, in terms of turbulence intensity as it trends asymptotically at low mean wind speeds. The standard suggests stochastic models for calculating the component power spectral density that satisfy these requirements on the basis of the turbulent velocity

fluctuations being assumed random with zero mean Gaussian statistics. These stochastic models are predicated on a turbulence scale parameter which adjusts the power spectral calculation in terms of the height of the hub height of the wind turbine. The standard further refers to an alternative simplified approach that employs a deterministic model, but only if the turbine response to rotationally sampled wind velocity is sufficiently well damped.

The application of the standard in its current form is challenging. Urban mean wind speeds can be low and at very low wind speeds, turbulence intensity - in how it is calculated - trends asymptotically. While micro/small wind turbines are designed to commence generating at low wind speeds, there will be a lack of confidence in modelling that is entirely predicated on a Normal/Gaussian distribution of wind speed. Furthermore, the NTM suggests that the utilisation of cosine corrected wind speeds based on mean wind directions (over the 10-minute sampling period). This implies that there could be outliers not considered as power producing.

6.2.2 Small Wind Generation and Turbulence Modelling

The IEC standard specifies requirements for the safety of small turbines in urban environments including design, installation, maintenance and operation. It does not present a means to determine the performance of these turbines in such turbulently saturated conditions. It is intuitively obvious that, whatever the cause, turbulence reduces the energy output from a wind turbine since turbulence dissipates energy over a larger volume. It is also well documented, that turbulence is extremely difficult to model in a fully deterministic sense, based on the principles of fluid dynamics.

Early explanations of the affects of turbulence on wind turbines employed Taylor series approximations [214, 220], which could replicate the characteristics as illustrated in Figure 6.1. This analysis prioritised the static performance of the turbine (i.e. not considering the dynamic effect of the turbine yawing reaction). The static model developed by Scheiman in [214] can be further developed into a quasi-steady approach to the problem whereas [221] presents a fully dynamic model taking into account both the turbulence and the turbine characteristics. However, in all these approaches, the second derivative associated with the Taylor series approximation results in implausible power results in the transition from below rated power to rated power, particularly if this transition is sharp (as is the case for the majority of turbine technologies).

Albers' approach considered an idealised power curve in terms of the normal distribution model (as utilised in [154]). More specifically, in [222], the wind turbine power can be simulated by considering the variation of wind speed within a window of measurement (10 minutes) as following a Gaussian distribution in terms of:

$$\overline{P_{sim}(u)} = \int_{u=0}^{\infty} P_{I=0}(u).f(u)du \qquad \textbf{(6.1)}$$

Where *u*, is wind speed (m/s), $f(u)$ is the associated wind speed distribution within the 10-minute period (Gaussian wind speeds being assumed that follow a normal distribution around the mean wind speed). $P_{I=0}(u)$, is the idealised wind turbine power curve in terms of the associated wind speed, i.e. not inclusive of the affects of turbulence.

Albers' hypothesis is that if the wind speed within an observation period (10 minutes) is Gaussian distributed, it is fully determinable by the average wind speed and by the turbulence intensity (or standard deviation of wind speeds within the observation period, $\sigma = TI \times \bar{u}$), based on (6.1).

$$\overline{P_{Normalised}(u)} = \overline{P(u)} - \overline{P_{sim(TI)}(u)} + \overline{P_{obs(TI)}(u)} \quad \textbf{(6.2)}$$

where $\overline{P_{Normalised}(u)}$ is the approximate power output based on consideration of how the turbine power curve is affected by turbulence, $\overline{P(u)}$ is the ten minute average of measured power output and $\overline{P_{sim(TI)}(u)}$ is the simulated 10-minute average of measured power output according to (6.1) applied in terms of the measured wind speed distribution and an *assumed TI* (nominally, 10% *TI* is assumed). Here, the standard deviation of the turbulent wind at an assumed *TI* (TI_{sim}) and measured mean wind speed ($\overline{u_{obs}}$) over the observation window accounts for the fact that there cannot be a zero turbulence wind ($\sigma_{sim} = TI_{sim} \times \overline{u_{obs}}$). The simulated 10-minute average of measured power output $\overline{P_{obs_{(TI)}}(u)}$, is similarly calculated to $\overline{P_{sim.(TI)}(u)}$, except in the evaluation of the standard deviation here (σ_{obs}), the *observed* standard deviation (σ_{obs}) is evaluated by incorporating the *observed TI* ($\sigma_{obs} = TI_{obs} \times \overline{u_{obs}}$). Essentially, the manufacturer's power curve is 'idealised' by assuming 10% *TI* within the derivation of the power curve and then subsequently modified to be representative of the *TI* within the 10 minute observation window. In other words, it is assumed that in the compilation of the associated power curve, that there was some level of turbulence (*TI*) influencing the site power measurements. This effect is essentially removed to render the power curve into

an idealised turbine power curve. This idealised power curve is thereafter normalised in terms of observed T.I. as measured by meteorology.

The Albers approach is the springboard from which two models are considered:

1. An adaptation of the Albers approach for small wind turbines and
2. A novel approach that utilises the Weibull distribution as an alternative to the Albers' approximation.

6.3 Methodology

The following sections detail how both models are developed in the MATLAB7^{TM} programming environment. For the analyses presented (and with respect to the analysis concerning how a turbulent wind resource affects the Distribution Network, which will be described in section 7.5.3), cosine-corrected wind speeds u (as described in Figure 6.2), are assumed/employed.

6.3.1 Wind Observations

Observations are made at the two urban locations in Dublin, described in Chapter 5. URB1 (prioritising the high platform observations at C_H) is located closer to the city centre than SUB1 (again prioritising the high platform observations, S_H) and is therefore more urbanised with a higher associated roughness length. This site is also characterised by a higher building density in comparison to SUB1[8]. As URB1 is closer to the city centre, the buildings consist mostly of office blocks and high-rise residential buildings. Buildings in the area often reach heights of 20 m and beyond with morphological complexities located at all angles relative to the anemometer used to record the wind

[8] While the wind data utilised in the analyses is with respect to the observation locations identified in Chapter 5 (S_H and C_H respectively), different notation is employed to distinguish both the different time period and the frequency of the observations involved

velocity data. SUB1 has a more consistent building morphology and the anemometer is surrounded by a relatively lower average building height that consists mostly of two-storey residential buildings and vegetation which is also at similar heights (as described in section 5.2).

At both sites, high-resolution wind speed measurements are taken with a Campbell Scientific CSAT3 three-dimensional sonic anemometer [200]. For the turbulence analyses presented here, 10Hz wind measurements were taken over a 40 day period from 4/4/2012 to 15/5/2012. Consistent with [154], a 10 minute sampling period bench mark was employed; this period is used on a moving window basis with each window consisting of 6000 samples (10 minutes at 10Hz). Data was subject to quality control: *i)* data are removed if the period of 10 minutes is incomplete; *ii)* erroneous data are removed; *iii)* if *TI* is calculated to be >100%, the *TI* for the observation period is set to 100% (note, this control is with respect to the turbine power modelling only; this constraint is not applicable in the discussion in section 6.5)

6.3.2 Model 1: Albers Approximation

The methodology uses a manufacturer's wind turbine power curve that is modified on the basis of varying *TI* and wind speed so that the turbine power output for each 10 minute summary of observed *TI* and mean wind speed, through a 'look-up table', can be obtained. The turbine power curve employed in this chapter was acquired from HOMER^{TM} (Hybrid Optimisation Model for Electric Renewables (version 2.81) as developed by the US National Renewable Energy Laboratory (NREL) [85] and is indicative of a standard manufacturer's power curve. The specific turbine power curve (Skystream 3.7, 2.4kW) is decomposed within MATLAB into a polynomial equation that can be applied to any set or subset of wind speeds; subject to limiting the power

curve in terms of both cut-in wind speed and for wind speeds in excess of the power curve's maximum specified wind speed.

Figure 6.3 illustrates how the *Skystream* power curve is applied in the analyses, with equation (6.3), providing a 10th order polynomial description, of the turbine power curve ($P_{power-curve}(u)$), in terms of wind speed (u), (as derived in MATLAB™).

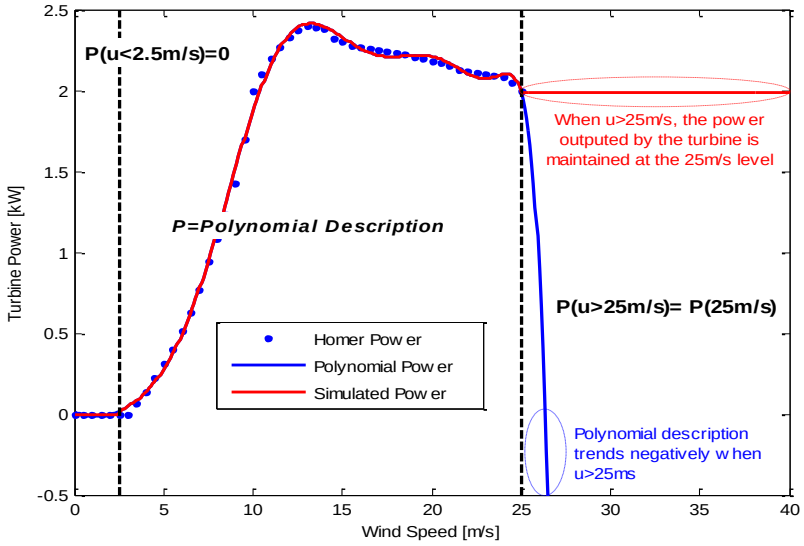

Figure 6.3 Modified Skystream 2.4kW Wind Turbine Power curve as employed in both models

$$P_{Power-Curve}(u) = -(1.62\times10^{-10})u^{10} + (1.89\times10^{-8})u^{9} - (9.17\times10^{-7})u^{8} + (2.38\times10^{-5})u^{7} - (3.55\times10^{-4})u^{6} + (3.07\times10^{-3})u^{5} - (1.50\times10^{-2})u^{4} + (0.04)u^{3} - (3.49\times10^{-2})u^{2} + (1.66\times10^{-2})u - (9.07\times10^{-3}) \quad \textbf{(6.3)}$$

The Albers approach, which quantifies the degradation of power performance of a wind turbine [222], is thus modified so as to predict the power performance based on raw wind resource observations. Employing an approximation to the Albers' approach, the turbine characteristic can be normalised to any level of *TI* as illustrated in Figure 6.4. The curves derived are consistent with observations [155, 215, 216].

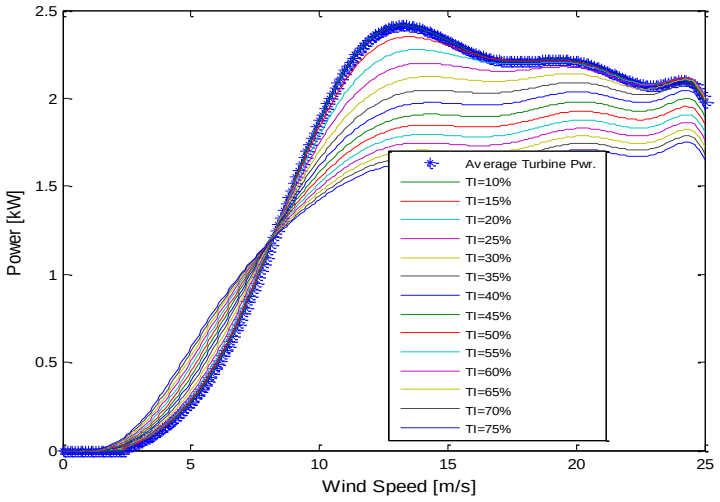

Figure 6.4 Albers Approximation of the Skystream 3.7 (2.4kW) Power curve in terms of varying TI and wind speed.

The procedure, which is implemented in MATLAB 7™ is presented in Figure 6.5.

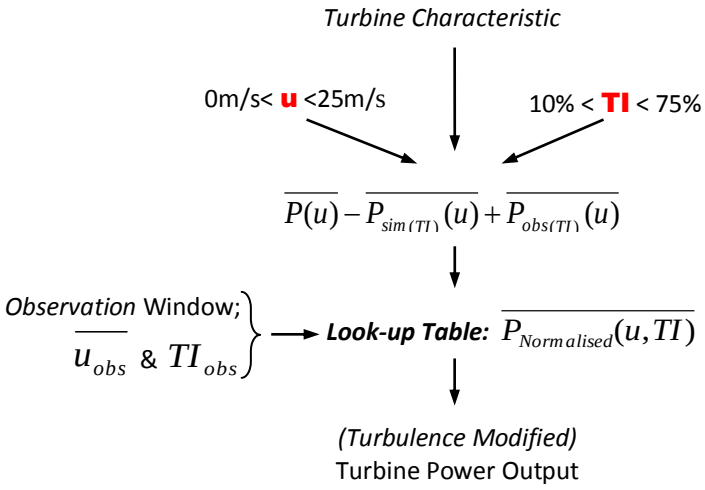

Figure 6.5 Flow Chart describing the Albers Approximation as utilised to derive the normalised turbine output in a turbulent environment.

The methodology outlined in Figure 6.5 illustrates how the turbine's *turbulence modified* output power for the power curve wind speed range and range of practicable *TI* percentages is predicated on a tabulation of the turbulence modified power curves presented in Figure 6.4. This approach facilitates a very simple approach that is transferable to any wind energy technology.

The Albers Approximation considers turbine output and each wind speed observation window in three ways. The *average power* output from the turbine is calculated based on the mean of the 6000 wind speed data-points[9]. This average wind speed is applied to (6.3) and the *average* power is calculated. This value of turbine power is based on an ideal power curve with the implications of turbulence removed. The power curve is therefore modified (in terms of (6.3)) to be representative of such effects by applying a Gaussian distribution with a mean wind equal to the mean of the 6000 data-points and a standard deviation based on a speculative *TI*. In the absence of specifics, the turbine characteristic is modified on the basis of *TI*=10%. Finally, the effect of the observed *TI* is applied to the turbine curve (again through (6.1)) by employing a Gaussian distribution with a standard deviation based on observations (6000/window).These calculations, collectively contained in (6.2) are facilitated through one look-up table. This approach however, loses validity at lower wind speeds as negative longitudinal wind speeds (derived through the application of a Gaussian distribution in the methodology) will arise, e.g. wind speeds with a mean wind of 1m/s and a *TI* value of 75%. However - as will be demonstrated - the methodology is robust for higher wind speeds incorporating high *TI*. The question arises: Is there an optimal frequency distribution other than a normal distribution that could more accurately represent lower wind speeds?

As with the NTM, the Albers' approximation could have issues at low wind speeds, so it makes to consider potential alternative probability density functions (PDF) other than Gaussian. Archer and Jacobson [223] suggest that wind speed PDFs are not static in nature and that they are dependent on the surface conditions. Based on data from 1327

[9] 10Hz sampling implies 6000 samples in 10 minutes

surface stations and 87 soundings in the U.S. for the year 2000, the PDF of wind speed with respect to turbulence and wind speed can be characterised as in Table 6.1.

Table 6.1 Turbulence and Wind Speed PDF Classification inferred from hourly records from 1327 surface stations and 87 soundings in the U.S. for the year 2000 [223]

Low Mean Wind Speed	Log PDF	Log / Rayleigh PDF	Rayleigh PDF
Medium Mean Wind Speed	Logarithmic/Rayleigh PDF	Rayleigh PDF	Rayleigh / Gaussian PDF
High Mean Wind Speed	Rayleigh PDF	Rayleigh / Gaussian PDF	Gaussian PDF

If we consider a Weibull distribution in the same context as the NTM the effects are similar at higher wind speeds to that of the normal distribution model. The fundamental difference however, is that the Weibull distribution gets progressively more logarithmic at lower mean wind speeds for higher values of *TI*. Figure 6.6 illustrates how a Weibull distribution with varying shape and scale can approximate the criteria presented in Table 6.1.

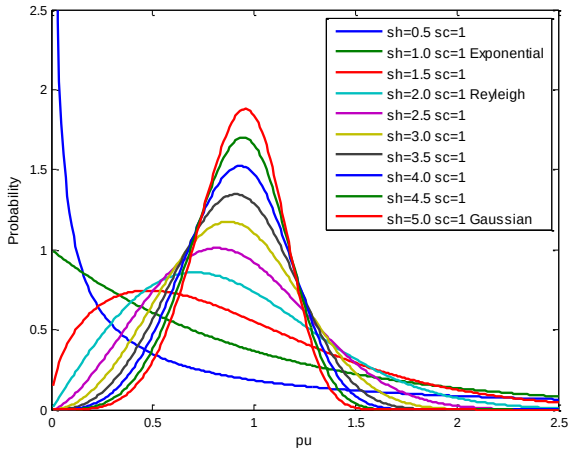

Figure 6.6 Weibull Probability Distribution with varying shape parameters representing the exponential, logarithmic and Gaussian probability distributions

6.3.3 Model 2Weibull Approximation

The Weibull distribution is commonly used to describe wind and wind energy [33, 34, 141] and this function has been shown to give a good fit to measured wind speed data [203]. The Weibull distribution function is described in (6.4).

$$P(u < u_i < (u + du)) = P(u > 0).\left(\frac{k}{c}\right).\left(\frac{u_i}{c}\right)^{k-1}.e^{(u_i/c)^k}\, du_i$$

(6.4)

The Weibull scaling factor, *c*, has the same units describing wind speed; *k*, represents the Weibull shape parameter; u_i is a particular wind speed; du is an incremental wind speed and $P(u < u_i < (u + du))$ is the probability that the wind speed is between u and $(u + du)$ [204]. The Rayleigh distribution is a special case of the Weibull distribution in which the shape parameter, *k*, has a value of 2.0.

The Weibull normalized power is calculated by implementing *Weibull* PDFs that meet the same sample criteria for mean wind speed and *TI* as that measured over the observation window. An average power value is calculated based on 6000 randomly generated data-points and the modelled Weibull PDF(s) in terms of the specific turbine characteristic (Skystream 3.7). Unlike the Albers approximation, the Weibull approximation has two stages, which are summarised in Figure 6.7. Multiple Weibull PDFs are created by varying shape and scale parameters. The shape factor is varied from 0.05 to 30 in 0.01 increments in conjunction with varying scale factors, from 0.05 to 15 in 0.01 increments (4.6 million PDFs). These PDFs are subsequently interrogated against practical wind speed and *TI* references, i.e. the best fit for a speed range from 0:25m/s (0.1m/s increments) and *TI* (10% to 75% in 5% increments). For each of the (4.6million) generated Weibull distributions, corresponding mean wind speed and standard deviation values are recorded. These values are formatted to a resolution of 0.1m/s wind speed and *TI* of 5% on the basis of best fit. The ‘best fit‘ is achieved by method of least squares difference between the generated values and the formatted vales. A table of shape and scale parameters, in terms of mean wind speed and *TI*, is

compiled and each entry is applied to a Weibull distribution to derive a simulated wind speed distribution. These Weibull simulated wind speed distributions are then applied to the polynomial description of the power curve. In this way, the table is enhanced to describe the turbine power in terms of a polynomial representation of the power curve, based on mean wind speed and *TI*.

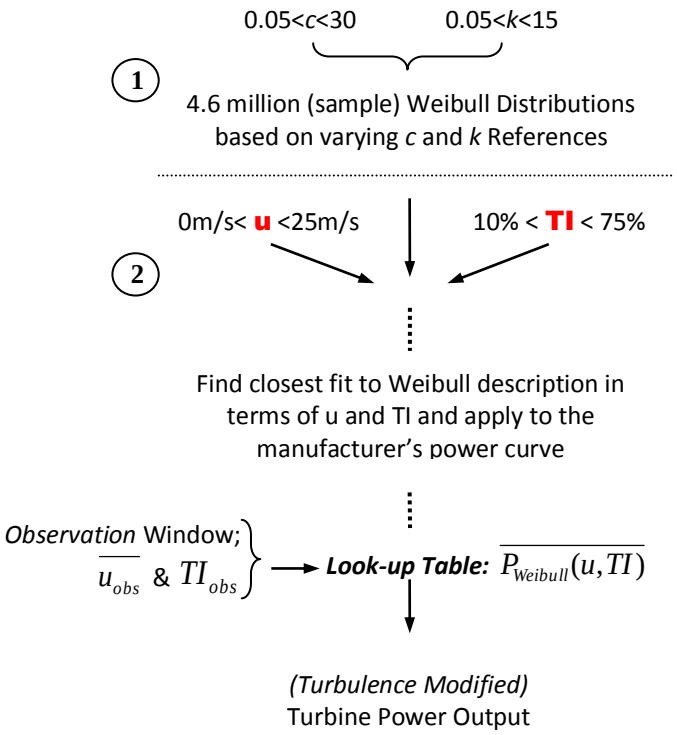

Figure 6.7 Flow Chart describing the Weibull Approximation as utilised to derive a turbine output estimate in a turbulent environment.

Figure 6.8 illustrates the *Skystream 3.7* power curve normalised to the range of practicable *TI* values (%).

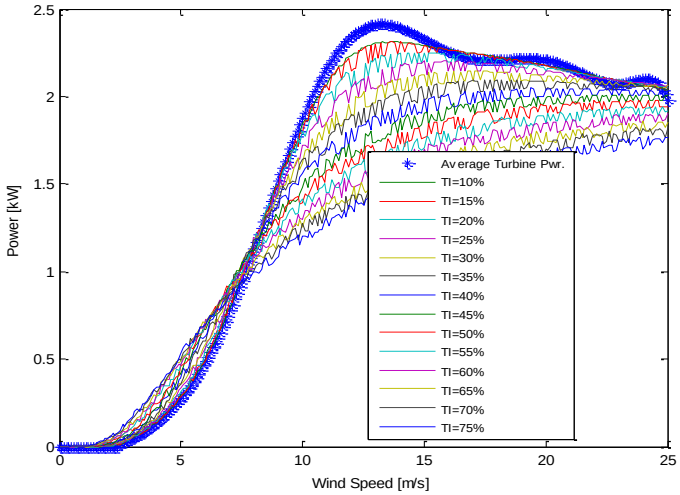

Figure 6.8 Weibull Approximated Skystream 3.7 (2.4kW) Power curves in terms of varying TI and wind speed.

The stochastic nature of the power curves is what is currently achievable with best fit mean and *TI* parameters, as there is a certain amount of rounding evident. A look-up table (similar to the Approximated Albers methodology) presenting the turbine output power with respect to varying *TI* and wind speed is thus derived.

6.4 Results

Over the 40 day period (from 4/4/2012 to 15/5/2012), 10Hz measurements are organised into 10 minute observation windows. As illustrated in Table 6.2, SUB1 and URB1 respectively contained 5.0% and 7.94% of erroneous observation 'windows', Each window considers three power measurements: the *Albers approximation* P_{norm}, the *Weibull approximation*, P_{weib} and the average power over the window, P_{mean}, which is calculated by considering the turbine characteristic with respect to the mean speed over the observation window. P_{mean}, is the industry norm for data logging of power output from wind turbines. Each of these calculations are benchmarked against the *absolute power*, P_{abs}, which is the average of individualised (6000) calculations of power over the observation window and represents the truest measure of generated power by the

turbine. Figure 6.9 illustrates scattergram comparisons of the three turbine output power measurements (P_{mean}, P_{norm} and P_{weib}) with respect to P_{abs} at URB1, (a) and SUB1, (b), respectively. An ideal comparison for either of the three calculation methodologies would give a 1:1 slope ratio (m=1) with an associated intersection and correlation of 0 and 1 respectively. This comparison shows that there is a strong correlation between the Albers (P_{norm}) and Weibull (P_{weib}) approximations to the absolute power generated over the observation window (P_{abs}). The average power (P_{mean}) at both locations is shown in general, to underestimate at lower wind speeds, whereas at higher wind speeds, there is a potential to overestimate.

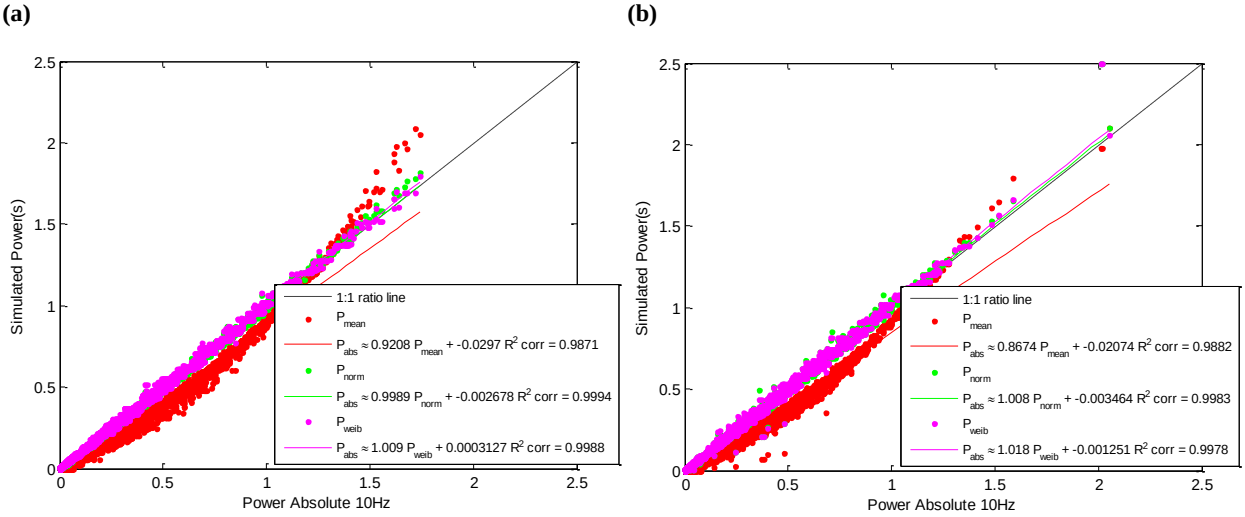

Figure 6.9 Scattergram comparisons of P_{mean}, P_{norm} and P_{weib} with respect to P_{abs} for both sites (URB1 (a) and SUB1 (b))

The comparison presented in Figure 6.9 is further considered to establish if there is an underlying trend in the power prediction methodologies and whether the simulated models under or overprescribe with respect to P_{abs}. Figure 6.10 presents a cumulative sum of differences that occur throughout the full set of 40 days of data with Figure 6.10(a) illustrates this trend analysis for URB1 and Figure 6.10(b) illustrates similar for SUB1.

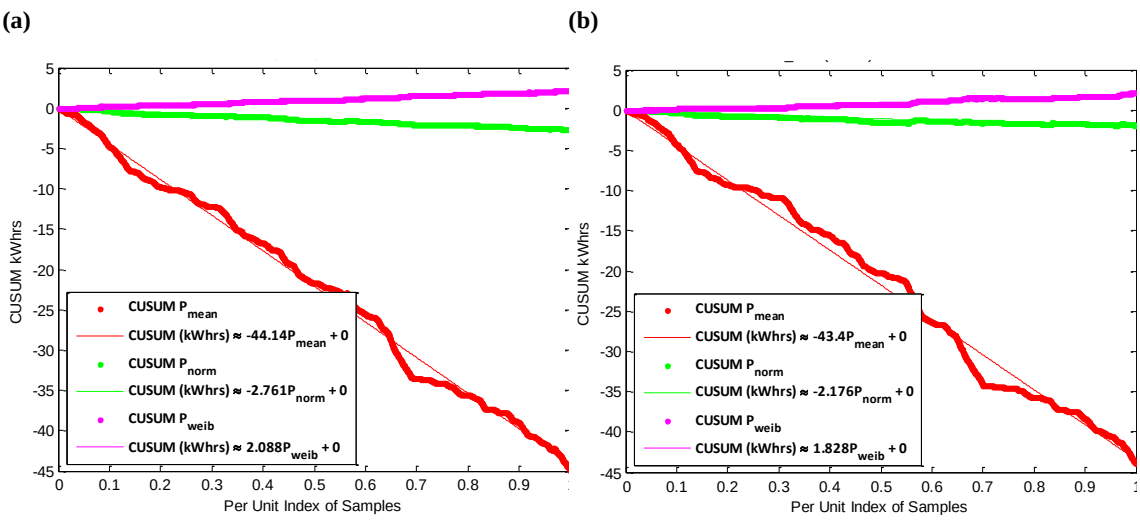

Figure 6.10 The cumulative error for each of the calculated power models (P_{mean}, P_{norm} and P_{weib}) for both sites (URB1 (a) and SUB1 (b)).

It is clearly evident that for both sites, P_{weib} and P_{norm} are virtually horizontal, with only a slight over prediction derived using P_{weib} and under-prediction using P_{norm} cumulatively derived over the 40 days of observations. This strongly implies that both models are consistent with the P_{abs} measurements and are accurate with respect to representing practically, the effect of turbulence on the wind turbine.

Table 6.2 Cumulative energy comparison: power estimation models (P_i) with respect to the absolute power (P_{abs}), calculated over successive observation windows.

	SUB1		**URB1**	
Erroneous Data/Observation-Windows (%)	5.0		7.94	
u_{MEAN} [m/s]	3.41		3.74	
U_{STD} [m/s]	1.70		1.73	
Prediction Methodology	*Total Power predictions*	*Relative error* $\left\{\frac{\sum(P_{abs})-\sum(P_i)}{\sum(P_{abs})}\right\}$	*Total Power predictions*	*Relative error* $\left\{\frac{\sum(P_{abs})-\sum(P_i)}{\sum(P_{abs})}\right\}$
$\sum(P_{abs})$ kWh	181.82		218.77	
$\sum(P_{mean})$ kWh	137.86	-24.2%	173.90	-20.5%
$\sum(P_{norm})$ kWh	179.93	-1.0%	216.04	-1.3%
$\sum(P_{weib})$ kWh	183.94	1.2%	220.94	1.0%

Table 6.2 presents the total energy (kWhr) derived from each of the methodologies and the results are consistent with Figure 6.10.

If the cumulative error characteristic is considered (in terms of a relative error calculation illustrated in Table 6.2), the probability of an error being below a given kW rating for a given simulated model, Figure 6.11 illustrates that both the P_{weib} model and the P_{norm} models derive 90% of their respective errors within 50W of the P_{abs} values at both sites.

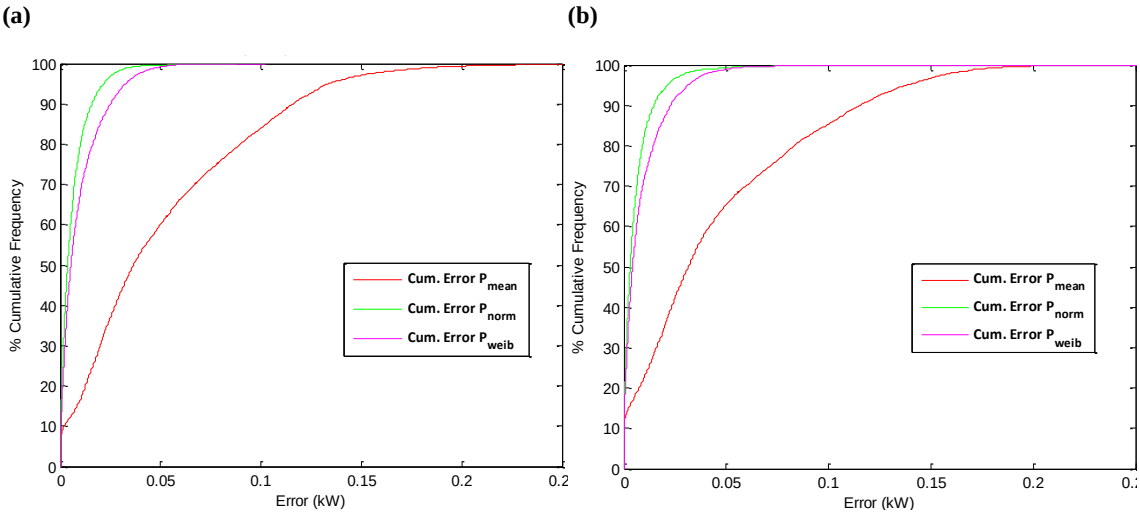

Figure 6.11 The cumulative error characteristic for each of the power prediction models at both URB1 (a) and SUB1 (b); highlighting the accuracy of both models.

Finally, the *mean absolute error* (MAE) between the power estimation models and the absolute power over the range of observation windows is considered. The MAE is the average, over each binned wind speed, of the absolute values of the differences between P_{abs} and the corresponding modelled power (P_{mean}, P_{norm} and P_{weib}), thereby measuring the average magnitude of the errors in each wind speed bin for each model.

$$MAE = \frac{1}{n}\sum_{i=1}^{n}\left|P_{abs} - P_i\right| \qquad \textbf{(6.5)}$$

where P_i is either P_{mean}, P_{norm} or P_{weib}. Figure 6.12 testifies that there is significant and consistent error derived with respect to P_{mean}. The albers and Weibull approximations (P_{norn} and P_{weib}) perform reasonably well across the spectrum of wind speeds with a tendency to introduce error (<75W) at high wind speeds. It is important to note that such wind speeds would be uncharacteristic across urban environments.

(a) **(b)**

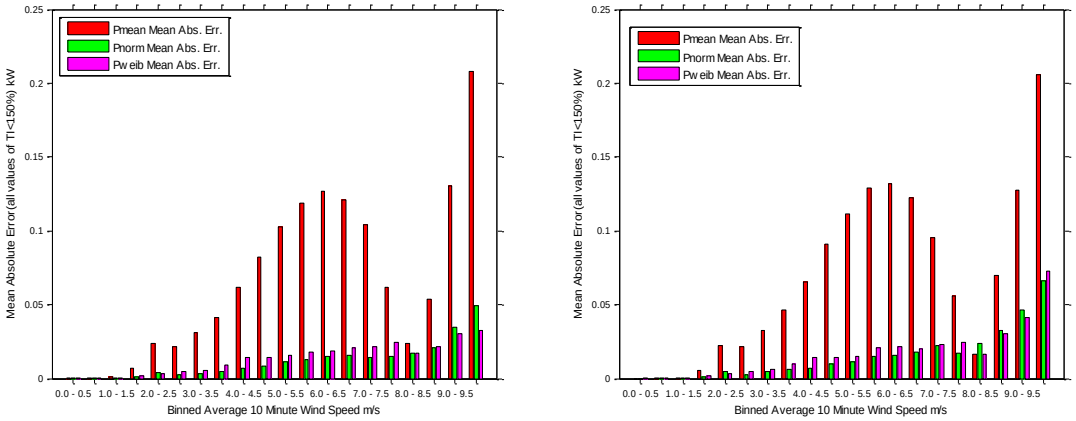

Figure 6.12 MAE comparisons of the power estimation models with respect to Pabs at both URB1 (a) and SUB1 (b)

6.5 Discussion

The analysis in the preceding section has shown that Gaussian and Weibull probabilistic statistics, considered in terms of *TI* observations, can provide an accurate means to estimate the electrical power output of a wind turbine at both a suburban and urban location. As the analyses employed anemometry installed at specific locations representative of their respective environments, with said observations within neutral atmospheric conditions, an obvious progression would be to characterise *TI* in terms of surface characteristics across all types of urban location. Table 6.3 summarises first order estimates of d and z_0 (displacement height and surface roughness length respectively) for the urban context. These estimates are collated within different categories of cityscape (based on a combination of measurement and informed

speculation) as presented by Grimmond and Oke in their work pertaining to the aerodynamic properties of urban areas, [167]. These estimates were utilised in developing a local climate zone classification system [187], where the diversity of landscape/topography is collated as inter-classifications under the urban umbrella. Mertens [72], further observed that *TI* is proportional to z_0 (4.8), but this equation requires z>z*, the wake diffusion height. The observations considered here are at the boundary between the RSL and ISL and as such, application of (4.8) to derive *TI* is not appropriate. Nor is it a viable approach for the majority of urban wind turbines when one considers the likely hub heights for these technologies. An objective for further research therefore, is to define the impact on turbine power output based on urban surface roughness classification by linking it to surface roughness length.

Table 6.3 Typical roughness of homogeneous zones in urban areas, ordered by height and density (source: excerpted from [40])

Urban Surface Form	z_H (m)	z_d (m)	z_0 (m)
Low Height and Density *Residential - one or two-storey single houses, gardens, small trees. Mixed houses and small shops. Warehouse, light industrial, few trees*	5-8	2-4	0.3-0.8
Medium Height and Density *Residential – two and three-storey large or closely spaced, semidetached and row houses, large trees. Less than five-storey blocks of flats with open surroundings. Mixed – houses with shops, light industry, churches, schools.*	7-14	3.5-8	0.7-1.5
Tall and High Density *Residential – closely spaced < six-storey row and block buildings or major facilities (factory, university, etc.), town centre.*	11-20	7-15	0.8-1.5
High Rise *Urban core or suburban nodes with multi storey tower blocks in dense urban surroundings. Major institutional complexes*	>20	>12	>2.0

According to Table 6.3, and with respect to the two locations in Dublin, SUB1 is characterised as ‘Low Height and Density’, whereas, URB1 is characterised as ‘Medium Height and Density’ and both sites have distinctive and different surface roughness lengths. Figure 6.13 illustrates the average filtered *TI* over wind speed bins

for the 40 days observed at both sites. Here the *TI* level is filtered on the basis of wind speed and potential for spurious *TI*. In the event of extremely high wind speed or exceptionally low wind speeds, in the equation describing *TI* (equation (4.6)), asymptotic values are derived. In the context of this research, said occurrences are treated as anomalies.

As Mertens describes in (4.8), higher surface roughness lengths (z_0), will derive a greater the level of *TI*. Relating *TI* to surface roughness requires an ability to trend *TI* across the spectrum of practical wind speeds. An obvious way to consider this is with respect to average *TI* in wind speed bins. Figure 6.13 (a) and (b) illustrate average *TI* is binned with respect to binned wind speeds for URB1 and SUB1 respectively, with average *TI* per wind speed bin superimposed for reference. First of all, the figure clearly illustrates that both sites have different wind speed distributions and this will affect how mean *TI* can be interpreted. This wind speed distribution inconsistency will bias the average *TI* so that above 3m/s, the average *TI* observed at SUB1 appears to be greater than observed at URB1, contrary to the position that at sites with increased surface roughness lengths, *TI* will be higher. Also, the number of observations at both sites within each wind speed bin will introduce biasing of *TI* averaging. Furthermore, the proliferation of unrealistically high *TI* at low wind speeds (0-1m/s) as illustrated in Figure 6.13 will contribute to this biasing effect. These abnormalities have the effect to skew the average *TI*. The same can be said for any *TI* 'outliers' within other wind speed bins along the practicable wind speed spectrum.

(a) **(b)**

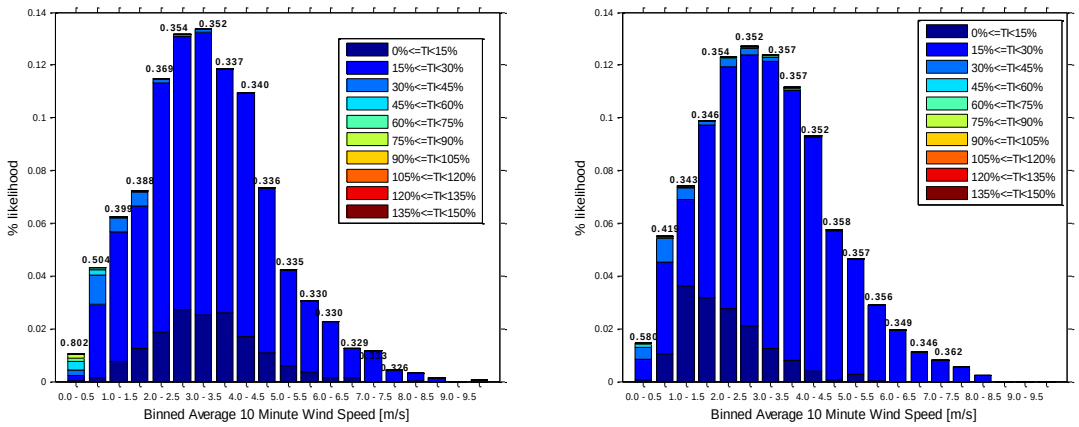

Figure 6.13 Binned TI (15% bins) with respect to binned wind speed (0.5m/s bins) representing observations at both urban locations (URB1 (a) and SUB1 (b)).

Speculative trending is considered on the basis of the lower wind speeds where *TI* and turbulence have the most effect and where biasing within the 40 days of observations were least prevalent. This concept leads to Figure 6.14, where said trending attempts to relate the different surface roughness characteristics describing both URB1 and SUB1 respectively. This trend is speculative; such empirical linkage requires further consideration and cross referencing to alternative wind speed observations at different sites with different surface roughness characteristics.

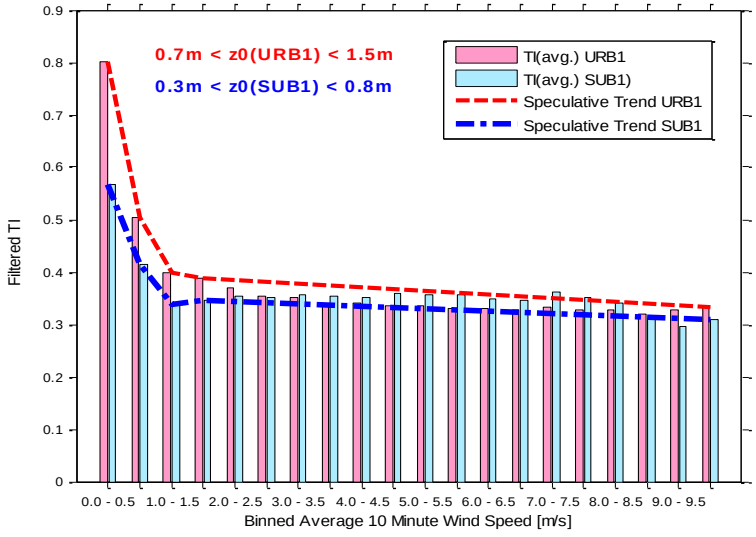

Figure 6.14 Average TI in terms of binned wind speeds at both urban locations (SUB1 and URB1). The TI bins are filtered so that only TI<150% are considered.

Future work in this area will consider the application of the fractal dimension to relate turbulence to surface roughness as a means for site classification based on generic turbulence bands. However, while potentially providing a quantification of the intuitive understanding that potential wind energy is less in urban regions [224], it does not establish the link from turbulent wind speeds to how they impact on the productivity of small wind turbines.

6.6 Conclusion

For a wind energy systems context, there are two aspects to understanding turbulent wind within urban environments. First of all there are the decisions pertaining to installation so that optimal performance can be achieved; hub-height with respect to the proximity/influence of adjacent buildings or obstructions. Secondly an appreciation and/or quantification of how turbulence affects the productivity of a wind turbine is required so that installers can be informed on the basis of installation location. The former was considered in Chapter 5 and the latter has been the focus of this Chapter, with the goal of predicting turbine productivity based on turbulence intensity.

Two mathematical models have been proposed. The first, an adaptation of Albers' work [222], and the second, employs an alternative to the Albers' Gaussian statistics approach to derive indicative TI by using the Weibull distribution. The structure of both models is similar with both models have an added advantage over current manufacturers data in that they calculate all instances of TI and wind speed in tabular form. These tables are therefore applicable for any wind speed reference over a 10 minute period. The Weibull is less cumbersome in that it utilises only one calculation whereas the Albers' approximation requires 3 equations to derive the turbine power output. Both

models were benchmarked using the *Skystream 3.7* (2.4kW) wind turbine, which is representative of commercially available technologies in similar ranges.

Two locations within Dublin City, Ireland, characterised as sub-urban (SUB1) and urban (URB1), were employed to investigate both models over a period of 40 days (from 4/4/2012 to 15/5/2012). At both locations, high resolution (sonic) anemometry samples the wind resource at 10Hz at a height of about 1.5 times the average building height at both an urban and suburban location (URB1/C_H and SUB1/S_H respectively). Therefore, consistent with Chapter 5, the anemometry is ideally positioned to be representative of where micro wind energy systems should be installed.

Benchmarking, cognisant of the industry standards (IEC61400-2) is achieved by comparing the power predicting capability of both models (P_{norm} and P_{weib} for the Albers and Weibull approximations respectively) against P_{abs}, which as the average of all powers produced (in terms of the Skystream characteristic) for each wind sample over the wind observation window (10 minutes). All three power measurements are contextualised with the industry standard method of measuring power, namely, by calculating the power based on the average wind speed over the 10 minute window (P_{mean}). Accuracy is determined on the basis of how well the models compare to P_{abs}.

The results confirm that both models are consistent with P_{abs} and indeed, as illustrated in Figure 6.8 it is evident that over 90% of all simulated powers are within 50W of the P_{abs}. The rating of the turbine is 2.5kW, so this would imply that 90% of readings are within 0.2% error. The Albers' approximation tends to over-predict (slightly) with the opposite outcome when using the Weibull approximation. Contrasted with the industry norm for evaluating power, it was observed that it significantly under-estimates at lower

wind speeds and over estimates considerably at higher wind speeds (Figure 6.6). Both models are observed to introduce errors with increasing wind speed, but in comparison to the industry norm, these errors are negligible whereby significant errors are produced across the spectrum of practical wind speeds (Figure 6.9). In an energy context, the errors derived by the industry standard approach, results in an under-estimation of 24.2% and 20.5% at SUB1 and URB1 respectively (as detailed in Figure 6.7 and Table 6.3). The error associated with the Weibull approximation may be minimised further by reducing the dependency on random numbers (that are used to generate the artificial wind speeds for successive 10 minute periods) and as such, is an area for future research. The Weibull approximation is currently generated by using a series of 6000 'Weibully' distributed random numbers that are then subsequently organised into suitably sized wind speed bins with a class width of 0.5m/s. As a consequence of this histogram with narrow bin width, the artificial Weibull distribution appears somewhat erratic in nature for this relatively small (6000) subset.

Another logical step for this research is to compare the models developed with output power observations from installed wind turbines of similar capacity to the power curve considered here.

However, there are issues with both models and in how they employ *TI*. The metric does not facilitate chronological and time-indexed trending of the wind speed observations, where inter-variability of wind speed perpetuates turbulence. There is also a potential for unrealistic levels of *TI* within observations owing to gusting and occurrences of very low wind speeds. Such effects limit the practicality of the average

TI as a metric, particularly if it is to be employed as a means to link a description of the urban environment (z_0) and average wind speed.

Notwithstanding these issues, with regard to distribution network analyses (as will be discussed in Chapter 7), the models developed here offer the ability to model the reaction of a distribution network considerate of a turbulent wind resource; consistent within an urban environment.

Chapter 7: Distribution Network Modelling In an Urban Wind Context

7.1 Introduction

The distribution network power flow analysis in Chapter 3 considered a representative network, generically described from 38kV to 400V [109]. There, both consumer load and micro generation were balanced across all three phases. As that analysis prioritised a balanced configuration, the neutral voltage and how the network voltage profile is affected by system earthing were not considered. Nor was there analysis relating to quality of supply issues such as those presented by voltage unbalance. Also, as only balanced load was considered in Chapter 3, network cabling was represented as positive sequence impedance only. Furthermore, the integration of the consumer generation was with regard to wind data at Dublin Airport, which is more indicative of a rural wind resource. This ultimately leads to over estimation of both the wind resource and the effects of wind energy system connections in an urban distribution network context. As concluded in Chapter 4, the effect of the city both diminishes and complicates the flow of the wind resource, with building morphology and associated landscape heterogeneity contributing to the increased fetch and turbulent characteristic of the resource.

This Chapter considers a representative urban network based on an actual section of the distribution network in suburban Dublin and employs the wind modelling developed in

Chapter 5 as a more realistic wind resource for the embedded generation. Furthermore, analyses of the effects of turbulence as modelled in Chapter 6 will also be considered. The section of network contains a substation and 74 consumers connected to individual phases across 10 mini-pillars. The network is described in terms of 3-phases and neutral with unbalanced load and generation and system earthing is also facilitated.

Power flow analyses is through an *Admittance Matrix Correction* (AMC) algorithm that utilises an admittance description of the network based on the approach developed by Benato *et al* [225]. This approach considers the core network (cabling and system earthing) separately to consumer load and generation, which are represented as shunt admittance elements; with both load and generation being modelled as constant power sources. Alternative models can easily be included with load/generation modelled as constant current or constant impedance. For a network model that facilitates both load and generation, shunt element admittances are 'corrected' iteratively in the power flow solution. This is a more general representation. A more particular case would be incorporating only load, which implies a direct solution with said load being described as a constant admittance.

The urban wind speed modelling described in Chapter 5 forms the basis for *driving* the consumer (micro) generation in the correction admittance power flow algorithm; effectively bridging the separate research themes presented in this thesis. Initially, a simplification of the model, as derived in Chapter 5, employs the surface roughness parameters for the suburban location (S_H) to facilitate a rural/urban logarithmic extrapolation. This simplification is employed to consider sample (seasonal) profiles derived in terms of similar load data profiles [187].

The detailed model that was designed to consider the wind resource at both a suburban and urban location (S_H and C_H respectively) [209] is subsequently considered to establish the network voltage profile over 8760 hours (one year). In this regard, a first order Markov chain is employed to 'extend' the model to facilitate statistical consistency so that generation capacity factor based on the same time reference at both observation sites, can also be investigated.

Finally, the turbulence modelling that was discussed in Chapter 6 is considered in terms of implications on a distribution network. The AMC power flow model is modified to integrate the 'turbulence affected' turbine output in ten minute intervals (over a 40 day period), so that an investigation of the consequences of a turbulent wind resource, from the turbine's perspective and the ramifications concerning network voltage profiling, could be investigated.

7.2 Distribution Network Structure

Details of a section of the low voltage (LV) network concerning a suburb of Dublin City were acquired from the Irish Distribution Network Operator (DNO), *ESB Networks* [226]. Figure 7.1 illustrates a schematic of the network[10]. 74 single phase consumers are supplied through a 10/0.4kV substation transformer. The 10/0.4kV transformer is not equipped with a tap-changer, but the sending end voltage is through a 38/10kV transformer which is facilitated with a tap-changer. Each mini-pillar accommodates consumer connections at single-phase (domestic installations), and each consumer has distinct earthing provision (TN-C-S). Service cabling from mini-pillars to consumers is modelled as overhead (25/16mm^2 concentric neutral), whereas, the cabling from the substation transformer to the first mini-pillar and for each successive mini-pillar

[10] The customer identification within Figure 7.1 have been appropriately disguised

thereafter, 4-core, underground cabling is employed (either 185/70mm^2 cross-linked polyethylene (XLPE), or 70mm^2 paper-insulated (NAKBA)).

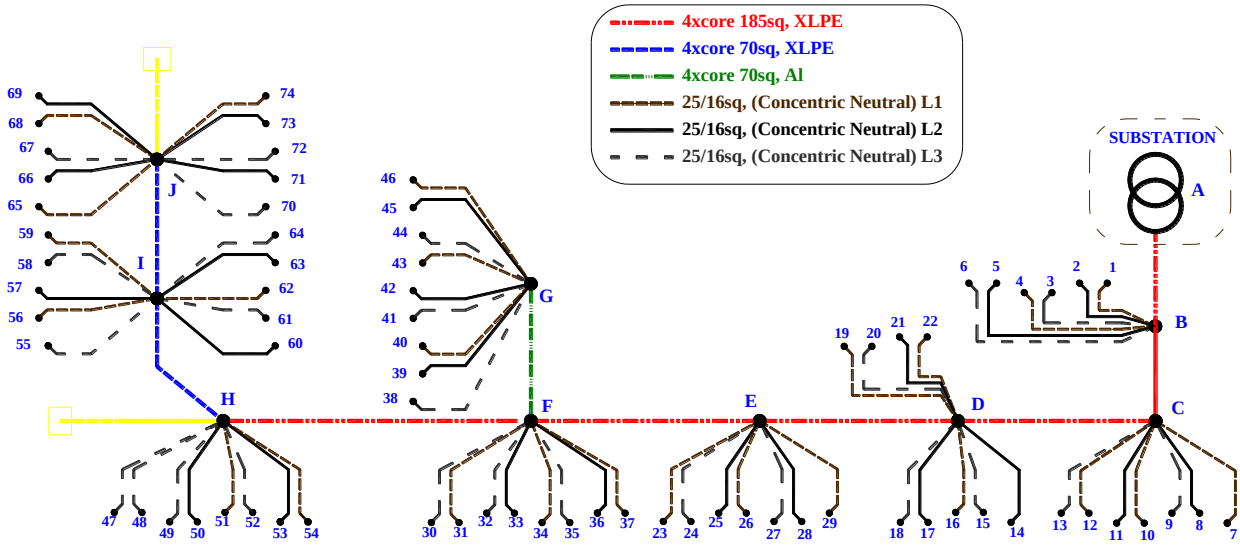

Figure 7.1 Representative Distribution Network [226]

Figure 7.2 illustrates a generic consumer/(mini) pillar configuration, incorporating individual consumer connections, with each consumer facilitated with a *TN-C-S* earthing system. Each consumer is supplied at single-phase (230V) and each consumer has a distinct earthing arrangement that complies to TNC-S.

A TN-C-S earthing system involves the direct connection to earth at the supply authority's sub-station transformer whereas the consumer earth is effectively connected to ground through an earth electrode. Within the installation, both earth and neutral are independent considerations. At each installation an earth electrode is provided. The earth electrode is connected to the installation's main earth terminal (MET) and therefore to the DNO neutral. This arrangement provides the consumer with an earth

terminal, which is connected to the neutral conductor of the system, thereby providing a low impedance path for the return of earth fault currents.

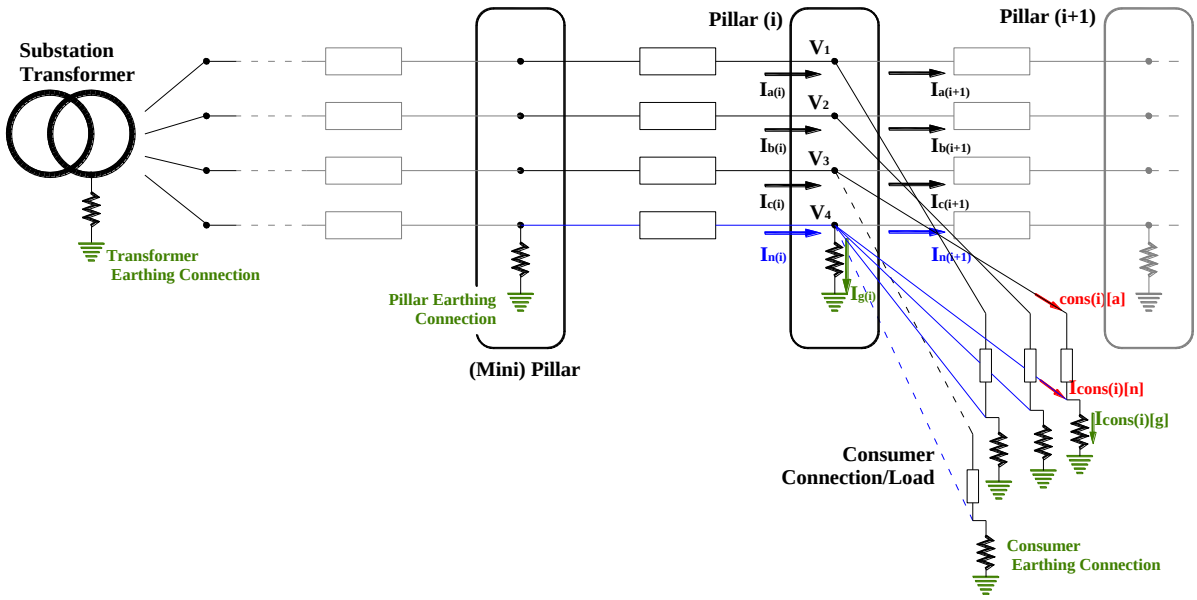

Figure 7.2 Generic Network Configuration incorporating consumer/pillar connections and the associated (TN-C-S) earthing arrangements

In terms of both Figure 7.1and Figure 7.2, the analyses presented in this thesis represents detailed modelling of the actual configuration of an urban network.

The sending voltage at the 10/0.4kV transformer operates in accordance with the assumed maximum voltage drop limits as defined in the EN50160 voltage standard [227] . Essentially, the DNO is prescribed to deliver electricity in a voltage range of 207V to 253V (±10% $V_{Nominal}$ of 230V).

The network has a radial configuration and comprises 4-core (three-phase and neutral) cabling between mini-pillars with individual consumer connections via a single phase service cable (Figure 7.2). It is important to note that exact network detail is difficult to

validate as it is not normal in practice to model such sections of the network. Furthermore, the DNO employs software (*SynerGEE*^{TM}) that utilises a sequence impedance description of network cabling, whereas modelling here is in terms of the full matrix (impedance) descriptions. The network details provided includes:

- Description of the Network topology
- Line and Cable impedance
    - As per Figure 7.1 the system cables include 4-core, 185mm^2 (XLPE), 70mm^2 (XLPE), 70mm^2 (NAKBA) and the customer service cable is a single-core, 25.16 mm^2 (concentric neutral)) cable
- Customer detail including phase allocation and respective distances from customer connection and associated mini-pillar
- Example spot load demands (kW) were provided for each customer

The network was developed in MATLAB^{TM} and the *Admittance Matrix Correction* (AMC) Power Flow methodology [225] forms the basis of voltage analyses. This power flow methodology is developed from research carried out by Benato *et al* [225] in which a *complex admittance matrix* (CAM) describing the network is employed. The following section will outline how the network cabling is considered. Cable models are very influential in deriving any power flow solution aiming to derive accurate voltage profile results. Before describing the methodology employed in this thesis, the rationale for the methodology is established by considering in general terms the requirements to facilitate an unbalanced power flow solution.

7.3 Unbalanced Power Flow Considerations & Preliminary Analysis

7.3.1 Network Cabling

Carson in his paper [228] employed image theory to develop equations that calculate the self-impedance with earth return and mutual impedances with common earth return (as illustrated in Figure 7.3). While initially developed to consider wave propagation in

communications cable systems, these equations have subsequently been adapted for the evaluation of power lines.

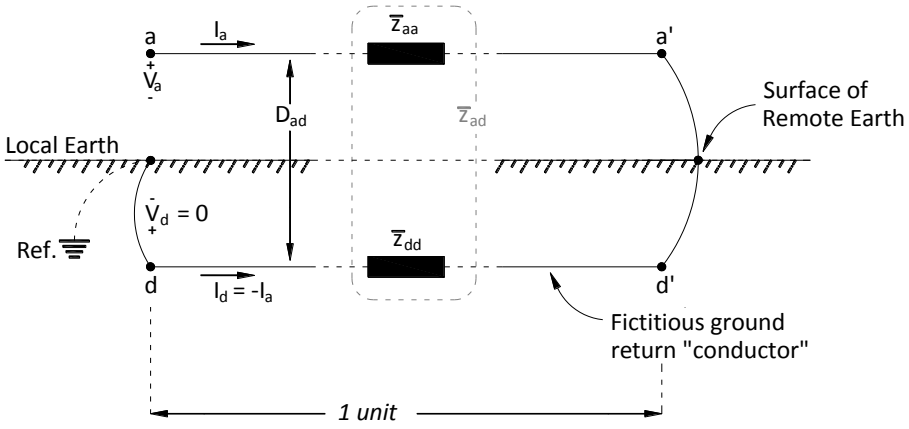

Figure 7.3 Carson's Line with Earth Return (source: interpreted from [229])

Line impedance evaluation is critical in any evaluation of power flow in a distribution network. Distribution feeders are inherently unbalanced and for accurate analysis assumptions should not be made regarding spacing between conductors, conductor cross-sectional areas, or cable transposition. Carson assumed the earth as an infinite, uniform solid, with a flat uniform upper surface and a constant resistivity. He made use of conductor *images*; i.e., every conductor at a given distance above ground has an image conductor the same distance below ground. As illustrated in Figure 7.4, the original Carson equations are provided in (7.1) and (7.2), which describe the self and mutual impedances of/between conductors *i* and *j* respectively.

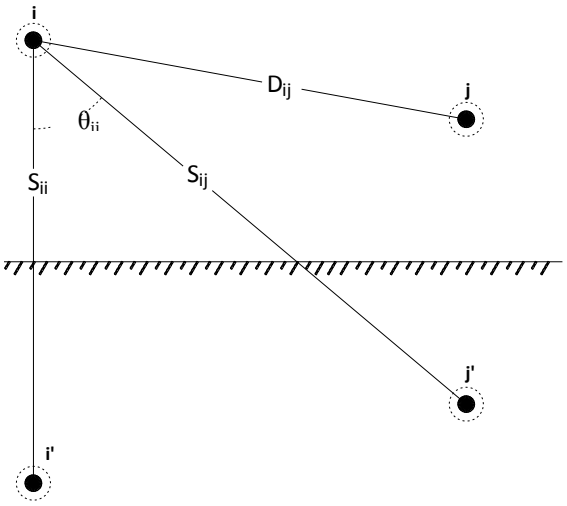

Figure 7.4 Conductors and images (source: extracted from [230])

$$z_{ii} = R_i + 4\omega P_{ii} G + j\left\{ X_i + 2\omega G.\ln\left(\frac{S_{ii}}{RD_i}\right) + 4\omega Q_{ii} G \right\} \ [\Omega/mile] \quad \textbf{(7.1)}$$

$$z_{ij} = 4\omega P_{ij} G + j\left\{ 2\omega G.\ln\left(\frac{S_{ij}}{D_{ij}}\right) + 4\omega Q_{ij} G \right\} \ [\Omega/mile] \quad \textbf{(7.2)}$$

where z_{ii} = self impedance of conductor *i* in Ω/mile

z_{ij} = mutual impedance between conductors *i* and *j* in Ω/mile

R_i = resistance of conductor *i* in Ω/mile

$\omega = 2\pi f$ = system angular frequency in radians per second

$G = 0.1609344 \times 10^{-3}$ Ω/mile

RD_i = radius of conductor *i* in feet

D_{ij} = distance between conductors *i* and *j* in feet

S_{ij} = distance between conductor *i* and image *j* in feet

θ_{ij} = angle between a pair of lines drawn from conductor *i* to its own image and to the image of conductor *j* in feet

$$X_i = 2\omega G.\ln\left(\frac{RD_i}{GMR_i}\right) \ \Omega/\text{mile}$$

GMR_i = Geometric Mean Radius of conductor *i* in feet

$$P_{ij} = \frac{\pi}{8} - \frac{1}{3\sqrt{2}} k_{ij} \cos(\theta_{ij}) + \frac{k_{ij}}{16} \cos(2\theta_{ij}) \cdot \left(0.6728 + \ln \frac{2}{k_{ij}} \right) \quad \textbf{(7.3)}$$

$$Q_{ij} = -0.0386 + \frac{1}{2} \ln \frac{2}{k_{ij}} + \frac{1}{3\sqrt{2}} k_{ij} \cos(\theta_{ij}) \quad \textbf{(7.4)}$$

$$k_{ij} = 8.565 \times 10^{-4} . S_{ij} . \sqrt{\frac{f}{\rho}}$$

f = system frequency in Hz

ρ = resistivity of earth in Ωm

Carson's (original) equations are described in Ohms/mile, but the subsequent cabling considerations that will be discussed here are described as Ohms/kilometre. In deriving a primitive expression of cable impedance and in consideration of the *ground*, Carson's formula involved an "infinite integral to formulate the effect of the finite conductivity of the ground" [228]. The terms P_{ij} and Q_{ij} are constants (correction terms) that are derived in the evaluation of this infinite integral.

The GMR_i the geometric mean radius, reflects the fact that there are magnetic flux lines not only outside of the conductor, but also inside. The GMR describes a hypothetical radius that replaces the actual conductor with a hollow conductor of radius equal to GMR such that the self inductance of the inductor remains the same. For distribution network cabling, with the exception of the service cables (concentric neutral cables), the GMR_i can be estimated in terms of the cable conductor radii as $GMR_i = 0.7788.r$ [229, 231], where *r* is the radius of the conductor.

The application of Carson's equations as they are described ((7.1) to (7.4)) is cumbersome and requires simplification. There are different approaches in literature to

describe Carson's equations - and in particular how the correction terms are considered. Kersting [230], employs *modified Carson's* equations in which approximations for P_{ij} and Q_{ij} are derived [232] to describe self and mutual impedance equations. In this regard, the first term of P_{ij} and the first two terms of Q_{ij} are employed.

Anderson [229], also derived equations to describe the self and mutual impedances of the line(s). Anderson, considers the Carson's line as a single return conductor with a self GMD of 1 foot (or 1 meter), located at a distance (unit length) above/below the oh/ug line, where said distance is a function of the earth resistivity p. In his description of the cable impedances, Anderson employs the concept of hypothetical return path of the earth current and is a function of both earth resistivity, ρ and frequency, f: $D_e = 2160\sqrt{\rho / f}\ [feet]$.

In terms of this thesis and the network model that is developed to facilitate the AMC power flow algorithm (which will be described in detail in section in 7.3.2), an approximation for Carson's equations analogous to Anderson's consideration is employed. The network cabling is modelled by considering the basic Carson equations ((7.17) to (7.19)) in terms of the electromagnetic coupling that is developed between parallel lines [233]. This approach segregates the self impedance into an internal and external component, whereas the mutual impedance is considered separately.

The following section discusses the relative cable parameters specific to the AMC power flow methodology as well as more generic considerations such as conductor arrangements and the evaluation of geometric spacing between line conductors.

7.3.2 Unbalanced System & Power Flow Considerations

The goal of any power flow algorithm is to robustly derive a solution for voltage profile (and power flows). In consideration of an LV power flow however, standard power flow algorithms such as standard *Gauss Seidel*, *Newton Raphson* (NR) or the decoupled NR algorithm [137] are not ideal due to the radial nature of the network, the inherent unbalanced load configuration as well as the extra complexity associated if earthing systems at a consumer level are included. Notwithstanding such complexity, the solution method should be reliable, versatile with inherent simplicity [38]. Therefore an approach initially considered in the research presented here was a form of forward/backward power flow solution; as a robust and simple methodology. In this context, a method developed by Ciric *et al* [234, 235] was initially considered and applied to the network described in Figure 7.1 and Figure 7.2 [236].

Figure 7.5 presents a flow diagram describing how the algorithm was applied. Cable modelling in the Ciric *et al* approach is predicated on the assumption that the ground can be represented as a fictitious conductor to compute the ground self and mutual impedances. Therefore, for a four wire system (including consideration of the neutral conductor and earth), a 5x5 impedance matrix is compiled.

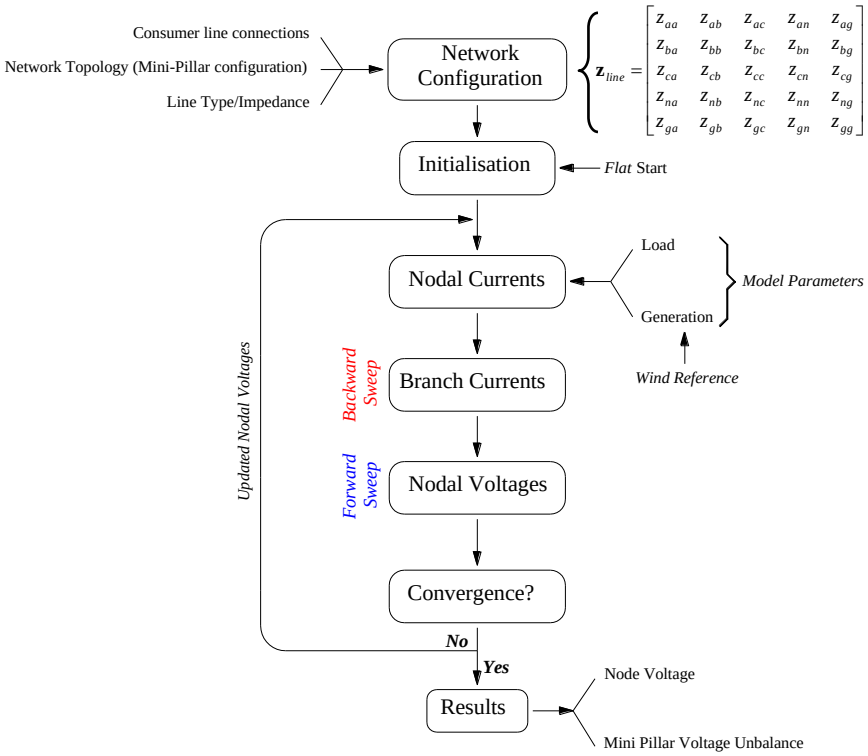

Figure 7.5 Flow Diagram illustrating the modified Forward/Backward Power Flow Methodology

Two (primary) concerns arise from the methodology described by Ciric *et al* [234, 235] relating to the evaluation of the neutral/earth currents and also the requirement to correct the neutral/ground connections. The current injected at each node is derived by

$$\begin{bmatrix} I_{ja} \\ I_{jb} \\ I_{jc} \\ I_{jn} \\ I_{jg} \end{bmatrix} = \begin{bmatrix} \left(\frac{S_{ia}}{V_{ia}}\right)^* \\ \left(\frac{S_{ib}}{V_{ib}}\right)^* \\ \left(\frac{S_{ic}}{V_{ic}}\right)^* \\ -\left(\frac{z_{gi}}{z_{nni} + z_{gi}}\right).\{I_{ia} + I_{ib} + I_{ic}\} \\ -\left(\frac{z_{nni}}{z_{nni} + z_{gi}}\right).\{I_{ia} + I_{ib} + I_{ic}\} \end{bmatrix} \quad [\text{A}] \tag{7.5}$$

where the subscript i and j respectively represent the current entering and leaving a line section (branch) with the earth specifically represented as a separate conductor;

z_{ggi} and z_{nni} are the ground and neutral self impedances respectively and z_{gri} is the grounding impedance at node *i* ($z_{gi} = z_{gri} + z_{ggi}$).

Voltage correction is performed on all nodes with grounded neutrals)

$$V_{n(j)} = z_{gr} \times J_{ig} \qquad [\mathrm{V}] \tag{7.6}$$

The Ciric *et al* forward/backward power flow methodology ([234, 235]) is based on consideration of the earth as a specific conductor and as such the neutral earth voltages (NEV) are calculated by considering the neutral/earth connection in terms of a current divider. While the approach is relatively simple and easy to apply, it is unclear what effects are manifested with regard to mutual line and earth couplings by considering the earth as a dedicated conductor, this potentially minimises the effects of said mutual couplings between the earth and respective line conductors. Further exasperating a diminished mutual coupling representation, the algorithm requires a voltage correction (7.6), which again is not (explicitly) justified. Furthermore, Ciric *et al* do not employ a direct 'current adjustment' and instead used a voltage correction which considers the effects of a current flow through the ground impedance on the neutral potential.

In light of these issues, a more developed description of the network, utilising a 4x4 line impedance construct (thereby incorporating the earth within the impedance description), that could explicitly include the affects of the system earthing was investigated. In this regard, the network (Figure 7.1) was modified in MATLAB facilitate a forward/backward solution, but without the adaptations inherent in the Ciric *et al* approach [234, 235]. Also, the algorithm devised by Ciric *et al* considered mutual coupling involving the earth as a 'correction caused by the ground influence' and used

"the effect of the finite conductivity of the ground (correction part) of the simplified Carson's equations for self-impedance". On that basis, and by prioritising frequency dependency, they manage to separate out explicitly the earth consideration. In pursuing a modified forward/backward power flow solution, the Carson-Clem approximations as described by Albano *et al* were employed [233].

These 'modifications' caused the modified forward/backward algorithm to have poor convergence. This issue was subsequently considered collaboratively with the power systems research group at the Department of Industrial Engineering, University of Padova, Italy, where the system described in Figure 7.1 was also analysed. In consideration of the problem, forward/backward, current injection power flow algorithms as well as analysis employing OpenDSS were applied to the Network model (5 pillar condensed version of the network illustrated in Figure 7.1). The *Open Distribution Simulator Software* (OpenDSS) software facilitates a comprehensive electrical power system simulation/analysis [237]. It contains many element models, such as relay, capacitor, PV and energy storage systems and in this regard includes all the different needs to simulate unbalanced DN including distributed generation [238].

The forward/backward approach converged (albeit with a different solution to the OpenDSS method), but for a full network description (Figure 7.1), convergence was not possible. Therefore a direct solution was explored; leading to the development of the Network in terms of a refined *Admittance Matrix Correction* power flow, based on the methodology derived by Benato *et al* [225].

7.4 A Full Analysis of a Distribution Network with unbalanced load/generation

This section outlines the methodology employed to fully consider the distribution network presented in Figure 7.1. It will outline load flow algorithm developed in this regard and present the considerations of how network cabling was modelled

7.4.1 Admittance Matrix Correction (AMC) Power Flow (adapted from [225])

The *AMC* methodology was developed on the basis of the *Complex Admittance Matrix* power flow algorithm described in [225]. The procedure is sufficiently robust to facilitate a multi-conductor asymmetrical network analysis. The methodology was originally developed for computing electromagnetic coupling of complex conductor geometries [233]. Figure 7.6 illustrates a schematic describing how the network model is built; incorporating network structure, load, generation and earthing elements. The network admittance matrix is composed of branch elements that represent the 4-wire (and earth) system. The shunt elements are then connected to the ports represented by the nodes with different configurations.

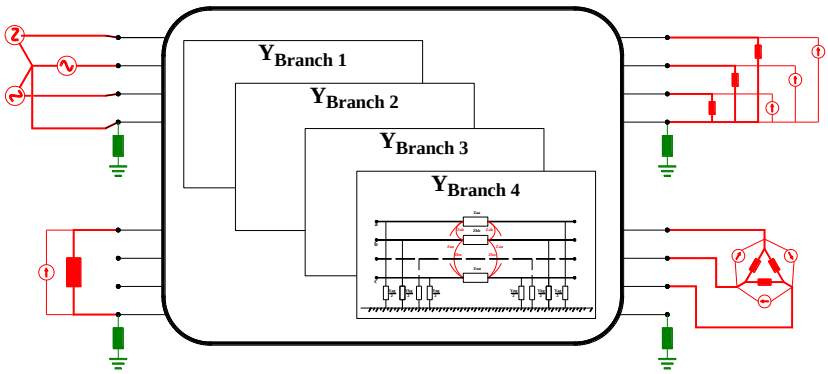

Figure 7.6 Network representation through an admittance network that individually incorporates (line) branch admittances and shunt element (red) and Earth connection admittances (green).

The approach involves ‘splitting’ the network into two parts: (i) a passive network, incorporating branch admittances and (ii) ‘shunt’ element consideration, in which the

shunt elements (load/generation) are represented as admittances (if no generation is present, load/generation can be represented as constant admittance; the overall network being passive so that a direct solution is possible). In this way, the shunt and network branch admittances can be combined (algebraically) to form a holistic network representation. Indeed, in the same way, the earthing network, as it is facilitated at network nodes, can also be included. Figure 7.7 illustrates how the network is split by considering the slack (generator) node as external to the network $(\mathbf{i}_{aSH} = 0)$. The shunt components (load/generation) are represented by a constant shunt admittance as defined by equations (7.7) and (7.8).

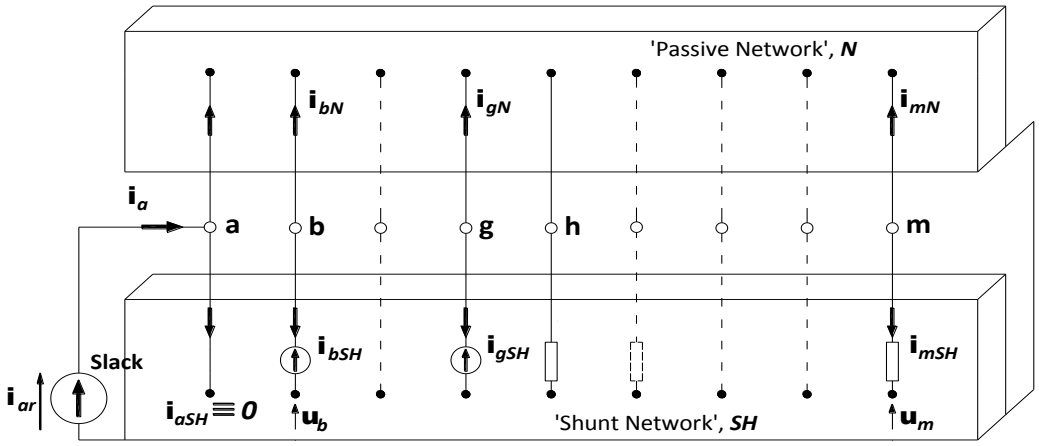

Figure 7.7 Decomposition of the system network admittance into passive and shunt branches (incorporating system load/generation) [source: extracted from[225]]

$$\mathbf{Y}_{Load(i)} = \frac{S_{Load(i)}^{\ *}}{\left|u_{Load(ph-N)(i)}\right|^2} \qquad [\mathrm{S}] \tag{7.7}$$

$$\mathbf{Y}_{Gen(i)} = \frac{S_{Gen(i)}^{\ *}}{\left|u_{Gen(ph-N)(i)}\right|^2} \qquad [\mathrm{S}] \tag{7.8}$$

The branch elements matrix is built by placing branch element sub-matrices into the system through a topology matrix. Similarly, earth connections may be defined by

adding self-admittances to the neutral conductor at the relative bus, as graphically represented in Figure 7.1. The general approach involves describing the 4-wire (3-phase) line network (pillar to pillar) as in Figure 7.1 and with regard to each single-phase consumer connection, this 4-wire network is expanded to include both the connection branch admittance and the shunt load/gen participation. In this way a (188×188) System matrix $((4\times Lines\times 10_{Pillars})+(2_{L+N}\times 74_{Consumers}))$; on the basis of Figure 7.8. The specifics of the approach are described in **Appendix A9**.

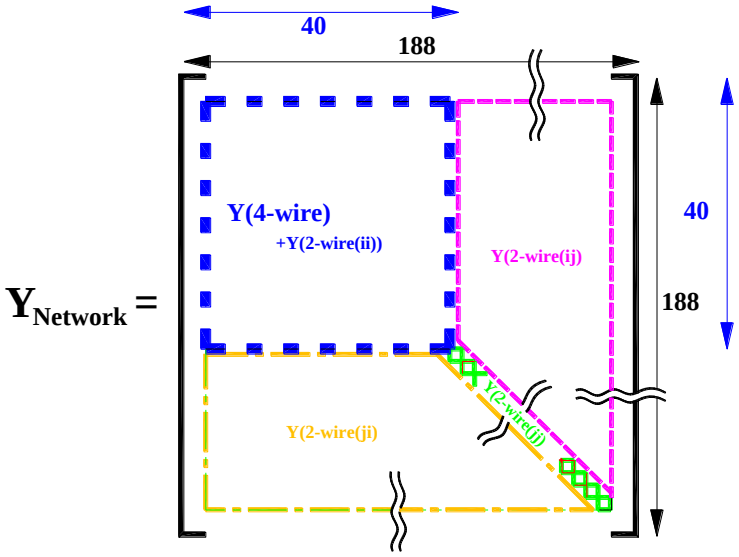

Figure 7.8 System Admittance Development in terms of the additional of single-phase shunt elements to the branch network representation

With regard to Figure 7.7 the shunt component admittance matrix is subjected to both absorption and injection of complex power; dependent on the application of the slack bus voltage $\mathbf{u}_{ar}$ at node a of the branch (passive) admittance matrix, *N*. In this regard, the system can be evaluated in terms of $\mathbf{i}=\mathbf{Y.u}$, where $\mathbf{Y}=\mathbf{Y}_N+\mathbf{Y}_{SH}$ and the shunt component currents can be transposed into the network admittance structure. Consider the system admittance matrix partitioned on the basis of Figure 7.9.

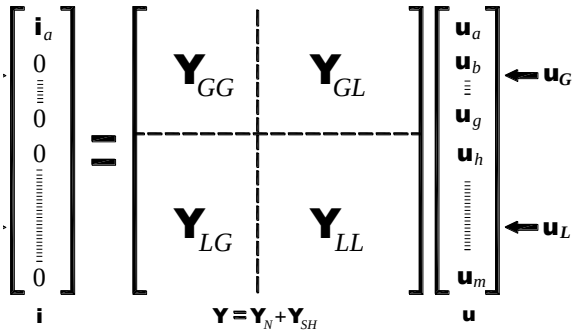

Figure 7.9 Partitioned form of $\mathbf{Y} = \mathbf{Y}_N + \mathbf{Y}_{SH}$

Therefore,

$$\mathbf{i}_G = \mathbf{Y}_{GG}.\mathbf{u}_G + \mathbf{Y}_{GL}.\mathbf{u}_L \ [\text{A}] \tag{7.9}$$

$$0 = \mathbf{Y}_{LG}.\mathbf{u}_G + \mathbf{Y}_{LL}.\mathbf{u}_L \tag{7.10}$$

$$\mathbf{u}_L = -\mathbf{Y}_{LL}{}^{-1}\mathbf{Y}_{LG}.\mathbf{u}_G \quad [\text{V}] \tag{7.11}$$

Reconfiguring (7.9) in terms of (7.10),

$$\mathbf{i}_G = \left[\mathbf{Y}_{GG} + \mathbf{Y}_{GL}.\left(-\mathbf{Y}_{LL}{}^{-1}\mathbf{Y}_{LG}\right)\right]\mathbf{u}_G \quad [\text{A}] \tag{7.12}$$

Figure 7.9 can be further partitioned in terms of (7.12) and described in Figure 7.10,

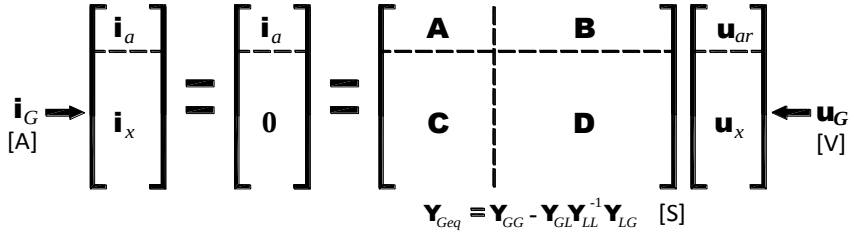

Figure 7.10 Partitioned form of $\mathbf{i}_G$ [A]

From Figure 7.10,

$$0 = \mathbf{C}.\mathbf{u}_{ar} + \mathbf{D}.\mathbf{u}_x$$
$$\mathbf{u}_x = -\mathbf{D}^{-1}\mathbf{C}.\mathbf{u}_{ar} \ [V] \tag{7.13}$$

Similar to the development of (7.12), the system (supply) current can be described as

$$\mathbf{i}_a = \mathbf{A}.\mathbf{u}_{ar} + \mathbf{B}.\left(-\mathbf{D}^{-1}\mathbf{C}.\mathbf{u}_{ar}\right)$$

(7.14)

The partitioning described above illustrates how the system node voltages can be generically described in terms of (7.13) and the system slack bus current is evaluated from (7.14). Therefore, power flow can be iteratively solved through an application of the slack voltage, in association with a system admittance matrix description. The solution is acquired by applying a flat start to the shunt elements (load/generation) and each network bus/node. For each iteration successive values of system voltage are acquired in terms of (7.13) on the basis of modulating the shunt admittances of both generator and load buses in order to satisfy scheduled voltage and power values. This iterative evaluation of the system voltages is depicted in Figure 7.11.

Figure 7.11 illustrates how a solution is achieved by updating the shunt element admittance representation, where (7.7) and (7.8) are updated in accordance with the iteratively derived network voltages (7.13). For generic *i-th* iteration, convergence is reached if the conditions (7.15) and (7.16) are verified:

$$\left|\underline{\mathbf{E}}_{(i+1)}\right| - \left|\underline{\mathbf{E}}_{(i)}\right| \leq \varepsilon_M$$

(7.15)

$$\angle\underline{\mathbf{E}}_{(i+1)} - \angle\underline{\mathbf{E}}_{(i)} \leq \varepsilon_A$$

(7.16)

where ε_M and ε_A are the magnitude and angle thresholds respectively.

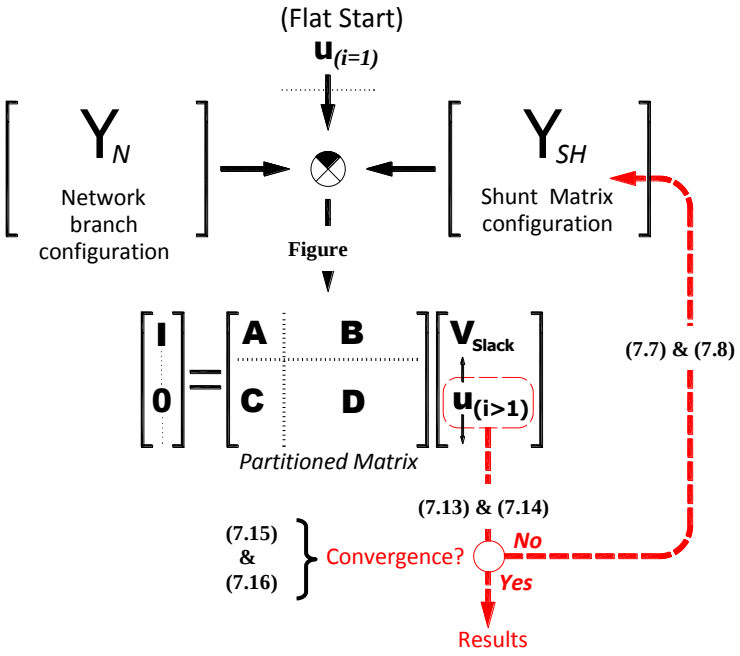

Figure 7.11 ***Admittance Matrix Correction*** **Flow Chart**

7.4.2 The AMC Power Flow Methodology & Cable Modelling

In modelling the distribution network cabling, the method described by Albano *et al* [233] is employed. For the analysis presented here, cable shields are not considered. There, the basic Carson equations ((7.17) to (7.19)) are considered in terms of electromagnetic coupling between parallel lines. The construction of the Z (and $Y_)$ sub-matrices utilises the Carson-Clem formulation for a n-phase branch; similar to the approximations described by Anderson [229]. Albano *et al* initially describe the self impedance is segregated into an internal and external component whereas the mutual impedance is considered separately

$$z_{oi} = \left(R_i + z + j.2.10^{-4}.\omega.\frac{\mu_r}{4} \right) \ [\Omega / km] \qquad \textbf{(7.17)}$$

whereas the external part of the self-impedance is provided by

$$z_{Ei} = j.\omega.\frac{\mu_0}{2.\pi}.\ln 2\frac{h_i}{r} + 2.(\Delta R_{ii} + j\Delta X_{ii}) \qquad [\Omega/km]$$

(7.18)

and the expression for the mutual impedance is given by

$$z_{ij} = j.\omega.\frac{\mu_0}{2.\pi}.\ln 2\frac{D_{ij}}{d_{ij}} + 2.(\Delta R_{ij} + j\Delta X_{ij}) \qquad [\Omega/km]$$

(7.19)

where D_{ij} is the distance between the ith conductor and the j-th conductor image

h_i is the average height above the ground

R_i is the DC resistance

d_{ij} is the direct distance between the i-th and j-th conductors

μ_0 /is the permeability of free space ($4.\pi,10^{-4}$ H/km)

ΔR_{ii}, ΔX_{ii} are correction terms; real and imaginary components of the external part of self impedance with earth return

ΔR_{ij}, ΔX_{ij} are correction terms of the mutual impedance

However, Albano *et al* refine both the internal and external reactance of a conductor as well as the mutual impedances to produce equations (7.20) and (7.21), in terms of two circuits *i* and *j*:

$$Z_{ii} = R_i + R_e + j\omega \cdot 2 \cdot 10^{-4} \cdot \ln\left(\frac{D_e}{GMR_i}\right) \qquad [\Omega/km]$$

(7.20)

$$Z_{ij} = R_e + j\omega \cdot 2 \cdot 10^{-4} \cdot \ln\left(\frac{D_e}{d_{ij}}\right) \qquad [\Omega/km]$$

(7.21)

where *R*: is the DC resistance [Ω/km];

GMR is the Geometric mean radius [m];

d is the mutual distance between conductors i and j [m].

In equations (7.20) and (7.21), the hypothesis of soil finite conductivity is duly considered by an earth return path with depth D_e and resistance R_e, defined in equations (7.22) and (7.23) below:

$$R_e = \pi^2 f \cdot 10^{-4} \qquad [\Omega / km] \tag{7.22}$$

$$D_e = 659\sqrt{\frac{\rho}{f}} \qquad [m] \tag{7.23}$$

where f is the system frequency [Hz] and ρ,is soil conductivity [Ωm] (typically 100 Ωm).

The advantage of the approach described by Albamo *et al* [233] is that an earth impedance is implicit in the description of both the self and mutual impedances and as such, the line impedance is described as a 4x4 impedance matrix.

7.4.3 Geometric Cable Spacing

The sub-distribution cable systems (i.e. from pillar to pillar) are modelled as 4-core underground (ug) cables with a quartile conductor arrangement at a depth of 2m. Figure 7.12 illustrates how image theory is employed to evaluate the relative distances between cables and their respective images. The consumer connections are simarly modelled, but as over head conductors (concentric neutral) connected to the consumer at a height of 4.5m.

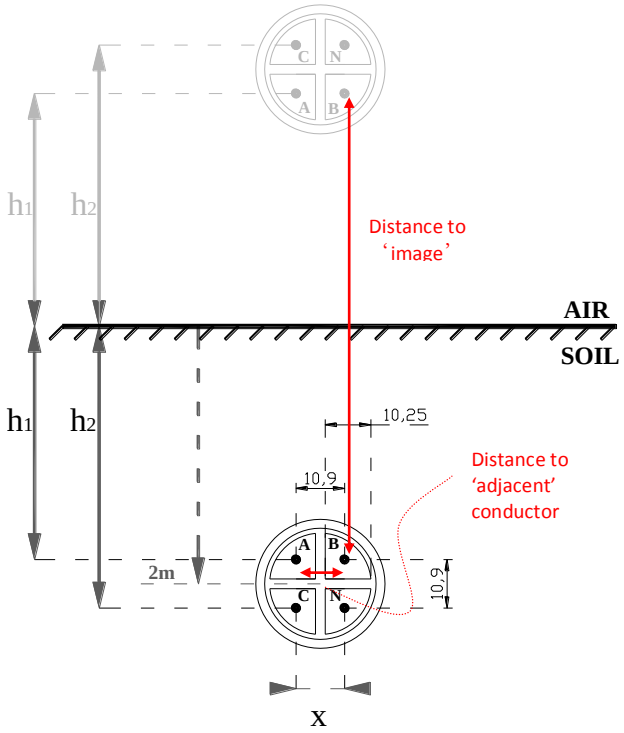

Figure 7.12 Spacing/height/depth for (quartile) underground (*ug*) (distribution) cable installation (same approach being applicable to overhead (*oh*) cabling)

Figure 7.13 illustrates how the geometric spacing between the 4-core quartile-arranged conductors of the sub-distribution ug cabling is calculated. Figure 7.13 specifically illustrates the relative values for the 70mm^2 XLPE cable as provided in manufacturers specification [226], but the same approach is applied for the 185mm^2 XLPE and 70mm^2 NAKBA cables. With regard to the service cables that connect the consumers to the mini-pillars, Figure 7.14 illustrates the geometric spacing for the 25/16mm^2 Concentric Neutral cable.

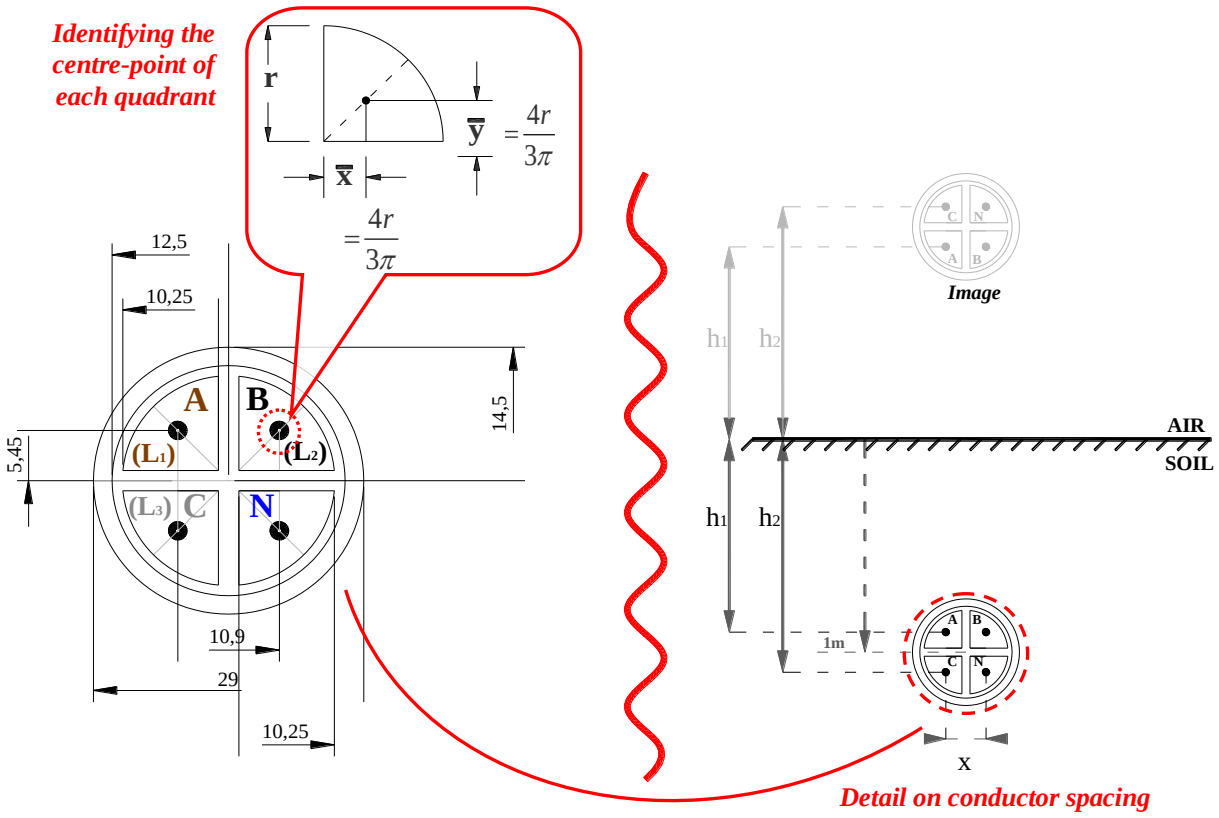

Figure 7.13 Geometric spacing (mm) for the 70mm^2 XLPE [226]

For the concentric neutral cable (as described in Figure 7.14) the equivalent geometric mean radius of the concentric neutral is computed using the equation for the geometric mean radius of bundled conductors used in high voltage transmission lines [232] as described in (7.24).

$$GMR_{cn} = \sqrt[k]{GMR_s.k.R^{k-1}} \quad [m] \tag{7.24}$$

where k is the number of concentric neutral strands and GMR_s is the geometric mean radius of a neutral strand

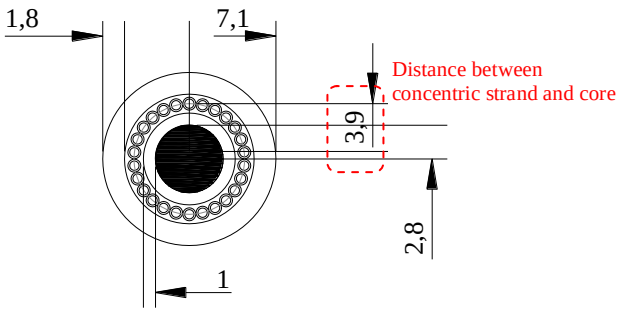

Figure 7.14 Geometric spacing (mm) for the 25/16mm^2 Concentric Neutral Cable [226]

7.5 AMC power flow analyses considering an urban wind profile

This section will consider a number of scenarios with respect to the developed distribution network model that employs the AMC power flow algorithm. Network cabling is modelled as underground from pillar to pillar with consumer connections considered as overhead connections complicit with the analysis presented in sections 7.4.2 and 7.4.3. The Substation send-end voltage was also modelled as 1.05pu, which is within the upper tolerances of [227]. The network topology and consumer phase connections are consistent with 7.4.1 and 7.4.2, but the consumer earth electrode impedances are modelled as 5Ω (with pillar earth electrode impedances of 1Ω).

First of all exemplar load/wind profiles are applied in terms of a standard wind speed extrapolation technique (Wierenga technique as discussed in Chapter 4 and 5). The extrapolation is based on parameterisation of the surface roughness, z_0, as established in Chapter 5. The network (Figure 7.1) is considered in terms of the AMC algorithm and the ensuing analyses are as presented in [239]. Whereas [239] is written and described in terms of a *Current Injection methodology* (CCM), the research presented here will concentrate on the AMC algorithm. **Appendix A10** provides a synopsis of this current correction algorithm. In that approach, once the network admittance matrix is solved

initially, it does not need to be iteratively updated thereafter. So the inversion in (7.11) is not repeated during the iterative solution procedure. Thus the consideration of different kinds of shunt elements (loads or generators) is through adaptation of the injected currents, $\Delta\mathbf{i}$.

The network model is subsequently considered on the basis of the empirical wind speed model developed in Chapter 5. The application of this wind speed model represents a holistic model that facilitates an improved power flow analyses that is cognisant of the effect of the urban environment and how it affects the available wind resource. Finally, the turbulent nature of the wind resource and how it impacts the voltage profile in an urban distribution network is considered by integrating the wind turbine (characteristic) model as developed in Chapter 6.

7.5.1 Exemplar load/wind profiles [239]

The wind resource is estimated in terms of the logarithmic profile (4.7), consistent with the Wierenga's and Mertens' rural/urban wind profile 'stepping' ([182] and [72] respectively). In this regard, the wind resource is extrapolated from a non-urban (e.g. Airport) site, to the site in question, using the surface roughness parameter acquired from the analysis in Chapter 5 (5.4.1). This extrapolation is with respect to the suburban location (S_H) in Dublin to an indicative turbine hub height which, for the purpose of this analysis is considered to be at 12m (the effective position of z* for the local area). The extrapolation is thereafter employed to acquire the wind speeds for the exemplar weeks.

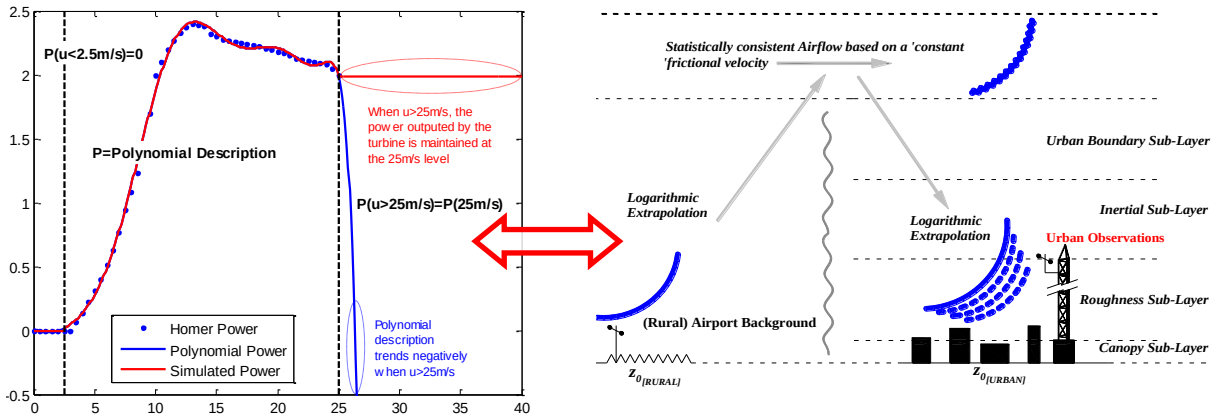

Figure 7.15 Exemplar *Wind Turbine* and *wind speed* profiling through logarithmic extrapolation cognisant of the surface characteristic length (z_0) pervasive within the specific rural and urban environments respectively [198]

The load data employed is representative of consumer demand at hourly intervals [145] (as in Chapter 3). In this regard, consumer hourly demand is based on an annual consumption of 5000kWh of electricity [61], which represents an average hourly demand of 0.571kW. Figure 7.16 illustrates a 24 hour seasonal *snapshot* in terms of the annual wind and load variation. In the analysis that will be presented here, spring and winter exemplar profiles (Figure 7.16), consistent with the methodology presented in [198], are considered.

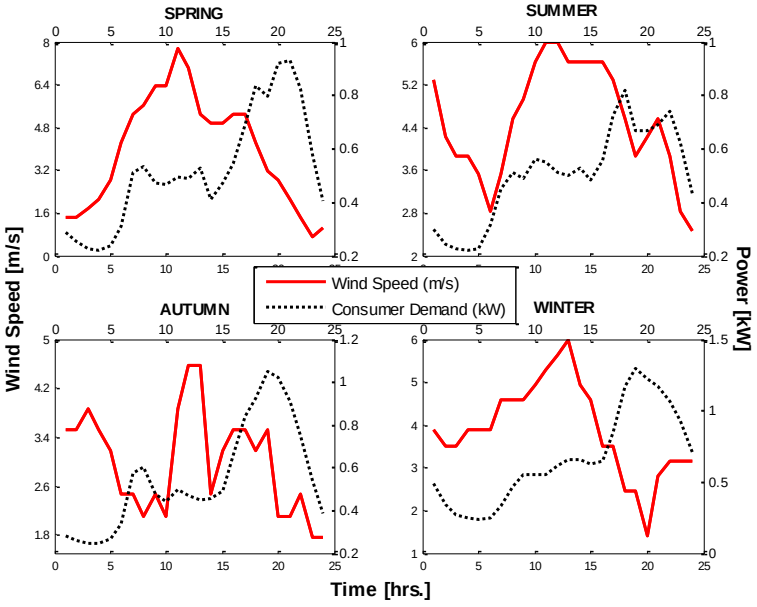

Figure 7.16 Daily seasonal urban wind speed and consumer demand (the first day of January, April, July and October (spring, summer, autumn & winter respectively)

The commencement of the second weeks in April and January are chosen to represent the seasons respectively. As Table 7.1 illustrates, these two exemplar days represent the opposite ends of consumer demand for the days considered and while the average wind speeds over both periods are the same, statistically, in terms of the output of a micro wind turbine, Spring will actually offer more by way of wind resource. The consumer demand over the winter day represents an increase of 27.5% over the spring day with 37.5% of the hourly wind speeds over the spring day being greater than 5 m/s compared to 12.5% for winter day. This paradoxical situation is something a distribution network needs to be cognisant of in consideration of embedded generation connection, as this implies that the spring profile could present issues with respect to network voltage (upper) limit breaches [227].

Table 7.1 Seasonal wind speed (u_{Seas}) and consumer load (P_{Cons}) profile statistical comparison

Spring		Summer		Autumn		Winter		
u_{Seas} [m/s]	P_{Cons} [kW]	u_{Seas} [m/s]	P_{Cons} [kW]	u_{Seas} [m/s]	P_{Cons} [kW]	u_{Seas} [m/s]	P_{Cons} [kW]	
7.74	0.93	5.98	0.82	4.57	1.05	5.98	1.29	$(u_{Seas.}/P_{Cons})_{Max}$
3.88	0.52	4.51	0.50	2.99	0.55	3.88	0.66	$(u_{Seas.}/P_{Cons})_{Mean}$
2.09	0.22	1.06	0.18	0.83	0.25	1.08	0.33	$(u_{Seas.}/P_{Cons})_{Std.}$
12.42		12.02		13.15		15.84		Energy [kWh]

The specific scenarios considered include:

1. A benchmark model; each consumer is allocated both the Spring and Winter profiles with no generation connected
2. The network is forcibly unbalanced with the load allocated in scenario 1 apportioned as follows: 100% load connected to L_1, with 200% and 300% load connected to L_2 and L_3 respectively
3. Scenario 2 is again considered but this time with generation connected (generator power factor of 0.95 applied) and the associated seasonal wind speeds forced to 300% nominal. The embedded generation considered in this analysis is the same as discussed in section 6.3.2.

An investigation into the effect of consumer earth electrode variation is also considered by increasing all consumer earth electrodes to an impedance of 50 Ω.

The following illustrations consider each network section mini-pillar (9) and the customer connections at pillars B and J (being the extreme ends of the network) are specifically highlighted. Box plots are employed so that network reaction over time can be represented. In this way, the maximum, minimum and median values of bus/pillar voltages are clearly visible. Box plots further illustrate the upper and lower quartiles of bus/pillar voltages over the period of investigation.

Figure 7.17[(a) & (b)] illustrate the voltage profile across each of the network lines for the benchmark spring and winter cases respectively (Scenario 1). The spring case derives a network voltage range of 4.73V between maximum and minimum voltage

with L_3 having the widest range at 5.2V. In contrast, the winter average voltage range is 6.65V with L_3 again having the widest range at 7.34V. The mini-pillar voltage unbalance (Figure 7.18) varies from 0.1463% for the spring day to 0.208% for the winter day, but both are within acceptable tolerances.

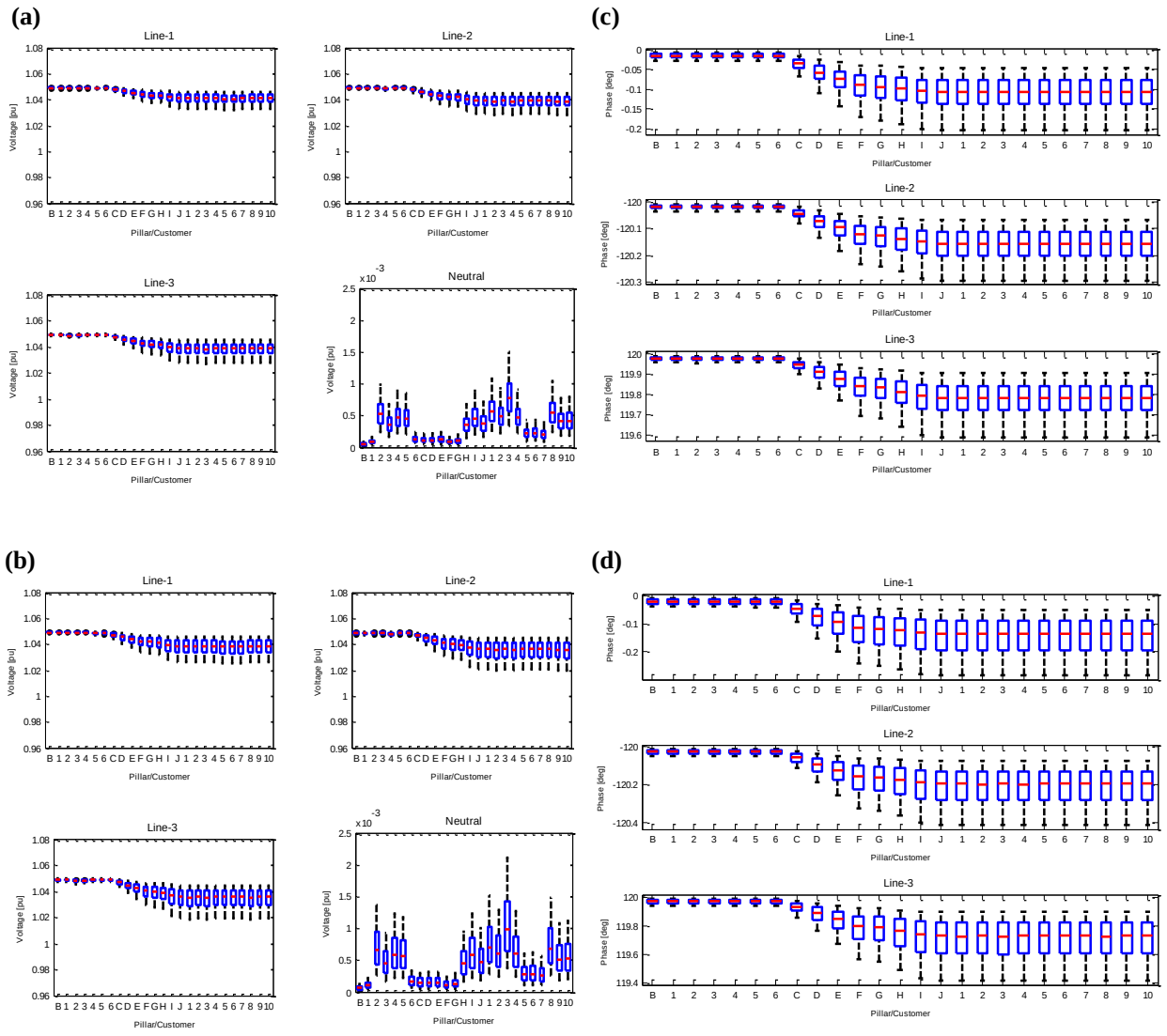

Figure 7.17 Network Voltage [(a) & (b)]/Phase [(c) & (d)] relationship for a Winter day (scenario 1)

Voltage unbalance can be described in terms of sequence components, with Fortescue's transformation facilitating a description of the sequence voltages in terms of the line voltages

$$\begin{bmatrix} V_1 \\ V_2 \\ V_0 \end{bmatrix} = \mathbf{F} \times \begin{bmatrix} V_a \\ V_b \\ V_c \end{bmatrix}$$

(7.25)

Where V_0, V_1, V_2 are the zero, positive and negative sequence voltages respectively. Equation (7.25) can be transferred so as to describe the sequence voltages as line voltages

$$F = \frac{1}{3}\begin{bmatrix} 1 & 1 & 1 \\ 1 & a & a^2 \\ 1 & a^2 & a \end{bmatrix}$$

(7.26)

The level of unbalance is defined by the ratio of the negative sequence voltage to the positive sequence voltage.

$$V_{Unbalance}(\%) = \frac{V_2}{V_1} \times 100(\%)$$

(7.27)

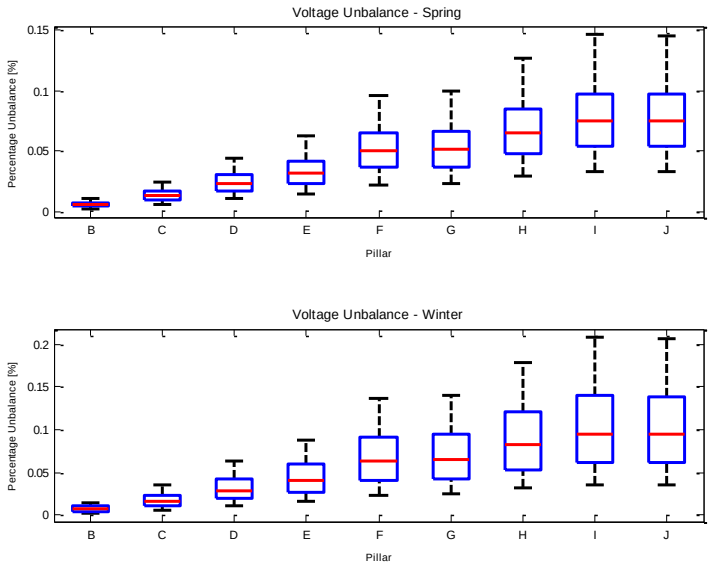

Figure 7.18 Network Voltage unbalance (%) for both the Spring and Winter day (Scenario 1)

When the network is unbalanced, as described in Scenario 2, the resultant network voltage is as depicted in Figure 7.19 for spring. There is an increase in V_{L1} as a

consequence of the increased unbalanced loadings over the other phases for the seasonal consideration.

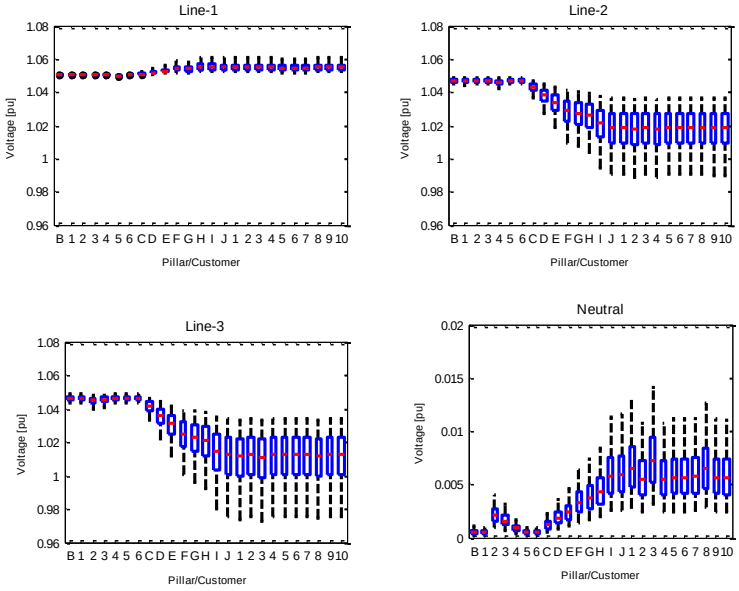

Figure 7.19 Network Voltage ($V_{L1}/V_{L2}V_{L3}/V_N$) for the Spring day (scenario 2)

The reaction of the network voltages is also evident in the phase angle and particularly in lines 1 and 2 with the respective line phase angles trending positive. Even with the level of voltage unbalance, there are still no voltage breaches. It is also notable that the neutral voltages, for both season considerations, increase significantly with the increased loading imbalance.

With the generation connected as in Scenario 3 and with respect to the unbalanced network considered in scenario 2, the mean wind speed for both spring and winter are respectively increased from 3.88m/s (both spring and winter profiles) to 11.65m/s. Figure 7.20 illustrates the voltage profile across the network with the 300% wind speed applied to the embedded generation. This scenario was specifically considered due to the minimal impact on the network voltage presented by embedded generation driven

by nominal (seasonal) wind speed. Indeed, for the nominal wind speed application, the average voltage range across each line for spring was 12.49V and 16.3V for winter. In comparison to the unbalanced consideration with no generation included (scenario 2), this range represented only a 10.4% and 0.2% increase for spring and winter respectively with an associated negligible impact on voltage unbalance.

With the wind speed at 300% of nominal (exemplar profiles being considered), the consequence of this level of wind speed increase on embedded generation is illustrated in Figure 7.20. There the effect of the increased generation is clearly evident on the network and with respect to voltage breaches, the voltage exceeds the 110% nominal voltage limit on the 5th, 6th and 7th consumer connections to the last network mini-pillar (J). This is in context with a total generation capacity (based on the *Skystream 3.7* operating at rated wind speed as deriving maximum generator output) of 185kW (60kW, 65kW and 60kW for lines 1, 2 and 3 respectively).

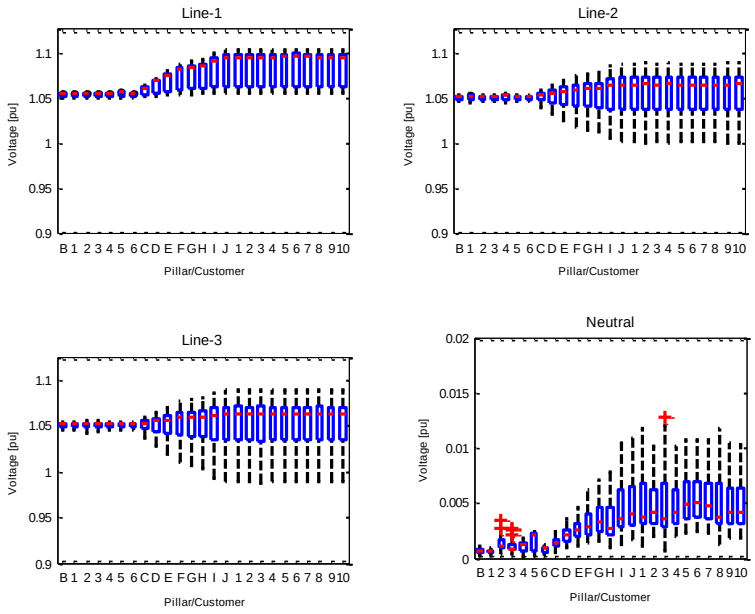

Figure 7.20 Network Voltage ($V_{L1}/V_{L2}/V_{L3}/V_N$) for the Spring day (scenario 3)

The inclusion of generation also reduces the percentage voltage unbalance by 10.5% and 9.6% for the spring and winter profiles as manifested in scenario 2 (Figure 7.21).

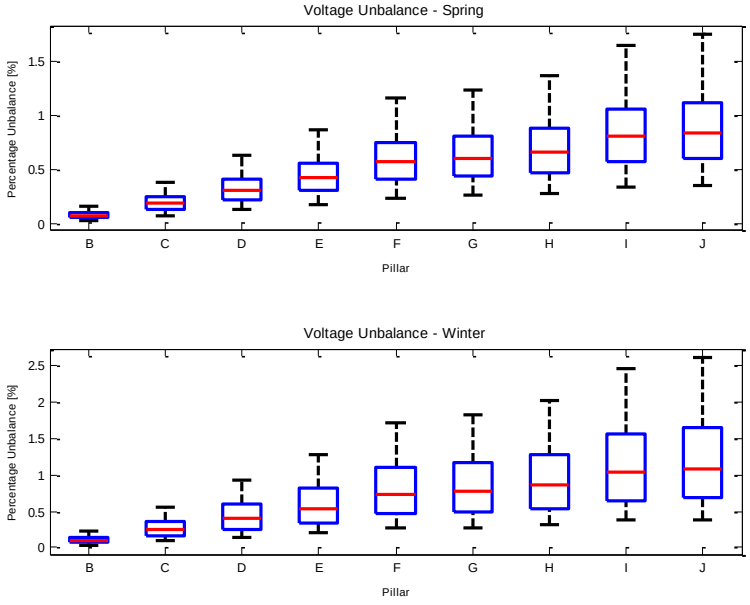

Figure 7.21 Mini-Pillar Voltage Unbalance (%) for both the Spring and Winter day (Scenario 2 with no embedded generation applied)

Finally, in consideration of the effect of the consumer earthing arrangements (TN-C-S), when the earth electrode impedances for all consumers are increased to 50Ω, the overall

network voltage decreases slightly, but the neutral voltages for both scenarios increase substantially (58% and 56% over the neutral voltages derived by scenario 3 for the spring and winter days respectively).

7.5.2 Power Flow using the developed Wind Speed Models

Whereas in Section 7.5.1, snap-shot (seasonal) periods over 24 hours were considered, this section will use this modelled wind speed data, in conjunction with a Markov Chain, to consider the affect of a typical mean year of wind speeds on the distribution network. The *markov chain* is employed to effectively extend both the urban and suburban locations (C_H and S_H respectively) to be statistically representative of a mean year or 8760 hours. The modelled wind references (section 5.4.1) are derived in terms of wind directional (120° to 300°) and (neutral) atmospheric stability filtering. This filtering process is with respect to the background reference, Dublin Airport, and through the empirical modelling, non-chronological wind data sets (of different length) at each site were acquired. Markov chain theory thereby facilitates an extension of these modelled wind speeds in a manner that retains the statistical significance contained within both models over a year (or 8760hrs).

Figure 7.22 illustrates a comparison of the filtered, modelled and Markov extended wind speeds at both S_H and C_H respectively with the respective representations closely aligned. The consistency between the modelled and Markov extended wind profiles is further evidenced in Table 7.2. The voltage reaction with respect to the Skystream 3.7 wind turbine and this typical mean wind speed model is presented in Figure 7.23. **Appendix A11** describes the Markov Chain model developed.

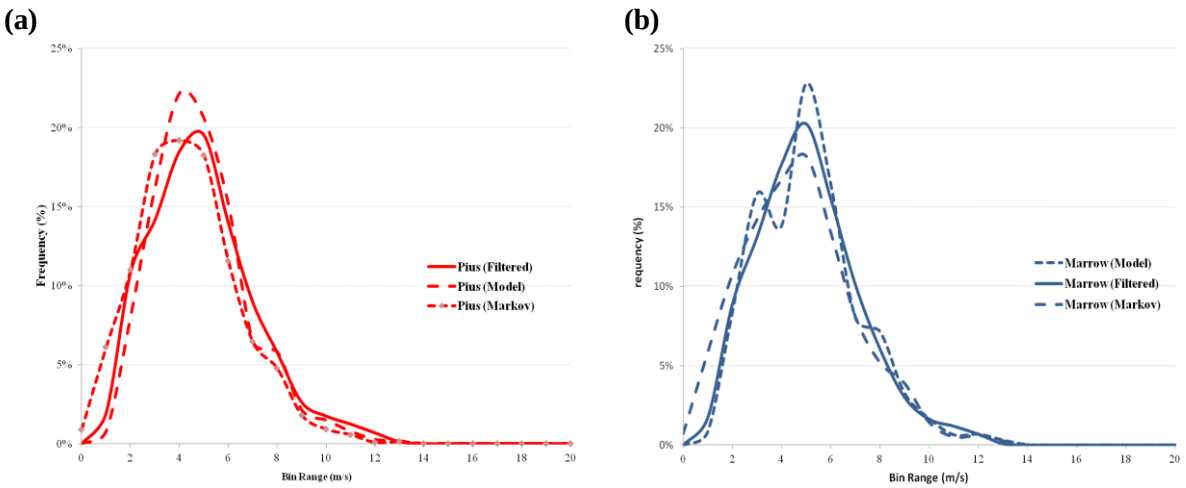

Figure 7.22 Comparison (frequency distribution) of the filtered, modelled and markov-chain extend wind resource at S_H (a) and C_H (b) respectively

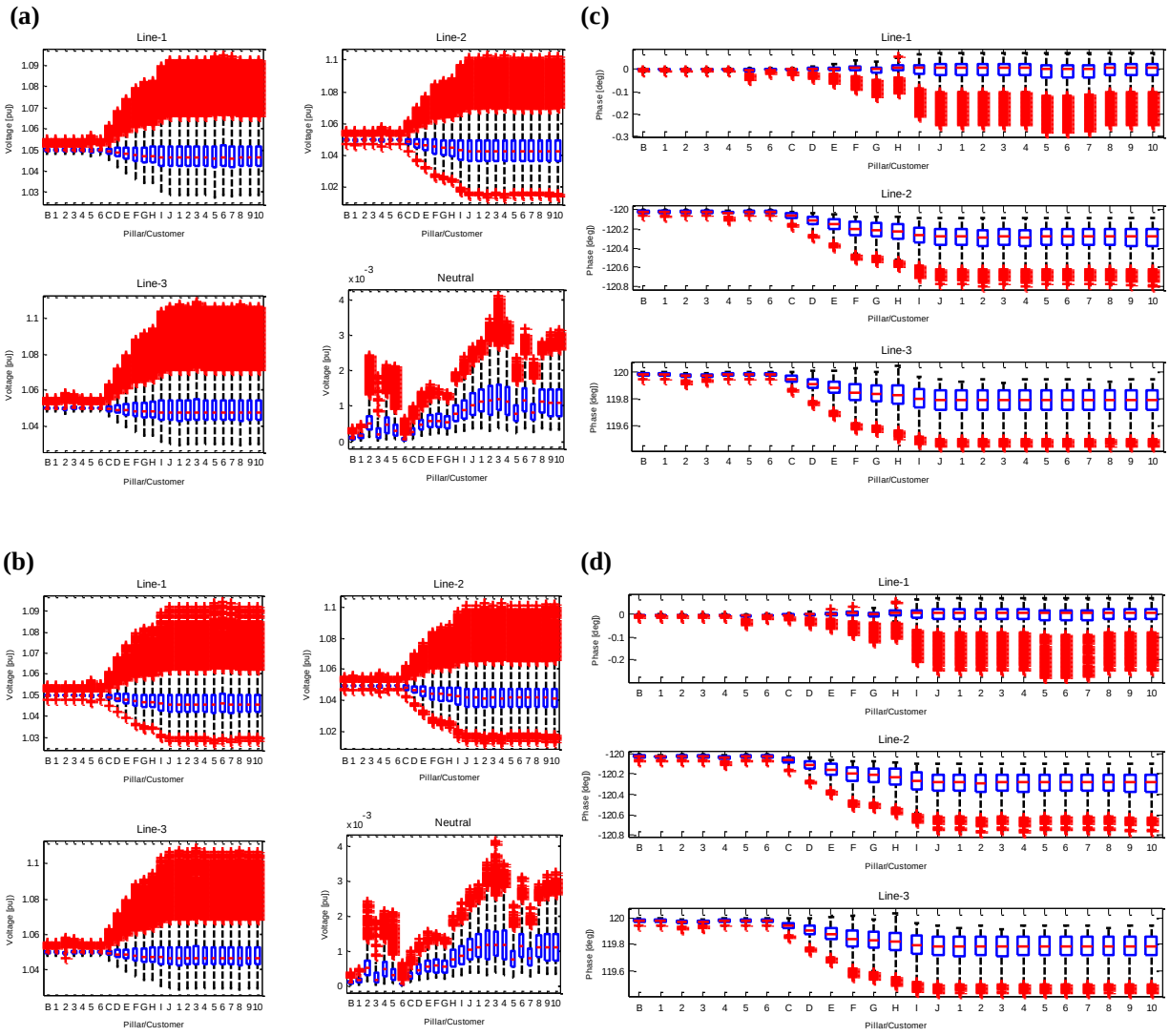

Figure 7.23 Network Pillar/Consumer Profiles: Voltage [(a) & (b)]/Phase [(c) & (d)] relationship, for a mean typical year

Table 7.2 Modelled Wind and Markov Extended Wind Comparison

Statistical Comparison	*Urban Modelled Wind Speed (C_H)*		*Suburban Modelled Wind Speed (S_H)*	
	Modelled Wind Data (4789 Hrs)	Markov chain Extended Data set (8760hrs)	Modelled Wind Data (5556 Hrs)	Markov chain Extended Data set (8760hrs)
$\mathbf{u_{Mean}}$	4.62	4.58	4.39	4.33
$\mathbf{u_{STD}}$	2.09	2.18	1.96	2.05

The analysis in this section considers the reaction of the distribution network as a result of the standard load profile over a year including embedded generation driven by the modelled wind speed derived in Chapter 5. The load and generation is consistent with Section 7.5.1. The network voltage profiles, over the 8760 hours considered, are illustrated Figure 7.23.

Comparing the network voltage profile derived from the (extended) modelled wind speed references at both the suburban and urban locations and concentrating on pillar J (furthest from the substation transformer), voltage breaches are incurred on L_2 and L_3 only. With respect to L_2, there are on average upper voltage breaches (>1.1pu) on 0.051% and 0.012% of the year at the urban and suburban sites respectively, with the urban wind speed causing the maximum breach of 1.10237pu . For a similar comparison of the voltage breaches incurred on L_3, there are on average upper voltage breaches on 0.715% and 0.183% of the year at the urban and suburban sites respectively. Once again, the urban wind resource derives the highest breach of 1.1086pu. Voltage unbalance was also relatively consistent for both wind speed references (as illustrated in Figure 7.24.

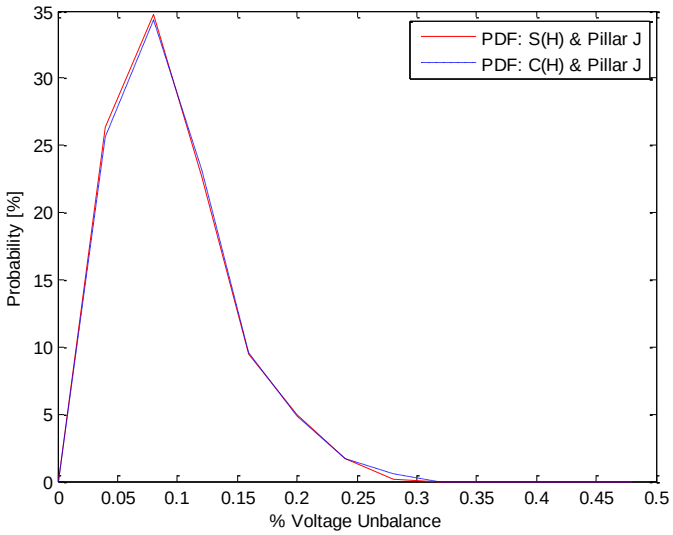

Figure 7.24 Network Voltage Unbalance PDF illustrating the voltage unbalance experienced at Pillar B with consumer load [145] and generation in terms of the extended wind speed model

In consideration of an unbalance range between 0.15% and 0.3%, the pillar voltage unbalance was within said range on 13.42% and 13.22% of the time at the urban and suburban locations respectively. The maximum voltage unbalance at pillar J was 0.296% and 0.294% at the urban and suburban location respectively.

Table 7.3 illustrates a comparison of the generator output with respect to the extended modelled wind resources at both the urban and suburban locations. The table also presents a consideration of the analysis contained in Chapter 5. Table 5.10 presented the performance of the WES5 Tulipo, which has a rated output of 2.5kW. In terms of the observed wind resource at both locations, Table 7.3 below instead presents a comparison of the modelled wind speeds on the basis of the Skystream 3.7 wind turbine as discussed in Chapter 6 (Figure 6.3) that utilises a polynomial description of the wind turbine for enhanced performance consideration. The comparison illustrates the consistency derived in employing the Markov Chain as a basis of extending the urban wind speed reference. The difference in generation capacity compared to Table 5.10 in

Chapter 5, is as a consequence of the more detailed wind turbine characteristic; the priority in Chapter 5 was to establish the extent of the wind resource.

Table 7.3 Generation capacity comparison of the extended (markov chain) wind speed reference and modelled wind speed as derived in Chapter 5

	Cumulative Energy [kWh]	Max Possible Generation [kWh]	Capacity Factor [%]
C_H Modelled	1629.2	11493.6	14.17
C_H Extended	3250.1	21024.0	15.46
S_H Modelled	1634.5	13334.4	12.26
S_H Extended	2727.0	21024.0	12.97

The capacity factors illustrated in Table 7.3, are comparable to those observed by Drew *et al.* in their analysis of micro wind generators across the greater London area [95].

7.5.3 Power Flow in terms of the Turbulence Models

Finally, an investigation into how the distribution network voltage profile as a consequence of turbulence affected wind turbine, is considered. The results from the modelling in Chapter 6 are utilised to acquire a perspective on how the industry standard in applying a mean wind speed over a observations period (10 minutes) compares to a consideration of higher resolution power data. The consumer load profile was organised into 30 minute intervals so that three 10 minute wind turbine data-points (for each model) were considered for each half hour consumer load data-point. The period investigated is consistent with the analyses in Chapter 6, 4th April to the 15th May 2012. Figure 7.25 illustrate the network voltage profile for the following considerations:

1. The *absolute* turbine output per observation window, in which an average of the of the 6000 samples of turbine power acquired in terms of the turbine characteristic 6.3.2),
2. The *mean* turbine power per observation window, in which the turbine power is an average of the wind speed measured over each 10 minute period.

3. An average of the *Albers* and *Weibull* approximations (as discussed in Chapter 6). As Chapter 6 concluded, both these approximations derived very similar results, so it is reasonable to expect similar consistency with regard to network voltage profile

Figure 7.25(a) illustrates the *maximum* voltage profile based on the turbulence models in consideration of wind speed and standard deviation observations and turbulence intensity measurements at the suburban location (S_H). Figure 7.25(b) illustrates the *average* voltage profile. Similarly, the voltage profile results are illustrated for the urban site (C_H) in Figure 7.25(c) and (d).

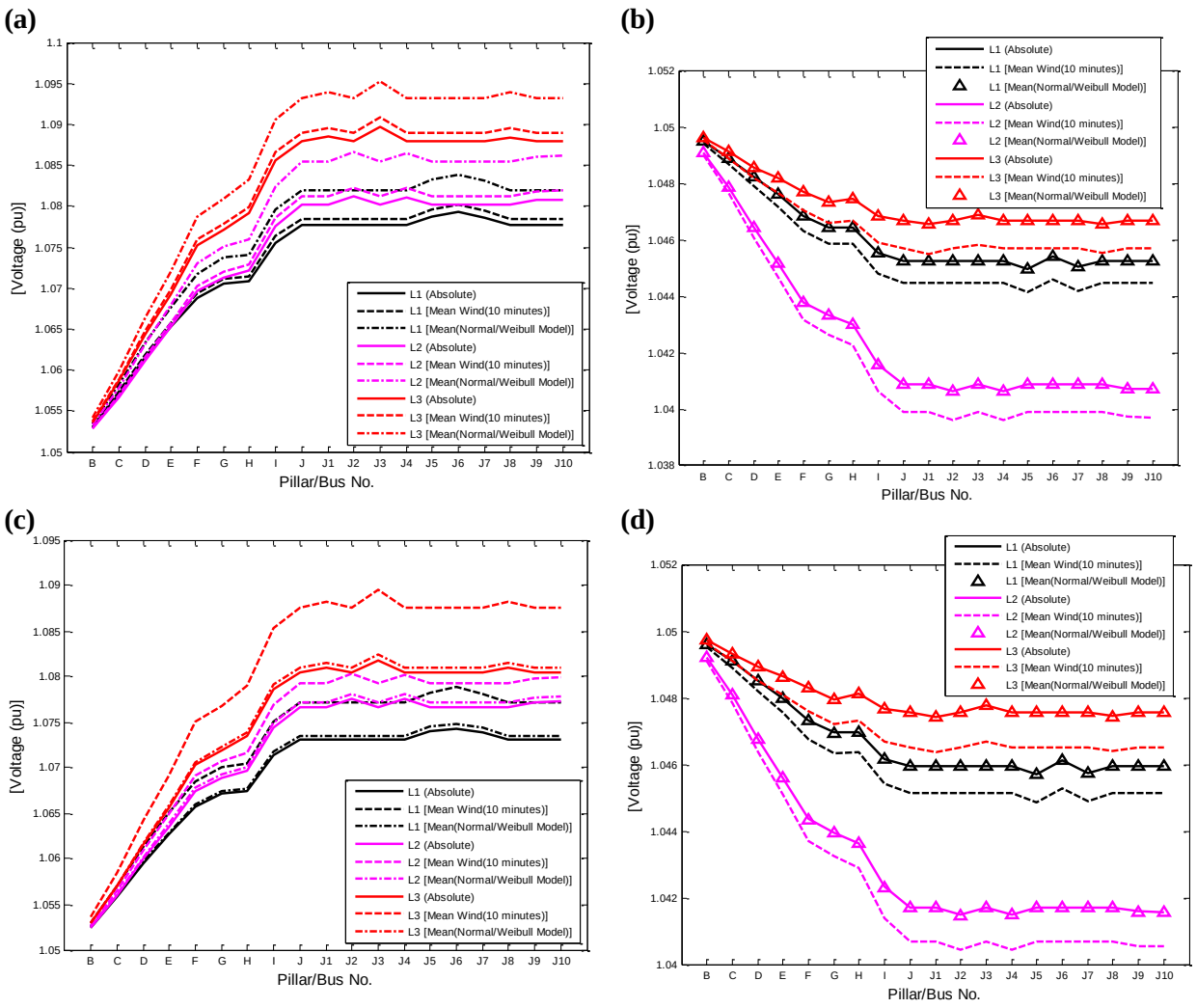

Figure 7.25 Maximum and Mean Voltage profiles derived from wind generation affected by turbulent considered wind resource

Figure 7.25 illustrates that, consistent with Chapter 6, where the turbine output turbulence models very closely approximate the absolute reference, the voltage profiles derived for both models are also very consistent. Therefore, the analyses presented here implies that a power flow solution for the network, incorporating significant wind generation, is achievable at very high resolution (wind speed resolution of 10Hz) based on observations of mean wind speed and standard deviation. This consistency is apparent in Figure 7.25(b) and (d). However, it is also apparent, that at the higher wind speeds, the Albers and Weibull approximations in modelling the turbine output over estimate leading to higher network voltage profiles being derived. Furthermore, the analyses described here, consistent with Chapter 6, do not incorporate the dynamics of the turbine. The dynamics of a wind turbine would affect the power output of a wind turbine, particularly in urban environments, but said dynamics are likely to reduce overall turbine productivity. In this regard, the overall system voltage profile would be somewhat depleted and over voltages would be less likely.

7.6 Conclusions

An accurate 4-wire, distribution network model is required to provide the platform on which a holistic understanding of the implications for an urban distribution network with increased levels of wind energy systems. Such a model must be able to facilitate dual voltage (400/230V) considerations with unbalanced load. Furthermore, as the generation involved is connected in parallel with the customer point of common coupling (PCC), it is important for such a model to be considerate of the network/consumer earthing arrangements.

This Chapter initially considers the logistical aspects involved in the development of an accurate distribution network model, but integration of both the empirical wind model

developed in Chapter 5 and the turbulence models developed in Chapter 6, were subsequently applied. The focus of these analyses is with respect to the effect on network voltage and voltage unbalance. Consideration of how the system earthing affects consumer voltages is also presented.

The basis for the network model parameters considered here is through information acquired from the DNO [226]. This information includes topological detail describing the network structure, and phase alignment for 74 consumers, with finer detail pertaining to cable systems and configurations involved. Network cabling was modelled in terms of Carson equations and through image theory describing geometric spacing between conductor cores, a full description of network cabling is facilitated. All modelling was implemented through the MATLAB^{TM} programming platform.

The power flow algorithm employed in the analyses is an admittance matrix correction (AMC) algorithm based on the methodology contained in [225]. Initially, a method proposed proposed by Ciric *et al* [234, 235] was considered, in which power flow is solved using a forward backward sweep methodology. The methodology is relatively straight forward to implement, but the approach has some inconsistencies. The algorithm, in considering the ground explicitly, employs a current divider approach to evaluate neutral and ground currents. This implies a lack of consideration for how mutual coupling between ground and the line conductors are affected. Furthermore, the algorithm requires that nodes with ground connections through ground electrodes need to be voltage corrected based on the neutral-ground current and said earth electrode impedance. Modification of the Ciric *et al* algorithm was explored, but convergence was an issue.

The AMC algorithm employs a holistic system admittance representation by combining separate 'blocks' of shunt admittances describing cabling, load, generation and earthing. Through a topology algorithm, power flow is solved by iteratively modulating the system admittance matrix until convergence is achieved. This AMC algorithm uses the Carson Chlem approximations of Carson's equations, thereby facilitating a more accurate representation of the earth. In comparing both methodologies, it is apparent that the cable impedance/admittance descriptions and the manner in which the ground is represented are critical.

Using the AMC algorithm, a number of network issues were considered. Initially, a sample seasonal wind and consumer load profiles (24 hours) were investigated. Representative load was acquired from [145] and a wind speed extrapolation model based on observations at Dublin Airport produced representative wind speeds at an optimal hub height at the suburban location [239]. The wind energy technology considered in the analysis was with regard to a polynomial description of the *Skystream 3.7* (2.4 kW) power curve (as described in section 6.3.2). It was ascertained that under nominal wind speed and load for spring and winter profiles, no voltage breaches occurred. Subsequent *forced* line unbalancing resulted in significant line voltage deviation that would have implications for the network, but even with significant unbalance, no network voltage breaches were experienced. The unbalancing also had implications on the neutral as increases in neutral voltage were derived. Indeed, over-voltage consequences only became prevalent at the last mini-pillar on the network when the wind speed was increased to 300%. With regard to the influence of the system earthing, this was tested by changing all consumer earth electrode impedances to 50Ω. This had the effect of significantly increasing the neutral voltages. In this regard, safety

concerns could be presented with respect to nuisance tripping of protective devices and even increased fire risk.

The application of the empirical wind speed model developed in Chapter 5 was considered next. The model developed in Chapter 5 optimises hourly wind speed wind observations at Dublin Airport on the basis of wind direction and stability for two sites in Dublin city. This optimisation derived, as a consequence, models with different numbers of hourly representations at both sites. Therefore, along with considering the network in terms of these models, a means to normalise the duration or number of hourly wind speed representations was also considered. Such normalisation implies a means to extend (or contract) the hourly wind speed representations for application to the distribution network. Such a consideration, while not being chronological, should retain the statistical proprieties of the modelled wind speed at both the urban and suburban sites. To that end, a Markov Chain algorithm was developed to extend the time reference for both sites to 8760 hours (1 year). These 'extended' wind speed models (58% and 88% for the suburban and urban models respectively) were applied to the Network model. Power flow analysis, based on the *Skystream* polynomial power curve description and half-hourly representations of consumer load, derived some occurrences of over voltage breach. But said breaches were relatively rare (<1% of 8760 hours). An advantage of extending the time reference for both wind speed models is that capacity factor based on consistent time frames is possible. Whereas the capacity factor for the city suggests a better wind harnessing capability at that site, the capacity factors calculated at both sites are comparable to the values acquired using the separate shorter time reference (Table 7.3). This implies that the empirical wind speed model, in conjunction with the Markov chain model can be employed to evaluate network reaction

for variable time references, thereby alleviating long term wind observation requirements.

Finally, the network model was indirectly subjected to the turbulence affected wind resource. Here, as opposed to a wind model, the network (model) was modified to accommodate turbine power considerations in terms of 10 minute, high resolution (10Hz), wind observations. The modelling described in Chapter 6, in which turbine power based on mean wind speed and two statistical models, was applied to the network to establish the effects on voltage profile. Half-hourly consumer load and the polynomial description of the *Skystream 3.7* power curve were once again employed. The results illustrate that in consideration of a turbulent wind resource, voltage breaches would not be an issue. Consistent with the results observed in Chapter 6, the voltage profiles developed by both mathematical models were practically identical.

Chapter 8: The Cost of Energy & Micro Wind Generation: A Rural/Urban Perspective

8.1 Introduction

National targets for increased renewable energy are common-place internationally and micro generation may help in achieving such goals. Micro wind generation is still at the early stages of market penetration, mainly due to the high capital cost and long payback period. Also, as discussed in Chapters 4 and 5, energy yield of such technologies is very location and site specific; particularly in an urban context. In the rural environment, the average wind speed is relatively high and the homogeneous landscape promotes statistically consistent wind speeds and wind directions. In the urban environment however, as illustrated in Chapters 4 and 5, the wind resource is characterized by lower mean wind speeds and increased levels of atmospheric turbulence due to heterogeneous surface forms and complicated building morphologies.

From an economical viability perspective and not withstanding broader issues such as market structure and associated regulation, the most important parameters in evaluating the viability of micro wind turbine systems are the initial cost and the value of potential energy generated. These parameters depend on the average wind speed, turbine type, size, mechanical design and the ability to optimise the generation output. The price per

kW installed will vary per country, but a conservative estimate would be $3000-$5000/kW [211], though manufacturers estimate that once mass production starts, this figure may drop to ≈1,500 $/kW. The actual value of 1 kWh of electricity produced by the turbine depends on the load profile, electricity tariff and whether a feed-in-tariff is applied.

This Chapter discusses the associated costs per unit of electricity generated by micro wind energy systems. This consideration follows on from the basic economic analysis presented in the discussion in Chapter 5 which prioritised simple payback for the capital costs associated with the wind energy system. This Chapter instead investigates the levelized cost of energy (LCOE) for such systems as this, in the context of a developing market, provides information to the bodies involved in incentivising such market.

Three case studies are presented, which consider national perspectives with varying renewable energy ambitions and micro wind embracement policies. The data used was acquired from collaborative work with research colleagues at the University of Northumbria. The case studies ascertain the cost of energy associated with micro wind generation in Sri Lanka, Ireland and the UK; countries that have progressive, conservative and ambitious goals respectively towards the integration of micro generation. Cost of energy analyses in this context facilitates viability assessments of micro wind systems and also assists in decisions pertaining to suitable feed-in tariff rates for such systems.

Sri Lanka[11] has a target of 10 % of electricity supply from renewable energy by 2016 [20]. Current electrification in Sri Lanka stands at 83 % [240] and rural electrification is identified as a way for enhancing rural economic and social development. In this regard, the Sri Lankan attitude is progressive and potentially open to embracing small wind energy systems. *Ireland* has a relatively robust distribution network with active engagement policies for the integration of large wind projects. Micro wind generation capacity currently represents 0.13 % of the national wind energy [241] and despite some incentive measures, uptake of micro wind generation opportunities are low. The Irish DNO therefore (and energy regulator (CER)), have a conservative attitude towards microgeneration in general. The *UK* on the other hand, has a strong commitment to the embracement of power generation from wind energy with 160.96 MWe capacity across the sector [25]. Indeed, the UK Government have ambitious targets and aspire to have 2% of national electricity demand supplied from small scale energy sources [103]. Whilst wind power at micro level currently represents only 0.35% of total wind capacity [20], with potential for micro generation as high as 30-40 % of the UK's electricity needs [120], micro wind generation capacity is expected to increase significantly.

The Chapter further presents the results of sensitivity analysis conducted through the *Hybrid Optimization Model for Electric Renewables* (HOMER^{TM}) optimisation software. This software facilitates such sensitivity analysis by considering cost parameters, performances and specifications of a small wind turbine system in the three countries considered. The annual energy production by a wind turbine at different annual mean wind speeds and the value of energy use are measured against the cost of energy production (based on the initial cost and maintenance costs over the life time of

[11] Sri Lanka was selected in this research through collaboration with a Sri Lankan who had an insight and data for Sri Lanka which would serve as a good contrast

the turbine). Accordingly, the viable initial cost per kW installation and cost of energy use of micro wind turbines are determined for the three countries. In the context of the main research themes considered in this thesis, this analysis offers insight into the economical challenge facing these systems in cities if they are to play a realistic role in a future renewable energy mix.

8.2 Renewable wind energy integration in the sample countries

Table 8.1 presents the contributions from renewable electricity production in the three countries and presents a context for the respective national ambitions towards renewable energy integration.

Table 8.1 Target Renewables Share of Electricity Production in selected countries[12]

	2010 [%]	Target [%]	Target Year
Sri Lanka	-	10	2015
Ireland	14.8	40	2020
UK	9.4	30	2020

The Ren21 Renewables 2012: Global Status Report [20] further provides a comparison for the selected countries in terms of the associated regulatory policies and fiscal incentives, as illustrated in Table 8.2.

Table 8.2 Renewable Energy (Electricity) Support Mechanisms (extracted from [20])

	Regulatory Policies				**Fiscal Incentives**		
	FiT (including premium payments)	*Electric Utility Quota Obligation/RPS*	*Net Metering*	*Tradeable Renewable Energy Certificate (REC)*	*Capital Subsidy, Grant or Rebate*	*Reduction in Sales, Energy. CO2, VAT or other taxes*	*Energy Production Payment*
Sri Lanka	✓	✓	✓		✓	✓	✓
Ireland	✓			✓			
UK	✓	✓		✓	✓	✓	✓

[12] In 2010, Sri Lanka did not have a renewable energy policy contribution policy

8.2.1 Sri Lankan Policy

Hydro power provides the major renewable energy contribution to the network in Sri Lanka. However, there are limited opportunities for further development of this resource. Demand for electricity in Sri Lanka is estimated to rise at an annual pace of 8-10% [242]. To tackle this demand, non-conventional renewable energy (NRE), including wind generation, are being encouraged.

Conventional grid extension has made good progress connecting nearly 83% of Sri Lankans to grid electricity; however accessibility still varies widely among regions. The Eastern Province of Sri Lanka has the lowest electrification level of 67.3% [240] . Harnessing of renewable energy, including micro PV, hydro and wind systems, is a possible option to meet the rural electric energy demand. The basic electricity requirement of a typical rural house is only for lighting, television and radio with a monthly gross electric energy requirement of approximately 50 kWh.

A tier type tariff mechanism is currently applied in Sri Lanka for grid electricity sales and then for a monthly block consumption, a mean electricity flat rate of €0.155 is applied [243]. For net-metering connections, the consumer is not paid for the export of energy, but is instead given credit (in kWh) for consumption of the same amount of energy later. In this study, for net-metering analysis, the same power price is taken for sales back to the grid as the mean electricity flat rate.

8.2.2 Irish Policy

According to the Sustainability Authority of Ireland [60] report, the, target of 13.2% RES-E by 2010 was exceeded (14.8%). That said, with regard to the Irish strategy for

renewable energy, there is still 26.2% more engagement required if the goal of 40% is to be achieved by 2020 [59].

As discussed in Section 2.5, from a regulatory perspective, there are a number of policies in place that could facilitate micro generation assisting in the 2020 RES-E goal. Building regulations require a reasonable proportion of energy consumption to be met by renewable energy [97] and the Irish Energy Performance of Buildings (recast) stipulates that alternative (green) energy supply systems *must* be considered for new buildings.

However, micro generation uptake has been relatively poor. Table 8.3 (extracted from Table 2.5) shows the total metered micro generation capacity in Ireland at the end of 2011[13]. There is nearly 3 MW of micro generation grid connected , but there is long way to go before the sector can make an impact on renewable energy targets.

Table 8.3 Irish micro generation capacity (Ireland, 31st December, 2011 (extracted from [241]))

	MW Installed Capacity (MWe)	Market Share by Capacity (%)	No. of Installations	Market Share by Installation (%)
Micro CHP	0.01	0.24%	7	1.13%
Micro Hydro	0.04	1.31%	8	1.29%
Solar PV	0.29	9.92%	114	18.39%
Micro Wind	2.60	88.52%	491	79.19%
TOTAL	**2.9**		**620**	

As explained in section 2.5, since April 2013, the price available for exported electricity on to the distribution network has fallen from the €0.19 offering under the Irish Micro Generation Scheme to an offering of €0.09. In this regard, one could consider the Irish micro generation policy as conservative.

[13] This table being indicative of data from the microgeneration scheme and does not consider commercial installations outside of this scheme. (https://www.electricireland.ie/ei/residential/price-plans/micro-generation-scheme.jsp)

8.2.3 UK Policy

The UK have a comprehensive approach towards micro renewable energy including micro wind generation [16]. The UK Department of Energy and Climate Change (DECC) expect that, by 2020, the feed-in-tariff (FiT) scheme will support over 750,000 small-scale, low carbon electricity installations [25]. An example of the progressive nature of the UK micro generation embracement is the Micro generation Government-Industry Contact group, which is set up to tackle the non-financial barriers facing mass deployment of micro generation [121].

Of the three countries being reviewed, the UK has the highest feed-in-tariff (FIT) options with the most progressive attitude towards the sector. Over the past three years, 160.96 MWe of low carbon electricity generation has registered under the scheme (representing 44,460 installations) [25]. Table 8.4 (Table 2.6) illustrates the breakdown of installed capacity considered under the scheme. Micro wind energy is not the most significant player in this market, where PV installations enjoy the most attractive FiT [104]. Indeed, in the comprehensive review of the feed-in tariffs (FITs) scheme in the UK [104], from December 2012, all forms of (small) wind energy installations less than 100 kW are paid €0.263/kWh [121] exported.

Table 8.4 UK Installed micro generation capacity (UK, 30th June, 2011 (extracted from [25]))

	MW Installed Capacity (MWe)	Market Share by Capacity (%)	No. of Installations	Market Share by Installation (%)
Micro CHP	4.99	3.10%	5	0.01%
Micro CHP	0.16	0.10%	157	0.35%
Micro Hydro	12.75	7.92%	218	0.49%
Solar PV	120.16	74.65%	42590	95.79%
Micro Wind	22.90	14.23%	1490	3.35%
TOTAL	**160.96**		**44460**	

8.3 Micro-Wind Generation Viability and Dependence on Mean Wind Resource

8.3.1 Levelized Cost of Energy

Cost of energy and initial cost of the system are the most important parameters in evaluating economic viability of small wind power systems. Levelized Cost of energy is the average cost per 1 kWh of useful electrical energy produced by the system, and may be defined by (8.1). The initial cost of small wind turbines depends on the size and type of the turbine. In this study, sensitivity analysis is carried out by considering cost parameters, performances and specifications of the *Skystream 3.7*, 2.4 kW small wind turbine system; so as to be consistent with Chapters 5, 6 and 7. Initial cost (including tax) is combined with annual maintenance requirements; such as oiling, regular safety inspections, checking of electrical connections, checking wind turbines for corrosion and the guy wires supporting the tower for proper tension, etc. The maintenance cost is estimated to be 1.5%-3% of the turbine cost but increases with time as the turbines get older [244]. The life time of the system is 25 years with replacement cost being considered as equal to initial cost of the system and salvage cost is neglected. Annual Energy Production (AEP) is computed based on power curves provided by the manufacturer. The cost of energy (COE) in (€)/kWh may be represented as:

$$COE = \frac{C_{ann,tot}}{E_{prim} + E_{def} + E_{grid,sales}} \tag{8.1}$$

where;

$C_{ann,tot}$ = Total annualised cost of the system (€Year)

E_{prim} = Primary load served (kWh/Year)

E_{def} = Deferrable load served (kWh/Year)

$E_{grid,sales}$ = Total grid sales (kWh/Year)

The total annualised cost of the system *($C_{ann,tot}$)* is the sum of the annualised capital cost ($C_{ann,cap}$), annualised replacement cost and annual operation and maintenance cost. The annualised capital cost is:

$$C_{ann,cap} = C_{cap}.CRF(i, R_{proj}) \tag{8.2}$$

$$CRF(i, N) = \frac{i(1+i)^N}{(1+i)^N - 1} \tag{8.3}$$

where;

C_{cap} = Initial capital cost (€)

$CRF(i, N)$ = Capital recovery factor

i = Annual real interest rate

R_{proj} = Project lifetime

N = Number of years

Power generation by small wind turbines is determined by considering the power curve of the wind turbine and wind potential. Grid sales and purchases are calculated by considering hourly based wind data, energy generation and demand data over the course of a year. In the analyses presented here, the *Hybrid Optimization Model for Electric Renewables* (HOMER^{TM}) optimisation software, as developed by the National Renewable Energy Laboratory, USA, was employed. *HOMER* was used to determine the optimal system configuration for given aspects and economic viability of wind turbines for different initial cost and various annual mean speeds. HOMER^{TM} is an hourly simulation model in which system components, available energy resources and load on an hourly basis are employed. The information on said resources as well as any associated control methods, costs or other parameters is required. A sensitivity analysis can vary a specific number of variables, thereby facilitating a systematic analysis of how a range of parameters affect the performance and overall efficiency of a system

[245]. In the analyses presented here, a wind energy system's sensitivity to varying mean wind resource is considered in both a rural and urban context.

Generally, small scale wind turbines are installed at lower heights in constricted areas. *HOMER* facilitates a logarithmic profile (or log law) extrapolation based on the assumption that the wind speed is proportional to the logarithm of the height above ground. The extrapolation (8.4) considers the ratio of the wind speed at hub height to the wind speed at anemometer height:

$$\frac{v_{hub}}{v_{anem}} = \frac{\ln\left(h_{hub} / z_0\right)}{\ln\left(h_{anem} / z_0\right)} \qquad \textbf{(8.4)}$$

where

h_{hub} is the hub height of the wind turbine [m]

h_{anem} is the anemometer height [m]

z_0 is the surface roughness length [m]

$v_{(hub)}$ is the wind speed at the hub height of the wind turbine [m/s]

$v_{(anem)}$ is the wind speed at anemometer height [m/s]

With regard to the wind resource (urban/rural), the primary variable within (8.4) is the surface roughness and in the absence of site-specific calculation, guidance on the selection of this parameter is provided in [170]. For the Irish context, the urban wind profile is based on the extrapolation model developed in Chapter 5 (section (5.4). The surface roughness parameters identified in Table 5.3, with the surface roughness for C_H chosen as being representative for the Irish urban consideration. For this study, Table 8.5 details the surface characteristics and associated turbine hub-height for the sites being investigated. For both the Sri Lankan and UK contexts, surface roughness lengths were ascertained on the basis of the Davenport scale [170]. For each case study,

HOMER^{TM} extrapolates based on (8.4) from 50 m to the hub height within the rural/urban environment. So the model developed in Chapter 5 for the urban consideration (C_H) was modified to facilitate an extrapolation to 50m above the urban location. The wind data used for Sri Lanka and the UK were sourced directly (as explained in sections 8.3.2 and 8.3.4 respectively).

Table 8.5 Turbine Height & surface roughness characteristics

	Turbine Hub Height (m)	**Surface Roughness, z_0 (m)**	
Sri Lanka	20	0.25	*Hambontoto (Rural)*
	20	1.5	*Colombo (Urban)*
Ireland	20	0.02	*Dublin (Rural)*
	20	0.8	*Dublin (Urban)*
UK	15	0.01	*Newcastle (Rural)*
	15	1.5	*Newcastle (Urban)*

The optimisation results indicate the correlation between the initial cost of wind turbine, the annual mean wind speed and the associated cost per kWh generated. For the case studies being considered, an analysis of the cost effectiveness of a grid-connected wind turbine as a source of electricity within rural and urban contexts is presented.

8.3.2 Optimal System: Sri Lanka

In this study, the viability of a micro wind system was reviewed at two locations in Sri Lanka; representing both a rural (Hambantota) and urban (Colombo) perspective respectively[14].

The *Wind Resource Assessment Model* (WRAM) map was employed to estimate wind speeds at an elevation of 50 m height [246]. Estimated wind speeds at a 20 m elevation (hub-height), based on the parameters listed in Table 8.5, are subsequently modelled employing the logarithmic profile translation within *HOMER*. The WRAM 50 m

[14] Specific 50m monthly wind speed estimates acquired through collaboration with the University of Northumbria

monthly wind speed estimates for both the Colombo suburbs and the rural location Hambontota are illustrated in Table 8.6.

Table 8.6 *Sri Lankan* Monthly average wind speeds at 50 m height

Months	Monthly average wind speed at 50m height (m/s)	
	Hambantota (rural)	**Colombo (suburbs)**
Jan	8.22	4.09
Feb	7.19	2.75
Mar	6.19	3.35
Apr	4.62	3.82
May	8.65	6.69
Jun	8.96	7.23
Jul	9.37	6.79
Aug	10.09	7.12
Sep	6.84	6.38
Oct	7.77	5.1
Nov	3.48	3.8
Dec	4.2	4.1
Average	7.14	5.12

According to the wind resource data for each location, the Skystream wind turbine can generate 1374 kWh/year in Colombo suburbs and 5670 kWh/year near Hambantota. A typical daily (domestic) electricity consumption pattern in Sri Lanka is shown in Figure 8.1 with an annual household electricity demand of around 1993 kWh/yr. A summary of annual grid sales/purchase at each location are shown in Table 8.7, with Figure 8.2 illustrating energy production and grid purchases/sales against the monthly mean wind speed.

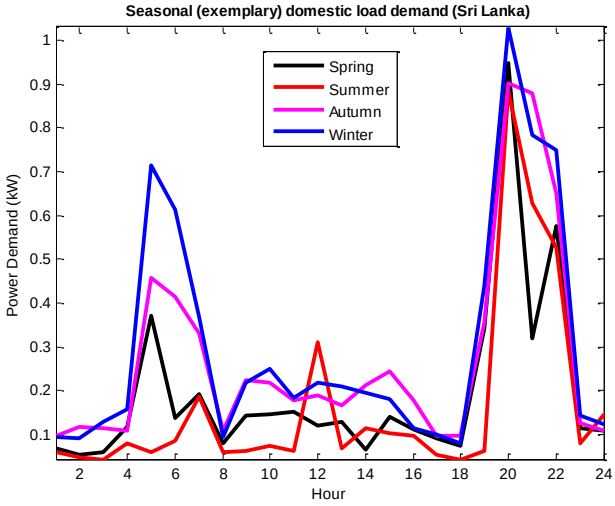

Figure 8.1 Seasonal (exemplary) domestic load demand (Sri-Lanka)

Table 8.7 Annual Sri Lankan Grid Sales/Purchases as percentages of annual load consumption of 1993kWh

	Colombo		Hambantoto	
Grid sales	613 kWh/yr	30.8 %	4250 kWh/yr	213.2 %
Net (€) purchases/sales	619 kWh/yr	31.1 % (Purchases)	3677 kWh/yr	184.5 % (Sales)

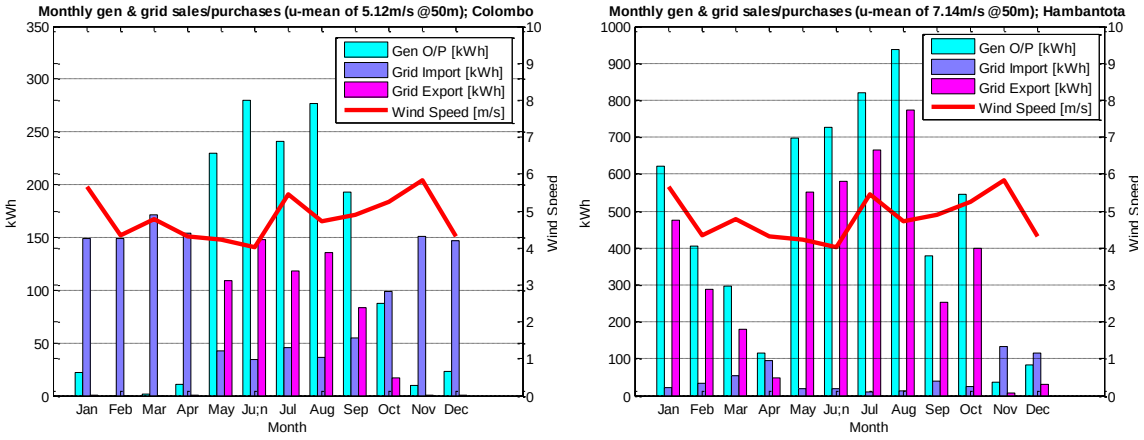

Figure 8.2 Monthly mean wind speed, energy production & grid purchases for Sri Lankan sites

The actual cost for the *Skystream* system in the Sri Lankan context was taken as *€7214.51+12% (VAT) = €8080.25*. Annual energy production by the wind turbine and cost of energy produced in terms of a unit cost of €0.163/kWh and variable wind speeds are illustrated in Table 8.8. This table shows the cost of kWh generated by the wind

turbine at both sites for the respective mean wind speeds observed at both sites. The significance of the (green) shading for this table (and the subsequent analyses in the other case studies) is to indicate at what wind speed with respect to initial cost per kW that a grid-connected wind turbine can provide a cost effective source of electricity (less than €0.163/kWh).

Table 8.8 Annual Energy Production (Sri Lanka) & associated cost of energy produced by the wind turbine (kWh)

HAMBONTOTA AIRPORT (Rural)

Initial Cost (€) per 1kW installation	Annual Mean Wind Speed								Unit cost €/kWh
	3m/s	4m/s	5m/s	6m/s	7m/s	**7.14m/s**	8m/s	9m/s	
4798.78	€ 3.42	€ 1.07	€ 0.53	€ 0.31	€ 0.21	**€ 0.21**	€ 0.16	€ 0.13	
3998.98	€ 2.85	€ 0.89	€ 0.44	€ 0.26	€ 0.18	**€ 0.17**	€ 0.13	€ 0.11	
3199.19	€ 2.28	€ 0.72	€ 0.35	€ 0.21	€ 0.14	**€ 0.14**	€ 0.11	€ 0.09	
2399.39	€ 1.71	€ 0.54	€ 0.26	€ 0.16	€ 0.11	**€ 0.10**	€ 0.08	€ 0.07	
1599.59	€ 1.14	€ 0.36	€ 0.17	€ 0.10	€ 0.07	**€ 0.07**	€ 0.05	€ 0.04	
799.80	€ 0.57	€ 0.18	€ 0.09	€ 0.05	€ 0.04	**€ 0.03**	€ 0.03	€ 0.02	
AEP (kWh by Skystream 3.7)	340	1083	2214	3700	5421	**5670**	7190	8855	

COLOMBO SUBURB (Urban)

Initial Cost (€) per 1kW installation	Annual Mean Wind Speed								Unit cost €/kWh
	3m/s	4m/s	5m/s	**5.12m/s**	6m/s	7m/s	8m/s	9m/s	
4798.78	€ 12.11	€ 2.12	€ 0.92	**€ 0.85**	€ 0.50	€ 0.32	€ 0.22	€ 0.16	
3998.98	€ 10.10	€ 1.77	€ 0.77	**€ 0.71**	€ 0.42	€ 0.27	€ 0.18	€ 0.14	
3199.19	€ 8.07	€ 1.41	€ 0.61	**€ 0.56**	€ 0.34	€ 0.21	€ 0.15	€ 0.11	
2399.39	€ 6.05	€ 1.06	€ 0.46	**€ 0.42**	€ 0.25	€ 0.16	€ 0.11	€ 0.08	
1599.59	€ 4.04	€ 0.71	€ 0.31	**€ 0.28**	€ 0.17	€ 0.11	€ 0.07	€ 0.05	
799.80	€ 2.02	€ 0.35	€ 0.15	**€ 0.14**	€ 0.08	€ 0.05	€ 0.04	€ 0.03	
AEP (kWh by Skystream 3.7)	96	548	1267	**1374**	2304	3642	5272	7093	

8.3.3 Optimal System: Ireland

For the Irish consideration, two sites were selected. The first is Dublin Airport, which would be indicative of a rural site with the second site being indicative of a sub-urban landscape within the city. Table 8.9 illustrates the monthly wind speed at respective site elevations.

Table 8.9 *Irish* Monthly average wind speeds

Months	Monthly average wind speed (m/s)	
	Airport (10m elevation)	**Dublin Suburb (50m elevation)**
Jan	5.650	6.168
Feb	4.344	4.741
Mar	4.794	5.233
Apr	4.322	4.718
May	4.228	4.615
Jun	4.013	4.380
Jul	5.439	5.937
Aug	4.707	5.138
Sep	4.908	5.357
Oct	5.253	5.734
Nov	5.821	6.353
Dec	4.316	4.711
Average	***4.821***	***5.26***

The urban wind reference is logarithmically extrapolated from the Airport wind resource to a height of 50m on the basis of the model described in Chapter 5. HOMER extrapolates from 50m to 20m (hub-height) thereafter.

Typical Irish load data is illustrated in Figure 8.3.

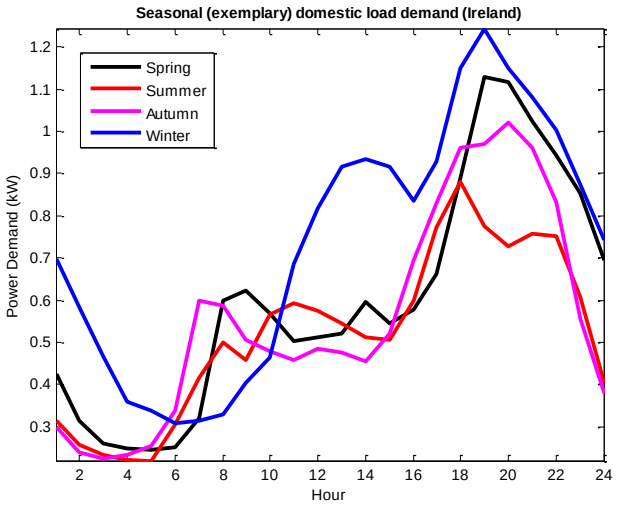

Figure 8.3 Seasonal (exemplary) domestic load demand (Ireland)

Annual energy output of the *Skystream* wind turbine system was evaluated and according to the wind resources data in each location, the wind turbine can generate 4472 kWh/year in rural Dublin and 2220 kWh/year in suburban Dublin. Typical annual

household electricity demand is around 5074kWh/yr. Hourly based energy demand and wind power generations, grid sales and purchase per year in each location are evaluated and shown in Table 8.10, with Figure 8.4 illustrating energy production and grid purchases/sales against the monthly mean wind speed.

Table 8.10 Annual Irish Grid Sales/Purchases as percentages of annual load consumption of 5074kWh

	Dublin Airport		**Dublin Suburb**	
Grid sales	1817 kWh/yr	35.81 %	555 kWh/yr	10.9 %
Net (€) purchases/sales	601 kWh/yr	11.8 % (Purchases)	2853 kWh/yr	56.2 % (Purchases)

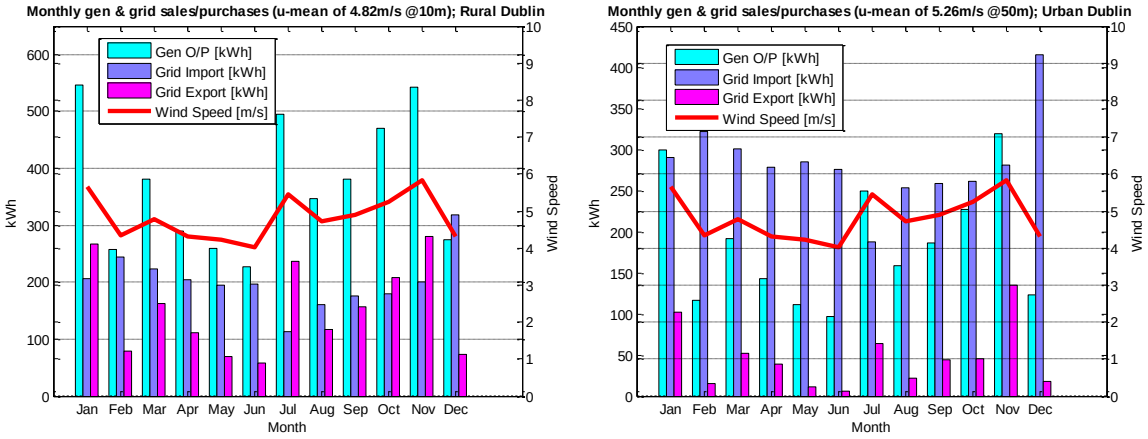

Figure 8.4 Monthly mean wind speed, energy production and grid purchases for Irish sites

The cost for the *Skystream* system for the Irish context was taken as €12000+21%(VAT) = €14521 [211]. Annual energy productions by the wind turbine and cost of energy production for a unit cost of €0.18/kWh and sale price of €0.09, with respect to variable wind speeds are illustrate in Table 8.11. This table shows the cost of kWh generated by the wind turbine at both sites for the respective mean speeds.

Table 8.11 Annual Energy Production (Ireland) and associated cost of energy produced by the wind turbine (kWh)

DUBLIN AIRPORT (Rural) [Airport]

Initial Cost (€) per 1kW installation	Annual Mean Wind Speed								
	3m/s	4m/s	**4.82m/s**	5m/s	6m/s	7m/s	8m/s	9m/s	
9075.63	1.40	0.91	**0.57**	0.52	0.36	0.27	0.23	0.20	Unit cost €/kWh
7563.02	1.17	0.76	**0.47**	0.44	0.30	0.23	0.19	0.17	
6050.42	0.94	0.61	***0.38***	0.35	0.24	0.18	0.15	0.14	
4537.81	0.70	0.45	**0.28**	0.26	0.18	0.14	0.12	0.10	
3025.21	0.47	0.30	**0.19**	0.17	0.12	0.09	0.08	0.07	
1512.60	0.23	0.15	**0.09**	0.09	0.06	0.05	0.04	0.03	
AEP (kWh by Skystream 3.7)	1812	2800	**4472**	4861	7115	9252	11040	12539	

DUBLIN SUBURB (Urban) [Site 1]

Initial Cost (€) per 1kW installation	Annual Mean Wind Speed								
	3m/s	4m/s	5m/s	**5.26m/s**	6m/s	7m/s	8m/s	9m/s	
9075.63	€8.77	€2.74	€1.33	**€1.15**	€0.80	€0.55	€0.41	€0.33	Unit cost €/kWh
7563.02	€7.31	€2.28	€1.11	**€0.95**	€0.67	€0.46	€0.34	€0.27	
6050.42	€5.85	€1.83	€0.88	**€0.76**	€0.53	€0.36	€0.27	€0.22	
4537.81	€4.39	€1.37	€0.66	**€0.57**	€0.40	€0.27	€0.20	€0.16	
3025.21	€2.92	€0.91	€0.44	**€0.38**	€0.27	€0.18	€0.14	€0.11	
1512.60	€1.46	€0.46	€0.22	**€0.19**	€0.13	€0.09	€0.07	€0.05	
AEP (kWh by Skystream 3.7)	290	929	1917	**2220**	3180	4650	6227	7760	

8.3.4 Optimal System: The UK

Power generation for the UK sites (Newcastle) was determined by considering a typical wind pattern [247] to evaluate hourly based energy generation of the wind turbine in the rural site. Table 8.12 illustrates the monthly wind speed at respective site elevations, with Figure 8.5 illustrating typical electrical energy demand of a house in UK.

Table 8.12 *UK* Monthly average wind speeds

Months	Monthly average wind speed (m/s)	
	Newcastle Airport (5m elevation)	**Newcastle Suburb (50m elevation)**
Jan	6.571	7.710
Feb	6.273	7.360
Mar	6.123	7.184
Apr	4.929	5.783
May	4.182	4.906
Jun	3.704	4.346
Jul	3.435	4.030
Aug	3.435	4.030
Sep	4.331	5.082
Oct	5.227	6.133
Nov	5.675	6.659
Dec	6.123	7.184
Average	***4.994***	***5.859***

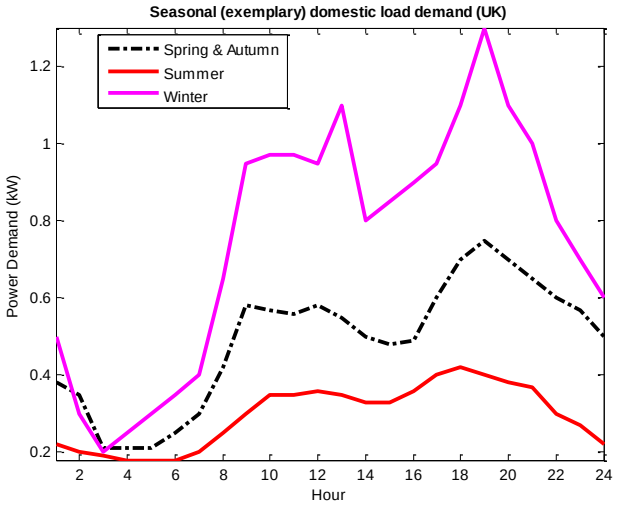

Figure 8.5 Seasonal (exemplary) domestic load demand (UK)

Calculated annual grid sales and purchase at each location are shown in Table 8.13, with Figure 8.6 illustrating energy production and grid purchases/sales against the monthly mean wind speed.

Table 8.13 Annual UK Grid Sales/Purchases as percentages of annual load consumption of 4616kWh

	Newcastle Airport		Newcastle Suburb	
Grid sales	2755 kWh/yr	62.4 %	417 kWh/yr	9.4 %
Net (€) purchases/sales	1301 kWh/yr	29.5 % (Sales)	2410 kWh/yr	55.6 % (Purchases)

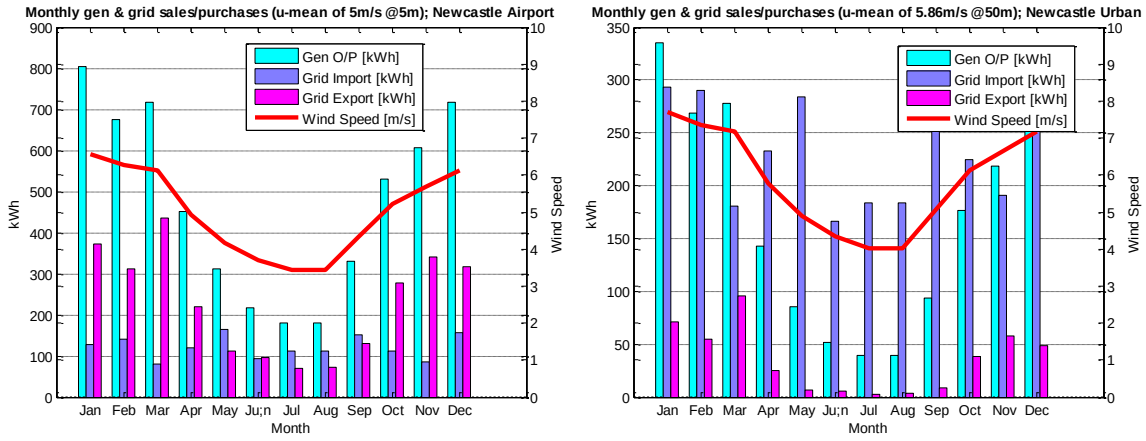

Figure 8.6 Monthly mean wind speed, energy production and grid purchases for UK sites

The actual cost for the Skystream 3.7 system was taken as €10063+20 % (VAT) = €12,076 [211]. Annual energy output of the wind turbine was evaluated and according to the wind resources data in each location, the wind turbine can generate 5717 kWh/year in rural Newcastle and 2007 kWh/year in suburban Newcastle. Typical annual household electricity demand is around 4417 kWh/yr. The cost of energy production based on different initial cost values for different annual mean speeds are illustrated in Table 8.14 on the basis of electricity buying price of €0.188/kWh and selling price of €0.263/kWh.

Table 8.14 Annual Energy Production (UK) and associated cost of energy produced by the wind turbine (kWh)

NEWCASTLE AIRPORT (Rural)

Initial Cost (€) per 1kW installation	Annual Mean Wind Speed							Unit cost €/kWh
	3m/s	4m/s	5m/s	6m/s	7m/s	8m/s	9m/s	
7437.67	€1.31	€0.59	**€0.36**	€0.26	€0.21	€0.18	€0.16	
6198.06	€1.09	€0.49	**€0.30**	€0.21	€0.17	€0.15	€0.14	
4958.45	€0.87	€0.39	**€0.24**	€0.17	€0.14	€0.12	€0.11	
3718.83	€0.66	€0.29	**€0.18**	€0.13	€0.10	€0.09	€0.08	
2479.22	€0.44	€0.20	**€0.12**	€0.09	€0.07	€0.06	€0.05	
1239.61	€0.22	€0.10	**€0.06**	€0.04	€0.03	€0.03	€0.03	
AEP (kWh by Skystream 3.7)	1548	3466	**5717**	7920	9844	11391	12516	

NEWCASTLE SUBURB (Urban)

Initial Cost (€) per 1kW installation	Annual Mean Wind Speed							Unit cost €/kWh
	3m/s	4m/s	5m/s	5.86m/s	7m/s	8m/s	9m/s	
7437.67	€13.11	€3.65	€1.65	**€1.01**	0.62	0.45	0.35	
6198.06	€10.92	€3.04	€1.38	**€0.84**	0.52	0.38	0.29	
4958.45	€8.73	€2.43	€1.10	**€0.67**	0.41	0.30	0.23	
3718.83	€6.55	€1.83	€0.83	**€0.51**	0.31	0.23	0.18	
2479.22	€4.37	€1.22	€0.55	**€0.34**	0.21	0.15	0.12	
1239.61	€2.18	€0.61	€0.28	**€0.17**	0.10	0.08	0.06	
AEP (kWh by Skystream 3.7)	155	556	1228	**2007**	3265.00	4496.00	5767.00	

8.4 Discussion

The viable initial costs per kW installation of small wind turbines were determined based on the results shown in Figure 8.2, Figure 8.4 and Figure 8.6 and Table 8.8, Table 8.11 and Table 8.14. A collated summary of the results are presented in Table 8.15. HOMER facilitates this sensitivity consideration as illustrated in Figure 8.8, which illustrates the Irish context.

Table 8.15 Viable initial cost per 1 kW generator capacity in terms of annual mean wind speed

Annual mean wind speed	***Viable initial cost per 1 kW capacity installed (€/kW)***					
	Sri Lanka		**Ireland**		**UK**	
	Rural	**Urban**	**Rural**	**Urban**	**Rural**	**Urban**
3 m/s	*NV**	*NV*	*NV*	*NV*	*NV*	*NV*
4m/s	*NV*	*NV*	<€1815	*NV*	<€2465	NV
5m/s	<€1600	<€673	<€2904	NV	<€4478	NV
6m/s	<€2626	<€1582	<€3933	<€1512	<€6541	<€1006
7m/s	<€3872	<€2525	<€4538	<€2783	<€8503	<€2264
8m/s	<€5050	<€3703	<€5082	<€3509	<€10063	<€3396
9m/s	<€6162	<€4882	<€5626	<€3933	<€11572	<€4402

**Not Viable*

In Table 8.15, the annual wind speed column represents a reference to which the wind speeds at the different locations are scaled to. Irrespective of the scale, the wind speeds (annual observed/modelled) considered in the preceding section (8.3) will retain the statistical characteristics and shape of the baseline data, but the wind speed magnitudes will vary depending on the factor required to achieve this scale reference. Figure 8.8 illustrates a frequency distribution comparison of the wind resource for the Irish rural and urban locations, illustrating statistical differences at both locations.

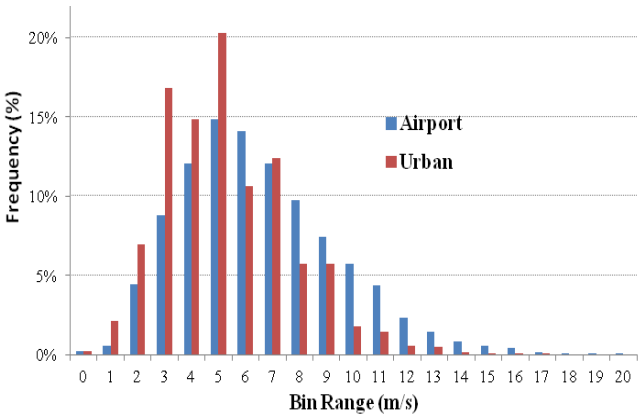

Figure 8.7 Frequency Distribution comparison of the rural/urban wind resource (Ireland)

Wind potential for power generation by a wind turbine is not dependent solely on mean wind speed. Wind speed variation is also a considerable factor. So for variable mean wind speed reference (as illustrated in Table 8.15), the wind speeds at for each location were scaled (to a greater or lesser degree) to be representative of that reference wind speed. But as the baseline statistics representative of both locations are also considered, a wind turbine positioned at any location could have different a different productivity for the same mean wind speed reference. In this way, Table 8.15 presents a comparison of wind turbine productivity at both rural and urban sites for respective countries in terms of a single mean wind speed value.

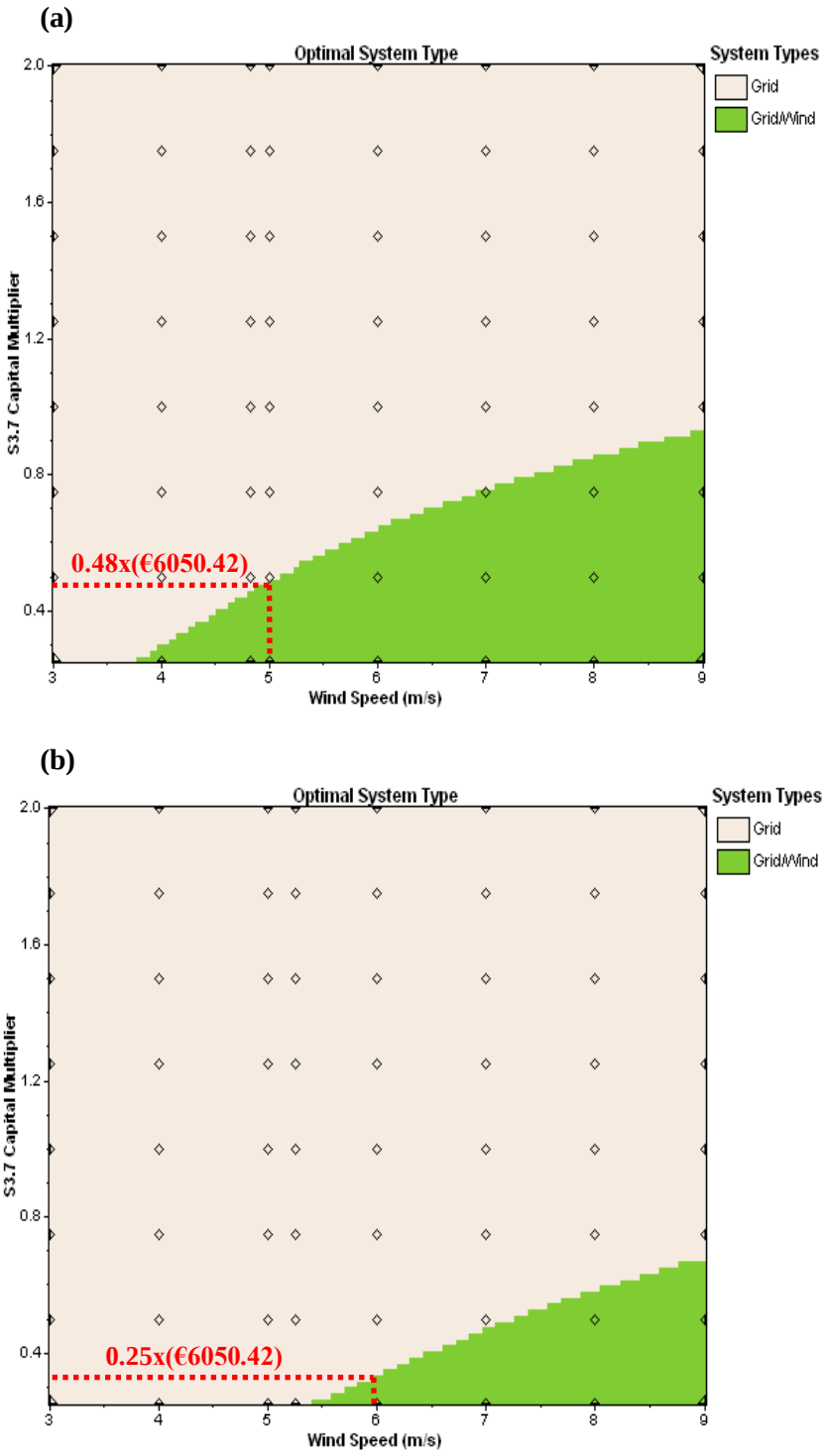

Figure 8.8 Viable initial cost per 1 kW generator capacity (*Skystream 3.7*) in terms of annual mean wind speed in terms of HOMER sensitivity analysis (Cost/kW = €6050.42)

The system cost of energy generation for each case study in terms of varying initial investment costs are illustrated in Figure 8.9. Table 8.16 offers further context by

illustrating the COE for each country in terms of their associated rural and urban installations at the current cost per kW of the micro wind system.

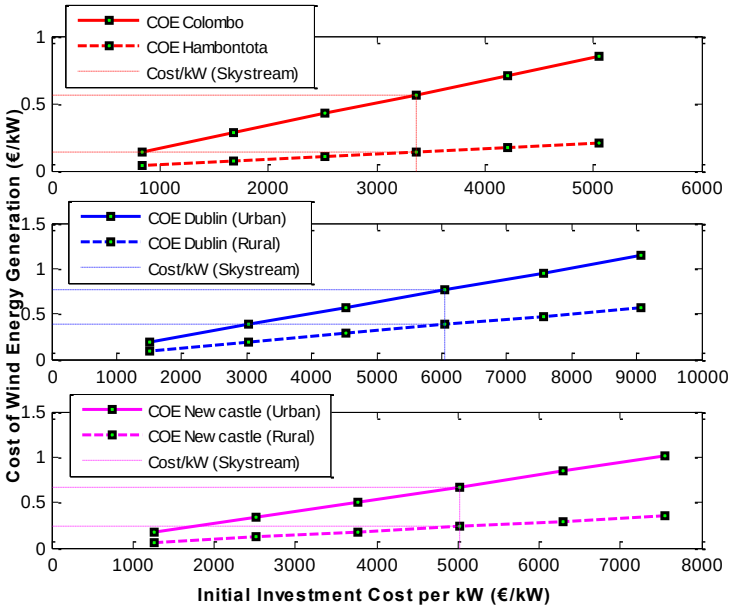

Figure 8.9 Wind Energy Generation vs. Initial investment

Table 8.16 COE associated with the wind generator at the annual mean wind speed in terms of capital cost of the generation system

Cost of Skystream 3.7 Wind Energy Generation (€)	***Rural Context***	***Urban Context***
Sri Lanka	€0.14	€0.56
Ireland	€0.38	€0.76
UK	€0.24	€0.67

The results suggest that the COE associated with micro wind systems installed in urban locations is preclusive from an optimisation perspective. For micro wind turbines to be viable in the urban environment, a reduced initial cost of the system is required. Improvements in the wind turbine aerodynamics and energy capture at low wind speed are essential in conjunction with reduced power losses in the generator and power electronic conversion modules. Outside of the technology itself, more generous Feed-In Tariffs (FIT) will be required for the foreseeable future.

In the context of increasing small/micro wind energy systems efficiencies, *Maximum Power Point Tracking* (MPPT) has been shown to have potential for fixed-pitch controlled wind turbines (dominant option for small/micro wind turbines). Such control strategies facilitate operating the turbine at maximum aerodynamic power points of the wind rotor. This approach has been shown to increase the energy capture of the system by 12% [247], which has the potential to offset the system costs.

Finally, from an Irish perspective a comparison is made with a Solar PV system of the same capacity. The balance of system costs for a PV system based on 2.4kWp was taken as €2600 per kWp, i.e. €6,240 for a 2.4kWp PV system [248]. Annual energy productions by the PV system and cost of energy production for a unit cost of €0.18/kWh and sale price of €0.09 (consistent with the Irish position), with respect to solar radiation are illustrate in Table 8.17. This table shows the cost of kWh generated by the PV system based on exemplar data for Ireland which was attained through NASA's Surface Solar Energy Data Set which provides monthly average solar radiation data for everywhere on earth (at http://eosweb.larc.nasa.gov/sse/).

Table 8.17 Annual Energy Production (Ireland) and associated cost of energy produced by the exemplar PV system (kWh)

		Annual Mean Solar Radiation							
		1kWh/m^2/d	2kWh/m^2/d	**2.43kWh/m^2/d**	3kWh/m^2/d	4kWh/m^2/d	5kWh/m^2/d	6kWh/m$^{\wedge}$2/d	7kWh/m^2/d
Initial Cost per 1kW installation	€3,900	€2.31	€0.94	**€0.71**	€0.56	€0.46	€0.41	€0.38	€0.37
	€3,250	€1.93	€0.79	**€0.60**	€0.47	€0.38	€0.34	€0.32	€0.31
	€2,600.00	€1.56	€0.63	**€0.48**	€0.38	€0.31	€0.28	€0.26	€0.25
	€1,950	€1.19	€0.49	**€0.37**	€0.29	€0.24	€0.21	€0.20	€0.19
	€1,300	€0.82	€0.33	**€0.25**	€0.20	€0.16	€0.15	€0.14	€0.13
	€650	€0.44	€0.18	**€0.14**	€0.11	€0.09	€0.08	€0.07	€0.07
AEP (kWh by Skystream 3.7)		72	177	**233**	298	364	404	432	454

Figure 8.10 contextualises the Irish wind energy system costs of energy generation (rural and urban) with regard to a Solar PV consideration and in terms of varying initial investment costs.

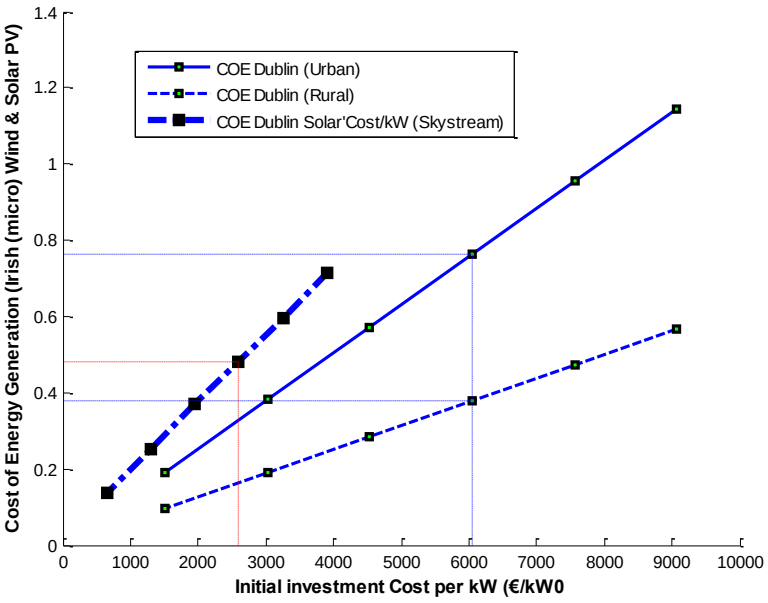

Figure 8.10 Irish Wind Energy Generation and Solar PV Generation vs. Initial investment

It is apparent from Figure 8.10 that the cheaper cost/kW available to the PV system is affording a competitive position for this technology with respect to the wind energy system

8.5 Conclusions

Available studies on the performance of micro wind turbines in the urban environment are generic, e.g. the technology can work if installed correctly and in appropriate locations. There is a need to establish the various factors that affect performance of small scale wind turbines, particularly in the urban environment, and find out minimum requirements to make such installations commercially viable.

The results of the COE analysis between three countries, with different national targets and renewable energy strategies, show that for urban wind, the cost in developing wind energy at micro level is preclusive. Moreover, in countries such as Sri Lanka where micro wind could support the developing rural distribution networks, the FiT is insufficient to enhance viability in urban environments. The UK Government is generally committed to the integration of microgeneration, with current FiTs offered to small/micro wind being considerably more favourable than for e.g. Solar PV [249, 250]. In Ireland, the microgeneration scheme saw micro wind as the technology of choice, but with the current payment for exported energy, neither rural nor urban sites are cost viable.

This study was based on small wind turbine systems and considered initial system's cost, (utility) electricity supply and (system) generation to determine the Levelized unit cost of electrical energy which is the parameter used to determine the optimal system configuration. Initial cost of the wind turbine is the main factor to determine cost of energy production by wind turbine as operation cost is comparatively low. *HOMER* was employed to determine optimal system configuration for given aspects of economic viability of the wind turbine with respect to varying initial costs and annual mean wind speeds. The viable initial costs per kW were determined on the basis of the representative load characteristic in each country and the available wind resource.

To advance the uptake of micro wind turbines, it is important to reduce the initial cost of the system, improve the wind turbine aerodynamics and energy capture at low wind speed by considering the use of advanced dynamic control techniques (e.g. wind speed forecasting, predictive control, active yaw control, etc.).

Chapter 9: Conclusions & Future Work

9.1 Summary

As obliged by the European Commission's energy policy goals for 2020, Ireland is committed to achieve a 20% increase in energy efficiency, coupled with a 20% decrease in greenhouse gas emission. Both goals are supported by a 20% increase in renewable energy integration. The Irish Government has further set a target that requires 40% of national electricity to be generated through renewable energy; the highest target in the EU for variable renewable electricity. However, this is not just an Irish concern. Globally, populations are increasingly migrating towards cities [22], and green solutions to electrification where the demand is highest are required.

Central generation systems are currently the predominant platforms for electricity supply and in terms of electrifying urban centres, transmission and distribution losses are preclusive for optimal system efficiency. From an increasing energy efficiency perspective, if improvements are to be realised, an energy paradigm is required where in conjunction with these centralised plant, there is a shift from "many loads – few sources" towards one advocating "many loads – *many sources*" [3]. Such a compromise should be cognisant of the economies of scale associated with central power systems, but be coupled with renewable energy sources that are closer to load centres, thereby also contributing to improved efficiencies and lower GHG contributions.

The renewable resource prioritised in this thesis is wind. Wind in cities is a complicated phenomenon, but to ignore wind energy here is counterintuitive when an over reliance on fossil fuels is so prevalent worldwide. Wind energy on a global scale is the most developed form of renewable energy. However, as with most countries, the majority of wind plant is on a large scale and remote from the urban populations, where the vast majority of load centres are located [62]. Therefore, as with central generation plant, distributed generation in this form also face transmission efficiency issues.

This logic is well understood and is a pillar on which future smart grids are being developed. But there are contrary views that believe that there should be alternatives to increasing the pursuit of renewable energy supply. In recent times such alternatives have been identified and these potentially offer respite to global energy price fluctuations [43, 50, 51]. But as these alternatives are themselves not sustainable, such *respite* will be (relatively) short lived and with their extraction, a delay in the inevitable is all that is achieved. Strategically therefore, electricity *greening* at multiple levels is the only sustainable energy future. A case for increased levels of distributed generation is therefore further established.

This thesis uses these issues as the rationale to consider a realistic context for the integration of small scale distributed generation into the distributed network. In other words, can small, distributable wind energy systems, for a large representation, operate in conjunction with current distribution network standards? In this regard, the work presented here prioritises cities and focuses on two themes: firstly, is there a viable wind resource in urban environments and secondly, on the basis of an accurate wind model, a representative and appropriate power flow algorithm is required to investigate the

implications for distribution network. Ultimately, the research attempts to ascertain the consequences of consumer connected micro wind generation to establish if it impacts detrimentally the distribution network operation at consumer level.

9.2 Research Findings: Contributions to Aims and Objectives

As highlighted in the literature considered throughout this thesis, there is evidence supporting the contention of the thesis that small renewable have a role in future distribution networks. While there are significant challenges ahead if micro/small wind energy systems are to play a contributory role in supplying the electricity demand within cities, the analyses supports their deployment and justifies international government engagement in this regard. The analyses here suggest a minimum height requirement with respect to where such generation systems can optimally extract the available resource in a viable manner. The research presented here demonstrates a methodology applicable for Dublin. Further work will investigate if the method developed for these two sites could be extrapolated to other urban sites.

It was also shown that increased proliferation of consumer connected wind generation systems within urban environments should not inhibit the operational concerns of DNOs from a consumer voltage and network voltage balance perspective. In the manner in which the distribution network model was developed and how it is configured, other network structures and forms of renewable energies could easily be integrated to investigate alternative energy scenarios.

The wind resource in cities significantly limits the installation potential. While the surface form and environmental heterogeneity are primarily responsible in this regard, an appreciation of the associated surface characteristics is employable as a parameter in urban wind profiling, as the associated modelling established.

Currently, the associated costs of such systems are preclusive from a consumer engagement perspective, but if this market was to develop and drive capital costs down, there is potential for consumers to both save on their electricity costs and contribute towards

9.2.1 Addressing the main research questions and their wider implications

Chapter 2, in an energy supply context, established that small and micro generation could have a role to play in a renewable energy paradigm. It is unrealistic to expect small embedded generation – as constituent elements of distribution networks – should dictate how electricity utilities are configured, but that does not mean small scale generation cannot contribute positively. Micro generation in Ireland is still at very early stages of embracement, but it is clear from the commitment of Ireland's closest neighbour, the UK, that micro generation has a key role to play in future distribution network configurations, albeit on the basis of collaboration with the DNO. Even with the current uncertainties surrounding the sustainability of such an agenda (due to alternative fossil fuels that have been identified), there is already significant traction towards micro grids that can optimise smaller embedded generation.

Chapter 3 discussed micro generation and the associated technical implications if it is to have a defined role in the micro grids of the future. The literature considered justified technical analysis pertaining to network tolerances with increased micro (wind)

generation capacity – particularly at consumer level – to underpin how this level of generation capacity can participate. Initial power flow analyses were applied to a generic representation of the Irish distribution network and with Dublin airport wind data, which would be more representative of a rural environment, the network can accommodate almost 100% of consumer connected micro wind generation capacity based on an after diversity maximum demand model. Two conclusions can be drawn from these initial analyses. First of all, the generic network description needs to be enhanced so that unbalanced (asymmetrical) power flow and also, an improved consumer representation in this regard is also required. Secondly, it was clear that any load flow analyses to accurately represent the urban environment needs to be cognisant of an accurate wind resource.

The primary energy resource issue was considered in Chapters 4 and 5. These Chapters considered firstly the limitations in understanding currently available to the engineering community – particularly with respect to urban distribution networks. The analytical models considered explored the limits of opportunity available to wind energy extraction and more importantly how this understanding is capable of application in any city where alternative forms of energy are needed most. Chapter 4 outlined the significant complexity associated with the wind resource in cities and prioritised analytical modelling by considering, in detail, two such models. Following-on from Chapter 4, Chapter 5 empirically links the wind resource available at the top of the urban roughness layer (RSL) at z*, to an urban reference site (Dublin Airport). Maybe more significantly, the associated analyses illustrated how in order to avail of a viable wind resource, the hub-height of a small/micro wind turbine needs to be between 2 and 4 times the average building height in a particular location. Modelling in this regard

further considered the wind resource within the roughness surface sublayer and found that the wind resource in this region would not be conducive to viable wind energy harnessing in an urban context. Due to the nature of the wind resource, it was further observed that modelling in said region is also inconclusive. Chapter 5 made use of previously unpublished wind speed (direction) data to validate the empirical modelling developed.

Chapter 6 further considered the urban wind resource but more from the perspective of how usable it is by the generator itself; particularly when turbulent air flows are so prevalent. Modelling therefore prioritised the turbulent component within the average wind speed (over a fixed duration). Here the emphasis was with respect to modelling the reaction of the wind turbine in turbulent environments and towards a model that could be used by the industry in such environments, based on the observation capabilities of current monitoring equipment. In this regard simplistic models were developed that utilise both the mean wind speed and standard deviation to model the effect of turbulence on the performance capability of a wind turbine. Two models were developed that utilise Gaussian and Weibull statistics respectively were developed by employing 10Hz data at the two locations considered in Chapter 5. The novelty of the approach developed (which could also be said for the wind profiling presented in Chapter 5), is with regard to the simplicity of the approach in which for both models, all that is required is the mean wind speed and standard deviation over a reference time frame. Both models employ the industry metric, turbulence intensity, to normalise the power characteristic of a standard wind turbine.

An analysis of how the resource affects the generation technology is extremely important to understand how the technology interacts with the network. The distribution network model is critical if an accurate understanding of how such technologies affect the power performance of said network is to be achieved. Chapter 7 devises a robust distribution network model that employs the complex admittance matrix to accurately evaluate power flow for a range of scenarios. A number of modelling scenarios were subsequently applied to this model. More specifically, seasonal load/wind speed profiles were considered, as were models that considered the empirical wind speed model developed in Chapter 5. Also considered was the specifics of embedded generation on the basis of it being normalised as a consequence of the turbulent urban wind resource. The verified model developed in this thesis was inclusive of the earthing system.

Finally, while Chapters 4 and 5 evaluated the viability of urban installed wind energy systems (i.e. with respect to minimum hub-height), if this form of renewable energy is to have a future, it is understood that the associated market will require some incentives. Such incentives require an appreciation of the *per kW* installed costs associated with these systems. In this regard, the levelized cost of energy was explored. The Hybrid Optimisation Model for Electric Renewables *HOMER*^{TM} was utilised in this regard. The cost of energy analyses highlighted that current capital costs associated with small wind energy systems are preclusive. The international comparison concluded that even with an improved offering for exported energy (as in the UK), while capital costs are excessive; the cost per kW will remain high.

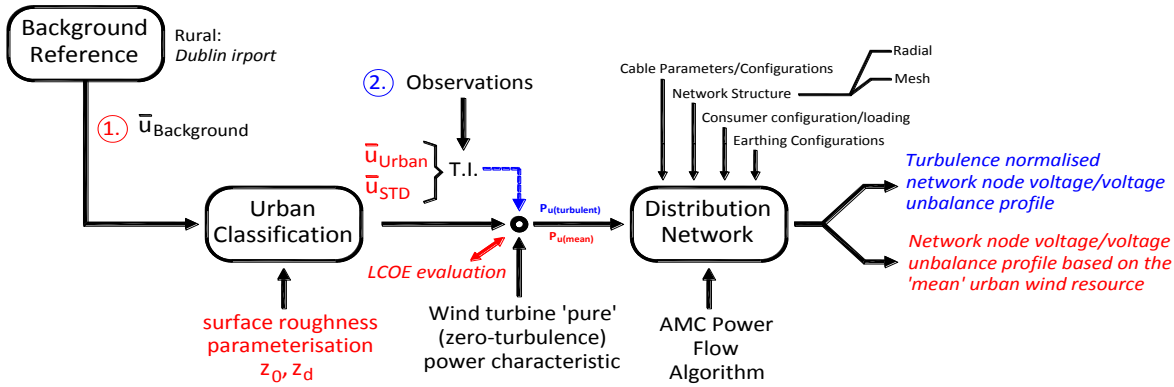

Figure 9.1 Thesis contribution: *'Towards Smart Energy Cities'*

The main modelling considerations as developed in the thesis are synopsised in Figure 9.1 above, in which said modelling was developed from the generic analyses described in Chapter 3. The research served to acquire a refined wind resource model that was available to establish a detailed description of how this resource was incorporated in the developed network model and power flow algorithm, which collectively facilitated an enhanced understanding of the potential for this form of embedded generation. The holistic contribution from this applied research can be described as follows:

1. This research investigated the context of '*many loads, many sources' (*wind energy) through a synergy of urban climatology that informs the limitations of a DN model capable of the granularity required to accurately represent individual 'prosumers. Both the mean wind airflow profiling and the consideration of how turbulence affects turbine productivity employed observations across Dublin city to inform the modelling
2. With increasing population migration to cities, wind energy in urban environments as considered in my thesis needs to be harnessed as a viable primary resource; analyses of resource limitations and in the context of the

future *smarter* grids, distribution network modelling reflecting the practicalities/limitations of this urbanised resource are required.

3. These smart grids will also require accurate power flow models such as the one I developed that incorporate correctly the participation of these prosumers

9.3 Limitations and Further Work

There are a number of questions arising from the achievements of the work presented here:

- The analytical model developed in Chapter 5 has scope for further consideration in terms of *Geographical Information Systems* (GIS). GIS are a readily available resource for cities and could be employed to both validate and refine the methodology developed in Chapter 5 towards an urban wide wind mapping resource that is based on the urban surface form. Such a development would have significant engineering applications as well as urban development potential, but also with regard to environmental concerns such as air pollution models.
- Chapter 5 highlighted how the Weibull and Rayleigh distributions as commonly employed by wind engineers in ascertaining the available resource within an urban environment have limited scope within the UCL. Further work in ascertaining if alternative probability distributions might derive improved accuracy in this regard is warranted.
- Chapter 5 in the consideration of the analytical models described in Chapter 4 identified scope for analyses concerning how frictional velocity within urban environments is linked to a rural reference. The research ascertained that current empirical considerations are insufficient and warrant further investigation as

current guidance could lead to significant errors in the absence of measured values. Improved empirical frictional velocity parameterisation based on rural/urban transitions may prove useful in the development of an enhanced profile model

- The primary energy modelling in this thesis prioritised the urban wind resource, but a further consideration would be a more diverse generation base involving PV. To achieve a similar level of understanding as developed for wind, similar considerations would be required for solar insolation; albeit, variations in this resource are less sensitive on a city scale
- Chapter 6 provided for an improved understanding of how turbulence affects the performance of a wind turbine. This modular modelling approach, while consistent with the current standard, needs to be extended to consider the inertia of the turbine, particularly in an urban context, if industry confidence is to be achieved.
- The distribution network model and power flow algorithm is sufficiently robust to facilitate other power quality issues. Alternative forms of generation at more divers capacity ranges should be considered. A further development of the model developed in Chapter 7 would to consider the MV network at the primary side of the substation transformer
- With regard to the cost of energy analyses as presented in Chapter 8, further work is required to establish if more refined feed-in-tariffs might be considered to encourage the development of a micro wind energy market as a precursor to facilitating reduced capital costs.

REFERENCES

[1] International Energy Agency. (2012, 18th November, 2012). Key World Energy Statistics. Available: http://www.iea.org/publications/freepublications/publication/kwes.pdf

[2] Patterson W., *Keeping the Lights On.* London: Earthscan, 2007.

[3] Burt G. M., Hammond G. P., and Infield D., "Guest Editorial - Special Issue on Highly Distributed Power Systems," *Proceedings of the Institution of Mechanical Engineers, Part A: Journal of Power and Energy,* vol. 222, , pp. i-iii, 2008.

[4] Momoh J.A., Meliopoulous S., and R. Saint, "Centralized and Distributed Generated Power Systems - A Comparison Approach," Power Systems Engineering Research Center,2012.

[5] Martin J. (2009, 4th April 2013). *Distributed vs. centralized electricity generation: are we witnessing a change of paradigm? An introduction to distributed generation* [on-line]. Available: http://www.vernimmen.net/ftp/An_introduction_to_distributed_generation.pdf

[6] IEA, "Distributed Generation in a liberized energy market," International Energy Agency,, Jouve: France2002.

[7] Patterson W., "Electric Opportunities," *European Energy Review,* vol. 1, 2007.

[8] Bouffard F. and Kirschen D. S., "Centralised and distributed electricity systems," *Energy Policy,* vol. 36, pp. 4504-4508, 2008.

[9] Cossent R., Gomez T., and P. Frias, "Towards a future with large penetration of distributed generation: Is the current regulation of electricity distribution ready? Regulatory recommendations under a European persopective," *Energy Policy,* vol. 37, pp. 1145-1155, March, 2009 2009.

[10] Council of the Eurpoean Union, "Council conclusions on Renewable Energy," 3204th Transport, Telecommunications and Energy Council Meeting,2012.

[11] El-Khattam W. and Salama M. M. A., "Distributed generation technologies, definitions and benefits," *Electric Power Systems Research,* vol. 71, pp. 119-128, 2004.

[12] Pepermans G., Driesen J., Haeseldonckx D., Belmans R., and D'haeseleer W., "Distributed generation: definition, benefits and issues," *Energy Policy,* vol. 33, pp. 787-798, 2005.

[13] Ayompe L., "Performance and Policy Evaluation of Solar Energy Technologies for Domestic Applications in Ireland," (Doctorate Degree) PhD, School of Civil and Building Services Engineering, Dublin Institute of Technology, Dublin, 2011.

[14] Bergman N., Hawkes A., Brett D.J. L., Baker P., Barton J., Blanchard R., Brandon N. P., Infield D., Jardine C., Kelly N., Leach M., Matian M., Peacock A. D., Staffell I., Sudtharalingam S., and Woodman B., "UK microgeneration. Part I: policy and behavioural aspects," *Proceedings of the ICE - Energy,* vol. 162, pp. 23-36, 2009.

[15] Watson J., Sauter R., Bahaj A.S., James P.A.B., Myers L.E., and Wing R., "Unlocking the power house: policy and system change for domestic micro-generation in the UK," Project Report2006.

[16] Peacock A. D., Jenkins D., Ahadzi M., Berry A., and Turan S., "Micro wind turbines in the UK domestic sector," *Energy and Buildings,* vol. 40, pp. 1324-1333, 2008.

[17] James P. A. B., Sissons M. F., Bradford J., Myers L. E., Bahaj A. S., Anwar A., and Green S., "Implications of the UK field trial of building mounted horizontal axis micro-wind turbines," *Energy Policy,* vol. 38, pp. 6130-6144, 2010.

[18] Infield D., "Integrating Micro-Generation into Distribution Systems - a review of recent research," *IEEE,* 2008.

[19] Manfren M., Caputo P., and Costa G., "Paradigm shift in urban energy systems through distributed generation: Methods and models," *Applied Energy,* vol. 88, pp. 1032-1048, 2011.
[20] Ren21, "Renewables 2012: Global Status Report," Renewable Energy Policy Network for the 21st Century, on-line2012.
[21] Ayhan D. and Sağlam Ş., "A technical review of building-mounted wind power systems and a sample simulation model," *Renewable and Sustainable Energy Reviews,* vol. 16, pp. 1040-1049, 2012.
[22] United Nations Human Settlements Programme (UN-HABITAT). (2008, 18/11/2012). *State of the World's Cities 2008/2009: Harmonious Cities,* [on-line].
[23] United States Energy Information Administration, "Annual Energy Review 2011 (Energy consumption by sector)," EIA2011.
[24] European Environment Agency, "Final electricity consumption by sector (EU-27)," EEA2012.
[25] AEA. (2011, 12th July, 2012). *The AEA Microgeneration Index* [on-line]. Available: http://www.aeat.com/microgenerationindex/reports/The%20AEA%20Microgeneration%20Index%20-%20Issue%204.pdf
[26] GWEC, "Global Wind Report - Annual Market Update," Global Wind Energy Council,2011.
[27] Reuther N. and Thull J-P., "Feasibility Study of Small and Micro Turbines for Residential Use in New Zealand," Land Environment and People Research Report No. 30, 2011.
[28] AWEA, "Small Wind Turbine Global Market Study," American Wind Energy Association, Ed., ed, 2010.
[29] EST, "Location, Location, Location: Domestic small-scale wind field trial report," Energy Savings Trust,2009.
[30] Encraft, "The Warwick Urban Wind Trial Project," 2009.
[31] Arifujjaman Md, Iqbal M. T., and Quaicoe J. E., "Energy capture by a small wind-energy conversion system," *Applied Energy,* vol. 85, pp. 41-51, 2008.
[32] Islam M. R., Saidur R., and Rahim N. A., "Assessment of wind energy potentiality at Kudat and Labuan, Malaysia using Weibull distribution function," *Energy,* vol. 36, pp. 985-992, 2011.
[33] Cabello M. and Orza J. A. G., "Wind speed analysis in the province of Alicante, Spain. Potential for small-scale wind turbines," *Renewable and Sustainable Energy Reviews,* vol. 14, pp. 3185-3191, 2010.
[34] Fyrippis I., Axaopoulos P. J., and Panayiotou G., "Wind energy potential assessment in Naxos Island, Greece," *Applied Energy,* vol. 87, pp. 577-586, 2010.
[35] Kavak A. E. and Akpinar S., "A statistical analysis of wind speed data used in installation of wind energy conversion systems," *Energy Conversion and Management,* vol. 46, pp. 515-532, 2005.
[36] Jowder F. A. L., "Wind power analysis and site matching of wind turbine generators in Kingdom of Bahrain," *Applied Energy,* vol. 86, pp. 538-545, 2009.
[37] Kavak Akpinar E. and Akpinar S., "A statistical analysis of wind speed data used in installation of wind energy conversion systems," *Energy Conversion and Management,* vol. 46, pp. 515-532, 2005.
[38] Mekhamer S. F., Soliman S. A., Moustafa M. A., and El-Hawary M. E., "Load flow solution of radial distribution feeders: a new contribution," *International Journal of Electrical Power & Energy Systems,* vol. 24, pp. 701-707, 2002.
[39] Stott B., "Review of load-flow calculation methods," *Proceedings of the IEEE,* vol. 62, pp. 916-929, 1974.
[40] "PLANNING AND DEVELOPMENT REGULATIONS 2007.," ed. Ireland: Deparment of the Environment, Heritage and Local Government,, 2007.

[41] IPCC. (2013, 27th September). *Human influence on climate clear, IPCC report says* [on-line]. Available: http://www.ipcc.ch/news_and_events/docs/ar5/press_release_ar5_wgi_en.pdf
[42] Kent S., "OPEC: U.S. Shale Oil to Cut into Demand," in *Wall Street Journal*, ed. New York, 2013.
[43] Charles C. M. (2013) What if We Never Run Out of Oil. *The Atlantic* [on-line]. Available: http://www.theatlantic.com/magazine/archive/2013/05/what-if-we-never-run-out-of-oil/309294/
[44] McCrone A., "Global trends in renewable energy investment,," Frankfurt School of Finance & Management,2012.
[45] EIA. (2012, 24/02/13). *Annual Energy Review* [on-line,]. Available: http://www.eia.gov/totalenergy/data/annual/pdf/aer.pdf
[46] EEA. (2012, 24/02/13). *Final electricity consumption by sector, EU-27* [on-line]. Available: http://www.eea.europa.eu/data-and-maps/figures/final-electricity-consumption-by-sector-4
[47] EEA, "Approximated EU GHG inventory: early estimates for 2011,," European Environment Agency, Technical Report 13/2012, 2012.
[48] Gaughan K., "Is there evidence that there are increasing fossil fuel deposits presenting a counter position to emphaising renewable energy sources in the future?," K. Sunderland, Ed., email ed, 2013.
[49] WEC, "World Energy Reserves and Production (2008 Figures from 2010 survey by the World Energy Council)," vol. 2013, ed: World Energy Council,, 2013.
[50] Williams S., "BP Says North America Shale Boom Will Pressure OPEC," in *Wall Street Journal*, ed. New York, 2013.
[51] National Geographic. (2013, 6th May,). *Japan's Burning Hope for New Energy* [on-line]. Available: http://news.nationalgeographic.com/news/energy/2013/03/pictures/130328-methane-hydrates-for-energy/
[52] Meitheal NaGaoithe, "Embedding Sustanability: The Business Case for Small Wind Energy," SEAI,2013.
[53] United Nations Climate Change Portal. 4th May 2013,). *Durban conference delivers breakthrough in international community's response to climate change* [on-line]. Available: http://www.un.org/wcm/content/site/climatechange/pages/gateway/the-negotiations/durban
[54] EEA, "Greenhouse gas emission trends and projections in Europe 2012,," European Environmental Agency, Luxembourg 6/2012, 2012.
[55] EREC, "Mapping Renewable Energy Pathways towards 2020," European Renewable Energy Council,2011,.
[56] EWEA, "Wind in Power: 2012 European Statistics," February 2013.
[57] Troen I. and Peterson E. L., "European Wind Atlas. ," Risø National Laboratory, Roskilde,1989.
[58] SEAI, "Ireland - Your Smart Grid Opportunity," Sustainable Energy Authority of Ireland,2010.
[59] DCENR, "Strategy for Renewable Energy: 2012 -2020," Department of Communications Energy and Natural Resources, Ed., ed, 2012.
[60] SEAI. (2011, 8th August). *Renewable Energy in Ireland 2011* [on-line]. Available: http://www.seai.ie/Publications/Statistics_Publications/Renewable_Energy_in_Ireland_2011.pdf
[61] Howley M., Dennehy E., ÓGallachóir B., and Holland M., "Energy in Ireland 1990-2011," Sustainable Energy Authority of Ireland2012.
[62] ESBN, "ESB Networks Key Statistics - 2012," ESB Networks2012.

[63] DCENR, "White Paper: Delivering a Sustainable Energy future for Ireland," Department of Communications Energy and Natural Resources Ed., ed, 2007.
[64] Howley M., Dennehy E., ÓGallachóir B., and Holland M., "Electricity & Gas Prices in Ireland (Annex Household Electricity Prices per kWh, 1st Semester (January-June, 2012))," Sustainable Energy Authority of Ireland2012.
[65] SEAI, "Renewable Energy in Ireland 2011," 2012.
[66] IWEA. (2012, 24/02/13). *Wind Energy in Ireland (FAQs)* [on-line]. Available: http://www.iwea.com/index.cfm/page/windenergyfaqs?#q21
[67] Eirgrid and SONI, "All-Island Generation Capacity Statement 2012-2021," Eirgrid & System Operator for Northern Ireland,December 2011.
[68] New Energy, "2012 Small Wind Report (Summary)," World Wide Energy Association, on-line,2012,.
[69] *EN 50438 Requirements for the connection of micro-generators in parallel with public low-voltage distribution networks,* CENELEC, 2007.
[70] Huleihil M., "Maximum windmill efficiency in finite time " *J. Appl. Phys.,* vol. 105, 2009.
[71] WWEA. (2012 Small Wind World Report (Summary), 24/02/13). [on-line]. Available: http://www.wwindea.org/webimages/WWEA%20Small%20Wind%20World%20Report%20Summary%202012.pdf
[72] Mertens S., "Wind Energy in the Built Environment: Concentrator Effects of Buildings," PhD,, Technische Universiteit Delft, 2006.
[73] World Wind Energy Association. (2013, 18th January). *Wind Energy Technology: An Introduction* [on-line]. Available: http://www.wwindea.org/technology/ch01/estructura-en.htm
[74] Ragheb M. and Ragheb A. M., *Wind Turbines theory - The Betz Equation and Optimal Rotor Tip Speed Ratio,*, 2011.
[75] Wineur, "Urban Wind Turbines, Technology review, A companion text to the EU UWT Catalogue," 2005.
[76] Bahaj A. S., Myers L., and James P. A. B., "Urban energy generation: Influence of micro-wind turbine output on electricity consumption in buildings," *Energy and Buildings,* vol. 39, pp. 154-165, 2007.
[77] Mithraratne N., "Roof-top wind turbines for microgeneration in urban houses in New Zealand," *Energy and Buildings,* vol. 41, pp. 1013-1018, 2009.
[78] Staffell I., Baker P., Barton J., Bergman N., Blanchard R., Brandon N. P., Brett D. J. L., Hawkes A., Infield D., Jardine C., Kelly N., Leach M., Matian M., Peacock A. D., Sudtharalingam S., and Woodman B., "UK microgeneration. Part II: technology overviews," *Proceedings of the ICE - Energy,* vol. 163, pp. 143-165, 2010.
[79] Stankovic S., Campbell N., and Harries A., *Urban Wind Energy*: Earthscan LLC, 2009.
[80] Liserre M., Sauter T., and Hung J. Y., "Future Energy Systems: Integrating Renewable Energy Sources into the Smart Power Grid Through Industrial Electronics," *Industrial Electronics Magazine, IEEE,* vol. 4, pp. 18-37, 2010.
[81] Giordano V., Gangale F., Fulli G., and Sanchez Jiménez M., "Smart Grid projects in Europe: lessons learned and current developments," European Commission Joint Research Centre Institute for Energy,2011.
[82] Santacana E., Rackliffe G., Le T., and Xiaoming F., "Getting Smart," *Power and Energy Magazine, IEEE,* vol. 8, pp. 41-48, 2010.
[83] DeBlasio D. 5th May, 2013,). *Connecting Small-scale Renewables to the Smart Grid,* [on-line]. Available: http://www.elp.com/articles/powergrid_international/print/volume-15/issue-9/features/connecting-small-scale-renewables-to-the-smart-grid.html

[84] A. Gaviano, K. Weber, and C. Dirmeier, "Challenges and Integration of PV and Wind Energy Facilities from a Smart Grid Point of View," *Energy Procedia,* vol. 25, pp. 118-125, 2012.
[85] Hamad A. A. and Alsaad M., "Asoftware application for energy flow simulation of a grid connected ohotovoltaic systems," *Energy Conversion and Management,* vol. 51, pp. 1684-9, 2010.
[86] Southwest Wind Power, "Skystream 3.7 Specifications," ed: Southwest Wind Power, 2009.
[87] Wholesaler Solar, "Technical Specifications: Whisper 200," South West Windpower, Ed., ed: Sout, 2005.
[88] CEI, "Proven 2.5 Specifications," in *Cell Energy Ireland*, ed, 2012.
[89] Wind Power Programme. (2013, 21st January). [on-line]. Available: http://www.wind-power-program.com/small_turbines.htm
[90] Muljadi E., Pierce K., and Milgliore P., "Control Strategy for Variable Stall-Regulated Wind Turbine," presented at the American Controls Conference, Philadelphia, 1998.
[91] Marathon Electric Generators, "Test Report WC1901," ed, 1999.
[92] Glass A. and Levermore G., "Micro wind turbine performance under real weather conditions in urban environment," *Building Services Engineering Research and Technology,* vol. 32, pp. 245-262, 2011.
[93] BRE, "Micro-Wind Turbines in Urban Envioronments - An Assessment," Building Research Establishment2007.
[94] EST, "Domestic small-scale wind field trial report," Energy Savings Trust2009.
[95] Drew D. R., Barlow J. F., and Cockerill T. T., "Estimating the potential yield of small wind turbines in urban areas: A case study for Greater London, UK," *Journal of Wind Engineering and Industrial Aerodynamics,* vol. 115, pp. 104-111, 2013.
[96] "DIRECTIVE 2009/28/EC OF THE EUROPEAN PARLIAMENT AND OF THE COUNCIL on the promotion of the use of energy from renewable sources," ed, 2009.
[97] Environment Community and Local Government, " Building Regulations 2011 Technical Guidance Document L: Conservation of Fuel and Energy - Dwellings," 2011.
[98] ESBN Asset Management, "Microgeneration connection statistics,," K. Sunderland, Ed., ed, 2012.
[99] SEAI, "Status Report on Microgeneration in Ireland," Sustainable Energy Authority of Ireland,2011.
[100] EU, "Directive 2010/31/EU of the European Parliament and of the Council of 19 May 2010 on the energy performance of buildings," 2010.
[101] *BUILDING REGULATIONS (PART L AMENDMENT) REGULATIONS 2011*, 2011.
[102] DCENR, "National Renewable Energy Action Plan," Department of Communications, Energy and Natural Resources,2010.
[103] DECC, "National Reneweable Energy Acion Plan," Department of Energy & Climate Change,2010.
[104] DECC, "Government Response to Consultation Comprehensive Review Phase 2B: Tariffs for non-PV technologies and scheme administration issues," Department of Energy and Climate Change, Ed., ed, 2012.
[105] Allen S., Hammond G., and McManus M., "Energy analysis and environmental life cycle assessment of a micro-wind turbine," *Power and Energy Magazine, IEEE,* vol. 222, pp. 669-684, 2008.
[106] Crawford R. H., "Life cycle energy and greenhouse emissions analysis of wind turbines and effect of size on energy yield," *Renewable and Sustainable Energy Reviews,* pp. 2653-2660, 2009.
[107] Clancy M. and Scheer J., "Energy Forecasts for Ireland to 2020 2011 Report," The Energy Modelling Group, SEAI,2011.

[108] Power P. B., "The Impact of Small Scale Embedded Generation on the Operating Parameters of Distribution Netowrks," Department of Trade & Industry2003.
[109] Power P. B., "Cost and Benefits of Embedded Generation in Ireland," SEI 2004.
[110] Gross R., Leach M., and Bauen A., "Progress in renewable energy," *Environment International,* vol. 29, pp. 105-122, 2003.
[111] CER, "Arrangements for Micro generation (Decision & Responser) (CER-07-208)," in *CER-07-208*, ed, 2007.
[112] Hearne T. & O'Connor B., "ESB Networks Perspective on Microgeneration," in *The Role of Microgeneration in Ireland's Energy Future*, Dublin 2009.
[113] *Planning and Development Regulations,* Oireachtas Eireann S.I. No. 83 of 2007, 20007.
[114] Thomson M., "High-Density Micro-Generation in UK Distribution Networks," presented at the CREST, Department of Electronic and Electrical Engineering, Loughborough University, UK, 2008.
[115] Barker P.P. and De Mello R.W., "Determining the impact of distributed generation on power systems: Part 1 - Radial distribution systems," in *PES Summer Meeting, IEEE*, 2000, pp. 1645-1656.
[116] Vu Van T., Woyte A., Soens J., Driesen J., and Belmans R., "Impacts of Distributed Generation on Distribution System Power Quality," presented at the 7th International Conference: Electrical Power Quality and Utilisation, Cracow, Poland, 2003.
[117] Gerwent R. Van, "Distribution Generation and Renewables - Integration and interconnection," *LEONARDO Energy,* vol. 8.3, 2006.
[118] Bloem J., "Distribution Generation and Renewables - Integration and interconnection," *LEONARDO Energy,* vol. 8.3.1, 2007.
[119] Energy Saving Trust. (2013, 2nd June). *Green Deal* [on-line]. Available: http://www.energysavingtrust.org.uk/Take-action/Find-a-grant/Green-Deal-and-ECO#details
[120] Watson J., Sauter R., Bahaj B., James P., Myers L., and Wing R., "Domestic micro-generation: Economic, regulatory and policy issues for the UK," *Energy Policy,* vol. 36, pp. 3095-3106, 2008.
[121] DECC, "Microgeneration Government-Industry Contact Group," Department of Energy and Climate Change,2011.
[122] DECC. (2088, 17th February, 2013). *Microgeneration Certification Scheme (MCS)*. Available: http://www.microgenerationcertification.org/about-us/about-us
[123] Energy Savings Trust, "Potential for MicrogenerationStudy and Analysis," Department of Trade and Industry, London,2005.
[124] McDonald M., "System Integration of Additional Micro-generation," URN NUMBER 04/1664, 2004.
[125] Douglas J., Roscoe N., and Andrews S., "Future network architecture & 2014; power network, protection, control and market requirements for 2020," in *Smart-Grids for Distribution, 2008. IET-CIRED*, 2008, pp. 1-4.
[126] Sunderland K. and Conlon M. F., "The role of micro wind generation in Ireland's energy future," in *Universities Power Engineering Conference (UPEC), 2008.* , 2008, pp. 1-5.
[127] CER, "Arrangements for Micro Generation: Decision and Response to Comments Received," Commission for Energy Regulation CER/07/208, 2007.
[128] Richardson P. and Keane A., "Impact of high penetrations of micro-generation on low voltage distribution networks," presented at the 20th International Conference and Exhibition on Electricity Distribution, CIRED Prague, 2009.
[129] Hub, "Seeing the light:the impact of micro-generation on the way we use energy - Qualitative Research Findings," October 2005 2005.
[130] Claudy M. C., Michelsen C., O'Driscoll A., and Mullen M. R., "Consumer awareness in the adoption of microgeneration technologies: An empirical investigation in the

Republic of Ireland," *Renewable and Sustainable Energy Reviews,* vol. 14, pp. 2154-2160, 2010.
[131] Cipcigan L.M., Taylor P.C., and Trichakis P., "The Impact of Small Scale Wind Generators on LV Distribution System Voltage " presented at the ICCEP '07, 2007.
[132] Cipcigan L.M., Taylor P., and Toshihisa F., "Large Scale Aggregation Effects of Small Scale Wind Generators," presented at the International Conference on Electrical Engineering (ICEE), Okinawa, Japan, 2008.
[133] MEES, "Sustainable Energy: Renreables-based electricity & Smart Grid - Smart Economy," Middel East Economic Survey,2010.
[134] Z. Fan and C. S. Cheng, "A modified Newton method for radial distribution system power flow analysis," *Power Systems, IEEE Transactions on,* vol. 12, pp. 389-397, 1997.
[135] W. Xu, Salmon J. C., Koval D., and Liu Y., "An investigation on the explicit solution of power system load flow equations," in *Electrical and Computer Engineering, 1998. IEEE Canadian Conference on*, 1998, pp. 97-100 vol.1.
[136] Jasmon G. B. and Lee L. H. C. C., "Stability of loadflow techniques for distribution system voltage stability analysis," *Generation, Transmission and Distribution, IEE Proceedings C,* vol. 138, pp. 479-484, 1991.
[137] Stott B. and Alsac O., "Fast Decoupled Load Flow," *Power Apparatus and Systems, IEEE Transactions on,* vol. PAS-93, pp. 859-869, 1974.
[138] Das D., Nagi H. S., and Kothari D. P., "Novel Method for solving radial distribution networks," *IEE Proc. - Gener. Transm. Distrib, Vol. 141, No. 4, July 1994,* 1994.
[139] Baran M. and Wu F., "Optimal capacitor placement on radial distribution systems," *EEE Trans. Power Deliv,* vol. 4, pp. 725–734, 1989.
[140] Tinney W. F. and Hart C. E., "Power Flow Solution by Newton's Method," *Power Apparatus and Systems, IEEE Transactions on,* vol. PAS-86, pp. 1449-1460, 1967.
[141] Nagrath I.J., Kothari D.P., and Desai R. C., "Modern Power System Analysis," *IEEE Transactions on Systems, Man, and Cybernetics,* vol. 12, 1982.
[142] Markiewicz H. and Klajn A., "Voltage Disturbances: Standard EN 50160 - Voltage Characteristics in Public Distribution Systems," 2004.
[143] ESB Networks, "Distribution Code," ed. Ireland: ESB Networks, 2007.
[144] CER, "Commission's Response to Submissions Received on Consultation Paper CER/03/298 (CER/04/100," ed, 2004.
[145] RMDS. *Retail Market Design Service: Standard Load Profiles,* . Available: http://www.rmdservice.com/guidance/standard_load_profiles.htm
[146] Burton T., Sharpe D., Jenkins N., and Bossanyi. E., *Wind Energy Handbook*: John Wiley & Sons, 2001.
[147] Planning Portal. (2012, 10th May). *Wind Turbines - Planning Permission* [on-line]. Available: http://www.planningportal.gov.uk/permission/commonprojects/windturbines/
[148] Millward-Hopkins J. T., Tomlin A. S., Ma L., Ingham D. B., and Pourkashanian M., "Mapping the wind resource over UK cities," *Renewable Energy,* vol. 55, pp. 202-211, 2013.
[149] MacDonald R. W., "Modelling the mean velocity profile in the urban canopy layer," *Boundary-Layer Meteorology,* vol. 97, pp. 24-45, 2000.
[150] Fisher B.E.A., Joffre S., Kukkonen J., Piringer M., Rotach M., and Schatzmann M., "Meteorology Applied to Urban Air Pollution Problems. Final Report of COST Action 715," Demetra Ltd. Publishers2005.
[151] Manwell J.F., McGowan J., and Rogers A., *Wind Energy Explained: Theory, Design and Application*: Wiley, 2002.
[152] Spera D.A., *Wind Turbiner Technology: Fundamental Concepts in Wind Turbine Engineering*, 2nd ed.: ASME, 1994.

[153] Van der Hoven I., "Power Spectrum of Horizontal Wind Speed in the Frequency Range from 0.0007 to 900 Cycles Per Hour," *Journal of Meteorology,* vol. 14, pp. 160-164, 1956.
[154] IEC, "International Standard 61400-2. Wind Turbines - Part 2: Design requirements for small turbines," ed, 2006.
[155] Lubitz W. D., "Impact of ambient turbulence on performance of a small wind turbine," Linkoping, Sweden, 2011.
[156] Oke T. R., *Boundary Layer Climates*, 2nd ed.: Routledge, 1988.
[157] Heath M.A., Walshe J.D., and Watson S.J., "Estimating the potential yield of small building-mounted wind turbines," *Wind Energy,* vol. 10, pp. 271-287, 2007.
[158] Watson S., Infield D., and Harding M., "Predicting the Performance of Small Wind Turbines in the Roof-Top Urban Environment,," presented at the EWEC, Milan, 2007.
[159] Landberg L., Myllerup L., Rathmann O., Petersen E. L., Jørgensen B. H., Badger J., and Mortensen N. G., "Wind Resource Estimation - An Overview," *Wind Energy,* vol. 6, pp. 261-271, 2003.
[160] Best M., Brown A., Clark P., Hollis D., Middleton D., Rooney G., Thomson D., and Wilson C., "Small-scale wind energy Technical Report," Met Office2008.
[161] Walker S. L., "Building mounted wind turbines and their suitability for the urban scale—A review of methods of estimating urban wind resource," *Energy and Buildings,* vol. 43, pp. 1852-1862, 2011.
[162] Millward-Hopkins J. T., Tomlin A. S., Ma L., Ingham D., and Pourkashanian M., "The predictability of above roof wind resource in the urban roughness sublayer," *Wind Energy,* vol. 15, pp. 225-243, 2011.
[163] de Wit M. H., Stathopoulos T., and Wisse J. A., "Airport wind speeds used for the design in urban environments: the Eindhoven case," *Journal of Wind Engineering and Industrial Aerodynamics,* vol. 90, pp. 1289-1298, 2002.
[164] Pal Arya S., *Introduction to Micrometeorology*: Academic Press, 1988.
[165] Stull R. B., *An introduction to Boundary Layer Meteorology*: Kluwer Academic Publishers, 1988.
[166] Garratt J. R., *The Atmpspheric boundary layer*: Cambridge University Press, 1992.
[167] Grimmond C. S. B. and Oke T. R., "Aerodynamic properties of urban areas derived from analysis of surface form," *Journal of Applied Meteorology,* vol. 38, pp. 1262-1292 1999.
[168] Folken T., *Micrometeorology*: Springer, 2008.
[169] Bianchi F.D., H. Battista, and R. J. Mantz, *Wnd Turbine Control systems Principles, Modelling and Gain Scheduling*: Springer, 2007.
[170] Oke T.R., "Initial guidance to obtain representative meteorological observations at urban sites," 2006.
[171] Rotach M. W., "Profiles of turbulence statistics in and above an urban street canyon," *Atmospheric Environment,* vol. 29, pp. 1473-1486, 1995.
[172] Roth M., "Review of atmospheric turbulence over cities," *Q.J.R. Meteorol. Soc., ,* vol. 126, 2000.
[173] Cheng H. and Castro I., "Near Wall Flow over Urban-like Roughness," *Boundary-Layer Meteorology,* vol. 104, pp. 229-259, 2002/08/01 2002.
[174] Ricciardelli F. and Polimeno S., "Some characteristics of the wind flow in the lower Urban Boundary Layer," *Journal of Wind Engineering and Industrial Aerodynamics* vol. 94, pp. 815-832 2006.
[175] Wood C. R., Lacser A., Barlow J. F., Padhra A., Belcher S. E., Nemitz E., Helfter C., Famulari D., and Grimmond C. S. B., "Turbulent Flow at 190 m Height Above London During 2006–2008: A Climatology and the Applicability of Similarity Theory," *Boundary-Layer Meteorology,* vol. 137, pp. 77-96, 2010/10/01 2010.

[176] Metzger M., McKeoin B.J., and Holmes H., "The near neutral atmospheric surface layer: turbulence and non-stationarity," *Philosophical Transactions of the Royal Society A: Mathematical, Physical and Engineering Sciences,* vol. 365, pp. 859-876, 2007.
[177] Yersel M. and Gorble R., "Roughness effects on urban turbulence parameters," *Boundary Layer Meteorology,* vol. 37, pp. 271-284, 1986.
[178] Fernando H. J. S., Zajic D., Di Sabatino S. , Dimitrova R., Hedquist B., and Dallman A., "Flow. turbulence and pollutant dispersion in urban atmospheres," *PHYSICS OF FLUIDS,* vol. 22, 2010.
[179] Millward-Hopkins J. T., Tomlin A. S., Ma L., Ingham D., and Pourkashanian M. , "Estimating Aerodynamic Parameters of Urban-Like Surfaces with Heterogeneous Building Heights," *Boundary-Layer Meteorology,* vol. 141, pp. 443-465, 2011.
[180] Hagishima A., Tanimoto J., Nagayama K., and Meno S., "Aerodynamic parameters of regular arrays of rectangular blocks with various geometries," *Boundary-Layer Meteorology,* pp. 315–337, 2009.
[181] Jiang D.H., Jiang W.M., Liu H.N., and Sun J.N., "Systematic influence of different building spacing, height and layout on mean wind and turbulent characteristics within and over urban building arrays," *Wind & Struct,* vol. 11, pp. 275-289, 2008.
[182] Wierenga J., "Roughness-dependent geographical interpolation of surface wind speed averages," *Quarterly Journal of Royal Meteorological Society,* vol. 112, pp. 867-889, 1986.
[183] Weekes S.M. and Tomliln A.S., "Evaluation of a semi-emperical model for predicting the wind energy resource relevant to small wind turbines," *Renewable Energy,* vol. 50, pp. 280-288, 2012.
[184] Raupach M.R., "Simplified expressions for vegetation roughness length and zero-plane displacement as functions of canopy height and are index," *Boundary-Layer Meteorology,* vol. 71, 1994.
[185] MacDonald R.W., Griffiths R.F., and Hall D.J., "An improved method for the estimation of surface roughness of obstacle arrays - a comparative study of the land use and built form of 110 schemes," *Atmospheric Environment,* vol. 32, 1988.
[186] Rafailidas S., "Influence of building areal density and roof shape on the wind characteristics above a town," *Boundary-Layer Meteorology,* vol. 85, pp. 155-17, 1997.
[187] Sterwart I. and Oke T. R., "Newly Developed "Thermal Climate Zones" For Defining And Measureing Urban Heat Island Magnitude In The Canopy Layer," 2009.
[188] Sterwart I. and Oke T., "Newly Developed "Thermal Climate Zones" For Defining And Measureing Urban Heat Island Magnitude In The Canopy Layer," 2009.
[189] Rotach M.W., Vogt R., Bernhofer C., Bathvarova E., Christen A., Clappier A., Feddersen B., Gryning S.-E., MArtucci G., Mayer H., Mitec V., Oke T.R., Parlow E., Richner H., Roth M., Roulet Y.-A., Ruffieux D., Salmond J.A., Schatzmann M., and Voogt J.A., "BUBBLE - an Urbn Boundary Layer Meteorology," *Theoretical and Applied Climatology,* 2005.
[190] Mertens S., "The energy yield of roof mounted wind turbines," *Wind Engineering* vol. 27, pp. 507-518, 2003.
[191] ESDU, "Mean fluid forces and moments on rectangular prisms: surface mounted structures in turbulent shear flow," in *Engineering Sciences Data Item Number 800053*, ed: Engineering Sciences Data Unit, 1980.
[192] Raupach M.R., Thorn A.S., and Edwards I., "A Wind Tunnel Study of Turbulent Flow Close to Regulary Arrayed Rough Surfaces,," *Boundary-Layer Meteorology,* vol. 18,, pp. 373-397, 1980.
[193] Rotach M.W., "Simulation of urban-scale dispersion using a lagrangian stochastic dispersion model," *Boundary Layer Meteorology,* vol. 99, pp. 379-410, 2001.
[194] Bottema M., "Aerodynamic roughness parameters for homogeneous building groups," ed: Lab de. Mécanique des Fluides, Ecole Centrale de Nantes, 1995.

[195] Taylor P.A. and Lee R.J., "Simple guidelines for estimating wind speed variations due to small scale topgraphical features," *Climatoligical Bulletin,* vol. 18, 1984.
[196] American Meteorology Society. (2013, 17 Feb). *2nd Edition of the Glossary of Meteorology* [on-line]. Available: http://glossary.ametsoc.org/wiki/Main_Page
[197] M. Bottema, "Aerodynamic roughness parameters for homogeneous building groups," ed: Lab de. Mécanique des Fluides, Ecole Centrale de Nantes, 1995.
[198] Sunderland K. and Conlon M. F., "Estimating the yield of micro wind turbines in an urban environment: A methodology," in *United Power Engineering Conference (UPEC), 2010*, Cardiff, Wales, 2010.
[199] Google Earth. Locations of the Wind Observations Across Dublin City [Online].
[200] Campbell Scientific. (2011, *CSAT3 , 3-D Sonic Anemometer*. Available: http://www.campbellsci.com/csat3
[201] Keogh S., Mills G., and Fealy R., "The energy balance of the urban surface:Two locations in Dublin," presented at the Urban Climatology on Tropical and Sub-Tropical Regions 2011, The Chinese University of Hong Kong, Hong Kong. , 2011.
[202] Davis. (2011, *WeatherLinkIP™*. Available: http://www.weatherlink.com/
[203] Justus C. G., Hargraves W. R., and Yalcin A., "Nationwide Assessment of Potential Output from Wind-Powered Generators," *Journal of Applied Meteorology,* vol. 15, pp. 673-678, 1976/07/01 1976.
[204] Seguro J. V. and Lambert T. W., "Modern estimation of the parameters of the Weibull wind speed distribution for wind energy analysis," *Journal of Wind Engineering and Industrial Aerodynamics,* vol. 85, pp. 75-84, 2000.
[205] Carta J. A., Ramírez P., and Velázquez S., "A review of wind speed probability distributions used in wind energy analysis: Case studies in the Canary Islands," *Renewable and Sustainable Energy Reviews,* vol. 13, pp. 933-955, 2009.
[206] Tsang-Jung C., Yu-Ting W, Hua-Yi H., C.-R. C., and Chun-Min L., "Assessment of wind characteristics and wind turbine characteristics in Taiwan," *Renewable Energy,* vol. 28, pp. 851-871, 2003.
[207] Jamil M., Parsa S., and Majidi M., "Wind power statistics and an evaluation of wind energy density," *Renewable Energy,* vol. 6, pp. 623-628, 1995.
[208] Celik A. N., "A statistical analysis of wind power density based on the Weibull and Rayleigh models at the southern region of Turkey," *Renewable Energy,* vol. 29, pp. 593-604, 2004.
[209] Sunderland K. M., Mills G., and Conlon M. F, "Estimating the wind resource in an urban area: A case study of micro-wind generation potential in Dublin, Ireland," *Journal of Wind Engineering and Industrial Aerodynamics,* vol. 118, pp. 44-53, 2013.
[210] WES. (10th October 2012,). *WES(5) Tulipo,* [on-line]. Available: http://www.cellenergy.ie/pdf/WES5_Tulipo_brochure_ds1.pdf
[211] SECO. (2012, 27th July). *Small Wind Systems* [on-line]. Available: http://www.seco.cpa.state.tx.us/re_wind_smallwind.htm
[212] Sunderland K., Woolmington T., Blackledge J., and Conlon M., "Small wind turbines in turbulent (urban) environments: A consideration of normal and Weibull distributions for power prediction," *Journal of Wind Engineering and Industrial Aerodynamics,* vol. 121, pp. 70-81, 2013.
[213] Pope S. B., *Turbulent Flows*: Cambridge University Press, 2000.
[214] Rosen A. and Sheinman Y., "The average output power of a wind turbine in a turbulent wind," *Journal of Wind Engineering and Industrial Aerodynamics,* vol. 51, pp. 287-302, 1994.
[215] Langreder W., Kaiser K., Hohlen H., and Hojstrup J., "Turbulence Correction for Power Curves," presented at the EWEC, London, 2004.

[216] Tindal A., Johnson C., LeBlanc M., Harman K., Rareshide E., Graves A-M., and America G. H., "Site-specific adjustments to wind turbine power curves," presented at the AWEA Wind Power Conference, Houston, 2008.
[217] Cochran B., "The Influence of Atmospheric Turbulence on the Kinetic Energy Available During Small Wind Turbine Power Performance Testing,," IEA Expert Meeting on: Power Performance of Small Wind Turbines Not Connected to the Grid,2002.
[218] Wagner R., Courtney S. M., Torben L. J., and Paulsen S. U., "Simulation of shear and turbulence impact on wind turbine power performance,," Riso DTU (National Laboratory for Sustainable Energy),2010.
[219] Carpman .N., "Turbulence Intensity in Complex Environments and its Influence on Small Wind Turbines," Dept. of Earth Sciences, Uppsalla University, Uppsalla, 2010.
[220] Albers A., Hinsch C., Klug H., and Westermann D. , "Einfluss verschiedener meteorologischer Parameter auf das Leistungsverhalten grosser Windenergieanlagen, ," presented at the Tagungsband Deutsche Windenergiekerenz,, Wilhwlmshaven, 1996.
[221] Sheinman Y. and Rosen A., "A dynamic model of the influence of turbulence on the ppwer output of a wind turbine," *Wind Engineering & Industrial Aerodynamics,* vol. 39, pp. 329-341, 1992.
[222] Albers A., "Turbulence Normalisation of Wind Turbine Power Curve Measurements," Deutsche WindGuard Consulting GmbH,2009.
[223] Archer C. L. and Jacobson M. Z., "Spatial and temporal distributions of U.S. winds and wind power at 80 m derived from measurements," *Journal of Geophysical Research,* vol. 108, p. 4289, 2003.
[224] Blackledge J., Coyle E., McCoy N., Kearney D., Sunderland K., and Woolmington T., "Analysis of Wind Velocity and the Quantification of Wind Turbulence in Rural and Urban Environments using the L´evy Index and Fractal Dimension," *ISAST Transactions on Computers and Intelligent Systems,* vol. 4, 2012.
[225] Benato R., Paolucci A., and Turri R., "Power flow solution by a complex admittance matrix method," *European Transactions on Electrical Power,* vol. 11, pp. 181-188, 2007.
[226] ESBNetworks, "Distribution Network: Parameters and Data," K. Sunderland, Ed., ed: ESB Networks, 2011.
[227] ESBNetworks. (2007, *Distribution Code*. Available: http://www.esb.ie/esbnetworks/en/downloads/Distribution-Code.pdf
[228] Carson J.R., "Wave propagation in overhead Wires with ground return," *Bell System Tech.,* 1927.
[229] Anderson P. M., *Analysis of Faulted Power Systems*: Wiley-IEEE Press; 1 edition June 26, 1995.
[230] Kersting W. H. and Green R. K., "The application of Carson's equation to the steady-state analysis of distribution feeders," in *Power Systems Conference and Exposition (PSCE), 2011 IEEE/PES*, 2011, pp. 1-6.
[231] Bayliss C. and Hardy B., *Transmission and Distributed Electrical Engineering*, 4 ed.: Elsevier/Newnes, 2011.
[232] Kersting W.H., *Distribution System Modelling and Analysis*: CRC Press, 2002.
[233] Albano M., Turri R., Dessanti R., Haddad A., Griggiths H., and Howat B., "Computation of the Electromagnetic Coupling of Parallel Untransposed Power Lines," in *Universities Power Engineering Conference*, 2006, pp. 303-307.
[234] Ciric R. M., Feltrin A. P., and Ochoa L. F., "Power flow in four-wire distribution networks-general approach," *Power Systems, IEEE Transactions on,* vol. 18, pp. 1283-1290, 2003.

[235] Ciric R. M., Ochoa L. F., and Padilha A., "Power flow in distribution networks with earth return," *International Journal of Electrical Power & Energy Systems,* vol. 26, pp. 373-380, 2004.
[236] Sunderland K. M. and Conlon M. F., "4-Wire load flow analysis of a representative urban network incoprating SSEG," in *Universities Power Engineering Conference (UPEC), 2012 47th International*, 2012, pp. 1-6.
[237] N. Song, F. Xiao-Peng, L. Peng, G. Fei, D. Cheng-Di, Y. Hao, and W. Cheng-Shan, "Analysis of the impact of DG on distribution network reconfiguration using OpenDSS," in *Innovative Smart Grid Technologies - Asia (ISGT Asia), 2012 IEEE*, 2012, pp. 1-5.
[238] D. Montenegro, M. Hernandez, and G. A. Ramos, "Real time OpenDSS framework for distribution systems simulation and analysis," in *Transmission and Distribution: Latin America Conference and Exposition (T&D-LA), 2012 Sixth IEEE/PES*, 2012, pp. 1-5.
[239] Sunderland K., Coppo M., Conlon M.F., and Turri R., "Application of a correction current Injection load flow algorithm to an unbalanced 4-wire distribution network incorporating TNC-S earthing," in *United Power Engineering Conference (UPEC), 2013*, Dublin, Ireland, 2013.
[240] CEB, "Initial Environmental Examination: Rural Electrification Expansion and Distribution Improvement, Sustainable Power Sector Support Project," Ceylon Electricity Board,2010.
[241] ESBN, "Micro-generation statistics, year ending 2011," K. Sunderland, Ed., ed, 2012.
[242] CEB. (2010, 22nd Mach, 2012,). *Statistical Digest* [on-line]. Available: http://www.ceb.ik/sub/publications/statistical.aspx
[243] CEB. (2012 29th July). *Bill Calculator* [on-line]. Available: http://www.ceb.lk/sub/business/billcalculator.aspx
[244] Verbruggen A. and Lauber V., "Basic concepts for designing renewable electricity support aiming at a full-scale transition by 2050," *Energy Policy,* vol. 37, pp. 5732-5743, 2009.
[245] Li Z., Boyle F., and Reynolds A., "Domestic application of micro wind turbines in Ireland: Investigation of their economic viability," *Renewable Energy,* vol. 41, pp. 64-74, 2012.
[246] Elliott D., Schwartz M., Scott G., Haymes S., Heimiller D., and George R. , "Wind Energy Resource Atlas of Sri Lanka and the Maldives," ed: National Renewable Energy Laboratory, USA,, 2003.
[247] Narayana M., Putrus G., Jovanovic M., and Lung P. S., "Predictive control of wind turbines by considering wind speed forecasting techniques," presented at the Universities Power Engineering Conference (UPEC), Universitiy of Strathclyde, Glasgow, 2009.
[248] Ayompe L.M. and D. A., "Feed-in tariff design for domestic scale grid-connected PV systems using high resolution household electricity demand data," *Energy Policy,* vol. 61, pp. 619-627, 2013.
[249] Ofgem. (2013, 21-01). *Feed-in Tariff scheme: Tariff Table 1 April 2013 to 31 March 2014 Non-PV Only* [on-line]. Available: https://www.ofgem.gov.uk/publications-and-updates/feed-tariff-scheme-tariff-table-1-april-2013-31-march-2014-non-pv-only
[250] Ofgem. (2014, 21-01). *Feed-in Tariff Scheme: Tariff Table 1 January 2014 - 31 March 2014 PV Only* [on-line]. Available: https://www.ofgem.gov.uk/publications-and-updates/feed-tariff-scheme-tariff-table-1-january-2014-31-march-2014-pv-only
[251] Hocaoglu F. O., Gerek O. N., and Kurban M., "The Effect of Markov Chain State Size for Synthetic Wind Speed Generation," in *Probabilistic Methods Applied to Power Systems, 2008. PMAPS '08. Proceedings of the 10th International Conference on*, 2008, pp. 1-4.
[252] Sahin A. D. and Sen Z., "First-order Markov chain approach to wind speed modelling," *Journal of Wind Engineering and Industrial Aerodynamics,* vol. 89, pp. 263-269, 2001.

[253] Srikanthan R. and McMahon T. A., "Stochastic generation of rainfall and evaporation data for Australia : user manual for computer programs " University of Melbourne, Dept. of Civil Engineering,, Melbourne1984.
[254] Thyer M. and Kuczera G., "Modeling long-term persistence in hydroclimatic time series using a hidden state Markov Model," *Water Resources Research,* vol. 36, pp. 3301-3310, 1999.
[255] Gringorten I. L., "A Stochastic Model of the Frequency and Duration of Weather Events," *Journal of Applied Meteorology,* vol. 5, pp. 606-624, 1966.
[256] Cheng E. D. H., "Wind data generator: A knowledge-based expert system," *Journal of Wind Engineering and Industrial Aerodynamics,* vol. 38, pp. 101-108.
[257] Jones D. I. and Lorenz M. H., "An application of a Markov chain noise model to wind generator simulation," *Mathematics and Computers in Simulation,* vol. 28, pp. 391-402, 1986.
[258] Kaminsky F. C., Kirchhoff R. H., Syu C. Y., and Manwell J. F., "A Comparison of Alternative Approaches for the Synthetic Generation of a Wind Speed Time Series," *Journal of Solar Energy Engineering,* vol. 113, pp. 280-289, 1991.
[259] Brokish K. and Kirtley J., "Pitfalls of modeling wind power using Markov chains," in *Power Systems Conference and Exposition, 2009. PSCE '09. IEEE/PES*, 2009, pp. 1-6.
[260] D.P. Bersekas and N. Tsitsiklis, *Introduction to Probability*: Belmont, Massacheusetts: Athena Scientific, 2002.
[261] Aksoy H., Fuat Toprak Z., Aytek A., and Erdem Ünal N., "Stochastic generation of hourly mean wind speed data," *Renewable Energy,* vol. 29, pp. 2111-2131, 2004.
[262] Shamshad A., Bawadi M. A., Wan Hussin W. M. A., Majid T. A., and Sanusi S. A. M., "First and second order Markov chain models for synthetic generation of wind speed time series," *Energy,* vol. 30, pp. 693-708, 2005.
[263] Dukes M. D. G. and P. J. P., "Estimation oof Extreme Wind Speeds with Very Long Return Periods," *Journal of Applied Meteorology,* vol. 34, 1950.

APPENDICES

A1: The Derivation of Bus Voltage: DISTFLOW approach

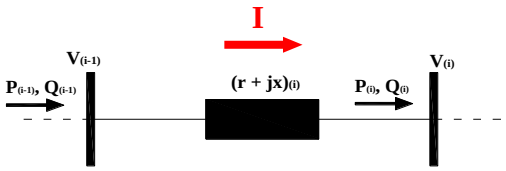

Figure A1 1 Radial Feeder in terms of sending and receiving buses

With respect to A1.1, the current in the radial section can be described in terms of (A1 1) and (A1 2)

$$|I| = \frac{\sqrt{P_{(i)}^2 + Q_{(i)}^2}}{V_{(i)}} \Rightarrow \frac{P_{(i)}^2 + Q_{(i)}^2}{V_{(i)}^2} = |I|^2$$

(A1 1)

$$|I| = \frac{\sqrt{P_{(i-1)}^{\ 2} + Q_{(i-1)}^{\ 2}}}{V_{(i-1)}} \Rightarrow \frac{P_{(i-1)}^2 + Q_{(i-1)}^2}{V_{(i-1)}^2} = |I|^2$$

(A1 2)

The active and reactive powers can be considered in (A1 3) and (A1 4) respectively,

$$P_{(i)} = P_{(i-1)} - P_{Loss} = P_{(i-1)} - |I|^2 . r_{(i-1)}$$

$$\Rightarrow\ P_{(i)} = P_{(i-1)} - \left\{ \frac{P_{(i)}^2 + Q_{(i)}^2}{V_{(i)}^2} \right\} r_{(i-1)}$$

(A1 3)

$$Q_{(i)} = Q_{(i-1)} - Q_{Loss} = Q_{(i-1)} - |I|^2 . x_{(i-1)}$$

$$\Rightarrow Q_{(i)} = Q_{(i-1)} - \left\{ \frac{P_{(i)}^2 + Q_{(i)}^2}{V_{(i)}^2} \right\} \times x_{(i-1)}$$

(A1 4)

Describing (A1 2) in terms of (A1 3) and (A1 4) respectively

$$|I|^2 = \frac{\left(P_{(i)} + \left\{ \frac{P_{(i)}^2 + Q_{(i)}^2}{V_{(i)}^2} \right\} r_{(i-1)} \right)^2 + \left(Q_{(i)} + \left\{ \frac{P_{(i)}^2 + Q_{(i)}^2}{V_{(i)}^2} \right\} x_{(i-1)} \right)^2}{V_{(i-1)}^2}$$

(A1 5)

Describing (A1 1) in terms of (A1 5),

$$\frac{P_{(i)}^2 + Q_{(i)}^2}{V_{(i)}^2} = \frac{\left[\begin{array}{l} P_{(i)}{}^2 + \left\{ \frac{P_{(i)}^2 + Q_{(i)}^2}{V_{(i)}{}^2} \right\}^2 r_{(i-1)}{}^2 + 2.P_{(i)}.\left\{ \frac{P_{(i)}^2 + Q_{(i)}^2}{V_{(i)}{}^2} \right\} r_{(i-1)} \\ \qquad + Q_{(i)}^2 + 2.Q_{(i)}.\left\{ \frac{P_{(i)}^2 + Q_{(i)}^2}{V_{(i)}{}^2} \right\} x_{(i-1)} + \left\{ \frac{P_{(i)}^2 + Q_{(i)}^2}{V_{(i)}{}^2} \right\}^2 x_{(i-1)}{}^2 \end{array} \right]}{V_{(i-1)}^2}$$

$$\frac{P_{(i)}^2 + Q_{(i)}^2}{V_{(i)}{}^2} = \frac{P_{(i)}^2 + Q_{(i)}^2}{V_{(i-1)}^2} + \left[\frac{\left\{ \frac{P_{(i)}^2 + Q_{(i)}^2}{V_{(i)}^2} \right\}^2 r_{(i-1)}{}^2 + 2.P_{(i)}.\left\{ \frac{P_{(i)}^2 + Q_{(i)}^2}{V_{(i)}^2} \right\} r_{(i-1)} + Q_{(i)}^2 + 2.Q_{(i)}.\left\{ \frac{P_{(i)}^2 + Q_{(i)}^2}{V_{(i)}^2} \right\} x_{(i-1)} + \left\{ \frac{P_{(i-1)}^2 + Q_{(i)}^2}{V_{(i)}^2} \right\}^2 x_{(i-1)}{}^2}{V_{(i-1)}^2} \right]$$

$$V_{(i-1)}{}^2 = \frac{P_{(i)}^2 + Q_{(i)}^2}{\frac{P_{(i)}^2 + Q_{(i)}^2}{V_{(i)}^2}} + \left[\frac{\left\{ \frac{P_{(i-1)}^2 + Q_{(i)}^2}{V_{(i)}^2} \right\}^2 r_{(i-1)}{}^2 + 2.P_{(i)}.\left\{ \frac{P_{(i-1)}^2 + Q_{(i)}^2}{V_{(i)}^2} \right\} r_{(i-1)} + Q_{(i-1)}^2 + 2.Q_{(i)}.\left\{ \frac{P_{(i-1)}^2 + Q_{(i)}^2}{V_{(i)}^2} \right\} x_{(i-1)} + \left\{ \frac{P_{(i-1)}^2 + Q_{(i)}^2}{V_{(i)}^2} \right\}^2 x_{(i-1)}{}^2}{\frac{P_{(i)}^2 + Q_{(i)}^2}{V_{(i)}^2}} \right]$$

$$\Rightarrow \qquad V_{(i-1)}{}^2 = V_{(i)}{}^2 + 2(P_{(i)}.r_{(i-1)} + Q_{(i)}.x_{(i-1)}) + \left\{\frac{P_{(i)}{}^2 + Q_{(i)}{}^2}{V_{(i)}{}^2}\right\}.(r_{(i-1)}{}^2 + .x_{(i-1)}{}^2)$$

$$V_{(i)}{}^4 + 2.V_{(i)}{}^2.\left(P_{(i)}.r_{(i-1)} + Q_{(i)}.x_{(i-1)}\right) + \left(P_{(i)}{}^2 + Q_{(i)}{}^2\right)\left(r_{(i-1)}{}^2 + .x_{(i-1)}{}^2\right) - V_{(i-1)}{}^2.V_{(i)}{}^2 = 0$$

$$V_{(i)}{}^4 + V_{(i)}{}^2\left\{2.\left(P_{(i)}.r_{(i-1)} + Q_{(i)}.x_{(i-1)}\right) - V_{(i-1)}{}^2\right\} + \left(P_{(i)}{}^2 + Q_{(i)}{}^2\right)\left(r_{(i-1)}{}^2 + .x_{(i-1)}{}^2\right) = 0$$

(A1 6)

Describing (A1 6) in terms of a quadratic:

$$x = \frac{-b \pm \sqrt{b^2 - 4.a.c}}{2.a}$$

Therefore:

$$V_{(i)}{}^2 = \left\{\frac{-\left\{2.\left(P_{(i)}.r_{(i-1)} + Q_{(i)}.x_{(i-1)}\right) - V_{(i-1)}{}^2\right\} \pm \sqrt{\left\{2.\left(P_{(i)}.r_{(i-1)} + Q_{(i)}.x_{(i-1)}\right) - V_{(i-1)}{}^2\right\}^2 - 4.\left(P_{(i)}{}^2 + Q_{(i)}{}^2\right)\left(r_{(i-1)}{}^2 + .x_{(i-1)}{}^2\right)}}{2}\right\}$$

$$V_{(i)} = \sqrt{\frac{-\left\{2.\left(P_{(i)}.r_{(i-1)} + Q_{(i)}.x_{(i-1)}\right) - V_{(i-1)}{}^2\right\}}{2} \pm \frac{\sqrt{\left\{2.\left(P_{(i)}.r_{(i-1)} + Q_{(i)}.x_{(i-1)}\right) - V_{(i-1)}{}^2\right\}^2 - 4.\left(P_{(i)}{}^2 + Q_{(i)}{}^2\right)\left(r_{(i-1)}{}^2 + .x_{(i-1)}{}^2\right)}}{2}}$$

(A1 7)

A2: Representative Distribution Network Configuration [109]

The Distribution Network model [109] is comprised of two 38/0.433kV transformers fed from a 500MVA source. The transformers are connected in parallel feeding a network containing five distribution feeders (10kV). One of these feeders is modeled in detail. The feeder length is 3km with half its length supplied via 185mm^2 (10kV) PICAS cable and the other half via 95mm^2 (10kV) PICAS cable. This detailed feeder contains ten substations (400kVA; 10/0.43kV @ 50% Load Factor) each supplying 312 consumers via four LV, 3-phase lines (0.4kV). One of these LV lines is also detailed. The LV lines are 300m in length; half of which is through 195mm^2 (415V) CNE cable and the remaining through 95mm^2 (415V) CNE cable. There is a further 30m of 35mm^2 CNE cable to each customer. With respect to consumer load, each consumer is represented as having an ADMD of 1.28kVA at unity power factor (minimum loading being 0.16kVA). The associated consumer microgeneration capacity is modeled as having a capacity of 2.2kVA at 0.95 power factor. The model developed in this section considers balanced load conditions. In this context, the generation is connected across the three-phases accordingly. The primary goal in this regard is to investigate voltage rise scenarios from a network integration perspective. Figure A2 1 illustrates the constituent components of the representative distribution network model with the highlighted sections (A→E) explained thereafter.

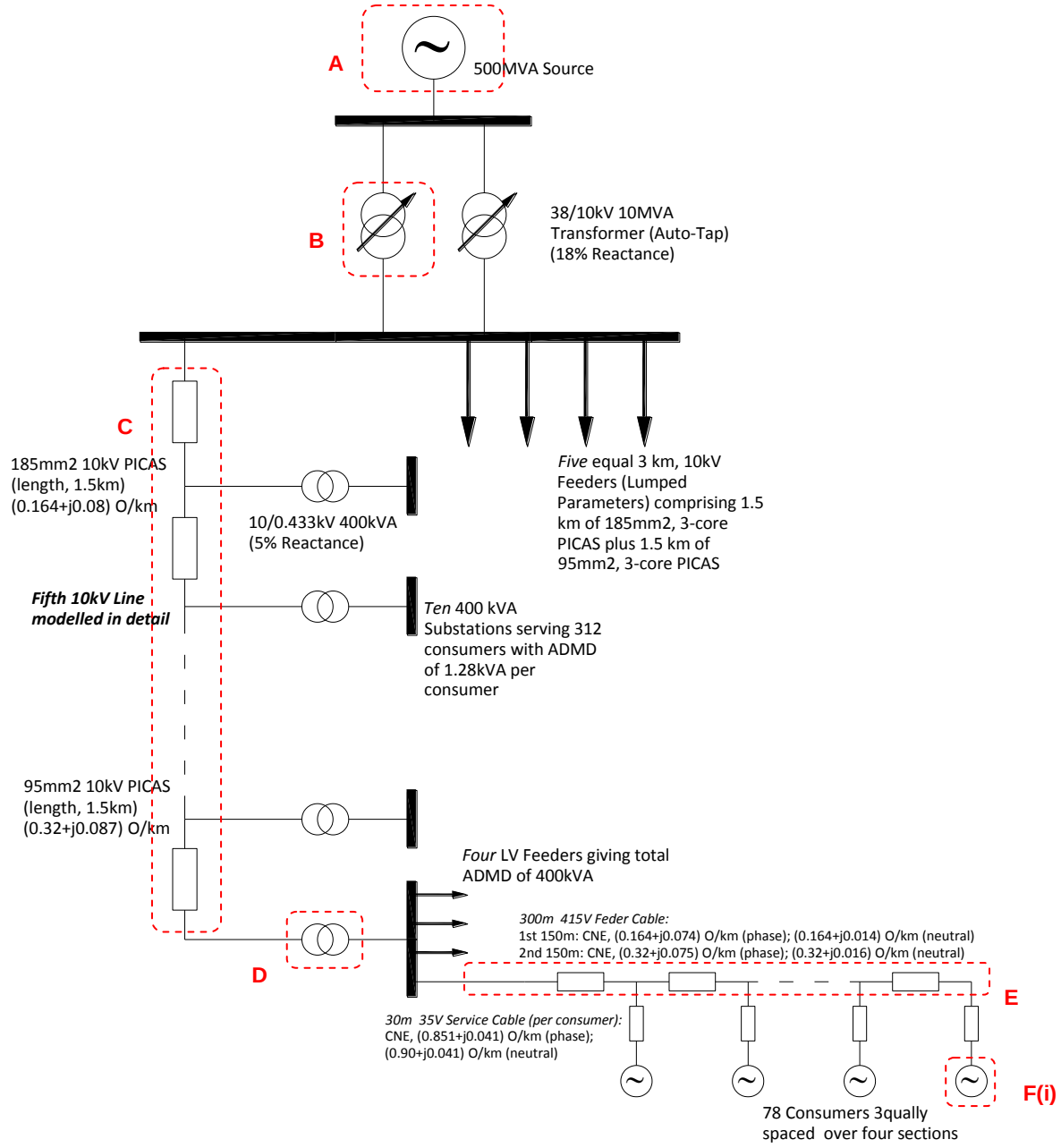

Figure A2 1 38/10/0.4kV Power System Model (Stage 1) [109]

A: ***Source;*** 2 no. 500MVA, 38kV source has an equivalent impedance of (0.003+j 2.888)Ω

B: ***Distribution Transformers;***

- 38/10.5kV
- Impedance of 18% (X/R of 15)

C: ***10kV Detailed Feeder Circuit***

- 4 no. 10kV feeders
- Each feeder supplies 10no.400kVA substations (ADMD of 50%)
- 1.5km of 185mm^2 PICAS Cable (0.164+j0.08)Ω/km
- 1.5km of 95mm^2 PICAS Cable (0.32+j0.087)Ω/km

D: ***10/0.433 Substation***

- 10no. 400kVA substations (ADMD of 50%)
- Transformer
  - 5% impedance
  - X/R Ratio of 15
  - Off-load ratio of 10/0.433kV
- Each substation supplies 312 consumers via four feeder cables
- Customers are supplied evenly along the LV feeders.

E: ***400V Detailed Feeder***

- 4 no. 400V feeders
- Each feeder facilitates 76 customers
- 150m of185mm^2 PICAS Cable (0.164+j0.074)Ω/km for the phase conductors
- 150m of 95mm^2 PICAS Cable (0.32+j0.075)Ω/km
- 78 customers per phase distributed evenly along each of the 300m feeder lines

F(i): ***Consumer connection***

- Feeder Cable to consumer is via 30m of 35mm2 (0.851+j0.090)Ω/km[15]
- The customer load/generator connection is developed from two perspectives:

  <u>*Stage 1:*</u> Static load/gen connection based on a range of load/gen ratios for specific load and capacity ratings (as defined in [108, 109] :ADMD of 1.28kVA, unity pf
  - Minimum Demand of 0.16kVA, unity pf
  - Micro generator, rating (generic) of 1.1 @0.95pf

  <u>*Stage 2:*</u> Hourly Consumer load [145] and Wind Speed observations (Dublin Airport, 2008) are employed to investigate network voltage reaction.

[15] The customer connection cabling modelled in [97,98] is with respect to a single phase CNE wiring system where impedances for both phase and neutral conductors are utilised. For the purpose of modelling balanced loads, the phase conductor impedance was utilised.

A3: Representative (Irish) Network Line Impedance Values (pu)

The line impedances were transferred into per-unit values based on the line voltages to which the lines are connected. Table A3 1 details the allocation of line/transformer impedances between network buses as per-unit values.

Table A3 1 Representative Distribution Network Line PU-Impedance

	kV	Connection Type	From	To	R (pu)	jX (pu)
Z_{base} = 1444	**38**	***Source***	1	2	0.000002	0.002000
Z_{base} = 100	**10**	***T: 38/10.5kV***	2	3	0.000662	0.009923
Z_{base} = 0.16	**0.4**	***Line***	3	4	0.000492	0.000240
		Line	4	5	0.000492	0.000240
		Line	5	6	0.000492	0.000240
		Line	6	7	0.000492	0.000240
		Line	7	8	0.000492	0.000240
		Line	8	9	0.000960	0.000261
		Line	9	10	0.000960	0.000261
		Line	10	11	0.000960	0.000261
		Line	11	12	0.000960	0.000261
		Line	12	13	0.000960	0.000261
		T: 38/10.5kV	13	14	0.000016	0.000234
		Line	14	15	0.030750	0.013875
		Line	15	16	0.030750	0.013875
		Line	16	17	0.030750	0.013875
		Line	17	18	0.030750	0.013875
		Line	18	19	0.030750	0.013875
		Line	19	20	0.060000	0.014063
		Line	20	21	0.060000	0.014063
		Line	21	22	0.060000	0.014063
		Line	22	23	0.060000	0.014063
		Line	23	24	0.060000	0.014063
		T: 38/10.5kV	4	25	0.000016	0.000234
		T: 38/10.5kV	5	26	0.000016	0.000234
		T: 38/10.5kV	6	27	0.000016	0.000234
		T: 38/10.5kV	7	28	0.000016	0.000234
		T: 38/10.5kV	8	29	0.000016	0.000234
		T: 38/10.5kV	9	30	0.000016	0.000234
		T: 38/10.5kV	10	31	0.000016	0.000234
		T: 38/10.5kV	11	32	0.000016	0.000234
		T: 38/10.5kV	12	33	0.000016	0.000234
		Consumer Connection	15	34	0.159563	0.007688
		Consumer Connection	16	35	0.159563	0.007688
		Consumer Connection	17	36	0.159563	0.007688
		Consumer Connection	18	37	0.159563	0.007688
		Consumer Connection	19	38	0.159563	0.007688
		Consumer Connection	20	39	0.159563	0.007688
		Consumer Connection	21	40	0.159563	0.007688
		Consumer Connection	22	41	0.159563	0.007688
		Consumer Connection	23	42	0.159563	0.007688
		Consumer Connection	24	43	0.159563	0.007688

A4: Network Transformer Impedances

The transformer impedances were derived in a similar fashion to the line impedances:

- ***38/10.5kV (Bus 2-3):***

HV Side, kV	38
LV Side, kV	10.5
Impedance, %	18
Rating, MVA	10
X/R Ratio	15

$$X : Z_{\%} \times \left\{ \frac{kV^2}{MVA_{Trafo}} \right\} = 0.18 \times \left\{ \frac{10.5^2}{10} \right\} = 1.9845\Omega$$

$$R : X / R \; ratio is 15 \;\therefore R = \frac{1.9845}{15} = 0.1323\Omega$$

There are two of these transformers connected in parallel feeding the system. Therefore the net impedance is given by:

$$Z_{Tot} : \left\{ \frac{Z_{T1} \times Z_{T1}}{Z_{T1} + Z_{T1}} \right\} = \left\{ \frac{(0.1323 + j1.9845) \times (0.1323 + j1.9845)}{(0.1323 + j1.9845) + (0.1323 + j1.9845)} \right\} = 0.06615 + j0.99225\Omega$$

Converting this to a per-unit value:

$$Z_{T_{pu}} : X_{pu} = \frac{X}{Z_{Base}} = \frac{0.99225}{\left\{ 10kV^2 / 1MVA \right\}} = 0.009923\, pu$$

$$R_{pu} = \frac{R}{Z_{Base}} = 0.000662\, pu$$

- ***10/0.433kV:***

HV Side, kV	10
LV Side, kV	0.433
Impedance, %	5
Rating, MVA	0.4
X/R Ratio	15

$$X : Z_{\%} \times \left\{ \frac{kV^2}{MVA_{Trafo}} \right\} = 0.05 \times \left\{ \frac{0.433^2}{0.4} \right\} = 0.0234\Omega$$

$$R : X / R \; ratio is 15 \;\therefore R = \frac{0.0234}{15} = 0.0016\Omega$$

Converting to a per-unit value:

$$Z_{T_{pu}} : X_{pu} = \frac{X}{Z_{Base}} = \frac{0.0234}{\left\{10kV^2 \diagup 1MVA\right\}} = 0.000234\ pu$$

$$R_{pu} = \frac{R}{Z_{Base}} = 0.000016\ pu$$

A5: Network Loading (Example): Max Demand

System Base (kVA)	1000

Bus no.	P_{Load}	P_{Gen}	P_{Net}	Q_{Load}	Q_{Gen}	Q_{Net}	P_{Net}	Q_{Gen}
1							0.0000	0.0000
2							0.0000	0.0000
3	2.4960	32.6040	-30.1080	0.0000	10.7164	-10.7164	-30.1080	-10.7164
4							0.0000	0.0000
5							0.0000	0.0000
6							0.0000	0.0000
7							0.0000	0.0000
8							0.0000	0.0000
9							0.0000	0.0000
10							0.0000	0.0000
11							0.0000	0.0000
12							0.0000	0.0000
13							0.0000	0.0000
14	0.4992	6.5208	-6.0216	0.0000	2.1433	-2.1433	-6.0216	-2.1433
15							0.0000	0.0000
16							0.0000	0.0000
17							0.0000	0.0000
18							0.0000	0.0000
19							0.0000	0.0000
20							0.0000	0.0000
21							0.0000	0.0000
22							0.0000	0.0000
23							0.0000	0.0000
24							0.0000	0.0000
25	0.0499	0.6521	-0.6022	0.0000	0.2143	-0.2143	-0.6022	-0.2143
26	0.0499	0.6521	-0.6022	0.0000	0.2143	-0.2143	-0.6022	-0.2143
27	0.0499	0.6521	-0.6022	0.0000	0.2143	-0.2143	-0.6022	-0.2143
28	0.0499	0.6521	-0.6022	0.0000	0.2143	-0.2143	-0.6022	-0.2143
29	0.0499	0.6521	-0.6022	0.0000	0.2143	-0.2143	-0.6022	-0.2143
30	0.0499	0.6521	-0.6022	0.0000	0.2143	-0.2143	-0.6022	-0.2143
31	0.0499	0.6521	-0.6022	0.0000	0.2143	-0.2143	-0.6022	-0.2143
32	0.0499	0.6521	-0.6022	0.0000	0.2143	-0.2143	-0.6022	-0.2143
33	0.0499	0.6521	-0.6022	0.0000	0.2143	-0.2143	-0.6022	-0.2143
34	0.0010	0.0125	-0.0116	0.0000	0.0041	-0.0041	-0.0116	-0.0041
35	0.0010	0.0125	-0.0116	0.0000	0.0041	-0.0041	-0.0116	-0.0041
36	0.0010	0.0125	-0.0116	0.0000	0.0041	-0.0041	-0.0116	-0.0041
37	0.0010	0.0125	-0.0116	0.0000	0.0041	-0.0041	-0.0116	-0.0041
38	0.0014	0.0188	-0.0174	0.0000	0.0062	-0.0062	-0.0174	-0.0062
39	0.0014	0.0188	-0.0174	0.0000	0.0062	-0.0062	-0.0174	-0.0062
40	0.0014	0.0188	-0.0174	0.0000	0.0062	-0.0062	-0.0174	-0.0062
41	0.0014	0.0188	-0.0174	0.0000	0.0062	-0.0062	-0.0174	-0.0062
42	0.0014	0.0188	-0.0174	0.0000	0.0062	-0.0062	-0.0174	-0.0062
43	0.0014	0.0188	-0.0174	0.0000	0.0062	-0.0062	-0.0174	-0.0062

1. Skystream 3.7 (2.4kW)

Dublin Airport (Recorded) Wind Data

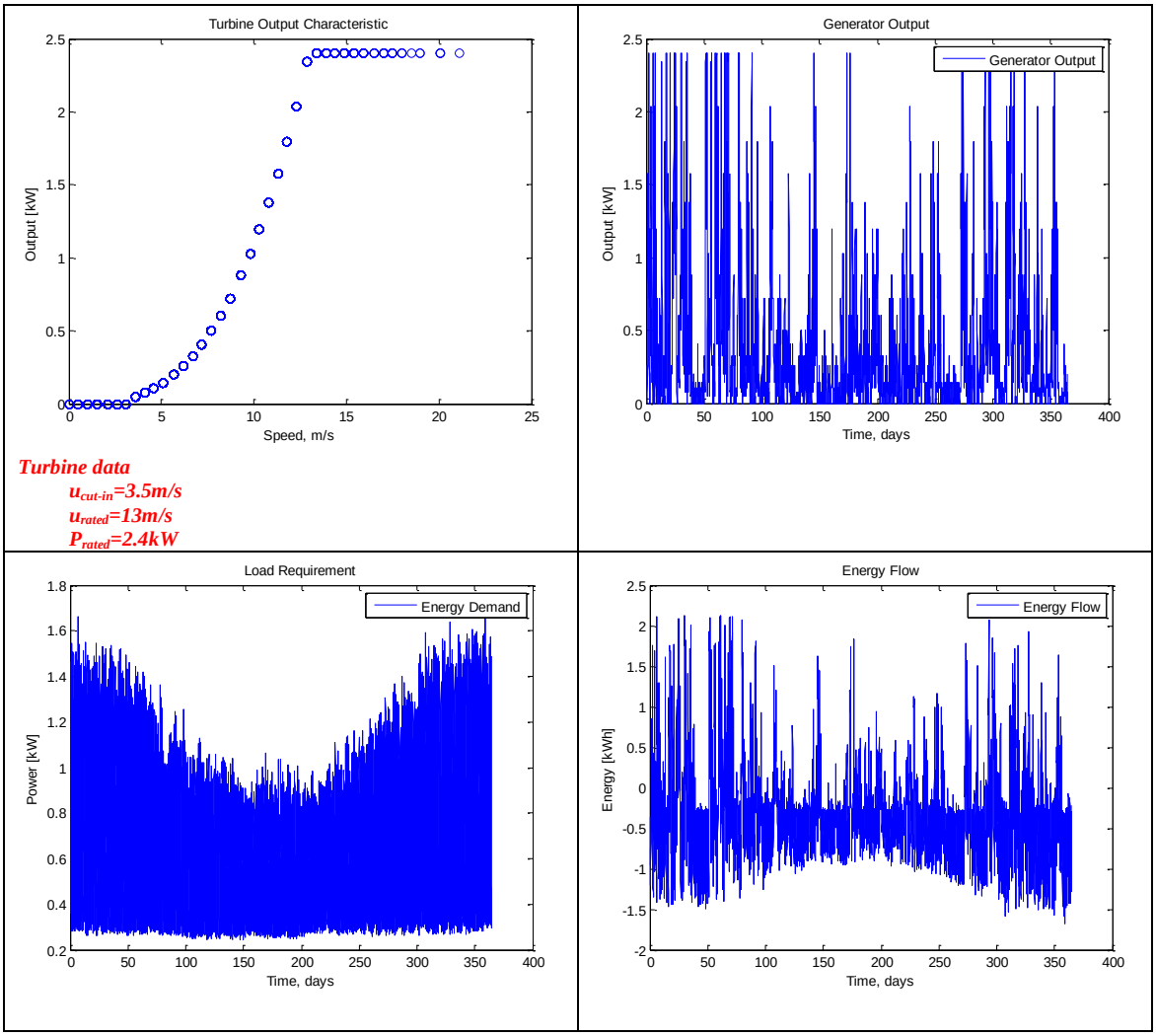

Figure A6 1 *Skystream* 2.4kW Micro Wind Turbine and its output characteristic and relative output based on the recorded Dublin Airport Wind Speed with respect to (hourly) consumer load

2. Whisper 200 (1kW)

Dublin Airport (Recorded) Wind Data

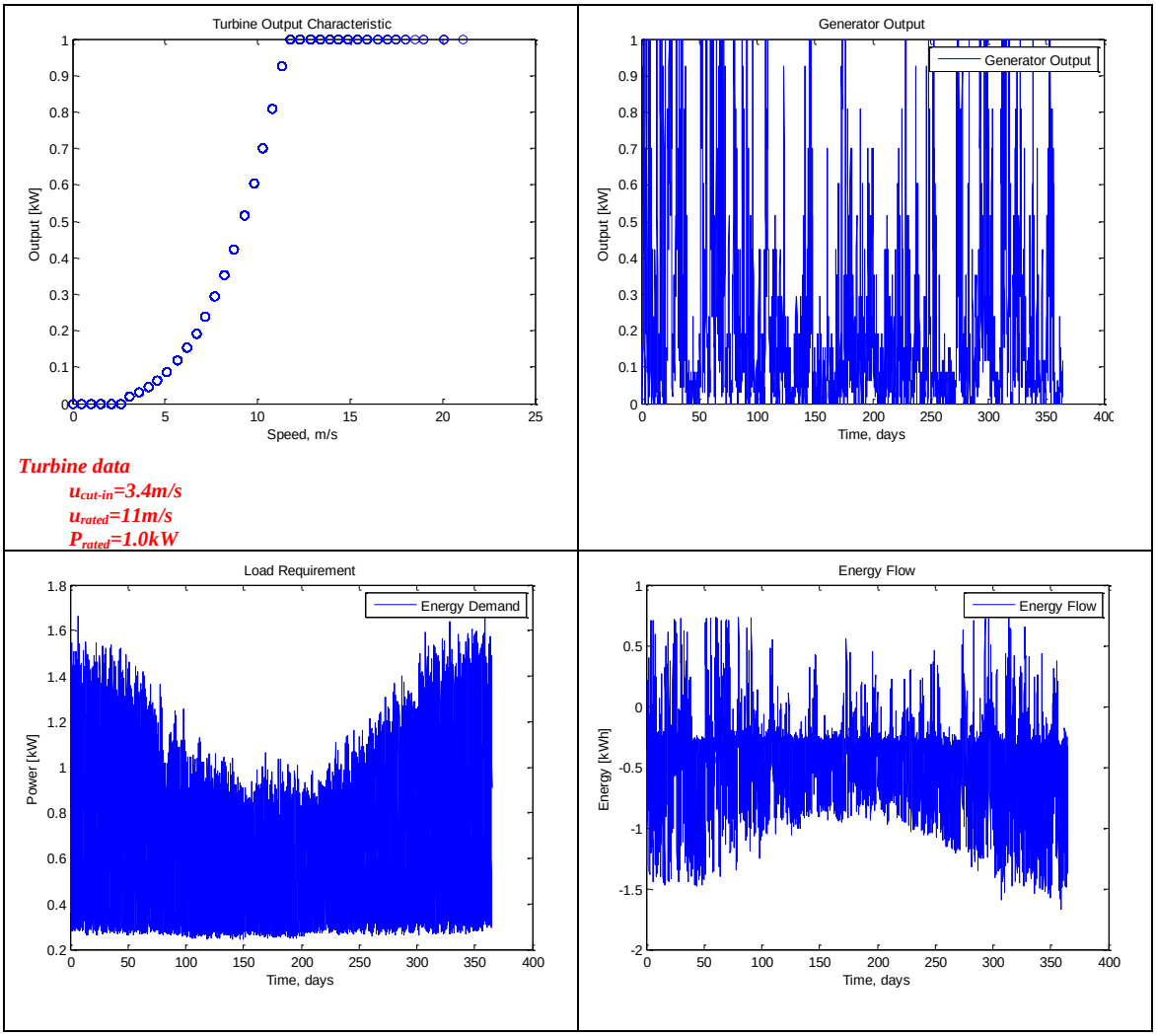

Figure A6 2 *Whisper 200 1.*0kW Micro Wind Turbine and its output characteristic and relative output based on the recorded Dublin Airport Wind Speed with respect to (hourly) consumer load

Zero Generation

Zero Generation	Tap	V_{Bus}[13] Vmax	Vmin	%		V_{Bus}[43] Vmax	Vmin	%	
	Neg-6				<90% V				<90% V
					>100% V				>100% V
	Neg-4				<90% V				<90% V
					>100% V				>100% V
	Neg-2				<90% V				<90% V
					>100% V				>100% V
	Nominal	0.99	0.86	2.26	<90% V	1.07	0.91	0.00	<90% V
				0.00	>100% V			0.00	>100% V
	Plus-2	1.02	0.89	0.03	<90% V	1.11	0.94	0.00	<90% V
				0.00	>100% V			18.95	>100% V
	Plus-4	1.06	0.93	0.00	<90% V	1.14	0.98	0.00	<90% V
				0.00	>100% V			68.80	>100% V
	Plus-6	1.09	0.96	0.00	<90% V	1.18	1.01	0.00	<90% V
				0.00	>100% V			90.64	>100% V

100% Generation Capacity

V_{BUS}[13]

100% Generation		Gen-1 V_{max}	Gen-1 V_{min}			Gen-2 V_{max}	Gen-2 V_{min}			Gen3 V_{max}	Gen3 V_{min}		
	Neg-6	1.05	0.76	58.80	<90% V	0.97	0.76	71.35	<90% V	1.05	0.76	45.06	<90% V
				0.00	>110% V			0.00	>110% V			0.00	>110% V
	Neg-4	1.09	0.80	17.95	<90% V	1.01	0.80	22.37	<90% V	1.09	0.80	14.11	<90% V
				0.00	>110% V			0.00	>110% V			0.00	>110% V
	Neg-2	1.12	0.83	3.98	<90% V	1.04	0.83	4.92	<90% V	1.13	0.83	3.12	5.70
				3.39	>110% V			0.00	>110% V			9.73	>110% V
	Nominal	1.16	0.86	0.55	<90% V	1.08	0.86	0.70	<90% V	1.17	0.86	0.47	<90% V
				7.01	>110% V			0.00	>110% V			15.70	>110% V
	Plus-2	1.20	0.89	0.01	<90% V	1.11	0.89	0.01	<90% V	1.20	0.89	0.01	<90% V
				13.39	>110% V			4.50	>110% V			24.05	>110% V
	Plus-4	1.23	0.93	0.00	<90% V	1.15	0.93	0.00	<90% V	1.24	0.93	0.00	<90% V
				23.26	>110% V			13.04	>110% V			37.50	>110% V

V_{BUS}[43]

100% Generation		Gen-1 V_{max}	Gen-1 V_{min}			Gen-2 V_{max}	Gen-2 V_{min}			Gen3 V_{max}	Gen3 V_{min}		
	Neg-6	1.18	0.81	4.28	<90% V	1.08	0.81	5.37	<90% V	1.18	0.81	3.32	<90% V
				7.41	>110% V			0.00	>110% V			16.48	>110% V
	Neg-4	1.22	0.85	0.84	<90% V	1.12	0.85	1.11	<90% V	1.22	0.85	0.71	<90% V
				13.18	>110% V			3.53	>110% V			23.94	>110% V
	Neg-2	1.26	0.88	0.05	<90% V	1.16	0.88	0.05	<90% V	1.26	0.88	0.05	<90% V
				22.12	>110% V			12.19	>110% V			35.81	>110% V
	Nominal	1.29	0.92	0.00	<90% V	1.20	0.92	0.00	<90% V	1.30	0.92	0.00	<90% V
				39.93	>110% V			27.52	>110% V			54.01	>110% V
	Plus-2	1.33	0.96	0.00	<90% V	1.24	0.96	0.00	<90% V	1.34	0.96	0.00	<90% V
				76.23	>110% V			69.75	>110% V			81.32	>110% V
	Plus-4	1.37	0.99	0.00	<90% V	1.27	0.99	0.00	<90% V	1.38	0.99	0.00	<90% V
				93.55	>110% V			91.55	>110% V			94.73	>110% V

75% Generation Capacity

V_{BUS}[13]

75% Generation	*Gen-1*				*Gen-2*				*Gen3*			
	Vmax	*Vmin*	*%*		*Vmax*	*Vmin*	*%*		*Vmax*	*Vmin*	*%*	
Neg-6	1.00	0.76	52.73	<90% V	0.95	0.76	84.27	<90% V	1.02	0.76	84.27	<90% V
			0.00	>110% V			0.00	>110% V			0.00	>110% V
Neg-4	1.03	0.80	16.31	<90% V	0.99	0.80	26.37	<90% V	1.06	0.80	28.37	<90% V
			0.00	>110% V			0.00	>110% V			0.00	>110% V
Neg-2	1.07	0.83	3.62	<90% V	1.02	0.83	6.34	<90% V	1.10	0.83	6.34	<90% V
			0.00	>110% V			0.00	>110% V			0.00	>110% V
Nominal	1.10	0.86	0.50	<90% V	1.05	0.86	0.89	<90% V	1.13	0.86	0.89	<90% V
			2.71	>110% V			2.71	>110% V			7.44	>110% V
Plus-2	1.14	0.89	0.01	<90% V	1.09	0.89	0.01	<90% V	1.17	0.89	0.01	<90% V
			17.01	>110% V			17.01	>110% V			17.01	>110% V
Plus-4	1.17	0.93	0.00	<90% V	1.12	0.93	0.00	<90% V	1.20	0.93	0.00	<90% V
			28.34	>110% V			28.34	>110% V			28.34	>110% V

V_{BUS}[43]

75% Generation	*Gen-1*				*Gen-2*				*Gen3*			
	Vmax	*Vmin*	*%*		*Vmax*	*Vmin*	*%*		*Vmax*	*Vmin*	*%*	
Neg-6	1.10	0.80	6.02	<90% V	1.04	0.80	9.82	<90% V	1.13	0.80	9.82	<90% V
			0.00	>110% V			0.00	>110% V			5.59	>110% V
Neg-4	1.14	0.83	1.59	<90% V	1.08	0.83	2.73	<90% V	1.17	0.83	2.73	<90% V
			14.25	>110% V			14.25	>110% V			14.47	>110% V
Neg-2	1.10	0.83	6.34	<90% V	1.17	0.87	0.15	<90% V	1.21	0.87	0.15	<90% V
			0.00	>110% V			22.61	>110% V			22.61	>110% V
Nominal	1.21	0.91	0.00	<90% V	1.15	0.91	0.00	<90% V	1.24	0.91	0.00	<90% V
			36.76	>110% V			36.76	>110% V			36.76	>110% V
Plus-2	1.25	0.94	0.00	<90% V	1.19	0.94	0.00	<90% V	1.28	0.94	0.00	<90% V
			66.78	>110% V			66.97	>110% V			67.40	>110% V
Plus-4	1.29	0.98	0.00	<90% V	1.22	0.98	0.00	<90% V	1.32	0.98	0.00	<90% V
			89.41	>110% V			89.59	>110% V			89.98	>110% V

A8: *Preliminary Analysis:* MacDonald and COST Wind Speed Profiling Methodologies

To facilitate preliminary investigations of the urban wind speed modelling methodologies and associated productivity of small wind energy systems, a tool was developed using EXCEL^{TM} (Figure A8 1). This tool facilities short-term visual (time series) wind speed profiling based on wind observations at an urban location (Dublin city) based on generic estimates of the modelling parameters identified in Sections 4.5.2 and 4.5.3 (over a three day period). The tool models the wind speed on the basis of a rural background (Dublin Airport) wind reference extrapolated into the urban environment which is refined to derive the representative urban wind resource based on the MacDonald and COST methodologies (as summarised in Figure A8 1 below).

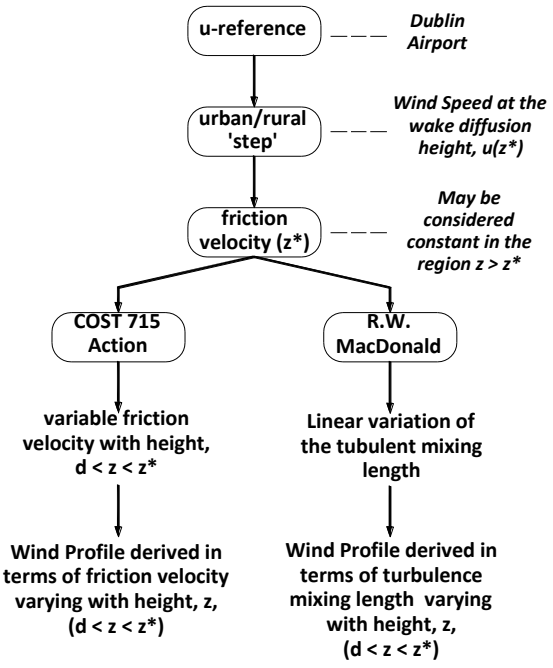

Figure A8 1 Summary of the urban wind speed methodologies [149] and [150] as applied in the EXCEL^{TM} Tool

Details on the urban location utilised for this preliminary analysis are as described in[198].

Figure A8 2 illustrates a screen Shot of the (EXCEL^{TM}) Urban Wind Estimation Tool [198]. The tool facilitates wind speed approximation based on the MacDonald methodology [149] and the COST approximation [150] in terms of the flow charts illustrated in Figure 4.12 and Figure 4.15 respectively. More specifically, the figure is broken into four parts:

a) The tool facilitates investigation of the variability of the wind speed approximations through variation of (urban) reference height (z) and fine-tuning of the surface roughness parameters ($z_{0[Rural]}$ and $z_{0[Urban]}$).
b) Short term wind speed profiling facilitating visual comparison of the different models
c) The tool further facilitates indication of the performance of a range of micro wind turbines based on their relative characteristics
d) Finally, the tool provides an illustration of Wind Turbine productivity based on the modelled/measured wind reference

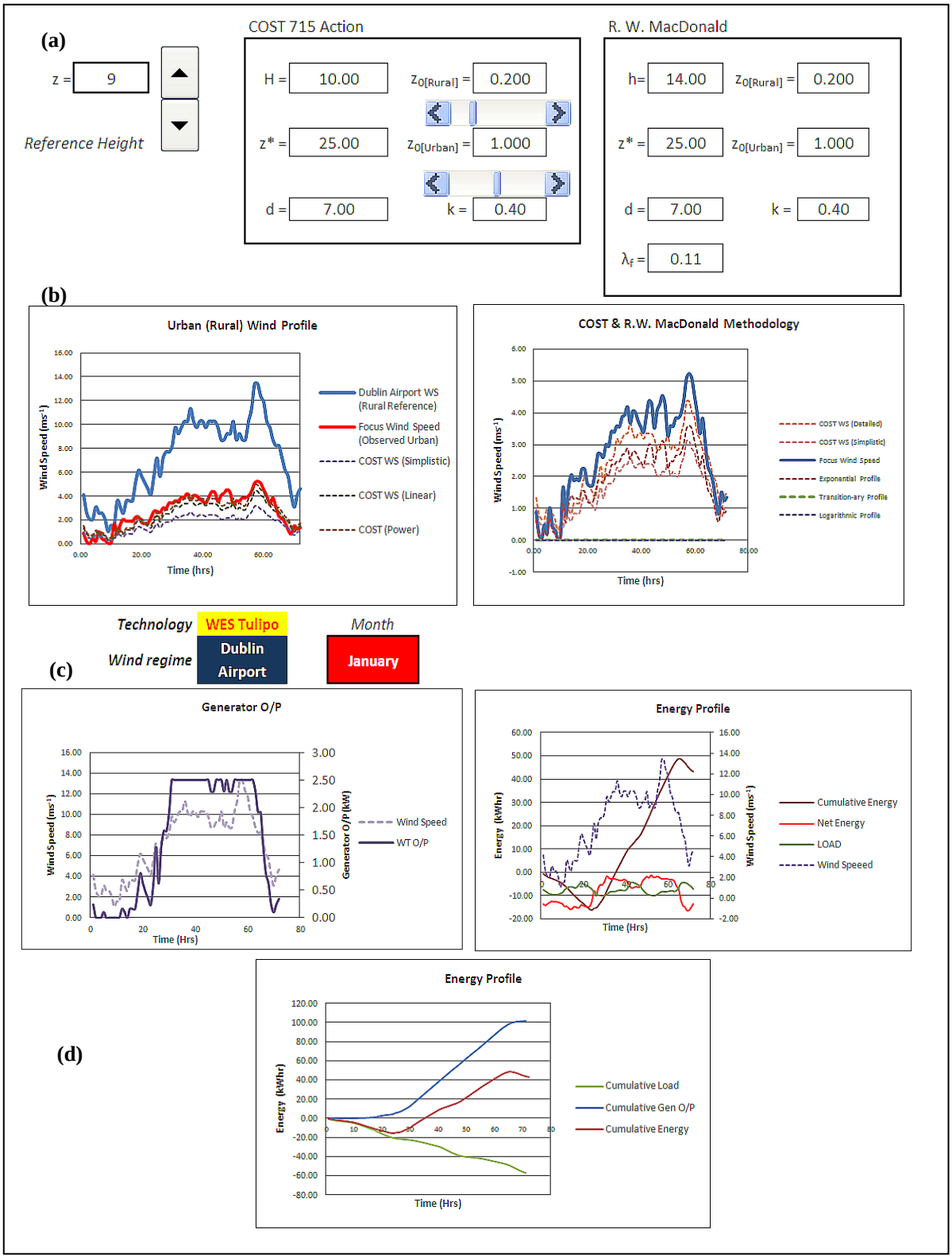

Figure A8 2 Screen Shot of the (EXCEL™) Urban Wind Estimation Tool.

The preliminary research in [198] used wind data acquired from *Dublin Airport* and the *Focus Research Centre* (Dublin Institute of Technology), over one year (2008). Focus Research Centre is located in the south inner city and the meteorological station at Dublin Airport is located 15km north west of The Focus Institute and is located in North county Dublin. A selection of months (with consideration applied over three consecutive days per month) was used to provide profiles in terms of:

- Wind speed
- Wind direction
- Modelled wind speeds

From these profiles, analysis was performed in terms of:

- Statistical accuracy
- Energy profile of a selection of readily available micro wind turbines.

Wind speeds/directions summaries that were employed in the analyses contained in [198] are presented in Table A8 1

Table A8 1 Wind Resource Summaries

	Dublin Airport		Focus Building	
	(ms^{-1})	Degrees	(ms^{-1})	Degrees
January	4.7	(180-240)	2.62	(150-240)
March	5.45	(180-240)	2.15	(210-360)
May	3.24	(30-90)	2.04	(60-150)
July	7.63	(210-300)	2.99	(210-330)
September	3.22	(210-330)	1.82	(210-330)
November	7.46	(210-330)	2.72	(120-270)

Referring to Figure A8 2, wind speed profiles can be selected for each month in terms of the modelled COST and MacDonald methodologies over a three day period, the model being developed primarily for initial investigations The COST *Simplistic* refers to a logarithmic extrapolation implementation of the COST methodology; whereas the

COST *Linear* and COST *Power* trace are approximations of the COST equation (4.29) and are approximated in (A8 3) and Figure A8 2) respectively.

$$\Rightarrow \quad u(z) = \frac{u_*(z^*)}{\kappa} \times \sqrt[3]{\frac{2}{\pi}\left(\frac{\pi}{2(z^*-z_d)}\right)^{1.28}} \times \frac{(z-z_d)^{0.42667}}{0.42667}$$

(A8 3)

$$u(z) = u_*(z^*)\left[\left\{\frac{1}{\kappa}\left(\frac{\pi}{2}\frac{1}{z^*-d}\right)^{1.28/3}\right\}\frac{(z-d)^{(0.43)}}{(0.43)} + \left\{\frac{\left[Sin\left\{\frac{\pi}{2}\right\}^{1.28}\right]^{1/3}}{\kappa(z^*-d)^{1.43}} - \frac{\left(\frac{\pi}{2}\cdot\frac{1}{z^*-d}\right)^{1.28/3}}{\kappa(z^*-d)}\right\}\frac{(z-d)^{(1.43)}}{(1.43)}\right]$$

(A8 4)

The derivations of both (A8 3) and (A8 4) are contained within the proceeding sections.

A8-1 Linear Approximation:

As explained in Section 4.5.3, for the neutral atmosphere

$$\frac{\partial u}{\partial z} = \frac{u_*(z)}{\kappa(z-z_d)}.1 \Rightarrow u(z) = \int_{z_1}^{z_2} \frac{u_*(z)}{\kappa(z-z_d)}dz$$

(A8 5)

Below z* an allowance for variation of friction velocity with height (i.e. within the roughness surface sub layer) as proposed by Rotach [193]:

$$\left(\frac{u_*(z)}{u_*(z^*)}\right)^b = \sin\left(\frac{\pi}{2}.Z\right)^a$$

Where $Z = \frac{z-z_d}{z^*-d}$

$$\Rightarrow u_*(z) = u_*(z^*) \times \sqrt[3]{\sin\left(\frac{\pi}{2}.Z\right)^a} \qquad \mathbf{a}=1.28;\ \mathbf{b}=3$$

(A8 6)

Combining (A8 5) and (A8 6),

$$u(z) = \int_{z_d}^{z^*} \left(u_*(z^*) \times \frac{\sqrt[3]{\sin\left(\frac{\pi}{2} \cdot \frac{z' - z_d}{z^* - z_d} \right)^{1.28}}}{\kappa (z' - z_d)} \right) dz'$$

$$u(z) = \frac{u_*(z^*)}{\kappa} \times \int_{z_d}^{z^*} \left(\frac{\sqrt[3]{\sin\left(\frac{\pi}{2} \cdot \frac{z' - z_d}{z^* - z_d} \right)^{1.28}}}{(z' - z_d)} \right) dz'$$

(A8 7)

A linear Approximation is applied on the basis of: $\sin x \cong \frac{2x}{\pi}$, $0 < x < \pi / 2$

$$\Rightarrow \sin x = \frac{2x}{\pi}$$

$$\Rightarrow x = \left(\frac{\pi}{2} \cdot \frac{(z - z_d)}{(z^* - z_d)} \right)^{1.28}$$

$$\sin x = \sin \left\{ \left(\frac{\pi}{2} \cdot \frac{(z - z_d)}{(z^* - z_d)} \right)^{1.28} \right\} \approx \frac{2}{\pi} \left(\frac{\pi}{2} \cdot \frac{(z - z_d)}{(z^* - z_d)} \right)^{1.28} \approx \frac{2}{\pi} \left(\frac{\pi}{2(z^* - z_d)} \right)^{1.28} \times (z - z_d)^{1.28}$$

$$\Rightarrow \sin x \approx \frac{2}{\pi} \left(\frac{\pi}{2(z^* - z_d)} \right)^{1.28} \times (z - z_d)^{1.28}$$

(A8 8)

Re-written in terms of a constant:

$$\sin x \approx a(z - d)^{1.28} \quad with \quad a = \frac{2}{\pi} \left(\frac{\pi}{2(z^* - z_d)} \right)^{1.28}$$

Returning to (A8 7) and in consideration of the approximation described in (A8 8)

$$u(z) = \frac{u_*(z^*)}{\kappa} \times \int_{z_d}^{z^*} \left(\frac{\sqrt[3]{\sin\left(\frac{\pi}{2} \cdot \frac{z'-z_d}{z^*-z_d}\right)^{1.28}}}{(z'-z_d)} \right) dz'$$

$$u(z) = \frac{u_*(z^*)}{\kappa} \times \sqrt[3]{a} \times \int_{z_d}^{z^*} \frac{(z'-z_d)^{\frac{1.28}{3}}}{z'-z_d} dz' = \frac{u_*(z^*)}{\kappa} \times \sqrt[3]{a} \times \int_{z_d}^{z^*} \frac{(z'-z_d)^{0.42667}}{(z'-z_d)} dz$$

$$\Rightarrow u(z) = \frac{u_*(z^*)}{\kappa} \times \sqrt[3]{a} \times \int_{z_d}^{z^*} F(y)\, dy$$

$$u(z) = \frac{u_*(z^*)}{\kappa} \times \sqrt[3]{a} \times \int_{z_d}^{z^*} \frac{(y-z_d)^{0.42667}}{(y-z_d)} d(y-z_d)$$

$$u(z) = \frac{u_*(z^*)}{\kappa} \times \sqrt[3]{a} \times \int_{z_d}^{z^*} (y-z_d)^{0.42667-1}\, d(y-z_d)$$

$$u(z) = \frac{u_*(z^*)}{\kappa} \times \sqrt[3]{a} \times \int_{z_d}^{z^*} (y-z_d)^{-0.57}\, d(y-z_d)$$

$$u(z) = \frac{u_*(z^*)}{\kappa} \times \sqrt[3]{a} \times \left\{ \frac{(y-d)^{0.57+1}}{(-0.57+1)} \right\} \Bigg|_{z_d}^{z^*} d(y-z_d)$$

$$\Rightarrow \quad u(z) = \frac{u_*(z^*)}{\kappa} \times \sqrt[3]{a} \times \frac{(z-z_d)^{0.42667}}{0.42667}$$

$$\Rightarrow \quad u(z) = \frac{u_*(z^*)}{\kappa} \times \sqrt[3]{\frac{2}{\pi}\left(\frac{\pi}{2(z^*-z_d)}\right)^{1.28}} \times \frac{(z-z_d)^{0.42667}}{0.42667}$$

(A8 9)

Therefore, for any height, z between z_d and z, a value for* ***u*** *can be calculated*

A8-2: Power-Series Approximation:

If $u_*(z)$ is considered in terms of a power expansion:

$$\frac{\sqrt[3]{\sin\left(\frac{\pi}{2}\cdot\frac{z'-z_d}{z^*-z_d}\right)^{1.28}}}{\kappa(z'-z_d)} \approx F(z)=\frac{a+b(z-z_d)}{(z-z_d)^{0.57}} \quad = a(z-z_d)^{-0.57}+b(z-z_d)^{1-0.57}$$

(A8 10)

$$\left.\begin{array}{l} z=z_d \,\|\, f(z_d)\equiv F(z_d) \\ z=z^* \,\|\, f(z^*)\equiv F(z^*) \end{array}\right\}$$ *Considering* (A8 10) *in terms of the two operational extremes with respect to a solution for 'a' and 'b'*

$$As\, z\to z_d: \qquad \frac{a}{(z-z_d)^{0.57}}=\frac{\left[\frac{\pi}{2}\left(\frac{z-z_d}{z^*-z_d}\right)\right]^{1.28/3}}{\kappa(z-z_d)}=\frac{\left[\frac{\pi}{2}\left(\frac{1}{z^*-d}\right)\right]^{1.28/3}\times(z-z_d)^{1.28/3}}{\kappa(z-z_d)}$$

$$\Rightarrow a=\frac{1}{\kappa}\left\{\frac{\pi}{2}\left(\frac{1}{z^*-z_d}\right)\right\}^{1.28/3}\times(z-z_d)^{0.42667+0.57-1}$$

$$=\frac{1}{\kappa}\left\{\frac{\pi}{2}\left(\frac{1}{z^*-z_d}\right)\right\}^{1.28/3}(z-z_d)^0$$

$$\therefore\ a=\frac{1}{\kappa}\left\{\frac{\pi}{2}\left(\frac{1}{z^*-z_d}\right)\right\}^{1.28/3}$$

Note: as $z \to z_d$, the second component of (A8 10), containing 'b', is much smaller and consequently irrelevant.

$$z\to z^*: \qquad \frac{\left[\frac{\pi}{2}\left(\frac{z-z_d}{z^*-z_d}\right)\right]^{1.28/3}}{\kappa(z^*-z_d)}=\frac{a+b(z^*-z_d)}{(z^*-z_d)^{0.57}}$$

$$\Rightarrow \frac{(z^*-z_d)^{0.57}}{\kappa(z^*-z_d)}\times\left[Sin\left\{\frac{\pi}{2}\right\}^{1.28}\right]^{1/3}-a=b(z^*-z_d)$$

$$b=\frac{(z-z_d)^{-1.43}}{\kappa}\times\left\{\sin\left(\frac{\pi}{2}\right)^{1.28}\right\}^{1/3}-\frac{a}{(z^*-z_d)}$$

(A8 11)

Recall from (A8 10), $F(z) = a(z-d)^{-0.57} + b(z-d)^{1-0.57}$

Therefore,

$$u(z) = u_*(z^*) \times \int_{z_d}^{z^*} F(y)\,dy = u_*(z^*) \times \int_{z_d}^{z^*} \left[a(y-d)^{-0.57} + b(y-d)^{1-0.57} \right] d(y - z_d)$$

$$u(z) = u_*(z^*) \times \left\{ a \times \left\{ \frac{(y-d)^{(-0.57+1)}}{(-0.57+1)} \right\} \Bigg|_{z_d}^{z^*} + b \times \left\{ \frac{(y-d)^{(-0.57+1)}}{(1-0.57+1)} \right\} \Bigg|_{z_d}^{z^*} \right\}$$

$$u(z) = u_*(z^*) \times \left\{ a \times \frac{(z-d)^{(0.43)}}{0.43} + b \times \frac{(z-d)^{(1.43)}}{1.43} \right\}$$

Therefore,

$$u(z) = u_*(z^*) \times \left\{ \left[\left(\frac{1}{\kappa} \left\{ \frac{\pi}{2} \cdot \frac{1}{z^* - z_d} \right\}^{1.28/3} \right) \times \frac{(z-d)^{(0.43)}}{0.43} \right] + \left[\left(\frac{\sin\left(\frac{\pi}{2}\right)^{1.28/3}}{\kappa.(z^*-d)} - \frac{\left\{ \frac{\pi}{2} \cdot \frac{1}{z^* - z_d} \right\}^{1.28/3}}{\kappa.(z^*-d)} \right) \times \frac{(z-d)^{(1.43)}}{1.43} \right] \right\}$$

A9: AMC System Matrix Development

In order to explain the approach, an example is presented here. Consider two three-phase (and Neutral) lines which subsequently facilitate a single-phase connection. Figure A10.1 below illustrates the 4-wire network configuration, with Figure A10.2 showing the development of a representative matrix.

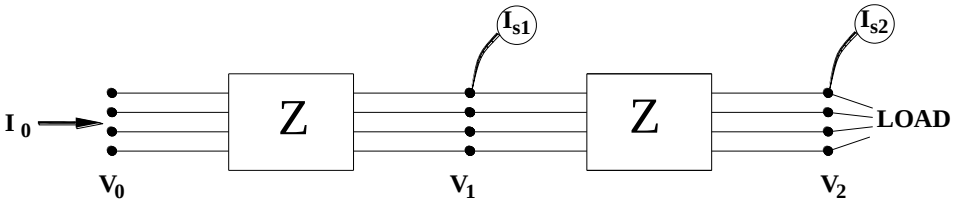

Figure A9.1 AMC & FCC - Y_{System} variation $(Y_N+\Delta Y_{SH}) / (Y_N+\Delta I_{SH})$ through voltage modulation

$$\begin{bmatrix} I_0 \\ I_{s1} \\ I_{s2} \end{bmatrix} = \begin{bmatrix} i_{01} \\ i_{02]} \\ i_{03} \\ i_{04} \\ i_{s1\_1} \\ i_{s1\_2} \\ i_{s1\_3} \\ i_{s1\_4} \\ i_{s2\_1} \\ i_{s2\_2} \\ i_{s2\_3} \\ i_{s2\_3} \end{bmatrix} = \begin{bmatrix} i_1 \\ i_2 \\ i_3 \\ i_4 \\ i_5 \\ i_6 \\ i_7 \\ i_8 \\ i_9 \\ i_{10} \\ i_{11} \\ i_{12} \end{bmatrix} = \begin{bmatrix} Y_{4\text{-wire}} \end{bmatrix} \begin{bmatrix} V_0 \\ V_1 \\ V_2 \end{bmatrix} = \begin{bmatrix} y_{11} & y_{21} & y_{13} & y_{14} & y_{15} & y_{16} & y_{17} & y_{18} & y_{19} & y_{110} & y_{111} & y_{112} \\ y_{21} & y_{22} & y_{23} & y_{24} & y_{25} & y_{26} & y_{27} & y_{28} & y_{29} & y_{210} & y_{211} & y_{212} \\ y_{31} & y_{32} & y_{33} & y_{34} & y_{35} & y_{36} & y_{37} & y_{38} & y_{39} & y_{310} & & y_{312} \\ y_{41} & y_{42} & y_{43} & y_{44} & y_{45} & y_{46} & y_{47} & y_{48} & y_{49} & & & y_{412} \\ y_{51} & y_{52} & y_{53} & y_{54} & y_{55} & y_{56} & y_{57} & y_{58} & & & & y_{512} \\ y_{61} & y_{62} & y_{63} & y_{64} & y_{65} & y_{66} & y_{67} & y_{58} & & & & y_{612} \\ y_{71} & y_{72} & y_{73} & y_{74} & y_{75} & y_{76} & y_{77} & y_{78} & & & & y_{712} \\ y_{81} & y_{82} & y_{83} & y_{84} & y_{85} & y_{86} & y_{87} & y_{88} & & & & y_{812} \\ y_{91} & y_{92} & y_{93} & y_{94} & & & & & & & & y_{912} \\ y_{101} & y_{102} & y_{103} & & & & & & & & & y_{1012} \\ y_{111} & y_{112} & & & & & & & & & & y_{1112} \\ y_{121} & & & & & & & & & & & y_{1212} \end{bmatrix} \begin{bmatrix} V_1 \\ V_2 \\ V_3 \\ V_4 \\ V_5 \\ V_6 \\ V_7 \\ V_8 \\ V_9 \\ V_{10} \\ V_{11} \\ V_{12} \end{bmatrix}$$

Figure A9.2 Admittance matrix representation of Figure A9.1

Figure A9.3 illustrates a two-port model of a single phase line with Figure A9.4 illustrating how and where (between line 1 and line 2 of the four-wire system) the single phase line is connected.

$$\begin{bmatrix} i_{1a} \\ i_{4a} \end{bmatrix} = \begin{bmatrix} y_{11} & y_{21} \\ y_{21} & y_{22} \end{bmatrix} \begin{bmatrix} v_{1a} - y_{1b} \\ v_{4a} - y_{4b} \end{bmatrix} \qquad \begin{bmatrix} i_{1b} \\ i_{4b} \end{bmatrix} = \begin{bmatrix} y_{11} & y_{21} \\ y_{21} & y_{22} \end{bmatrix} \begin{bmatrix} v_{1b} - v_{1a} \\ v_{4b} - v_{4a} \end{bmatrix}$$

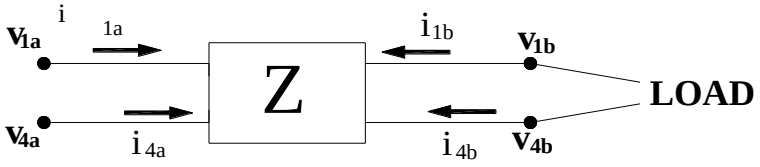

Figure A9.3 Two port model of a single –phase line

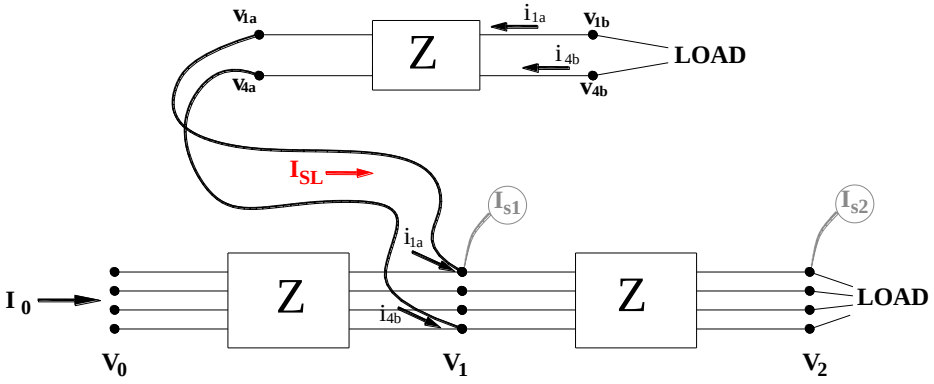

Figure A9.4 Connection of a single phase line to the 4-wire system (3-phase cabling) network

The system network as illustrated in Figure A9.4 is comprised of a partitioned matrix with 4 quadrants and with respect to the system network being considered, is configurable as follows (Figure A.9.5):

1. The 4-wire sub distribution network lines incorporating the connection of the single phase connection (as illustrated in Figure 7.1)

2. The four wire network matrix is essentially expanded to include the single-phase lines so as to facilitate the currents (phase and neutral) derived from the connection of the single phase line

3/4. These sections facilitate the evaluation of the single phase currents at the load connection point as a consequence of the 2-wire connection to the 4-wire network

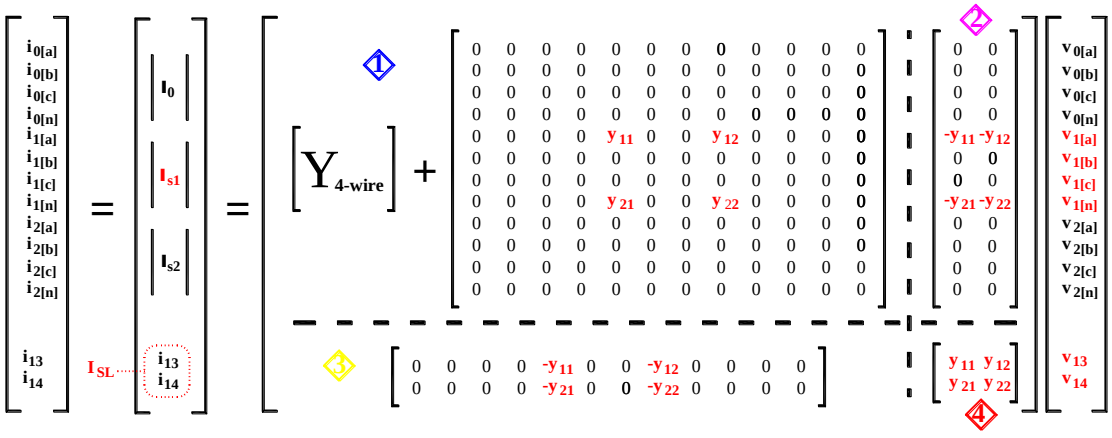

Figure A9.5 Matrix description of system presented in Figure A9.4

Described mathematically and concentrating specifically on where the single-phase line is connected (and in terms of system matrix positions),

$$i_{s1[5]} = y_{51}.v_{0[a]} + y_{52}.v_{0[b]} + \ldots + y_{54}.v_{0[n]} + y_{55}.v_{1[a]} + \ldots + y_{58}.v_{1[n]} + \ldots + \ldots y_{512}.v_{2[n]} + i_{1a} \quad \textbf{(A9.1)}$$

where i_{1a} in this regard represents the contribution from the single phase line/load.

Therefore:

$$i_{s1[5]} = y_{51}.v_{0[a]} + y_{52}.v_{0[b]} + \ldots + y_{54}.v_{0[n]} + (y_{55} + y_{11}).v_{1[a]} + \ldots + (y_{58} + y_{12}).v_{1[n]} + \ldots + \ldots y_{512}.v_{2[n]} + (-y_{11}v_{13} - y_{12}v_{14}) \quad \textbf{(A9.2)}$$

And in terms of a neutral current at the point of connection to the 4-wire system admittance matrix,

$$i_{s1[8]} = y_{81}.v_{0[a]} + y_{82}.v_{0[b]} + \ldots + y_{84}.v_{0[n]} + (y_{85} + y_{21}).v_{1[a]} + \ldots + (y_{88} + y_{22}).v_{1[n]} + \ldots + \ldots y_{812}.v_{2[n]} + (-y_{21}v_{13} - y_{12}v_{14}) \quad \textbf{(A9.3)}$$

In terms of the expanded system matrix, the currents flowing in the single phase line connection are therefore calculated as:

$$i_{13} = -y_{11}v_{1[a]} - y_{12}v_{1[n]} + y_{11}v_{13} + y_{12}v_{14} \quad \textbf{(A9.4)}$$

$$i_{14} = -y_{21}v_{1[a]} - y_{22}v_{1[n]} + y_{21}v_{13} + y_{22}v_{14} \quad \textbf{(A9.5)}$$

A summary of how the system admittance matrix is developed for *m* number of single-phase (customer additions to the 4-wire network configuration is illustrated in Figure A10.6.

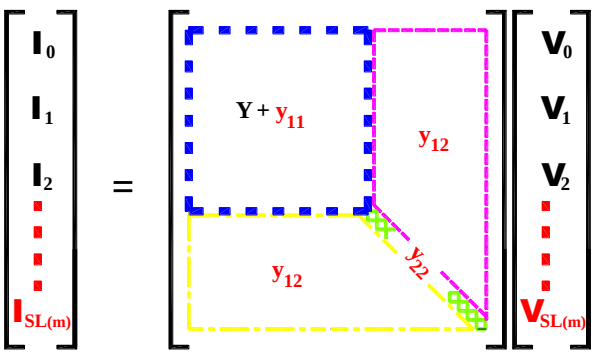

Figure A9.6 Summary of system admittance matrix description

A10: Current Correction Power Flow Algorithm

This approach applies (conceptually) the same kind of correction as the AMC ***but*** without the need to invert the admittance matrix. Here, instead of updating the shunt admittances (as the node bus voltages update iteratively), a suitable set of currents are injected. This approach has two steps:

1. $Y_{\{Network]}$ (compiled of the system branch description and the shunt element matrix) is defined in the first iteration. This matrix is thereafter used in each subsequent iteration
2. The iterative process involves the shunt element matrix modifications being represented as modulating current – i.e. $\Delta I_{SH} \leftrightarrow \Delta Y_{SH}$

Figure A10.1 illustrates a synopsised comparison of the AMC and FCC methodologies.

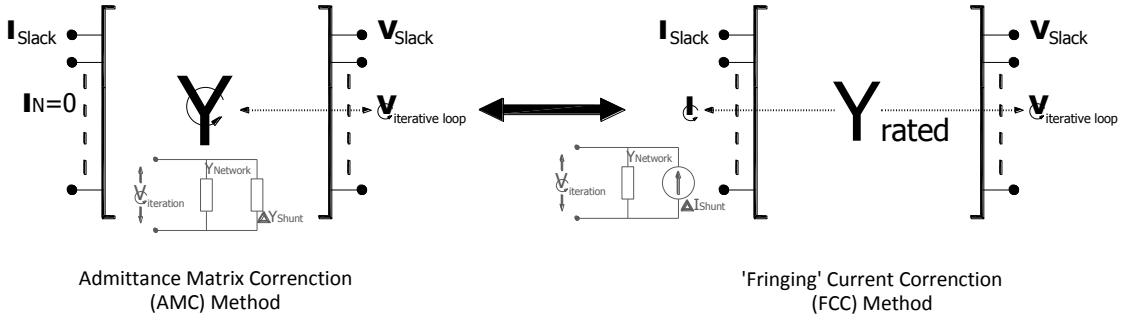

Figure A10.1 AMC & FCC - Y_{System} variation ($Y_N+\Delta Y_{SH}$) / ($Y_N+\Delta I_{SH}$) through voltage modulation

Recalling equations (7.9) and (7.10) in the development of (7.11) in describing how the system/network matrix can evaluate the network voltages directly in the AMC approach, a general solution to equation (7.13) is provided:

$$\Delta \mathbf{i}_L = \mathbf{Y}_{LG}.\mathbf{u}_G + \mathbf{Y}_{LL}.\mathbf{u}_L \qquad \textbf{(A10.1)}$$

leading to

$$\left(\mathbf{Y}_{LL}\right)^{-1}.\left(\Delta\mathbf{i}_L - \mathbf{Y}_{LG}.\mathbf{u}_G\right) = \mathbf{u}_L$$

and substituting into (7.9):

$$\mathbf{i}_G = \mathbf{Y}_{GG}.\mathbf{u}_G + \mathbf{Y}_{GL}.\left[\left(\mathbf{Y}_{LL}\right)^{-1}.\left(\Delta\mathbf{i}_L - \mathbf{Y}_{LG}.\mathbf{u}_G\right)\right]$$

$$\mathbf{i}_G = \left(\mathbf{Y}_{GG} - \left(\mathbf{Y}_{LL}\right)^{-1}.\mathbf{Y}_{LG}.\mathbf{Y}_{GL}\right)\mathbf{u}_G + \mathbf{Y}_{GL}.\left(\mathbf{Y}_{LL}\right)^{-1}.\Delta\mathbf{i}_L$$

(A10.2)

$$= \left(\mathbf{Y}_{G(Eq.)}\right)\mathbf{u}_G + \mathbf{Y}_{GL}.\left(\mathbf{Y}_{LL}\right)^{-1}.\Delta\mathbf{i}_L$$

(A10.3)

Consistent with Figure 7.10 which is the partitioned version of Figure 7.9, (A10.2) and (A10.3) can be partitioned in terms of Figure A10.2 below

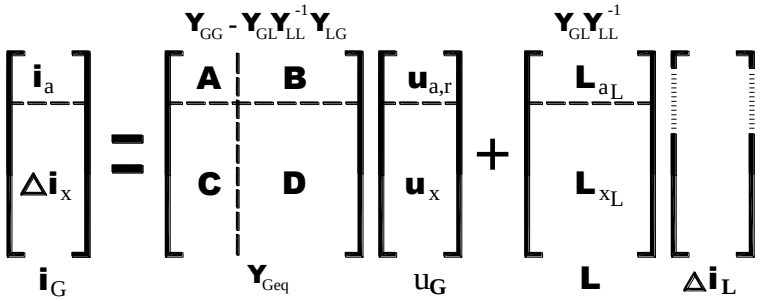

Figure A11.2 Partitioning of the system admittance matrix in terms of the 'fringing current', $\Delta\mathbf{i}_L$

With respect to Figure A10.2,

$$\Delta\mathbf{i}_x = \mathbf{C}.\mathbf{u}_{ar} + \mathbf{D}.\mathbf{u}_x + \mathbf{L}_{xL}\Delta\mathbf{i}_L$$

(A10.4)

and written in terms of u_x

$$\mathbf{u}_x = \left(\mathbf{D}\right)^{-1}\left(\Delta\mathbf{i}_x - \mathbf{L}_{xL}\Delta\mathbf{i}_L - \mathbf{C}.\mathbf{u}_{ar}\right)$$

(A10.5)

The fringing current, $\Delta\mathbf{i}_L$, is decoupled from (A10.4) and (A10.5) by considering how the shunt elements are evaluated (7.7) and (7.8).

If the approach outlined above is specifically modified so as to incorporate the *fringe* current into the description of the constant complex power description.

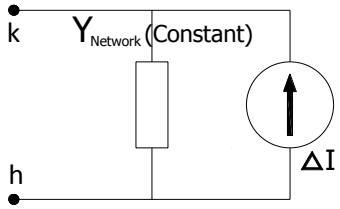

Figure A10.2 Shunt element representation through which a set of nominal constant admittances including fringe currents can be added

Under the hypothesis of constant complex power S_k, a term ΔI can be introduced:

$$S_k^* = Y_{kh} \cdot \left|U_{kh(0)}\right|^2 = Y_{kh} \cdot \left|U_{kh(i)}\right|^2 - U_{kh(i)} \Delta I_{kh(i)}$$

(A10.6)

where $U_{kh(0)}$ represents the rated voltage and the subscript (i) stands for the updated i-th iteration values. The implications of (A10.6) is that the complex power may be expressed as a function of the $U_{kh(i)}$ voltage, by using a correction current term as evaluated in (A10.7):

$$\Delta i_{kh} = \frac{Y_{kh}}{U_{kh(i)}} \left(\left|U_{kh}\right|_{(i)}^2 - \left|U_{kh}\right|_{(0)}^2 \right)$$

$$\Delta i_{kh} = \frac{Y_{kh}}{U_{kh(i)}} \left(\left|U_{kh}\right|_{(i)}^2 - \left|U_{kh}\right|_{(0)}^2 \right)$$

(A10.7)

A direct solution is iterated updating the shunt currents, through the system showed in Figure 11.3. The approach can be described in terms of (A10.8) and (A10.9):

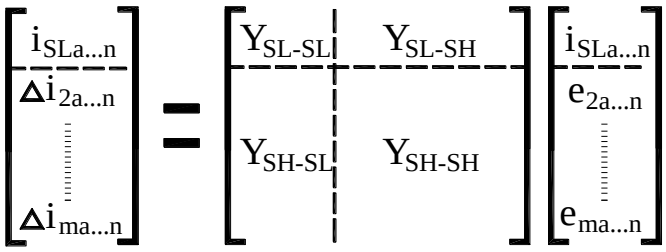

Figure A10.3: Representation of the power flow solution, using the Y matrix. The currents and potentials are arrays containing the values related to each circuit of the n-phase system

$$\mathbf{i}_{SL} = \mathbf{y}_{SL-SL}\mathbf{e}_{SL} - \mathbf{y}_{SL-SH}\mathbf{e}_{2-m}$$

(A10.8)

$$\Delta\mathbf{i}_{2-m} = \mathbf{y}_{SH-SL}\mathbf{e}_{SL} - \mathbf{y}_{SH-SH}\mathbf{e}_{2-m}$$

(A10.9)

An iterative loop is applied to find a solution for the system represented in (A10.8) and (A10.9). Equation (A10.10) shows how the $\mathbf{e_k}...\mathbf{e_h}$ potentials may be related to the $\Delta\mathbf{i}$ currents evaluated as in (A10.7):

$$\mathbf{e}_{2-m} = \mathbf{y}_{SH-SH}^{-1}\left(\Delta\mathbf{i}_{2-m} - \mathbf{y}_{SH-SL}\mathbf{e}_{SL}\right)$$

(A10.10)

A11: Markov Chain Wind Speed Generation

Theoretical *probability density functions* (PDFs) such as Weibull, Rayleigh etc. are commonly employed in predicting the magnitude of the wind speed. However, these theoretical PDFs assume independence of successive wind speeds in any synthetic data generation model. Markov chain modelling is based on transitional probabilities between successive wind speed data. As cited by Hocaoglu *et al* [251] and Sahin and Sen [252], there are a number of studies in which different natural processes are modelled using Markov chains. For example Srikanithan and McMahon [253] and Thyer and Kuczer [254] use a first order Markov chain model to generate annual rainfall data. Indeed, weather event modelling and simulation are extensively studied through Markov Chains [255] as well as being used to synthesize wind speed time series [256-258].

Markov chains are stochastic processes that can be parameterized by empirically estimating transition probabilities between discrete states in the observed system [252]. Therefore, a Markov Chain is a model for representing a stochastic process whereby a state *changes* at discrete time steps [259]. As described by Bersekas and N. Tsitsiklis [260], in such a model, a finite set of states is defined and the Markov chain is described in terms of transition probabilities p_{ij}, which determine the probability of transitioning from state *i* to *j*, regardless of previous states that were visited. In the Markov chain approach, the state of the wind speed in the current hour can be defined depending only upon the previous state – the first order, or one step Markov chain [261, 262]. A first order Markov chain model is generally used for modelling and simulation of wind speed

data, but is higher order chains could can improve the results of this synthetically generated wind speed data [262].

General Approach:

a) The wind speed time series are converted to wind speed states – a state contains wind speeds between certain values

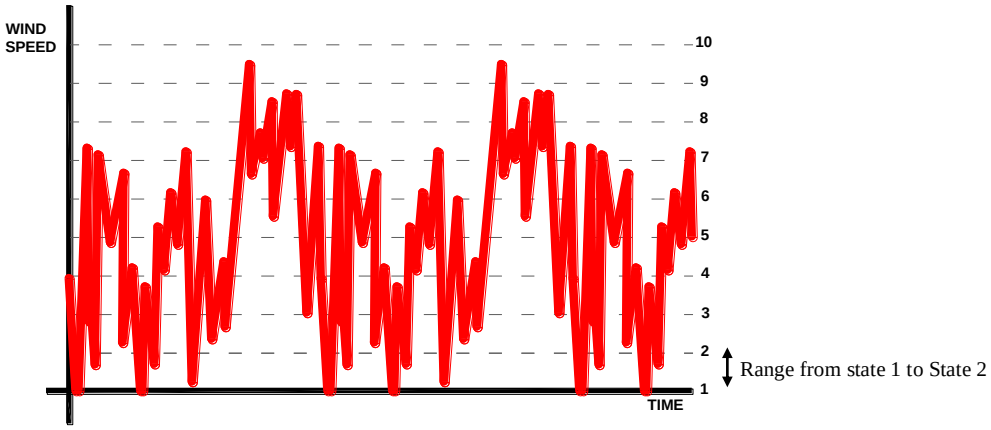

Figure A11.1 'State' variation representation of wind speed

b) Probability transition matrix is developed

- This matrix provides the basis of future likely synthetic wind speed generations and is based in simplistic terms, on the probability of wind speed transitions from one value to another; the number of transition probabilities, p_{ij}, from a state at time *t* to another state at time *t+1*.
- If the transition probability in the 'i'th row at the 'k'th state is P_{ik}, then the cumulative probability, P_{ik} can be expressed as

$$P_{ik} = \sum_{j=1}^{k} P_{ij}$$

$$P = \begin{bmatrix} P_{ij} & - & - \\ - & - & - \\ \vdots & \vdots & \ddots \end{bmatrix}$$

n x n Matrix ….. where 'n' refers to the number of states

Each element of the Matrix is derived as illustrated below:

$$P_{ij} = \frac{n_{ij}}{\sum n_{ij}}$$

No. of **transitions** from the specific state to other states (e.g. 1-2; 1-3; 1-4) etc

No. of states

$$P = \begin{bmatrix} P_{ij} & P_{i(j+1)} & - \\ - & - & - \\ \vdots & \vdots & \ddots \end{bmatrix}$$

The successive elements of each row sum to the cumulative probability of the row (Cumulative Probability Matrix)

c) Synthetic Generation of Wind Speed based on the derived cumulative probability transition matrix:

Step 1: Arbitrarily, a row is chosen representing the initial state. A random number (between 0 and 1 is used to generate a specific wind speed.

Arbitrarily chosen →

$$\begin{bmatrix} - & - & - & - & - & - & - \\ - & - & - & - & - & - & - \\ - & - & - & - & - & - & - \\ - & - & - & - & - & - & - \\ - & - & - & - & - & - & - \end{bmatrix}$$

The following 'representative' matrix (Cumulative Probability Matrix) is for illustrative purposes to aid explanation of methodology

$$\begin{bmatrix} - & - & - & - & - & - & - \\ 0.056 & 0.156 & 0.356 & 1.000 & 1.000 & 1.000 & 1.000 \\ 0.024 & 0.120 & 0.459 & 0.679 & 0.753 & 1.000 & 1.000 \\ 0.006 & 0.106 & 0.285 & 0.388 & 0.598 & 0.885 & 1.000 \\ - & - & - & - & - & - & - \end{bmatrix}$$

Step 2: A random number is generated and employed to the specific row. For the purposes of example, the random number generated is **0.43**

Step 3: As described by A. Shamshad *et al* [262] and Ahmet D. *et al* [262]:

- The next state speed is found where this random value is compared to the cumulative probability transition elements (of the highlighted/selected row).
- The column where the number resides represents the state for the next wind speed (remember, state really refers to a range of wind speeds)

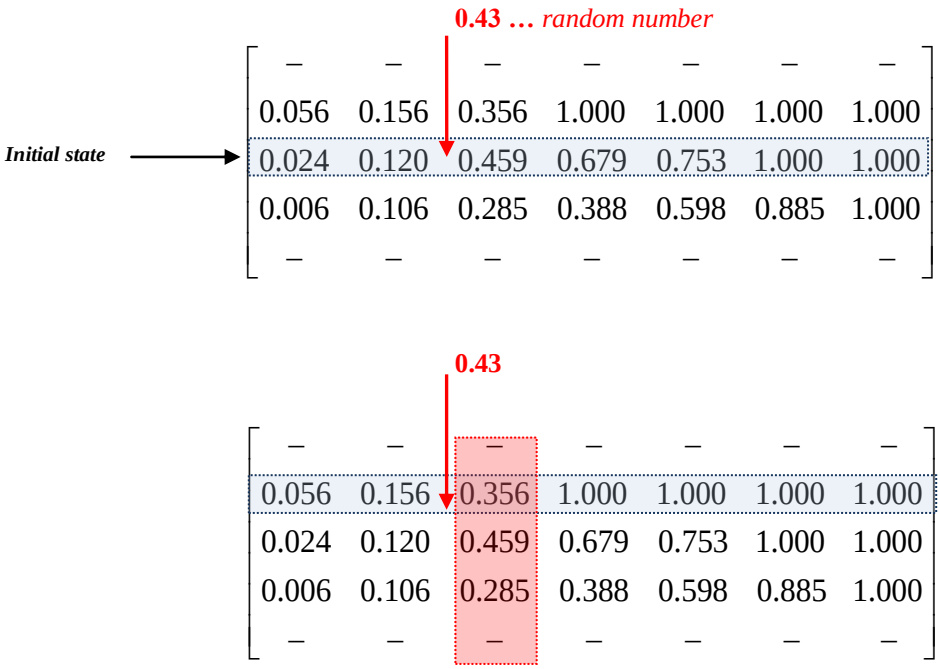

- For this example, the third column is acquired representing the third state

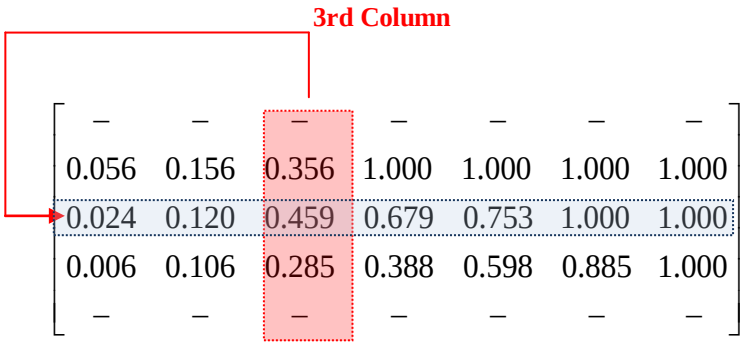

- For the next state another number (random) is generated, say ***0.82***

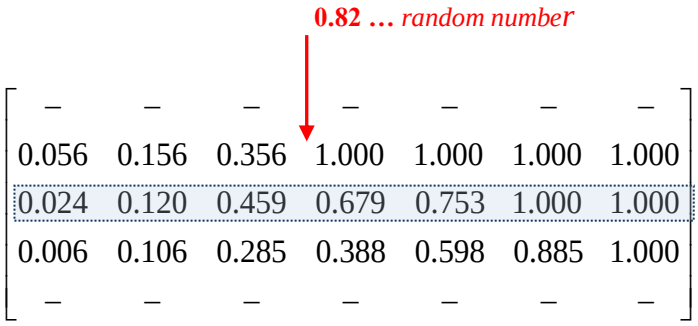

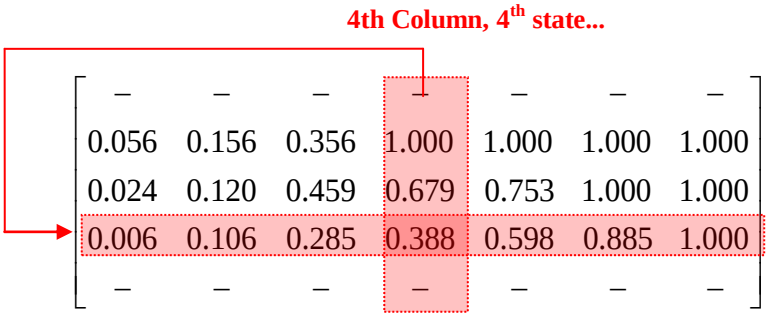

Step 4: To ascertain a value for wind speed form the above approach:

$$v = v_l + z_i(v_l - v_r)$$

where V_l and V_r represent the wind speed boundaries of the state;

Z_i = the uniform random number

The upper and lower limits of the states are highly subjective. For instance, in [252], *states* are defined depending on the standard deviation of the data set, or as per [263], Dukes and Palutiknof used a fixed width for the states of 2m/s. The approach employed in this research is to use a fixed width for the states of 1m/s.

In consideration of the urban and suburban sites discussed in Chapter 5 (C_H and S_H respectively), MATLAB^{TM} code was developed to employ a *markov chain* (first order) to 'pad' the modelled wind speed to encapsulate a representative year.

Figure A12.2 illustrates the derived markov chain extended time series as hourly data represented in terms of a number of days (including a weekly average) over a single year period, with Table A12 1 providing statistical comparison between the extended data and modelled wind speed as derived in Chapter 5.

Table A11 1 Modelled Wind and Markov Extended Wind Comparison

	Urban Modelled Wind Speed (C_H)		***Suburban Modelled Wind Speed (S_H)***	
Statistical Comparison	Modelled Wind Data (4789 Hrs)	Markov chain Extended Data set (8760hrs)	Modelled Wind Data (5556 Hrs)	Markov chain Extended Data set (8760hrs)
$\mathbf{u_{Mean}}$	4.62	4.58	4.39	4.33
$\mathbf{u_{STD}}$	2.09	2.18	1.96	2.05

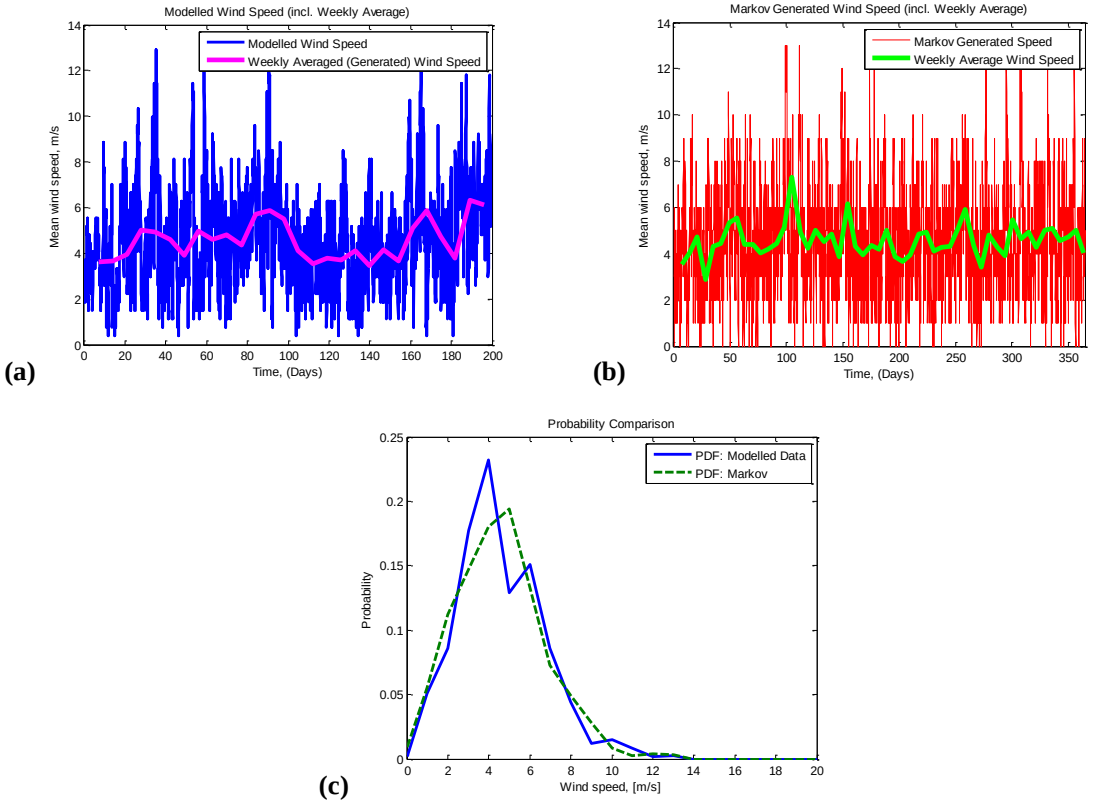

Figure A12 1 (a) Modelled Wind Speed; (b)Markov Extended Wind Speed & (c) PDF comparison for the *Urban* site (C_H)

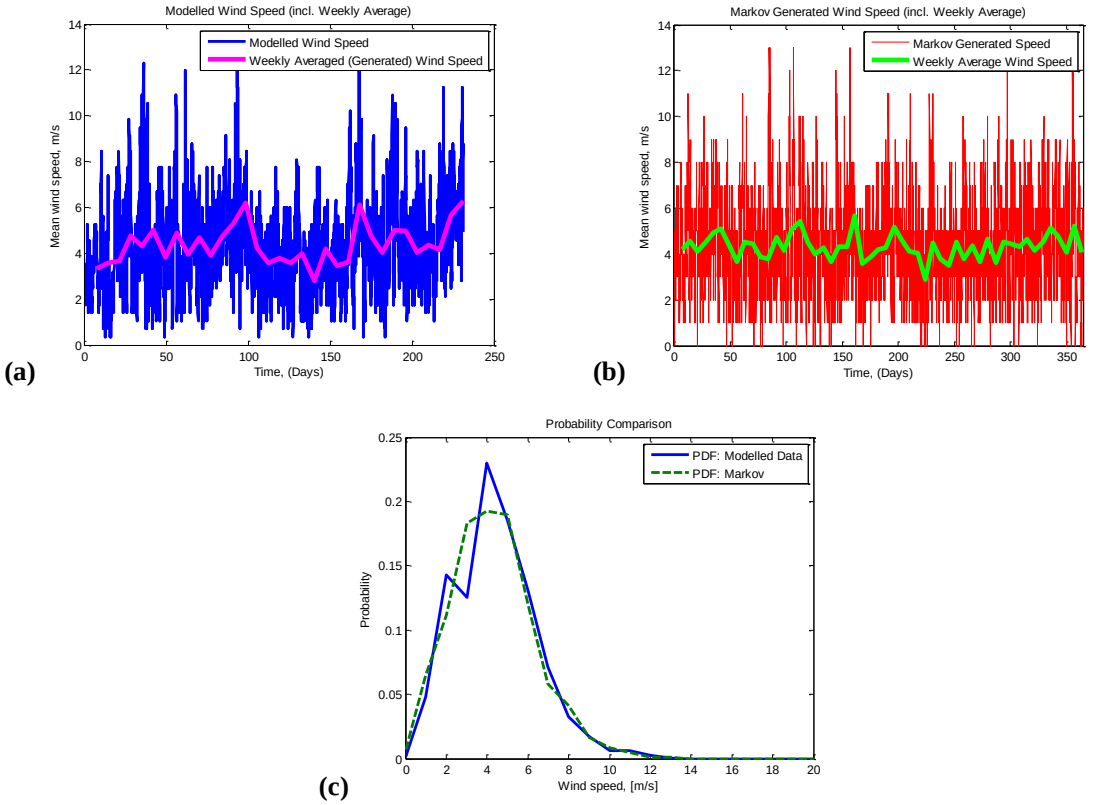

Figure A11 2 (a) Modelled Wind Speed; (b)Markov Extended Wind Speed & (c) PDF comparison for the *Suburban* site (S_H)

List of Publications

Journal Publications

Published:

Estimating the wind resource in an urban area: A case study of micro-wind generation potential in Dublin, Ireland, Sunderland K. M., Mills G., and Conlon M.F.; *Journal of Wind Engineering and Industrial Aerodynamics*, vol. 118, pp. 44-53, 2013.

Small wind turbines in turbulent (urban) environments: A consideration of normal and Weibull distributions for power prediction, Sunderland K., Woolmington T., Blackledge J., and Conlon M.; *Journal of Wind Engineering and Industrial Aerodynamics,* vol. 121, pp. 70-81, 2013

Analysis of Wind Velocity and the Quantification of Wind Turbulence in Rural and Urban Environments using the L´evy Index and Fractal Dimension, Blackledge J., Coyle E., McCoy N., Kearney D., Sunderland K., and Woolmington T.; *ISAST Transactions on Computers and Intelligent Systems*, vol. 4, 2012.

Peer Reviewed Conference Papers

Published:

Urban deployment of small wind turbines: power performance and turbulence, Sunderland K., Woolmington T., Blackledge J., Conlon M.F.; *Universities' Power Engineering Conference (UPEC), 2013*, 48th International, Dublin, Ireland, 2013.

Application of a correction current injection power flow algorithm to an unbalanced 4-wire distribution network incorporating TN-C-S earthing, Sunderland K., Coppo M., Conlon M.F., Turri R.; *Universities' Power Engineering Conference (UPEC), 2013*, 48th International, Dublin, Ireland, 2013.

Impact of Urban Atmospheric Turbulence on the Electrical Generation Capability of a Micro Wind Turbine, Beer E., Conlon M.F., Sunderland K.; *Universities' Power Engineering Conference (UPEC), 2013*, 48th International, Dublin, Ireland, 2013.

The Quantification of Wind Turbulence By Means of the Fourier Dimension, Woolmington T., Sunderland K., Blackledge J., Conlon M.F.; *24th IET Signals and Systems Conference (ISSC), 2013*, Letterkenny, Ireland, 2013.

Advances In The Quantification of Turbulence: A Wind Resource Characteristic, Woolmington T., Sunderland K., Blackledge J., Conlon M.F.; *The Sustainable Energy and Environmental Protection conference (SEEP)*, Slovenia 2013

An evaluation of the wind resource across an urban area, Sunderland K.; *International Conference on Urban Climates (ICUC8), 2012*, 8th International, 2012, pp. 1-4, Dublin Ireland, 2012

4-wire power flow analysis of a representative urban distribution network Incorporating SSEG, Sunderland K. and Conlon M. F.; in *Universities Power Engineering Conference (UPEC), 2012*, 47th International, pp. 1-6, London, 2012

Observations of the wind resource across the Dublin urban Area, Sunderland K., Conlon M.F., Mills G., Fealy R.; in *Universities' Power Engineering Conference (UPEC), 2011*, 46th International, 2011, pp. 1-6, Soest, Germany, 2011.

Estimating the yield of micro wind turbines in an urban environment: A methodology, Sunderland K. and Conlon M. F., in *Universities Power Engineering Conference (UPEC), 2010*, 45th International, 2010, pp. 1-6, Cardiff, 2010.

The probabilistic integration of demand -side load and generation in a representative Irish Distribution Network, Sunderland K. and Conlon M. F. in *International Conference on Environment and Electrical Engineering, (EEEIC), 2009*, 8th International, 2009, pp. 1-5, Karpacz, Poland, 2009.

The role of micro wind generation in Ireland's energy future, Sunderland K. and Conlon M. F. in *Universities Power Engineering Conference, (UPEC), 2008*, 43rd International, 2008, pp. 1-5, Padova, 2008.